KTH ROYAL INSTITUTE
OF TECHNOLOGY

Doctoral Thesis in Civil and Architectural Engineering

Reducing Radon Gas Emissions in Concrete

MAGNUS DÖSE

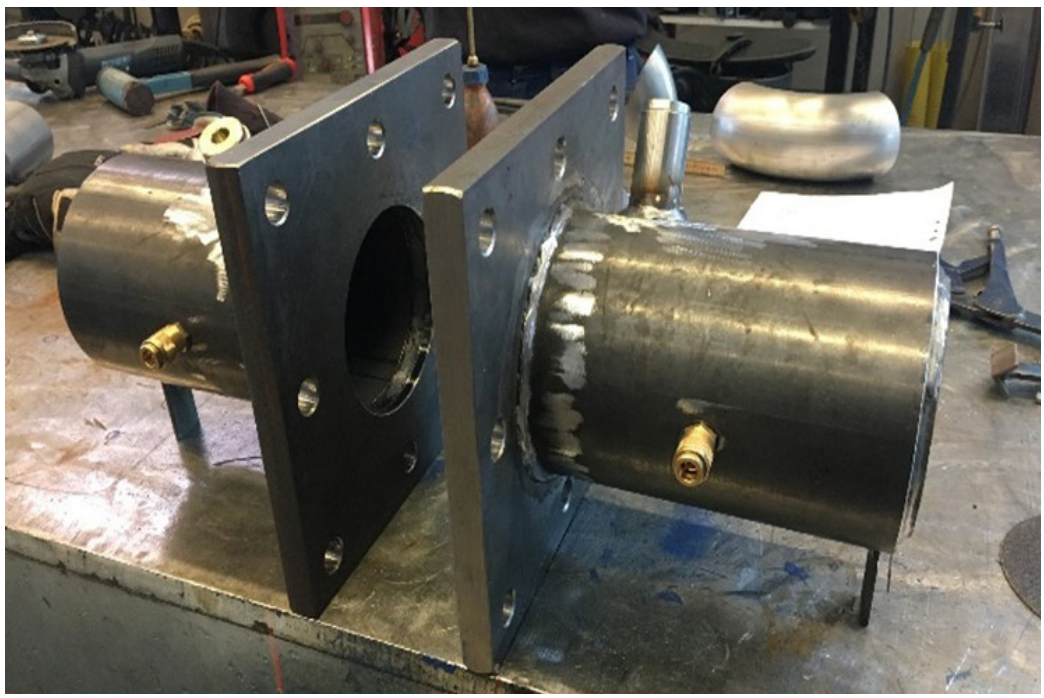

Stockholm, Sweden 2022

Reducing Radon Gas Emissions in Concrete

MAGNUS DÖSE

Academic Dissertation which, with due permission of the KTH Royal Institute of Technology, is submitted for public defence for the Degree of Doctor of Philosophy on Friday the 2nd of December-2022, Kollegiesalen 8, KTH, Stockholm

Doctoral Thesis in Civil and Architectural Engineering
KTH Royal Institute of Technology
Stockholm, Sweden 2022

ISBN: 978-91-8040-395-5
TRITA-ABE-DLT-2240

Printed by: Universitetsservice US-AB, Sweden 2022

Preface

The experimental work of this doctoral thesis was mainly carried out at RISE (Research Institutes of Sweden) in Borås, with complementary discussions at the Royal Institute of Technology (KTH) in Stockholm, Sweden. The PhD research project was initiated in February 2017 and finished in November 2022.

The project was financed by the Swedish Consortium on Financing Basic Research in the Concrete Field and the Construction Industry´s Organization for Research and Development (SBUF).

The project had a reference group with people from the different members of the Swedish Consortium as well as tutors representing the Royal Institute of Technology (KTH), the Department of Civil and Architectural Engineering, the Division of Concrete Structures (Johan Silfwerbrand), the Swedish Geological Survey (Cecilia Jelinek), the Swedish Cement and Concrete Research Institute (Jan Trägårdh) and the Department of Radiation Physics, Sahlgrenska Academy, University of Gothenburg (Mats Isaksson). From the Swedish Consortium, the following researchers participated as members in the reference group: Kent Slade (Strängbetong), Anders Selander (Cementa) and Monica Soldinger Almefelt (Peab/Swerock AB).

The author is very grateful to his supervisors and especially Professor Johan Silfwerbrand, who always tried to make time for discussion, evaluation and fruitful guidance in the process of finalising the thesis. Many thanks to my assistant supervisor Cecilia Jelinek, at the Swedish Geological Survey, who contributed with great quality in the reference group discussions. Many thanks as well to my assistant supervisor Professor Mats Isaksson, who gave me the necessary means to understand the complex issues of radiation even further. Finally, special thanks to Jan Trägårdh, who contributed with valuable discussions and support when needed, and the reference group for raising all sort of questions during our meetings.

A passionate thought is also addressed to my colleagues at Borås, who aided me in swiftly getting some measurement results, such as those on compressive testing, during the project.

Also, I address a sincere thanks to Eva Lundgren at RISE, Stockholm, who came to my rescue, more than once, when literature references seemed impossible to obtain.

Gothenburg, November 2022

Magnus Döse

Summary

Several compulsory regulations and recommendations regarding ionising radiation for building products have been introduced in recent years. Furthermore, industry-affiliated aggregate and concrete companies strive to implement environmental goals that should be fulfilled regarding building materials. In Sweden, a certification system for high-level environmental quality assurance has been designed by the Green Building Council (Miljöbyggnad 3.0). The certification system is used in procurements of buildings to achieve a high standard and good quality environment for habitants inside the new buildings. One of these environmental goals, as part of this certification system, concerns acceptable levels of radon within the indoor environment.

In recent decades it has become increasingly common for the concrete industry to use combinations of different Supplementary Cementitious Materials (SCMs) in concrete to reduce the carbon dioxide emissions of cement production. Additions of SCMs and different admixtures can also improve the properties of concrete, such as increased strength and durability. However, knowledge of ionising radiation and radon is still limited. How do SCMs and hydrophobic admixtures contribute regarding radon gas exhalation from concrete? Are there any advantages? Disadvantages? Can one make use of specific properties in specific indoor climate environments? What is the effect of moisture?

The main part of the thesis embraces these concerns. Twelve different concrete recipes were cast to investigate the ^{222}Rn radon exhalation rate of these concrete mixtures in relation to their relative humidity (RH). Ten recipes consisted of different mixes of binders and hydrophobic admixtures containing crushed rock with a slightly enhanced ^{226}Ra-activity concentration (Bq/kg), while two other recipes included crushed rock with low levels of radioactivity. As a reference cement, a CEM I, 52.5 R produced by Cementa AB/HeidelbergCement Group (Skövde cement factory) was used. The concretes´ composition had a water binder ratio (w/b) of 0.55.

For radon gas analysis and radon diffusion measurements, a method using the decay rate of alpha energies from ^{222}Rn and ^{218}Po was employed. The amount of decay per unit time was calibrated in relation to a well-defined radon gas level. The readings or output from the radon gas monitor were then displayed as ^{222}Rn content in air in the unit Bq/m^3. Diffusion measurements included an instrument named RAD 7 from Durridge, Inc. The instrument´s measuring technique uses a solid-state detector.

The results imply that SCMs and hydrophobic admixtures (liquid) have a moderate to fairly large impact on the radon exhalation rate, with a humidity of 75 % and 60 %. The largest impact at a relative humidity of 75 % is shown by micro-silica (SF-30), which reduces the radon exhalation rate by up to 57 %. However, at a relative humidity of 45 %, the radon exhalation of the reference concrete is in line with most other concrete mixes regarding their radon exhalation rates.

Also, the natural process of carbonation affects the radon exhalation rate. The study performed as part of the thesis, relating to carbonation and its influence, generated different results depending on the concrete recipe, but can be summarised as follows: (i) concrete with only CEM I or CEM I combined with an hydrophobic admixture indicated a reduced radon exhalation rate; and (ii) for a concrete recipe containing CEM I as a binder combined with slag or fly ash, the radon exhalation rate increased.

Another study, as part of the thesis, embraced induced cracks and their influence on the radon exhalation rate. The study showed that the influence of cracks can be quite large. In two cases an increase of 200-250 % was calculated compared to the radon exhalation rate of the same concrete without cracks. In the other cases, the increase was proportional to the increase of the concrete surface.

In the study, the radon gas exhalation rates from the concrete mixes generally decreased with decreasing relative humidity. The radon gas diffusion, however, increased in general as the relative humidity decreased. Several factors influence the final rate of radon gas being exhaled from a building material. The radon gas exhalation in the examined building materials can also be addressed as the

production rate of radon (exhalation of radon per unit volume) for the investigated concrete mixes. The production rate is mainly governed by the emanation coefficient, the content of radium in the materials and the material´s density (volume and mass) and its diffusion coefficient. Since the investigated concrete mixes have a similar density and radium content, these variables are of less importance when assessing the differences between the concrete mixes' exhalation rates. Consequently, the influence of the radon emanation becomes one major parameter when comparing the different concrete mixes. The radon emanation has in the ongoing assessments been demonstrated to show substantial variation due to the influence of the relative humidity. Initially, in a water filled system (100 % RH), the water acts as a barrier, and radon gas are accumulated in the pores (e.g., the recoil theorem). When the moisture level decreases, the initially high radon gas levels in the pore system are enabled to diffuse into the free air. The initially high concentration of water molecules also acts as a carrier for some of the radon atoms. This entails, that when the relative humidity decreases in the concrete mixes, the portion of radon atoms reaching the concrete surface is also diminished, which consequently reduces the radon exhalation rate. In other words, the most important factor for differences in the radon exhalation rate can be dedicated to its radon emanation, which refers to the number of radon atoms being released from the material itself into the free air. Hence, the tightness of the concrete, or its permeability, is also very important. This is in part reflected in the diffusion coefficient or radon diffusion length being assessed for the different concrete samples.

The fact that the radon gas diffusion increases with a lower relative humidity in the concrete is reasonable since the diffusion rate in water is markedly lower than in air. The diffusion rates in the investigated concrete samples have a subordinate role, however, when one evaluates the final exhalation rate. The high radon exhalation rate in this study is foremost due to (i) the material´s high radium content and (ii) higher emanation coefficient at higher relative humidities. It is of importance to note that the materials´ slightly elevated radium content has a large influence on the high radon exhalation. Comparing concrete recipe C (only OPC as binder) with a recipe replaced with a low radioactive content aggregate (i.e., a low amount of radium), the production rate is very limited, which means a low radon exhalation rate, even though a moderate emanation coefficient can be shown.

Conclusively, this implies that the relation between the relative humidity (RH), radon concentration and diffusion within a concrete wall, ceiling or floor is a complicated interaction. In practice, the influence of relative humidity is the dominant factor for the final radon exhalation rate from a building material. Consequently, the radon exhalation rate, in general, decreases over time as the concrete dries out and the relative humidity decreases.

Some essential conclusions derived from the thesis are that SCMs and hydrophobic admixtures can effectively reduce the radon gas exhalation rate, specifically at higher relative humidity levels; cracks in concrete may generate substantial radon concentration increases; and, depending on the choice of binders, the carbonation of concrete may have a positive or negative effect on the radon exhalation rate.

Sammanfattning

Flera krav och rekommendationer avseende joniserande strålning i byggprodukter har introducerats under de senaste åren. Även branschanslutna ballast- och betongföretag har en strävan att uppnå miljömål som skall efterlevas avseende byggmaterial. I Sverige har det utvecklats ett certifieringssystem för en hög nivå av miljösäkerhet vilket har designats av Green Council Building (Miljöbyggnad 3.0). Certifieringssystemet används i upphandlingar för huskonstruktioner för att uppnå en hög standard och trygg inomhusmiljö i nya byggnader för boende. Ett av dessa miljömål är acceptabla krav på radon i inomhusmiljö.

Under de senaste årtiondena har det också blivit vanligare att betongbranschen använder olika kombinationer av alternativa bindemedel i betong för att reducera koldioxidutsläppen från cementtillverkningen. Tillsatser av alternativa bindemedel och olika tillsatsmedel kan även förbättra betongens egenskaper som ökad hållfasthet och beständighet. Men kunskapen utifrån joniserande strålning och radon är fortfarande begränsad. Vad medför alternativa bindemedel och hydrofoba tillsatsmedel avseende radonavgång från betong? Finns det fördelar? Nackdelar? Kan man nyttja vissa egenskaper i specifika inomhusmiljöer? Hur påverkar fukt?

Huvuddelen av avhandlingen har omfattat dessa frågeställningar. Tolv olika betongrecept göts där avgången av ^{222}Rn från dessa betongblandningar i relation till deras relativa fuktighet (RF) undersöktes. Tio recept utgjordes av olika blandningar av bindemedel och tillsatsmedel, med en bergart med något förhöjd nivå av ^{226}Ra-aktivitetskoncentration (Bq/kg). Två recept innehöll en lågstrålande bergart. Som referenscement och bindemedel användes ett CEM I, 52.5 R (Skövde cementfabrik). Betongernas sammansättning hade ett vattencementtal (vct) av 0,55.

För radongasutvärdering och radondiffusionsmätningar användes en metod där alfa-sönderfall från ^{222}Rn och ^{218}Po utnyttjas (joniserande pulsationskammare). Mängden av sönderfall per tidsenhet är kalibrerad mot en väldefinierad radongashalt. Mätvärdena, eller resultaten från analysen av instrumentet, visas som halten av ^{222}Rn i luft i enheten Bq/m^3. Vid diffusionsmätningar användes ett instrument benämnt RAD 7 från Durridge Inc. Instrumentet är av typen halvledardetektor.

Resultaten indikerar att alternativa tillsatsmaterial och hydrofoberande tillsatsmedel har en moderat till stor påverkan på radonavgången vid en relativ fuktighet mellan 75 % och 60 %. Den största påverkan vid en relativ fuktighet på 75 % kan påvisas med mikro-silika (SF-30), som reducerar radonavgången med upp till 57 %. Vid en relativ fuktighet av 45 %, är radonavgången för referensbetongen i linje med en del andra betongsammansättningar och deras radonavgång.

Även betongens naturliga karbonatisering påverkar radonavgången. Den inom avhandlingen utförda studien av karbonatiseringens inverkan gav olika resultat beroende av betongrecept, men kan sammanfattas som: (1) betong med enkom CEM I eller CEM I som bindemedel tillsammans med hydrofoberande tillsatsmedel indikerade en sjunkande radonavgång medan för (2) ett betongrecept som innehöll CEM I bindemedel tillsammans med slagg eller flygaska, så ökade radonavgången.

En annan studie i avhandlingen omfattade inducerade sprickor och deras betydelse med avseende på radonavgången. Studien visade att påverkan av sprickor kan vara mycket stor. I två fall beräknades en ökning av radonavgången med 200–250 % jämfört med radonavgången i motsvarande betong utan sprickor. I övriga fall var ökningen proportionell mot ökningen av ytan.

Radonavgången minskade generellt med minskad relativ fuktighet för de undersökta betongsammansättningarna. Radongasdiffusionen i betongproverna ökade däremot generellt med minskad relativ fuktighet. Flera faktorer spelar in i den slutliga halten av radon som avges från ett byggmaterial. Radonavgången i undersökta byggmaterial, kan också benämnas produktionshastigheten (radonavgång per volymenhet) för undersökta betongprover. Produktionshastigheten bestäms av främst emanationskofficienten, materialens radium-innehåll och materialens densitet (volym och

massa) och diffusionskofficienten. Då de undersökta betongproverna har en ungefär likvärdig densitet och radium-innehåll blir dessa variabler av mindre betydelse för att undersöka skillnader mellan betongprovernas radonhaltsavgång. Härav blir i stället inflytandet av radonemanationen stor vid en jämförelse mellan de olika undersökta betongproverna. Radonemanationen har i utförda försök visat sig variera mycket beroende av den relativa fukthalten. Initialt i ett vattenfyllt system (100 % RF) utgör vattnet en barriär och radon ackumuleras i porerna (s.k. rekyl-tesen). När fuktnivån minskar, så tillåts de initiala höga radonnivåerna i porsystemet att diffundera till den fria luften. De initialt höga koncentrationerna av vattenmolekyler agerar också som bärare för en del radonatomer. Detta medför att när den relativa fuktigheten successivt minskar i betongproverna, minskar också andelen radonatomer, som når ytan av betongen, vilket till följd medför en lägre radonavgång. Mao, den mest betydande faktorn för skillnader i radonavgången från ett byggmaterial, kan beskrivas som dess radonemanation, dvs antalet radonatomer som avgår från ett material till den fria luften. Mao, blir betongens täthet, eller dess permeabilitet också väsentlig. Detta återspeglas delvis via diffusionskofficienten eller radonlängden som uppmättes för de olika betongproverna.

Att radongasdiffusionenen ökar med mindre relativ fukt i betongen är rimligt då diffusionshastigheten i vatten är betydligt långsammare än i luft. Diffusionshastigheten i de undersökta betongproverna har dock en underordnad roll när man utvärderar den totala radonavgången. Den höga radonavgången beror i denna studie främst av (i) materialets höga radiuminnehåll och (ii) en högre emanationsfaktor vid högre relativ fuktighet. Det är dock viktigt att poängtera att materialets något förhöjda radium-innehåll är av stor betydelse för den höga radonavgången. Vid en jämförelse med betongrecept, C (bara OPC som bindemedel), där betongens ballast ersattes med en lågstrålande ballast (låg halt av radium), blir produktionshastigheten mycket låg, dvs låg radonavgång, trots en moderat emanationskofficient.

Detta innebär sammantaget att sambandet mellan betongens RF, radonavgången och diffusion i en betongvägg, tak eller golv är ett komplicerat samspel. I praktiken dominerar ändå inverkan av den relativa fukthalten i betong mest för den slutliga radonavgången från ett byggmaterial. Således minskar radonhalten generellt över tid i takt med att betongen torkar ut och RF sjunker.

Några väsentliga slutsatser från avhandlingen som kan härledas är att alternativa bindemedel och hydrofoba tillsatsmedel effektivt kan minska radonavgången och härav produktionshastigheten vid högre luftfuktigheter samt att sprickor kan ge betydande ökningar av radongashalten. Beroende av valet av bindemedel kan betongens karbonatisering antingen ge en både positiv eller en negativ effekt med hänsyn till radonavgången.

List of publications

The following papers are included in the thesis

I. M. Döse, J. Silfwerbrand, C. Jelinek, J. Trägårdh & M. Isaksson: "Naturally occurring radioactivity in some Swedish concretes and its constituents – Assessment by use of I-index and dose-model". Journal of Environmental Radioactivity, 2016, Vol. 155-156, pp. 105-111.

II. M. Döse, J. Silfwerbrand: "Reduction of Radon Gas in Concrete Using Admixtures and Additives". Nordic Concrete Research, No 58, 2018, pp. 17-34.

III. M. Döse, J. Silfwerbrand: "Supplementary Cementious Materials and Additives – Effective Measures to Hinder Radon in Concrete". Journal of Advanced Engineering, Vol. 2, No. 1, 2018, pp. 1-8.

IV. M. Döse, J. Silfwerbrand: "Effect on Radon Exhalation Rate Due to Cracks in Concrete". Nordic Concrete Research, No. 61, 2019, pp. 79-90.

V. M. Döse, J. Silfwerbrand: "Effect of Carbonation on Radon Exhalation Rate in Concrete". American Concrete Institute, Materials Journal, Vol. 119, No 3, 2022, pp. 67-78.

The planning, writing and analysis were primarily performed by the main author. The co-authors have guided the work and contributed to all papers with fruitful comments, suggestions and amendments. The author has performed most of the analysis and preparations of the tests as well as the measurements, which includes carbonation testing, crack analysis, porosity, water absorption and radon gas exhalation, as well as diffusion measurements and the calculations thereof. Compressive tests and some carbonation testing using phenolphthalein were performed by Jesper Olsson or Lukas Andersson under the supervision of the author. The gamma-energy analysis of the natural radionuclides of each constituent as well as the analysis of the final concrete recipes were performed by the accredited gamma spectrometry laboratory at the Finnish Radiation and Safety Authority (STUK), Helsinki, Finland. The analysis of Mercury Intrusion Porosimetry was performed at the Federal Institute for Materials Research and Testing (BAM) in Berlin, Germany.

Notations

Terminology	Explanation
Activity, *A*	Decay per unit time (Bq).
Activity concentration, *C*	Decay per unit time and volume (Bq/m^3).
Activity concentration, *Cm*	Decay per unit time and mass (Bq/kg).
Activity Median Aerodynamic Diameter (AMAD)	The median particle size of the activity distribution of aerosols (d_{ae}) such that 50% of the activity in the aerosol is associated with particles of an aerodynamic diameter greater than the AMAD.
Addition	Inorganic constituent used in part as a replacement for the cementitious binder to improve certain properties or achieve special properties, cf. SCM.
Admixture	Material that is added during the concrete mixing process to provide the concrete with specific desired properties.
Aeorosol	Liquid/solid particles in a gaseous medium. Normal ranges, 0.5 nm to 10 µm.
Attached fraction, unattached fraction	Fraction of short-lived radon progeny that is attached to the ambient aerosol particles. Its counterpart is an unattached fraction moving freely in the air.
Decay (alpha decay)	Type of radioactive disintegration in which some unstable atomic nuclei dissipate excess energy by spontaneously ejecting an alpha particle.
Decay constant λ	Coefficient inversely proportional to the half-life time $T_{1/2}$, $\lambda = \ln 2 / T_{1/2}$
Diffusion	Movement of substances from one region of higher to one of lower concentration.
Diffusion cofficient *D*	Ability of radon or other elements to be transferred by diffusion through a medium (m^2/s).
Diffusion length, radon *L*	Characteristic distance travelled by the radon atoms during one half-life (3.8 days for ^{222}radon).
Dose	Energy absorbed by the human body. Several distinctions, absorbed dose, ambient dose, equivalent dose, effective dose and collective dose, exist.

Emanation	Radon atoms produced by radium decay that escape from the building material's solid phases into the pores of that material.
Emanation cofficient, ϵ	Portion (percentage) of radon atoms produced by radium decay that escapes into the pores in relation to the total amount of radon atoms within that material. Dimensionless (%).
Emission	Generation of gamma energy (photons) or radon (particles) due to the natural decay of radionuclides or their progenies.
Emitters	Atoms in the radionuclide's chains generating either alpha, beta and gamma rays or combinations thereof.
Equilibrium factor, F	State of equilibrium between the radon progeny and the radon gas in the air. Used in calculations of effective dose.
Equilibrium (secular equilibrium)	Condition where the mother nucleus has the same activity (Bq) as its progeny.
Exhalation, *E*	Areal release rate of radon gas from a surface (Bq/m^2)/h.
Exhalation, mass, *Em*	Release rate of radon gas per unit mass (Bq/kg)/h.
Half-life, $T_{1/2}$	The time (h) for the activity of radionuclide to be reduced to half its initial activity.
Hydration	Formation of complex bindings generating strength increase due to calcium-silicate hydrate formation when water and constituents of clinkers such as C_3S, C_2S, C_3A, C_4AF or $Ca(OH)_2$ are combined.
Hydrophobic admixture	Liquid admixtures used to reduce the speed of transfer of water molecules through the gel and capillary pore system
I-index, *I*	Activity concentration Index. Used for assessment of building materials. Conservative estimate of the maximum "effective dose" under circumstances, where a given "point-dose" is calculated within a room (Markkanen, 1995). Specific conditions presented in RP 112, EC (1999).
Potential Alpha Energy (PAE)	Sum of energies emitted during decay of this atom to its progenies. For radon gas, PAE is 19.2 MeV.
Porosity, *p*	The ratio, usually expressed as a percentage (%), of the volume of voids in a material to the total volume of the material including the voids.
Production, *P*	Total production of radon gas ((Bq/m^3)/h). A function of radium activity, emanation, mass density and the radon decay constant.

Progeny	Decay products of a specified decay chain.
Radon	The element ^{222}Rn, being a noble gas.
Radon flux, *J*	Concentration of radon that traverses in one direction (one dimensional) per unit time ($Bq/m^2/h$).
Recoil	Energy release causing a rebound deflection of the newly formed atoms in a liberation process of decay such as a mother nuclide transferring to its progeny, e.g., ^{226}Ra decay to ^{222}Rn and a 4He (α-particle).
Release rate	Release rate or radon gas release rate (Bq/s) is a function of diffusion, emanation, radium activity concentration and porosity of the material. Can also be defined as areal release rate (exhalation rate).
Relative humidity, *RH*	Amount of vapour (%) with regard to the maximum water vapour content, which can be upheld in the material´s pore system.
SCM	Supplementary Cementitious Material also named alternative binders. Includes fly ash, slag and silica fume.
Thin section	Thin sheet of concrete (25µm) placed on a glass for examination by polarising microscope.
Transport	Movement of particles (aerosols), liquids or gas in a material. Transport mechanism can be diffusion driven, ion migration, or advective flow. In this context it is mainly related to diffusion driven transport.

Table of Contents

1 Introduction

1.1 The issue with radon and gamma emitters

The second largest cause of lung cancer, in the world after smoking, is related to radon (^{222}Rn) and its progenies in our environment (WHO, 2009). Among the first studies aimed at radon were those performed by Hultqvist (1956), but these initially drew only minor attention. From the 1970s onwards an increasing number of elevated radon level measurements were made in dwellings in some countries (ICRP, 2014), and radon was formally identified as a cause of lung cancer in 1986 (WHO, 1986).

Building materials, such as concrete, contribute to the release of radon gas through the natural decay of ^{238}U (uranium-238). ^{238}U is a natural radioactive element with a very small abundance (part per million, ppm) in most silicate and calcareous rocks, soils and water in our environment. The abundance of ^{238}U activity in the earth´s crust is 12-37 Bq/kg or expressed as ppm, 1-3 (Isaksson & Rääf, 2017). Concerning gamma emitters, those naturally occurring radionuclides of interest are represented by ^{40}K, ^{226}Ra (^{238}U) and ^{232}Th and their progenies (daughter isotopes). ^{40}K constitutes 0.012 % of all natural potassium within bedrock and occurs in rock-forming minerals such as potassium feldspar (10-14 % K) and micas (9-10 % K) (Jelinek & Eliasson, 2015). Uranium and thorium, on the other hand, occur only as trace elements in rocks, mostly in accessory minerals, e.g., uraninite, allanite, apatite, titanite and xenotime (Jelinek & Eliasson, 2015).

Many national radiation authorities or municipalities have as of today performed and documented the effects of elevated radon gas levels in indoor environments (Mustonen, 1984, Valmari et al., 2012, Catelinois et al., 2006, Tse et al., 2011, Tomásek et al., 2008, Kropat et al., 2014). A large-scale study by Darby et al. (2005, 2006) incorporating 13 nations in Europe (with a minimum of 20,000 people in the study) revealed an increased risk of lung cancer due to enhanced levels of radon gas but with large uncertainties. In most studies on the elevated risks that radon gas poses to habitants in households a close relation is also drawn to the high content of aerosols derived from cooking or inhaling cigarette smoke (Scofield, 1988, Porstendörfer, 1994, Darby et al., 2005, Isaksson, 2011). Most case studies show that an increased risk of lung cancer caused by radon gas varies in the span of 5-15 % (Porstendörfer, 1994, Catelinois et al., 2006, Isaksson, 2011).

In recent years some thorough work by the national authorities of most member states within Europe, in collaboration with the European Commission (EC), has laid the basis of an outlook concerning the European situation with respect to radon gas concentrations in households. A compilation of the current situation in the basements of households (ground floor) in each country within the EC was calculated from national documentation and then mapped, creating an European indoor radon map (Figure 1.1).

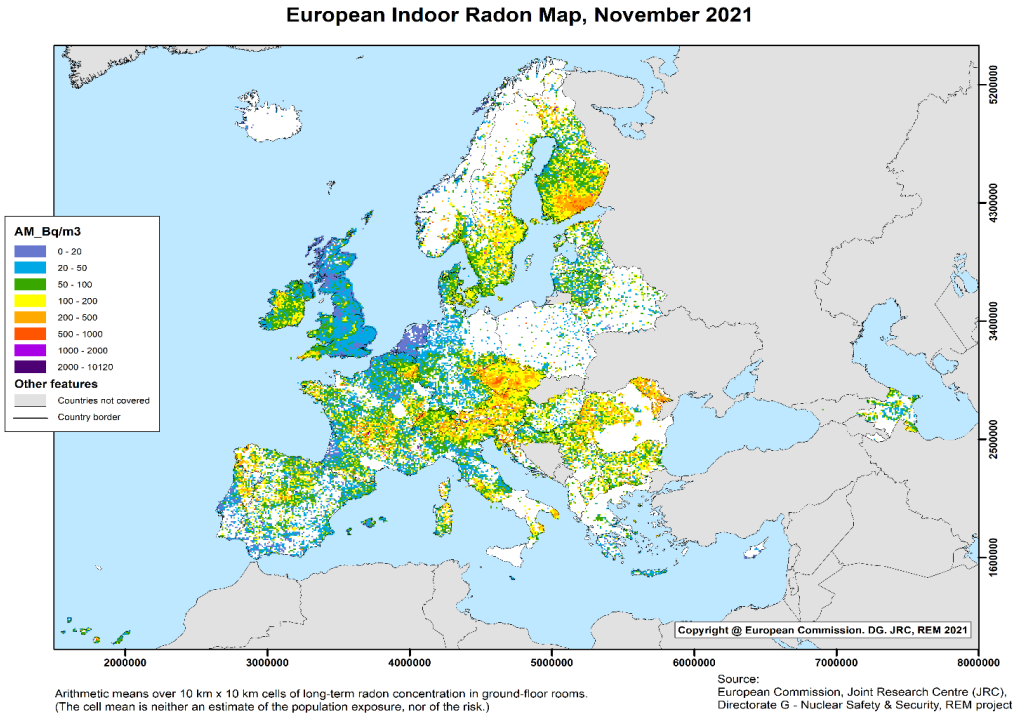

Figure 1.1 European Indoor Map presenting radon concentrations in Bq/m^3 with a colour legend to the left in the figure (EC, 2021, Hoffmann et al., 2017). The radon concentrations (Bq/m^3) in the map are presented as an arithmetic mean (AM) in ground floor rooms.

As can be seen in Figure 1.1, the Nordic countries in most cases have arithmetic means below 200 Bq/m^3. Noticeably, some areas of Finland show elevated radon levels of up 500 Bq/m^3 (orange colour, Figure. 1.1) or even 1000 Bq/m^3 (red colour). Acceptable indoor levels in European countries today are at a threshold level of 300 Bq/m^3 (EC, 2014). However, within Sweden a stricter threshold level of 200 Bq/m^3 has been set (National Board of Housing, Building and Planning, 2011 with updates).

Swedish bedrock, from a radon point of view, concerns mostly granitoids and sediments such as black shales (alunskiffer) that are enriched in uranium. Shales occurs in different parts of Sweden, but are geographically mostly found in the Västergötland, Skåne, Öland, Gotland, Närke and Jämtland regions. Shale was earlier used as part of aeriated concrete, while in granitoids, which originate from melted or partially melted magma, an enrichment of radioactive elements is common (Jelinek & Eliasson, 2015). For example, K-feldspar, which constitutes part of micas, is often enriched in a late stage crystallisation of a magma. Generally, accessory minerals, such as monazite, zircon, apatite or allanite, contain the radioactive isotopes uranium and thorium, which also accompany the late-stage crystallisation phases (Klein & Hurlbut, 1993). The relation between the mineral composition in Swedish bedrock and the minerals that contain natural radioactive elements is well described and summarised by Jelinek & Eliasson (2015). An overview of Swedish bedrock and its gamma radiation levels, as well as its contribution to the release of radon gas, can also be found in Möre (1985), Petterson et al. (1982), Mjönes et al. (1984) and Åkerblom & Clavensjö (2004, 2007). Risks regarding inhalation of radon gas and its progenies is well described by Schofield (1988), Isaksson (2011) and Isaksson & Rääf (2017).

For the Swedish production of concrete, the corner stone was earlier natural aggregates (glaciofluvial sediment) but is more commonly today crushed bedrock (aggregates) in combination with cement and

water. All three constituents, which are the basis for concrete, can accordingly contain substantial amounts of the radioactive isotopes ^{40}K, ^{232}Th and ^{238}U.

It should be addressed that a human being liberates gamma radiation merely through the intake of different foods and beverages. As an example, a person with a weight of ca 70 kg generates approximately 4200 Bq (Isaksson & Rääf, 2017), which corresponds to approximately 60 Bq/kg. In a rough estimate typical granite or crushed granite as an aggregate generates approximately 1000 Bq/kg of ^{40}K, which hints at the difference in activity concentration.

1.2 Radon in buildings – relative humidity and moisture influence

In Sweden, several studies were conducted in the 1980s to investigate the current situation concerning radon and its progenies in different households (Mjönes et al. 1984). Simultaneously, several investigations of the gamma energies from the Swedish bedrock were conducted. Moreover, a large study, including measurements of each radionuclide (^{40}K, ^{226}Ra and ^{232}Th) for different rocks and glaciofluvial sediments (gravel) used by the industry, was conducted by Möre (1985). These data can still be used to calculate the potential risks associated with using different building materials.

Concerning radon in households and dwellings, and with regard to the mentioned studies, a compilation report was presented by Andersson et al. (2007). The general mean of the radon concentration (Bq/m^3) within an average household (including, apartments, semi-detached houses, houses) in Sweden was at the time ca 108 Bq/m^3. Higher radon concentrations were in general documented in relation to houses or dwellings made up of concrete or bricks compared to dwellings constructed with other building materials such as wood.

There are few studies on the radon exhalation rate and effects of moisture in the indoor climate of dwellings. Some experiments are presented and compiled by Porstendörfer (1994) regarding radon attachment and aerosols (particles). Yu et al. (1999) conducted studies concerning the deposition of aerosols (particles) regarding the relative humidity in buildings in Hong Kong. At least 32 different sites (building places) showed that high moisture conditions in buildings (>79 % RH) gave concentrations of ^{222}Rn and ^{220}Rn, which were lower in the buildings compared to a lower relative humidity (<79 %). The summary concluded that a higher water content in the air will also enhance the deposition of aerosols onto the building walls, thus decreasing the aerosol content (including ^{222}Rn) in the air. In a second study by Yu et al. (2000) including 65 office buildings a similar result was obtained. Highlighting the influence of humidity regarding radon gas and aerosols, an interesting result was documented when using dehumidifiers in Taiwan (Chen et al., 1998). A strong negative shift in the potential alpha energy (PAE) of radon gas in the air occurred when dehumidifiers were installed and started to be used in the hospitals (ICRP, 2012). This indicates that a considerable amount of radon is attached to aerosols such as vapours and water molecules in the air, while at lower relative humidity levels the aerosol content as well as ^{222}Rn concentrations are greatly reduced.

Regarding the relative humidity in Sweden some data were presented by Nevander and Elmarsson (2006). They used meteorological data compilations of the annual variations for some major cities in Sweden. For three locations spanning from south to north (Malmö, Västerås, Kiruna) the relative humidity varies between ca 60 and 90 %. The span is much less in the south, due to less variations in temperature. For indoor climate conditions considerations needs to be taken to temperature and the vapour content contribution by external factors (washing, cooking, exhalation of vapour from humans). Given a mean value of external contributions of moisture (V_{FT}-2,9 g/m^3) to the indoor climate the relative humidity varies between 30 and 80 % RF considering the same locations as previously mentioned (Nevander & Elmarsson, 2006).

A doctoral thesis by Bagge (2011) presented measurements of the relative humidity regarding indoor and outdoor climate conditions at four different locations in Sweden. Thorough data for a full year were measured and presented from two of these regions (Karlstad and Malmö). In Karlstad five

buildings with ~150 apartments were included, and in Malmö this consisted of five buildings with ca 80 apartments. The relative humidity, indoors, varied roughly between 30 and 50 % during the year, where the period between May and October normally had a relative humidity above 40 %. The results from each site (Karlstad and Malmö) were very similar. The limitation of the study may be the placement of the equipment, which was situated in conjunction to the exhaust ventilation system. But, the results are similar as results obtained by Tolstoy (1993). Tolstoy (1993) reported a slightly larger span from ca 25 to 60 % in RH for small houses.

A study by Fridh and Lagerblad (2013), concerning the relative humidity of concrete exposed to carbonation in households indicates a relative humidity of around 50 % at the top surface (0-20 mm) of an inner wall, while concrete floors had a slightly higher relative humidity at the surface (0-20 mm) of ~55 % in RH.

1.3 Emissions, emanation, emanation coefficient and exhalation

Emissions, as a term in this dissertation, include both gamma ray ionising radiation (electromagnetic and photons) as well as particle ionising radiation, i.e., radon gas. The radon exhalation rate ((Bq/m^2)/h) is in the dissertation discussed in the context of radon gas being measured in a defined volume of air that stems from the exhalation of radon gas through a defined concrete surface area. The exhalation rate can also be defined related to a unit mass of the investigated material ((Bq/kg)/h).

Emanation is a term for radon atoms, produced by radium decay, that escape from the building material's solid phases into the pores of that material (in our case, the concrete). The emanation coefficient is the portion (percentage) of radon atoms produced by radium decay that escapes to the pores in relation to the total amount of radon atoms within that material. The emanation coefficient has among previous authors been given different names. de Jong P & van Dijk W (1996) called it emanation power, while other commonly used terms are release ratio or emanating fraction (Kovler, 2012). The emanation coefficient indicates the ability of a building material to release radon gas from its internal solid phases (aggregates, cement) for further transport into the free air. As an example, an aerated concrete will have a much larger emanation coefficient than dense concrete.

The emanation coefficient, as will be shown, is influenced by the relative humidity (moisture content), a material's porosity and interconnectivity between the pores (Figure 1.2). Pores in this context are gel, capillary pores and air voids. A concrete's emanation coefficient (%) can be deduced from its ^{226}Ra concentration (Bq/kg) in a specimen, mass and the radon gas ^{222}Rn concentration in equilibrium (Bq/m^3) in a predefined volume of air.

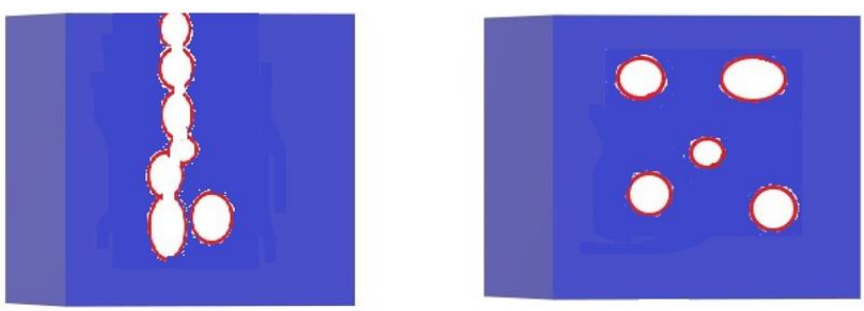

Figure 1.2. Identical concrete mixtures where red circles exemplify differences in the distribution of pores resulting in different transport properties.

In this research, we are interested in different concrete mixtures as radium and radon sources and their contributions of radon gas to the ambient air (Sections 4.14-4.15). However, in the case of diffusion measurements, the radon flux or flow density at different relative humidity levels is of interest. In the case of radon diffusion measurement, there is a problem since the radon flux or flow density of radon gas through a concrete material is disturbed by the concrete itself as a radon source. There is, however, a possible solution to this problem. To overcome this "disturbance", we can measure the diffusion by placing a strong radium source on one side of the concrete, which yields a marked radon concentration build-up on the other side of the concrete (Section 4.16). The contribution from the concrete itself (as a radon source) to the radon concentration build-up will thus be comparatively small.

This Thesis´s experimental programme of concrete mixtures covers different amounts of SCMs including three mixtures with admixtures (hydrophobic agents). This approach was selected to consider the variation in moisture content indoors (Section 1.2). In Sweden, the indoor relative humidity varies roughly between 40 and 80% during the year (Nevander & Elmarsson, 2006). Since moisture in materials such as concrete (Cozmuta et al., 2003, van der Graaf and Meijer, 2005, Fournier et al., 2005) has a significant effect on both the diffusion rate and the emanation coefficient (Cozmuta et al., 2003), its final influence on the exhalation rate was considered of great interest. Hydrophobic admixtures, with a known repellent effect (or mitigation) on the free transport of water molecules, should thus affect the diffusion rate of the concrete. This motivates why three of the concrete mixtures in the experimental programme contained a hydrophobic agent.

1.4 Principle of experiments regarding exhalation and diffusion coefficients

All experimental data regarding radon exhalation measurements have their origin in the radon gas concentration (Bq/m^3) build up within a fixed volume of air. The nature of radon as a noble gas is discussed in Chapter 2, and the mathematical modelling for the different set-ups in these experiments is described in Chapter 3. Nonetheless, all experiments apply the initial condition of proportionality between the radon gas concentration increase (Bq/m^3) and time. Applying the principle of proportionality, a constant defined as the exhalation rate ($(Bq/(m^2/h)$) can be used to further assess the radon gas concentrations within an air volume such as a room. The constant itself can be used relatively simply, comparing the radon exhalation rates of the different examined concrete specimens.

In the case of measuring the radon gas concentration build-up from a concrete specimen, this is conducted by inserting it into a closed container and thereafter sealing the container. Thus, a closed system of air is monitored since the measurement device is connected by hoses to the container. A small air flow is monitored by an electric pump in the measurement device (2 liter/min) as to ensure a continuous air stream through the container and the measurement device.

Diffusion at different relative humidity levels (75%, 60% and 45%) were examined for each concrete recipe. The calculated diffusion coefficients of each concrete recipe should be regarded relatively and not as absolute values. This is due to (i) the initial radon source concentration in the primary chamber causing a gradient that will be different depending on the final steady state concentration of radon gas and (ii) the chosen thickness of the concrete samples (Kovler, 2012). In the case of diffusion measurements, a concrete slab thickness of 50 mm for each investigated concrete mixture was placed between two hollow iron airtight chambers (Section 4.16). The concrete slab was secured in place by nuts and bolts, and a thick aluminium tape was used for sealing to assure no leakage. One of the hollow iron chambers (primary source) contained a radium rich source that was placed inside the chamber prior to locking the concrete slab in place. Thus, as soon the system was closed, the radon concentration in the primary chamber built up. The radon concentration in the primary chamber was continuously measured by an electronic device (RAD 7). Prior to the measurements of the radon concentration in the secondary chamber, secular equilibrium (radon concentration was constant, "steady state") was attained in the primary chamber. At the onset of these "diffusion measurements", the secondary chamber (one of the two chambers) was gently flushed with air to achieve a "zero

value" of the radon gas concentration (Bq/m^3). Immediately after flushing, two hoses were connected to the secondary chamber, which was in turn connected to the measurement device. Consequently, a fixed volume of air was circulated during the radon concentration build-up in the secondary chamber. The measurement procedure of the radon concentration (Bq/m^3) build-up in the secondary chamber for the radon diffusion measurements was as such identical to the measurement procedure conducted for radon exhalation measurements of concrete prisms enclosed within a container.

Knowing the radon concentration (Bq/m^3) in the primary source chamber at the "steady state" as well as the rate of the radon concentration build-up in the secondary chamber, one may calculate the diffusion of radon gas (radon flux) through the concrete slab.

1.5 Aim of the Thesis

The aim of the thesis is primarily to obtain increased knowledge about the behaviour of the noble gas radon under different conditions in concrete. A central role is the relative humidity (moisture content) of concrete and how this effects the radon release rate of the concrete.

Part of the thesis also aims to investigate the release mechanisms of radon gas under different relative humidity levels. In the thesis, three levels have been chosen: RH 75 %, RH 60 % and RH 45 %. Influencing factors due to the release mechanism of radon gas is a material's (i) porosity, (ii) pore structure, (iii) emanation (release of radon from its constituents to its pores) and (iv) moisture content. Do these properties/variables interact, or which property dominates the behaviour within concrete regarding the final radon exhalation from the concrete?

Secondly, the thesis entails what role different SCMs and additives play in promoting or mitigating the radon exhalation rate in different concrete mixes. However, it also helps to understand how these SCMs and admixtures (hydrophobic agents) in different proportions influence the radon exhalation rate as well as the diffusion rates in different concrete mixes.

Thirdly, some external effects are considered and evaluated regarding their contribution to the radon gas exhalation. External effects in this context are cracks and carbonation of concrete.

A minor part of the thesis also aims to briefly examine and explain studies relating to gamma radiation. This is due to the natural linkage of ^{226}Ra (radium) as the mother nuclide to ^{222}Rn (daughter). ^{226}Ra is also used as part of the activity concentration index (I-index), used in regulatory work and regulations. The activity concentration (Bq/kg) of ^{226}Ra is generally also used as a guideline in different practices and regulatory documents to estimate what activity concentrations (Bq/m^3) of ^{222}Rn could be expected from different rock materials or aggregates. Consequently, a minor part of the thesis also aims to explain and clarify some relations of gamma radiation, threshold values and the consequences of an effective dose to humans.

Finally, the thesis intends to serve as a tool for the concrete industry or individuals in regulatory positions influencing requirements of housing and buildings. The thesis hopefully contributes to an increased knowledge of what effects could be anticipated using different concretes and binders and serve as an assessment of when and under what circumstances some SCMs or admixtures can be used to fulfil the necessary regulatory requirements. In the end, increased safety for the citizens living in houses and apartments is the ultimate goal. If the thesis can contribute to better concrete products that reduce the radon gas exhalation rates, then the thesis has fulfilled its purpose. Optimisation according to one of the guiding lines of the International Commission of Radiological Protection (ICRP, 2006, 2007) is subsequently achieved.

1.6 Research questions

RQ 1. Regarding the relative humidity and exhalation of radon, how much does the relative humidity contribute to a change in the radon exhalation rate?

The research question aims to clarify which variations could be expected between a relative humidity in the range of 75 to 45 %. These conditions in relative humidity reflect the seasonal variations within an apartment building.

RQ 2. Will use of Supplementary Cementitious Materials (SCMs) aid in reducing the carbon dioxide imprint as well as reducing the radon exhalation rate?

This research question highlights the question of reducing the carbon dioxide output produced by the cement clinker production. A substitute by an alternative binder may in fact serve both aims: reduce the radon exhalation rate and use less Ordinary Portland Cement in the recipe.

RQ 3. How do hydrophobic admixtures affect the radon exhalation rate?

The research question highlights an optional way to reduce the radon gas release rate, without any other means.

RQ 4. How does porosity influence the radon exhalation rate?

The question is fundamental to understanding the mechanisms of the radon rate release due to the formation of the capillary pore system and the gel pores within the concrete in combination with air voids. The distributions of capillary pores and gel pores, and their proportions in the cement paste, may serve a vital role.

RQ 5. How do cracks in the concrete affect the radon exhalation rate?

The research focuses on the effect of induced cracks into concrete specimens. The study aims on answering whether theoretical calculations are in line with measured data.

RQ 6. Does the carbonation of concrete have an influence on the radon exhalation rate?

The carbonation of concrete was initially not considered as imposing a change in the radon exhalation rate. But what role does it play? A study was executed to investigate its influence on the radon exhalation rate in concrete with different binder systems.

1.7 Limitations

The experiments in the main study are limited to one defined water cement ratio (w/c = 0.55) in order to compare different binder systems (SCMs) as well as hydrophobic admixtures (hydrophobic admixtures) with a rapid hardening reference Portland cement concrete. It is well established that the water cement ratio in a concrete affects the radon exhalation rate (De Jong P & van Dijk W, 1996), but on the other hand, w/c = 0,55 for concrete represents concrete for modern buildings well.

A limiting factor is, apart for SCMs, that only hydrophobic admixtures are assessed. There are numerous admixtures (hydrophilic and hydrophobic), which may inflict problems on the concrete's matrix structure, porosity and final diffusion rate or radon gas exhalation; nevertheless, in this study only admixtures with hydrophobic properties were assessed. The reason for selecting hydrophobic admixtures was that humidity has a major influence on radiation.

In part, there are, of course, limitations when just assessing the concrete recipes using one type of aggregate as a reference aggregate. Nevertheless, the thesis's focus was primarily to gain a deeper

understanding of the different binder combinations and how these could affect the radon gas exhalation rate.

Also, the results rely in part on the equipment used within the project, ATMOS 33 delivered by Gammadata AB and RAD 7 delivered by Durridge, Inc. These are indirect methods (ionisiation chambers) and do not directly measure the exact content of radon gas. Other methods measuring the flow of radon should, of course, be beneficial to the project to limit any uncertainties of measurement techniques. These methods would, however, need major investments, for which the budget of the project was inadequate.

Measurements of the relative humidity were performed using equipment from Vaisala Oy. The different techniques used for measurements would indeed need a deeper technical review, but the mere time frame made this impossible. A brief explanation is found in Chapter 4, Section 4.8.1. The yearly calibrations of the equipment in part serves as a guidance for the reliability to give trustworthy results.

1.8 Outline of the Thesis

The content of the thesis embraces some aspects of the radioactivity of natural isotopes, which is of current interest. As such, a minor part also includes the influence of gamma radiation on habitants. The desire to enhance conditions for habitants in housing is a key issue and constitutes the core of the thesis, although from a radon gas point of view.

A major part of the thesis focuses on areas that may inflict on the radon gas release mechanisms and as such are vital tools for a further and deeper understanding of effectively reducing radon gas in concrete buildings.

The thesis entails five papers that, in short, contribute to the understanding of ionising radiation with a focus on radon gas production from the building materials themselves. It also addresses internal processes such as carbonation and its effect on the radon gas release rate, effects of cracks and use of different binder combinations, admixtures, and their impact on the final radon gas exhalation rate. It also embraces mitigation measures and the effect on equivalent doses from building materials due to gamma radiation.

Paper I embraces the concept of ionising radiation with a specific focus on gamma radiation in building materials and its final equivalent/ effective dose. Comparisons are made between measured values of the rock material aggregates used and the final concrete products containing the aggregates.

Paper II addresses the difference in the radon gas exhalation rates of concrete mixes and more clearly the difference between an ordinary recipe compared to a recipe containing SCM (fly ash), and in one case, a hydrophobic admixture. The radon exhalation rates of the concrete recipes are compared, and measures to hinder radon are addressed.

Paper III focuses on the source of radon gas in concrete buildings and how much of the concrete contributes with radon in its exhalation phase. The paper specifically addresses the difference in the diffusion coefficient between different concrete mixes at a fixed relative humidity (75 %). A comparison is made between the different recipes including the effects of different SCMs and hydrophobic admixtures and to what extent this influences the diffusion coefficient. This is also presented as the radon diffusion length (L).

Paper IV investigates the influence of induced cracks in concrete and the difference in the radon gas exhalation rate, both prior to the induced cracks and after. Two different concrete recipes are assessed. One using an ordinary rapid Portland cement (CEM I 52.5 R) and one with the same binder but with the addition of a hydrophobic admixture. The initial differences in the exhalation values are addressed as well as the large increase that is introduced by the cracks in the concrete.

Paper V focuses on the issue of the carbonation of different concrete mixtures used in housing structures by applying a w/b ratio of 0.55. An accelerated carbonation test is performed at a fixed relative humidity of 75 %. Four different recipes are assessed, and the depth of carbonation is measured simultaneously as the concrete specimen's radon gas exhalation rate is measured/calculated. The diffusion coefficient is also measured for two of the recipes in order to compare and validate the results of the radon mass transport through the materials compared to their exhalation rates at different stages of carbonation.

The different chapters are briefly summarised below.

- Chapter 1 discusses the outline of the thesis, its content and limitations but also its research contributions.
- In Chapter 2 some fundamentals of ionising radiation are directed, with a special focus on radon gas.
- Chapter 3 addresses the basics in modelling, including some fundamental physical laws and equations used in calculating the exhalation rates, emanation coefficients, diffusion coefficients and radon diffusion lengths of the investigated concrete specimens. It also briefly includes the background of the carbonation of concrete.
- Chapter 4 describes the methodologies used and the setup of different experiments.
- Chapter 5 presents the results of the thesis with occasional short comments on the results.
- Chapter 6 focuses on the analysis and discussion of the results.
- Chapter 7 presents and discusses some uncertainties and errors as part of the results.
- Chapter 8 contains the general conclusions of the thesis and studies performed.
- Chapter 9 addresses recommendations concerning the conducted experiments.
- Chapter 10 addresses some future research within the area.

1.9 Investigated variables in the study

Apart from some theoretical mathematical equations to explain the influence of moisture/water and its effect on the final exhalation rate of radon, there are still other factors or variables that are in part unclear. Fractures in concrete have been addressed by Daud & Renken (1999) and Landman (1982), but the research is often linked to the underlying radioactive soil and its contribution to indoor air. The contribution from the concrete itself, in this aspect, is not often mentioned. Secondly, there has rarely been, if ever, any considerations taken regarding the concrete material as a material in continuous change, apart from the issue of moisture. As such, the process of the carbonation of concrete may also be a variable of consideration for concrete with different binders, which should be taken into account with regard to the radon exhalation rate.

In this study a scheme to evaluate some properties that relate to the radon exhalation rate of the concrete recipes are summarised in Table 1.1. Four different variables are mentioned. A best estimate based on literature (Cozmuta et al. 2003, Fournier et al. 2005, Porstendörfer, 1994) and investigations by Döse (2016) give us, in part, an indication of the influence of the "water content or moisture" in concrete, see Table 1.1.

"Hydration" of the concrete specimens (Table 1.1) has been assumed to have a very low impact on the exhalation rate, due to the fact that all studies/measurements in this study commenced approximately 5-6 months after casting. Generally, rapidly hardening cement and w/c ratio´s around 0.50-0.55 (as in these tests) can be assumed to have a hydration degree of at least 95 % after 5-6 months (Neville & Brooks, 2010, Hewlett & Liska, 2019). The degree of hydration is further addressed in Section 4.1.2. The hydration of the cement paste has inevitably had an impact on the final microstructure of the concrete. Part of the microstructure constitutes the formation of the concrete's pore system (air voids, gel and capillary pores). Due to previous studies (Cozmuta et al., 2003, Mehta & Monteiro, 2006) the C-S-H gel formation of the concrete specimens can be assumed to be fairly limited after this time

interval. Consequently, most hydration products, such as the C-S-H gel formed from C_3S and C_2S and the secondarily formed calciumhydroxid ($Ca(OH)_2$) that reacts with pozzolanic SCMs such as silica and fly ash are assumed to be at their final stage of growth. This is also in line with studies by Zeng et al. (2012), who examines the hydration rate of cement pastes with different amounts of fly ash (20-60% wt.) with a w/b ratio of 0.3 and 0.5. For the cement pastes with a w/b ratio of 0.5, the paste had after 90 days hydrated to at least 90 %. For certainty, a minor "control study" of the effect of hydration at 3 and 6 months was launched and evaluated within this project, including a few of the used cast recipes.

"Cracks" and the effect of "carbonation" are variables that are explicitly investigated as specific studies in the thesis, and wherever the knowledge is limited and scarce, if any information is found in literature.

Table 1.1. Some properties that likely influence the radon exhalation rate at different RH for concrete.

	Influence on radon exhalation		
Variables	**RH 75**	**RH 60**	**RH 45**
Water content, moisture	Rather high	Medium	Rather low
Hydration	Medium to low	Low	Low
Cracks	Possible	Possible	Possible
Carbonation	Possible	Possible	Possible

The effect of these different properties will most likely affect the emanation coefficient, which in turn generates a gross estimate of the final exhalation rate or radon production rate.

1.10 Research contribution

As the concrete industry strives to improve its environmental imprint simultaneous with the stricter imposition of current regulations, it is most adequate to investigate the contributions of different constituents in concrete mixes. The concrete industry has for many years been successful in incorporating waste materials from the coal and metal industry processes. Typical examples are fly ash and slag (blast furnace slag). These bi-products or waste products are often today important parts of blended cements. These "waste materials" and other Supplementary Cementitious Materials (SCMs) have also in the recent decades been shown to improve to a large degree some properties of the concrete mixes (Mehta & Monteiro, 2006). Consequently, the aim of the thesis focuses largely on demonstrating the influence of using concrete with different SCMs and hydrophobic admixtures and their effect on the radon exhalation rate, compared to a reference cement binder, traditionally used. Thus, will SCMs and hydrophobic admixtures promote a decrease in the radon exhalation rate? Secondly, the research also clarifies the important difference between concrete´s diffusion coefficient and the radon exhalation rate under different moisture conditions.

Another contribution concerns the testing procedure of concrete and what time frame needs to be considered prior to testing. Not only because of the condition of the water saturation degree in concrete, but also with respect to the other properties considered. This question thus embraces the testing of the radon exhalation of concrete at an early age and whether an analysis of the radon exhalation rate of a concrete at a specific humidity level represents a correct value over time. Secondly, from a standardisation point of view a mutual agreement for when testing would be appropriate needs to be addressed.

Another contribution to research includes evaluating the different concrete mixes' emanation coefficient as a function of the relative humidity. These data can be used to anticipate which radon exhalation rates could be expected from different concrete mixes containing SCMs and/or hydrophobic admixtures.

Other parts of the thesis embrace (i) the effects of induced cracks in concrete as well as (ii) the effect of carbonation on the radon exhalation rate. In the project these "external impacts" were given specific attention with one separate study each. These studies are further contributions that lead to an increased understanding of what to expect regarding the concrete used during its lifetime.

Other valuable contributions are to enlighten these different options, such as using combinations of SCMs as part of binders to reduce the radon gas exhalation using appropriate measures. Since radon gas can largely be mitigated by a very low diffusion coefficient, this contribution for an increased understanding of the mechanisms of mitigation is considered valuable. The effect of reducing the radon gas (as a risk in our environment) has a much stronger impact on our health (more hazardous) than the effects of gamma radiation (Harrison & Marsh, 2011).

2 Ionising radiation

2.1 Fundamentals

Ionising radiation is radiation that carries enough energy to free electrons from atoms or molecules, thereby creating ions; thus ionisation occurs (Isaksson, 2011). In a natural decay process one element is transformed into another element. This occurs as the change in the number of protons of each element due to decay (α- or β-decay). In this process of, e.g., α-decay, a given excess of energy is also released as γ radiation, which creates a more stable form of the new element (Isaksson & Rääf, 2017).

For the elements ^{238}U and ^{232}Th the decay process starts with α-decay (Cember & Johnson, 2009). As the decay in these natural decay processes are continuous, β and γ radiation are also emitted, and a chain of other elements are formed. As an example, the ^{238}U decay chain contains various alkali-metal ions, radon gas and its daughter nuclides (^{218}Po, ^{214}Po), and finally reaches the stable lead isotope ^{206}Pb. Alpha emission (α) causes the element to emit two neutrons and two protons, Consequently, the mass number decreases by four, while the atomic number (number of protons) decreases by two. In the decay process, including negative β-emission (emission of an electron and anti-neutrino), a neutron is converted into a proton, hence leaving the mass number intact, while the atomic number increases by one (one more proton), as depicted in Figure 2.1.

With consideration of the noble gas ^{222}Rn, the process involves the α decay and transformation process by ^{222}Rn to its daughter nuclide ^{218}Po and secondly also the transformation process of ^{218}Po to ^{214}Pb. However, the decay process of ^{222}Rn and its transformation of elements yet further involves a chain α emissions and β capture, where continued α emission may take place. The α emission causes ionisation of its surroundings and can cause internal damage to the human cells if ^{222}Rn in the air is inhaled and stuck on the respiratory organs (Cember & Johnsson, 2009).

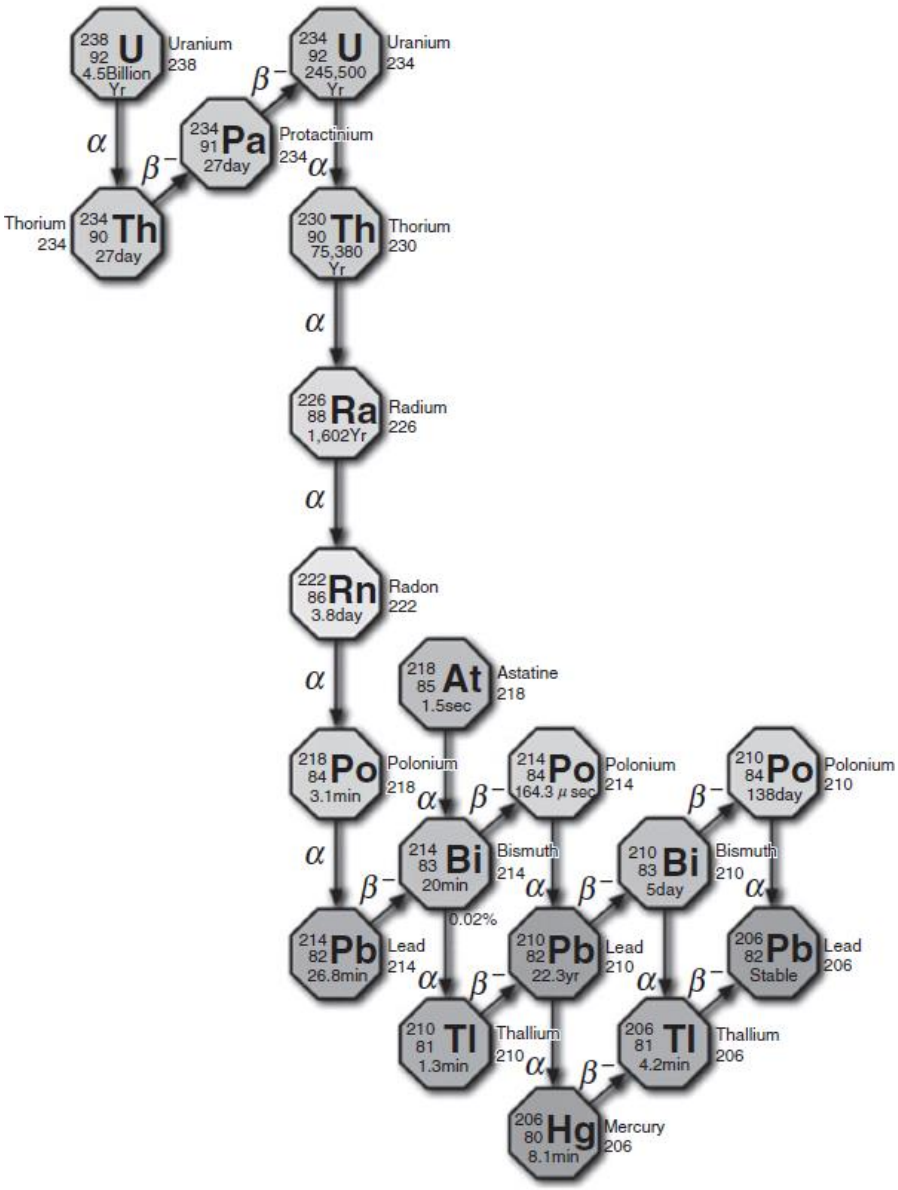

Figure 2.1 The ^{238}U decay chain illustrating the change of its elements during α- and β emission. Within the figure the gamma emissions are not presented. Data from Kovler (2012).

2.1.1 α-emission

The α-particle is a double-charged particle, quite slow in velocity and hence quite easily stopped. It is identical to a helium-nucleus, consisting of two neutrons and two protons. The double positive charge of the ion attracts other electrons from their parent atoms. Hence, when α -particles travel through a

material, some electrons will be attracted and depart from their outer parent atom shells and consequently ions will be produced in the material. In other words, ionisations occur (Isaksson, 2011).

An α-particle is a large particle compared to β-particles and especially photons (γ -rays), which are considered as only energy quanta or electromagnetic radiation, constituting no weight. An α-particle weighs 8000 times more than a β-particle, which is an electron (Isaksson, 2011). Table 2.1 depicts some of the characteristics of different energies, which are due to the ongoing decay of natural radionuclides.

Table 2.1. Some characteristics of α-, β-particles and γ-energies.

Particle	Constituents	Charge	Comparative weight	Energy (keV)	^{222}Rn (keV)	Wavelength (m)
α	2 protons + 2 neutrons	+2	8000	~ 4500-6000	6 000	
β^-	1 electron	-1	1	800-1400*		
γ	Energy	-	-	> 100		$<10^{-12}$

*Most frequent energy-interval of a β-particle

2.1.2 β-emission

β-particles are negatively charged particles, with a very high speed (close too speed of light). The negative charge of the particle will deflect other electrons in their parent atoms. Due to its speed and closeness to other electrons, it could deflect electrons out of their parent atom shells, and as such, ionisation occurs.

2.1.3 γ-emission

γ-emission occurs as a consequence of α- or β-decay. (Isaksson, 2011a). γ-radiation could also be described as electromagnetic radiation with very high frequency, i.e., with energies above 100 keV and wavelengths of less than 10 pm (10^{-12} meter), which is less than the diameter of an atom (Isaksson, 2011). γ-radiation is thus a form of electromagnetic radiation, such as x-rays and light. The difference between x-rays and γ-rays are dedicated to the origin of the ionising radiation source. For γ-rays, the origin is at the nucleus as a consequence of decay, whereas for x-rays the origin is related to the electronic shells (M, L, K) of the atom (Cember & Johnson, 2009).

The ionisations of material by γ-rays occur through several processes. Two of importance are (i) compton scattering and (ii) the photoelectric effect. These are the most prominent ones in the field of measurements for natural radiation (40-3000 keV). At higher energies, yet another process, called pair production, increases in importance (Turner, 2012). Compton scattering occurs when a high energy photon transmits some of its energy to another electron and deflects it (pushes it out of the parent atom shell). The remaining energy of the photon continues in another direction (scattered) through the material (Isaksson, 2011b). The photoelectric effect is slightly different compared to compton scattering. Here the incident photon rams into an electron, transfers its energy into the electron, which is ejected out of its parent shell (ionisation). An *photoelectron* is the final product, which continues its transfer in the atom. At the end the loss of energy to other electrons will result in the absorption of the remainder of the energy by the atoms in the material (Isaksson, 2011).

Pair production occurs when a photon is converted to one positron and one electron. (Isaksson, 2011).

2.2 Material characteristics of radon

General

Radon is the heaviest of all noble gases. Noble gases are considered as a class of chemically inert gases with low reactivity; they have a total of 36 isotopes (same number of protons, change in number of neutrons) ranging from ^{193}Rn to ^{228}Rn (Baskaran, 2016). The first paper reporting the release of radioactive gas (^{222}Rn) from the decay of radium (^{226}Ra) was published by a German scientist in 1900 (Dorn, 1900).

2.2.1 Chemical properties

The atoms of radon and other noble gases (six different elements in total) have a closed-shell electronic structure and are extremely stable, as the ionisation enthalpies are high (Baskaran, 2016). There are no ordinary electron-pair interactions among the noble gas atoms. The weak forces (van der Waals type or London type) are proportional to the polarisability and inversely proportional to the ionisation of the enthalpies of the atoms (Cotton et al. 1988). The first ionisation energy (the energy needed to remove one electron from the outermost filled shell) for radon is 1,037 kJ/mol, and it increases with the decreasing atomic number for the other noble gases (Fig. 2.2). The solubility in a column (periodic table) also increases with the increasing atomic number, hence radon is more soluble than the other noble gases, such as, e.g., Xenon or Argon. Radon is also more soluble in organic liquids than in water (Baskaran, 2016).

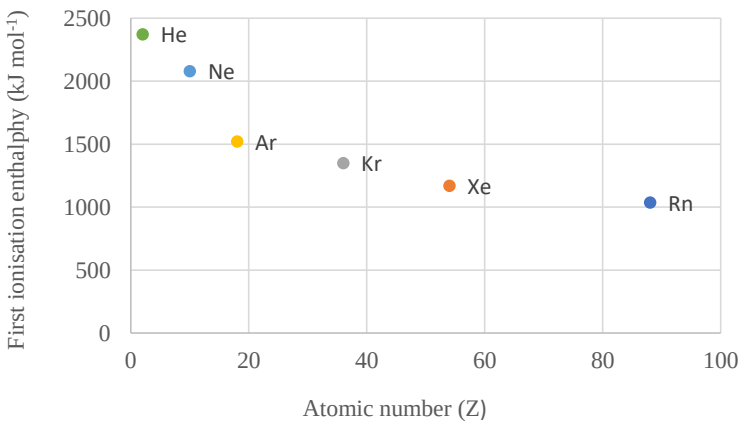

Figure 2.2. First ionisation energy (energy required to remove the most loosely held electron from one mole of noble gas ions each with a charge of +1) versus atomic number (redrawn from Cotton et al. 1988).

2.2.2 Atomic, physical and chemical properties of radon

Since radon is a noble gas, it will interact poorly with its surroundings (Isaksson & Rääf, 2017). When Rn exists in an ionic state, it is able to displace the ions of the first group elements (H^+, Na^+ , K^+ , Cs^+) and some of the second group elements (Ca^{2+} , Ba^{2+}). It may also form molecules with some flourides and salts at normal room temperature (Stein, 1987). Table 2.2 presents some atomic, physical and chemical properties of ^{222}Rn.

Table 2.2. Atomic, physical and chemical properties of ^{222}Rn. Data taken from Baskaran (2016).

Property	Values
Atomic number	86
Atomic weight	222
Density (kg/m^3)	9.73 (at 0ºC, 1.013·10^5 Pa)
First ionisation enthalpy (kJ mol^{-1})	1037
Electronegativity	2.2 (Pauling scale)
Melting point (K)	202
Covalent radius (nm)	0.150
van der Waals radius (nm)	0.220

2.2.3 Nuclear and physical properties ^{222}Rn and ^{220}Rn

Table 2.3 presents some nuclear and physical properties of ^{222}Rn and ^{220}Rn. ^{222}Rn is the radon gas being measured in the experiments as part of the alpha decay of ^{226}Ra (^{238}U). The ^{220}Rn (in earlier literature named thoron, Porstendörfer, 1994) is also referred to here as one of the radon progenies in the decay chain of ^{232}Th.

Table 2.3. Nuclear and physical properties of ^{222}Rn and ^{220}Rn. Data taken from Baskaran (2016).

Parameter	Symbol	^{222}Rn	^{220}Rn
Half-life	$T_{1/2}$	3.823 d	55.83 s
Decay constant	λ	2.098·10^{-6} s^{-1}	1.242·10^{-2} s^{-1}
Average recoil energy on formation	E_F	86 keV	103 keV
Diffusion coefficient in air	D_a	1·10^{-5} m^2 s^{-1}	
Diffusion coefficient in water	2.2 (Pauling scale[1])	1·10^{-9} m^2 s^{-1}	

[1] Pauling scale is a numerical scale of electronegativities based on bond-energy calculations for different elements joined by covalent bonds.

2.2.4 Solubility of radon

Radon is a noble gas that reluctantly diffuses in solutions. The solubility of radon can be described by Henry´s law, stating

$$C_w = KC_a \quad (2.1)$$

where C_w is the radon concentration in water (Bq per m^3 of water), Ca represents the radon concentration in the gas phase (Bq per m^3 of pore air), and K is the dimensional partition coefficient, which is a function of temperature. The reported partition coefficient for radon between distilled water in air is 0.245 at 20ºC (Nazaroff 1992). Another partition coefficient often used in experiments is the Ostwald coefficient (van der Graaf & Meijer, 2005). The Ostwald coefficient is derived as an extension of Henry´s law, but with the minor difference of molar concentrations of liquids and gases due to measurements at specified temperatures and pressures (Battino, 1984). The difference between the coefficients is, however, very small.

In the experiments undertaken as part of the thesis, the temperature is considered constant at 23°C because all experiments related to the radon exhalation rates and radon flux densities were performed within the climate chamber with its pre-set temperature (23°C±2) and relative humidity (50±5%). Thus, the solubility of radon gas is considered constant, but was never measured in the experiments.

2.2.5 Radon decay

^{222}Radon decay products are divided into two groups (Porstendörfer, 1994). The “short-lived” radon daughters all have half-lives of less than 30 min, which clarifies that half of the activity of the radon atom has decayed within half an hour. The “short lived” radon progenies’ half-lives are marked with parentheses and include ^{218}Po (3.05 min), ^{214}Pb (26.8 min), ^{214}Bi (19.7 min) and ^{214}Po (164µs).

The “long-lived” radon daughters include ^{210}Pb (22.3 years), ^{210}Bi (5 days) and ^{210}Po (134.4 days). The short lived-radon daughters are used in measuring equipment due to their rapid decay, which will enable a fast response by the instrument.

2.2.6 Radon and progenies attachment to aerosols

In most theories of attachment, the attachment process is diffusion controlled under consideration of electrostatic forces and gas kinetic laws (Porstendörfer, 1994). For large aerosol particles (> 1 mm) the attachment process is determined mostly by diffusion laws. For small aerosol particles (< 0.1 mm) the attachment is foremost due to the surface and size of the particle and electrostatic forces (Porstendörfer, 1994).

The radon atoms and its progenies are defined as “attached” and “unattached” fractions, depending on their charge (positive or neutral). Figure 2.3 depicts the different scenarios of decay from a radon atom to final attachment onto an aerosol.

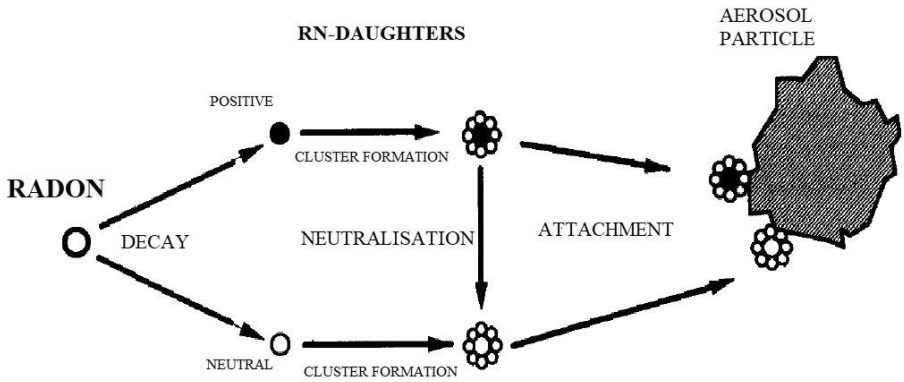

Figure 2.3. Basic process of Rn decay product behaviour in air defining "unattached" (bottom chain) and "aerosol-attached" (top chain) activities. Figure redrawn from Porstendörfer (1994).

The "unattached progeny" reacts rapidly (<1s) with trace gases and vapour and grows by cluster formation to form aerosol particles of ~1 nm in size (Harrison & Marsh, 2011). Reineking & Porstendörfer (1988) measured the activity size distribution of ^{218}Po, ^{214}Bi/^{214}Po and ^{214}Pb in homes. The dominant aerosol particle size regarding ^{218}Po was around 20-1000 nm with a mean value at 200 nm. However, the distribution was bimodal, which means that almost one third of the ^{218}Po nuclides attached to aerosols as "unattached" in a cluster mode. A similar size distribution regarding ^{214}Pb was also calculated. The largest part of aerosols (two thirds) constitutes the "attached" mode. The "attached" mode can have a trimodal activity size, with particles >1 um. The most dominant fraction is the activity median aerodynamic diameter (AMAD) of 100-450 nm (Porstendörfer, 1994, 2001).

A compilation by Porstendörfer (1994), where different authors used different experimental set ups to increase the aerosol content in the air, revealed very strong indicators. Smoking (which produces aerosols in air), cooking (vapour) or using a stove evidently largely increases the attachment rate of ^{222}Rn or different progenies to different aerosols.

2.2.7 Attenuation of radon and α emissions (radon and daughter isotopes)

The reduction (attenuation) of α particles, which reduce the rate of radon gas exhalation, can be controlled by different variables. One is to use paint on the walls or put-up wallpaper. This significantly reduces (~30-50 %) the radon gas release (Petterson et al., 1982).

A second approach to regulate the rate of radon gas emitted from building materials inside a room is through external influences, such as circulation of air from outdoors, where an increased air flow within the building through ventilation is an acceptable measure. This will mitigate or dilute the radon gas concentration build up within the room/building.

A third approach is to select low-radioactive building materials (aggregates), whereas a fourth is to identify other factors reducing the radiation emissions from the concrete into the ambient air and counter these factors. This is what the current thesis basically embraces.

2.3 Radon gas and dose quantities (internal radiation)

2.3.1 General

The ionisation of human cells due to the decay of radon gas and its progenies through α-particle emission is caused by the decay of ^{222}Rn, as well as the daughter nuclides ^{218}Po and ^{214}Po, all of which emit α-particles. The largest risk with radon gas is (i) the inhalation through air whereby different organs are exposed to different degrees of radiation. The intake of food and drinks also relates to the same subject. However, related risks, in the context of α-, β- and γ emitters, are considered most severe when α-decay occurs due to the much higher mass of the α-particle compared to the other emitters, and as such there is a much higher potential for ionisation of the human cells (Isaksson & Rääf, 2017). This is also explained in more detail by Döse (2016). Therefore, the whole uranium- and thorium decay chain as α-emitters should, in the end, be considered (Figure 2.1) when calculating the final effective dose received by the human body.

2.3.2 What is being measured by the radon instruments?

A vital key to understanding the outcome of the results lies in the understanding of the equipment and what is being measured. The techniques measure α-particles, and each registered particle could be transferred to a specific energy often defined in MeV (Baltzer et. al, 1992). For example, alpha particles of ^{222}Rn have a distinct energy of 5.5 MeV. ^{218}Po has a distinct energy of 6 MeV, and ^{214}Po has a distinct energy of 7.7 MeV. As for the ^{232}Th radioactive decay chain, the radioactive radon gas of ^{220}Rn corresponds to energy peaks at 6.8 MeV and 8.8 MeV. These energy peaks represent ^{216}Po and ^{212}Po, respectively. Hence, each a-alpha decay is registered as a detector pulse during one measurement and could be counted and transferred into a number per counts of unit time, giving a measure of the quantity of the particles (or elements) for each specific nuclide investigated. Thus, for ^{222}Rn it is appropriate to measure the alpha decay of ^{218}Po. This is due to the short half-life of ^{218}Po, which verifies that the activity of ^{218}Po is in equilibrium with ^{222}Rn within ten minutes. Thus, the frequency of alpha decay of ^{218}Po is used as the "radon activity concentration" radionuclide.

From what has been addressed, it should be clear that it is not the sample, samples or materials themselves that are being measured, but only the particles emitted into the air, adsorbed by molecules (water or dust aerosols) and transferred via the air into the ionising chamber of the instrument.

There are different techniques for how to measure γ-radiation, such as (i) semi-conductor gamma ray spectrometry, used in laboratory environments, or (ii) gamma spectrometry, used for equipment in the field where a doped crystal (NaOI) registers the electromagnetic energy in the medium and transfers it into an electric pulse that could be registered by the instrument. The reader is here referred to Döse (2016) for further reading.

2.3.3 Quantities and units used in calculations

For clarification, some quantities and units, with definitions and short explanatory notes, are presented in Table 2.4. Only the most essential quantities and units in relation to the thesis are presented for gamma radiation. A more comprehensive γ-radiation outlook is presented in Döse (2016).

Table 2.4. Quantities and units within radioactivity.

Quantity	Unit (full name)	Unit (abbreviation)	Definition/ short explanation
Radioactivity	Becquerel	Bq	One Bq is defined as the activity of a quantity of radioactive material in which one nucleus decays per second.
Radioactivity radon			
Radioactivity-Radon	Bequerel per cubic metre	Bq/m^3	Activity in the medium per unit volume. Decay of nucleus per second per cubic meter (volume)
Radioactivity-Radon	Bequerel per weight	Bq/kg	Activity per unit mass. Decay of nucleus per second per mass (often kg)
Radon exhalation rate/ radon flux	Bequerel per surface area per unit time	$(Bq/m^2)/h$	Number of decays per second per square meter per hour. Often also defined as the radon flux over a cross sectional area
Emanation coefficient		-	The portion (percentage) of radon atoms produced by radium decay that escapes to the pores in relationship to the total amount of radon atoms within that material. Dimensionless (%).
Radioactivity (gamma radiation)			
Absorbed dose (D)	Gray (Gy)	1 Gy = 1 J/kg	The energy absorbed per unit mass. Basic physical dose quantity. Stochastic quantity – measurable.
Equivalent dose (H_T)	Sievert (Sv)	1 Sv = 1 J/kg	The Sievert represents the equivalent biological effect of the deposit of 1 J of ionising radiation energy in a kilogram of human tissue. The dose equivalent encompasses the radiation weighting factor, W_R, which depends on the type of radiation ($D_{T,R}$) – absorbed dose. Not a measurable quantity.
Effective dose	Sievert (Sv)	1 Sv = 1 J/kg	The effective dose is the summation of all different equivalent doses by a factor, $W_{T,}$ as defined by the ICRP, 2007. Assuming full body irradiation for gamma rays (photons) the Equivalent dose and Effective dose could be considered equivalent.
I-index	-	Dimensionless	Conservative estimate of the maximum "effective dose" under circumstances, where a given "point-dose" is calculated within a room (Markkanen, 1995). Specific conditions presented in RP 112, EC (1999).

2.3.4 Monitoring and operational quantities

Different techniques are applied to measure the content of radon gas. The techniques may be classified as active or passive (Isaksson, 2011, Knoll, 2010). Active detectors require electrical power to measure the diffusion of radon gas. Passive techniques do not require any power source.

Some active techniques are as follows:

1. **Solid surface barrier detectors or solid-state detectors**, making use of α-spectrometry. A cell is coated on the inside with an electric conductor. A solid state, planar silicon alpha detector is often at the centre of the cell. A high voltage circuit creates an electric field throughout the volume of the cell. The electric field propels positively charged particles onto the detector, such as ^{218}Po. The ^{218}Po- nucleus decays upon the detector's active surface where the alpha particle produces an electrical signal proportional in strength to the energy of the alpha particle of ^{218}Po. Filters are used to separate each radon progeny to enhance reliable calculations.

2. **Scintillation cells** are enclosed cylinders coated with scintillation material, such as silver activated zinc sulphide powder. The interaction of alpha particles with the scintillation material causes the production of light photons, which are detected and amplified by a photomultiplier and converted to an electrical signal. Each progeny could be distinguished by complementary counting techniques and as such the methodology is considered to give high resolution and hence good control of uncertainties.

3. **The ionisation chamber** has a central collecting anode within a metal cylinder. The alpha particles upon decay ionise the gas within the chamber, and the liberated electrons in the ionisation process are collected at the anode (Isaksson, 2011). The registration of α-particles (or electrons) is measured by an ion current by use of an electrometer. The ionisation chamber could be used with both flow-through and closed operational modes.

Equipment used by RISE during experiments

RISE utilises a pulsating ionisation chamber, called ATMOS 33 DPX 12 used in all the measurements during this study. The working principle of the instruments and the transformation process of α-decay converted to radon gas activity concentration (Bq/m^3) in the air is further explained in Chapter 4, section 4.12. The other instrument used chiefly to monitor a state of secular equilibrium during diffusion measurements is a RAD 7. The equipment consists of a solid-state alpha detector.

Some passive techniques are as follows:

1. **Activated charcoal** is used as an absorber. The charcoal is weighted before measurement and sealed, then exposed to the air that is to be investigated. As soon as one measurement is finalised, the charcoal is measured again, and the radon activity concentration is determined by gamma spectrometry.

2. **A nuclear track detector** works on the principle of a selected film material, which due to the release of α-particles is damaged, where each α-particle leaves a small track. The tracks are enhanced by the use of NaOH or KOH to increase the size of the tracks to simplify the calculation. The tracks are counted by use of optical microscopy or by automated scanning. With knowledge of the decay rate of ^{220}Rn in relation to the density of the tracks, these variables/parameters can be correlated to the ^{222}Rn concentration in the air.

2.3.5 Protection quantities – radon and effective dose

The protection quantity of radon is given in Bq/m^3 but could also be recalculated to an effective dose (UNSCEAR, 2000). In the UNSCEAR report of 2008 (UNSCEAR, 2008), the total effective dose is summarised as

$$E_{eff} = E_{int} + E_{ext} \quad (2.2)$$

where E_{eff} = the total effective dose, E_{int} = the internal effective dose caused by inhalation (radon gas) and E_{ext} = the external effective dose caused by gamma rays.

Estimates of the absorbed dose to the critical cells of the respiratory tract per unit of ^{222}Rn exposure related to the general population can be derived from the analysis of information concerning the aerosol distribution, breathing rate, fractional deposition in the airways, clearance rate and location of the target cells in the airways (UNSCEAR, 2000, Scofield, 1988). However, these different variables are all subject to a certain degree of uncertainty. A simplified relation that takes into consideration all the above can relate the radon gas concentration in Bq/m^3 to an effective dose (UNSCEAR, 2000).

For indoor exposure this relation gives:

$$\frac{40\text{Bq}}{\text{m}^3} \times 0.4 \times 7000\ h \times 9\ \text{nSv}\ (\frac{\text{Bqh}}{\text{m}^3})^{-1} = 1.0\ \text{mSv} \quad (2.3)$$

where 40 Bq/m^3 represents the mean indoors value of the human population worldwide, 0.4 an equilibrium factor of ^{222}Rn and its related decay products, 7000 hours = 80 % of the time spent indoors annually and 9 nSv/(Bqh/m^3) = the mean average value of the dose conversion between the inhalation of radon and the above variables. The equilibrium factor is a measure of to what degree radon is in equilibrium with its short-lived daughters in the air (Equilibrium = 1).

The mean average radon concentration indoors (Bq/m^3) also varies significantly between countries (Darby et al., 2005). Thus, it can be noted that the mean average value of radon gas concentrations in the air in, e.g., Swedish households is approximately 110 Bq/m^3 (Andersson et al. 2007). Earlier estimates of Swedish habits also suggest that approximately 90 % of residents' time is spent indoors (Andersson et al. 2007). Considering this percentage (90 %) and converting it to hours indicates that the average person spends approximately 7900 hours indoors, which would result in an estimate higher than that used by UNSCEAR (2000).

There is also a wide range of dose conversion factors (ICRP, 1996, 2014, 2017; Unscear, 2000, 2008), The range of dose conversion factors for radon, derived from epidemiological studies and physical dosimetry, varies from 6 to 15 nSv (UNSCEAR, 1988, 2000). In the UNSCEAR (2008) report a mean value of 10 nSv/Bqh/m^3 has been recommended. It should also be addressed that the equilibrium factor may vary largely (0.1-0.9), but as an overall mean it has been justified by the committee (UNSCEAR, 2000). The equilibrium factor, as described above, is a measure of to what degree radon is in equilibrium with its short-lived daughters in the air (Equilibrium = 1). It can be defined as "the activity of the short-lived radon daughters at the location under investigation, divided by the corresponding activity that would result if the daughters were in equilibrium with radon" (Isaksson & Rääf, 2017).

The conversion of the activity concentration of ^{222}Rn in the air into the effective dose to the human organs is inevitably the primary goal using correct dose conversions, which set up a workable regulatory framework of safety limits for public health. As an example, Nuccitelli et al. (2015) calculated according to the formula (eq. 2.2), using a dose coefficient of 10 nSv/Bqh/m^3 as a mean average instead of 9 nSv/Bqh/m^3 as recommended by ICRP (Harrison and Marsh, 2011). For Swedish regulations, a corresponding effective dose$_{\text{int}}$ of ~6 mSv per year at 200 Bq/m^3 of ^{222}Rn in the air would be the result. This is a factor ~**6** in an effective dose in relation to the reference value of allowed γ-radiation for building materials presented in the Euratom directives by EC (2014). Other factors

influencing the total effective dose (E_{eff}), such as ingestion (e.g., intake of food/water containing natural radionuclides) are numerically negligible compared to the quantity of effective dose produced by the inhalation of ^{222}Rn and its progenies (ICRP, 2007, UNSCEAR 2008).

2.4 Risk aspects and regulatory framework

2.4.1 Decay, elements, and risk aspects of radon gas with decay

The production of radon gas is an ongoing process in the uranium decay chain (Figure 2.1), where the ^{226}Ra atom releases an α-particle and hence by decay becomes the new element, the noble gas ^{222}Rn. Radon gas has a half-life of approximately 3.8 days and its continuing decay results in the release of yet another α-particle and the production of a new element, one metal-ion, namely ^{218}Po. Nevertheless, further ^{218}Po radon-daughter decay releases another α-particle and reduces it to ^{214}Pb and subsequently to ^{214}Bi. The ^{214}Po atom arises through the β-decay of the former. The ^{214}Po-atom could hereafter release yet another a-particle before the more stable form of ^{210}Pb is reached. ^{218}Po, ^{214}Pb, ^{214}Bi and ^{214}Po are as earlier mentioned the so-called short-lived radon-daughter isotopes (Scofield, 1988, Porstendörfer 1994). In the process of the decay of ^{218}Po to ^{214}Pb and ^{214}Bi, beta- and gamma radiation are also emitted (Figure 2.1). Due to the release of gamma radiation between ^{218}Po and ^{214}Bi, the ^{214}Bi – atom is used as a progeny to calculate the gamma activity of ^{226}Ra assuming a state of equilibrium between ^{226}Ra and ^{214}Bi.

The decay of ^{222}Rn gives rise to a manifold of health aspects. The radon progeny (radon daughter) ions namely stick to particles in the air (aerosols) and are inhaled. As such, the particles in the air (aerosols) are troublesome and different places within a house give rise to different risks (Scofield, 1988, Åkerblom & Clavensjö 2007). For example, the kitchen area, when making food, gives rise to numerous particles in the air and as such increases the risk of inhaling larger doses of the daughter nuclides within certain areas of the house (Scofield, 1988). Cigarette smoke and humidity are variables that largely affect the number of aerosols in the air and consequently the risk of bonding with radon and its progenies (Scofield, 1988).

In view of the risks for external exposure α-emissions exerted to the human body from the outside could easily be stopped by the skin (β-particles and γ-rays are, however, more deeply penetrating into the skin). Nevertheless, if ^{222}Rn and its progenies are inhaled or digested by the intake of food, the human cells are more sensitive to the decay and α -emission exposure that occurs within the respiratory organs. The ICRP (2007) describes these internal exposures in terms of an index (W_R) correlating to the total equivalent dose or effective dose where α -emissions are 20 times as powerful in ionising within internal organs (surroundings) compared to β- and γ-rays. In part, this is due to its charge (W_R) but more importantly its comparatively slow speed giving it time to ionise the atoms more intensely (Isaksson, 2011, Isaksson & Rääf, 2017, Cember & Johnson, 2009).

A few large-scale studies on the effects of the risk of ^{222}Rn in regard to an elevated risk of lung cancer have been conducted in several countries (France, Finland, Switzerland, Sweden). In a large-scale interpolating study (thirteen national studies were combined) by Darby et al. (2005, 2006) the increasing relative risk of triggering lung cancer could be illustrated as a function of radon gas activity concentration (Figure 2.4). The study was performed on a large European population. Independent of the origin of habitants, a similar trend could be shown.

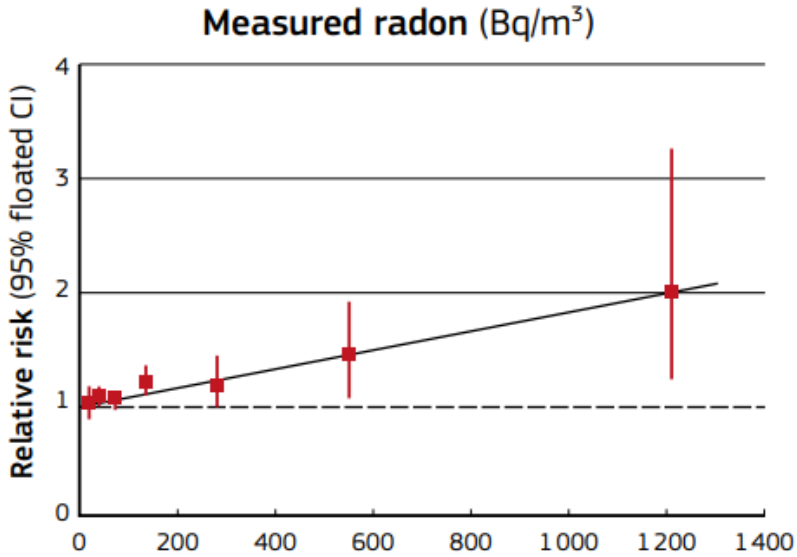

Figure 2.4. Relative risk of lung cancer according to measured residential radon concentration, with best fitting straight lines (risks are relative to that at 0 Bq/m^3, Darby et al., 2005).

2.4.2 Regulatory framework of γ-radiation and radon in building materials

The regulatory framework of radon is assembled in the Swedish radiation act (law) defined as "Radiation act 2018:396" defining responsibilities for anyone working with ionising radiation. The regulations are in part a direct consequence of the Council Directive 2013/59/Euroatom of 5 December 2013 (EC, 2014) laying down basic safety standards for protection against the dangers arising from exposure to ionising radiation including building materials. For building materials, under the Swedish legislation, a clearer guidance of threshold values of radon and gamma radiation are found in the "Radiation act directive (strålskyddsförordningen) 2018:506", which in turn addresses building materials with guidance to the national documents "The Radiation and Safety directives /Strålsäkerhetsmyndighetens föreskrifter) on naturally occurring radioactive materials (NORMS) and building materials, defined as directive "SFSM 2018:4". In the national radioactive directive, 2018:506, the acceptable levels of radon and γ- radiation for building materials are expressed. These values are also referenced in the National Board of Housing, Building and Planning regulatory framework (BBR 2018). The European union proposed a threshold value for radon, which is higher than the national regulations. Table 2.5 presents an overview of current European and Swedish threshold values of gamma- and radon levels from building materials.

Table 2.5 The reference and threshold values in relation to ionising the radiation of γ -radiation and radon gas

Definition	Quantity	Unit	Value	Regulatory framework
Levels of ionising γ-radiation within a specified room	Effective dose	mSv per year	1	Regulations, Strålskyddsförordningen 2108:506 and Eu´s Basic Safety Standards (EC, 2014)
Levels of ionising radiation (γ-energies) within a room	Ambient dose equivalent ($H^*(10)$)	µSv/h	0,3	Regulations from the Swedish National Board of Housing, Building and Planning (2011) and the Swedish Radiation and Safety regulatory act 2018:506 (2018)
Levels of radon gas in new buildings	Activity concentration	Bq/m^3	200	
Levels of radon gas proposed by the European Union (BSS)	Activity concentration	Bq/m^3	300	EU´s Basic Safety Standard (EC, 2014)

In should also be noted that the European countries with national protocols regarding radon and gamma radiation have had different approaches on how to calculate the risks of radon. Most countries assess alpha radiation (radon) and gamma radiation separately and with set requirements. However, as an example, the Austrian regulations, a combination of the activity concentrations of the different naturally occurring radionuclides, which take into account the potential emanating factor of radon, have earlier been considered. In this context, the risk of radon from an inhalation point of view is combined in the total risk assessment of the natural radioactive elements (Maringer et al. 2010).

These discrepancies concern what (i) is the best approach for how to calculate risk from natural radionuclides with respect to a human health perspective, something that has in recent years been addressed by the European Union to demonstrate how to evaluate natural radiation correctly. Specifically, attenuation has been drawn to building materials and a proper assessment of γ-radiation.

Regarding measurements of γ-radiation, several methodologies can be applied. Gamma-ray spectrometry has been found to be used by many laboratories within Europe. A large intercomparison study was performed in 2017 (Wiedner & Maringer, 2018) under the service of CEN/TC 351/WG 3. At least nine different laboratories participated. The results were, according to the authors, as expected but left room for improvement. Specifically, the activity concentration of ^{226}Ra was sometimes underestimated (by up to 35 %). The authors stressed that the results should be comparable within a 10 % margin if the instrumentation was calibrated correctly.

Reports and guidance on how to relate measured values in the field area to an internal effective dose inside a human residing within a building are still scarce. The currently used I-index only presents a rough estimate on how to assess building materials properly. Some guidance on how to calculate the yearly dose perceived as inhaled by habitants can regarding building materials be found in CEN/TR 17113 (2017). The technical report addresses a simplified model approach on how to calculate the final effective dose of a building material, such as concrete, used in a predefined room (2.5 x 4 x 3 m).

3 Radon, build-up and properties influencing the exhalation rate

3.1 General

In the following chapter a guidance concerning the decay process of natural radionuclides is presented. It also entails the numerical models used that relate to results in the dissertation. Decay is, as previously mentioned, a transformation phase where one element is transformed into a new element by decay (Isaksson, 2011). The rate of decay is described by its activity *A*, that is, by the number of atoms that decay per unit of time. The unit of activity is Bequerel (Bq), defined as one decay per second: 1 Bq = 1 s^{-1} (Turner, 2017).

3.1.1 Decay and equilibria

If *N* represent the number of atoms (nuclei) of a radionuclide in a sample at any given time, then the change d*N* in the number of atoms during a short time d*t* is proportional to *N* and to d*t*. Letting λ be the constant of proportionality (decay constant), the following applies:

$$dN = -\lambda N dt \tag{3.1}$$

where the negative sign indicates a decrease of *N* as time increases.

The activity *A* is the quotient between -d*N* and d*t*, consequently:

$$A = -\frac{dN}{dt} = \lambda N \tag{3.2}$$

If Equation 3.1 is rearranged according to

$$\frac{dN}{N} = -\lambda\, dt \tag{3.3}$$

and integrated, it will yield to

$$\ln N = -\lambda t + \ln N_0 \tag{3.4}$$

where N_0 is an arbitrary constant representing the initial number of atoms (N_0 at $t = 0$) for any given radionuclide. If rewritten with the exponent, the expression becomes

$$N(t) = N_0 \cdot e^{-\lambda, t} \tag{3.5}$$

The equation reflects the radioactive decay law. Combining Equations 3.2 and 3.5, we obtain

$$A = A_0 \cdot e^{-\lambda t} \tag{3.6}$$

or

$$\frac{A}{A_0} = e^{-\lambda, t} \tag{3.7}$$

where A_0 is the activity of the first radionuclide at time $t = 0$. In Figure 3.1, Equation 3.7 is depicted for ^{222}Rn. An activity of 1000 Bq has been chosen for illustrative purposes. After approximately 90 hours (3.8 days) half of the ^{222}Rn has decayed (red lines in Figure 3.1). Consequently, the activity of the ^{222}Rn atom is reduced by 50 % (halved) and has a remaining activity of 500 Bq. This time defines the so-called half-life ($T_{1/2}$) of ^{222}Rn.

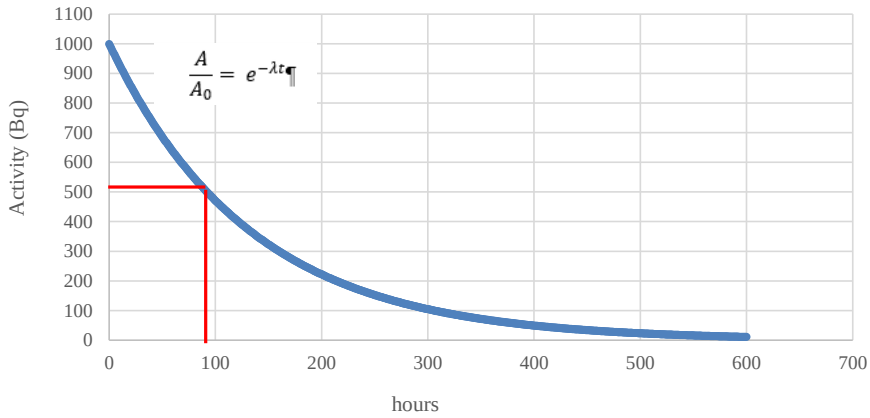

Figure 3.1 The decay of ^{222}Rn as a function of time. Red lines mark the approximate half-life of ^{222}Rn (~90 hours)

It could also be shown from Equation 3.7 that λ, the decay constant, is inversely proportional to the half-life $T_{1/2}$ and is given by

$$T = \frac{\ln 2}{\lambda} = \frac{0{,}0693}{\lambda} \quad (3.8)$$

If Equations 3.5 and 3.7 are written in terms of half-lives, the exponential decay laws become

$$\frac{N}{N_0} = \frac{A}{A_0} = e^{-0{,}693/T} \quad (3.9)$$

Secular equilibrium

If the half-life of the parent is much longer ($T_1 >> T_2$ or $T_1/T_2 > 100$), then it can be mathematically shown that the daughter (progeny) radionuclide will obtain an activity that by time is equal to its parent, i.e., activity A_1 of the parent = activity A_2 of the daughter radionuclide. The total activity will be A_1+A_2 (Cember & Johnston, 2009, Isaksson & Rääf, 2017). The condition applies when the activity of the parent A_1 can be considered as a constant in relation to the successive build-up of its daughter's isotope activity A_2. Consequently, if a secular equilibrium exists, the natural radioactive decay can be addressed in relation of the parents' and daughter's decay rate and number of atoms (N) as:

$$\lambda_1 N_1 = \lambda_2 N_2 \text{ or as activities } A_1 = A_2 \quad (3.10)$$

where λ_1 represents the decay rate of the parent atom, N_1 represents the number of molecules of the parent atom, λ_2 represents the decay rate of the daughter and N_2 represents the number of molecules of the daughter. The build-up of activity for the daughter isotope can be described as the rate of change dN_2/dt in the number of daughter atoms N_2 per unit time, equalling the rate at which they are produced, A_1, minus their rate of decay $\lambda_2 N_2$ as:

$$\frac{dN_2}{dt} = A_1 - \lambda_2 N_2 \quad (3.11)$$

As time increases, the result is that the secular equilibrium will eventually occur as depicted in Figure 3.2.

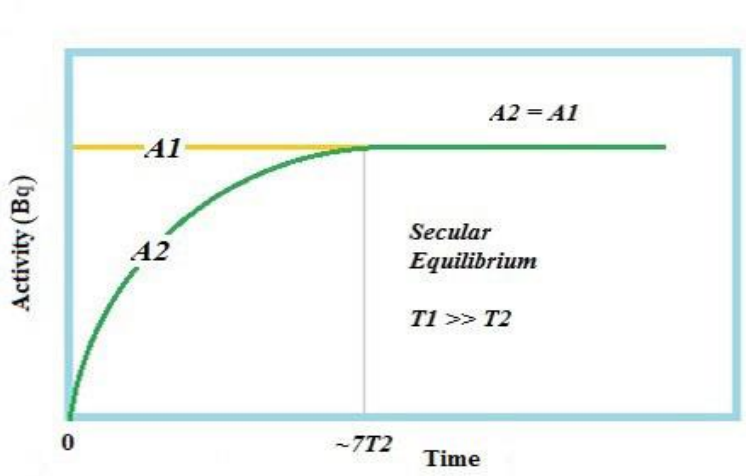

Figure 3.2 State of equilibrium between different isotopes in a decay chain expressed as "activity (Bq) as a function of time". When the build-up in activity of the daughter isotope (A_2) has reached ~7 half -lives, the activity of the parent (A_1) = activity of the daughter (A_2) and secular equilibrium is said to exist. Figure redrawn from Turner (2012).

The build-up process and the time before secular equilibrium is attained varies between the radioisotopes of interest, but in most aspects of radioactive decay, secular equilibrium will prevail after ~7 half-lives of the daughter (Turner, 2012).

The time dependency, i.e., the condition, $T_1 >> T_2$, is of significance between ^{226}Ra, ^{222}Rn and ^{218}Po, where the half-lives are 1600 years, 3.8 days and 3.1 min, respectively, indicating that their relationships in half-lives are in the order of more than 1000 times. As noted, the time prior to secular equilibrium within the material will vary strongly depending on the half-life of the daughter radionuclide.

Several decay scenarios may occur, where T_1 may be equal to T_2 (transient equilibrium) and so forth, but the scenarios described above (secular equilibrium prevails) are assumed in some calculations of the dissertation, i.e., when the emanation coefficient € is calculated. Secular equilibrium between ^{226}Ra and ^{222}Rn is in this specific situation subsequently assumed.

Secular equilibrium between the parent and the daughter progeny is a set of requirements for correct calculations. It is thus of importance to understand (i) why a specific radionuclide is used, e.g., the ^{218}Po as for the radon gas measurements. The reason is the decay rate of the ^{218}Po. The half-life of ^{218}Po is 3.1 minutes. Consequently, and as an example, ^{218}Po is in approximate equilibrium with ^{222}Rn after approximately 10 minutes (3 to 4 half-lives) in a material, and thus it can be accepted that equilibrium prevails shortly after the initiation of a measurement that will occur during several hours.

These relations between radioisotopes are as such also vital prior to measurements, when material or constituents have been blended. For a material such as concrete, this is primarily to ensure that equilibrium prevails in the concrete after being a mix of several constituents and cast. Normally, one would after casting wait at least 21 days prior to measurement to ensure that ^{222}Rn is in equilibrium with ^{226}Ra. The state of equilibrium between different radionuclides (secular equilibrium) is also

described as a condition of "steady state" (Chauhan & Kumar, 2013; Kovler, 2012) by many authors in different set ups or experiments.

3.1.2 Equilibria in a volume of air.

In a volume of air being exposed to a source of radioactive material, there is initially a disequilibrium between the concentration of ^{222}Rn in the source material and the concentration in the volume of air. Thus, enclosing a potential radon source in a closed volume of radon free air will, according to Fick´s first law, generate an increase of the radon activity concentration (Bq/m^3) in the air. As time progresses, the growth of ^{222}Rn into the air and its simultaneously continued decay into its progeny ^{218}Po will result in a slower and slower growth of ^{222}Rn until it ceases, and then it will be in equilibrium with its progeny (^{218}Po) in the air. This function of growth, and initial activity concentration accumulation of ^{222}Rn, can be expressed as (ISO 11665-7:2012):

$$C(\mathrm{t}) = \frac{E \cdot A}{V \cdot \lambda} \cdot (1 - e^{-\lambda t}) \qquad (3.12)$$

where C(t) = concentration as a function of time in Bq/m^3, E = the exhalation rate of source in (Bq/m^2)/h, A = the surface area of the source in m^2, λ = the decay constant of ^{222}Rn in h^{-1} (0,00755) and t = time in hours. The typical initial build-up of radon in a closed chamber is shown in Figure 3.3. Two different scenarios are shown, where only the volume of the container is different. All other parameters are set equal. Volume 2 (V2) is half the size of Volume 1 (V1). A reduced volume in a chamber will generate a higher activity concentration in the volume (V2) compared to V1.

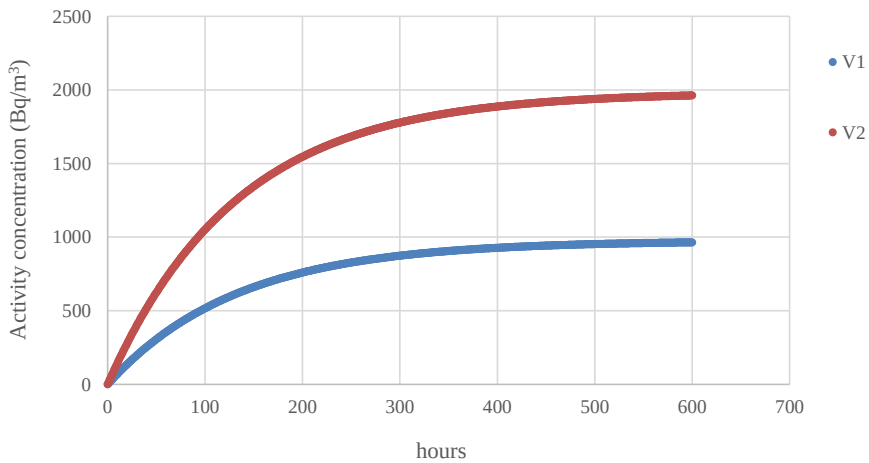

Figure 3.3 Build of ^{222}Rn in air in a closed chamber reaching secular equilibrium.

Through the Mclaurin derivation of Equation 3.12 the exhalation rate of ^{222}Rn can be assessed using a linear build up for the first 24 hours (Equation 3.8), assuming the background concentration is very low or can be subtracted from the final concentration. Thus, the following expression (ISO 11665-7:2012) can be used to calculate the radon exhalation rate of the material:

$$E = \frac{V \cdot C(\mathrm{t})}{A \cdot t} \qquad (3.13)$$

where V = volume in a closed chamber (m^3), C = the concentration of radon during build-up (Bq/m^3), A = the area of sample assessed (m^2) and t = the time for build-up (h).

The linear build-up also assumes no leakage or back diffusion of radon during this initial period of accumulation in the chamber.

3.2 Influences on radon exhalation rate

3.2.1 External influences

The major influencing external forces of the exhalation rate of radon gas are as follows:

1. Temperature
2. Pressure
3. Water

Stranden et al. (1984) showed the major influence of temperature (pressure) and to some extent also moisture. An increase in pressure or temperature follows the ideal gas law:

$$pV = NkT \tag{3.14}$$

where, p = pressure, v= Volume, N = number of molecules, k = Boltzman´s constant and T=temperature.

The external forces, in this context, are seen as parameters that will influence the radon release/exhalation rate, due to changes in the surroundings (environmental changes such as stormy weather, fire exposure, rainfall). As examples one may adress an advective flow (pressure driven) in a concrete wall or a sharp temperature increase within a building or the material itself within a short time span. It is well known that rain fall (water – 100 % relative humidity) on the soil surface initially dampens the radon relase from a surface (Ishimori et al, 2013).

3.2.2 Internal influences

According to Ishimori et al. (2013), there is a clear relation between increased moisture content and an increase in radon emanation coefficient of soils. The variation of the emanation coefficient ϵ in relation to humidity (degree of water saturation) can for soils be expressed by the radon production rate per unit volume, P ($Bqm^{-3}s^{-1}$). The production rate P is another way of expressing the exhalation rate (E) but with regard to the volume and not the radon exhaling surface (area) as in Section 3.1, Equation 3.12. The production rate P is expressed as:

$$P = \lambda R \epsilon \rho_b \tag{3.15}$$

where λ = the decay constant for radon (s^{-1}), ϵ = the emanation coefficient (dimensionless), R = the radium activity concentration in the material (Bq/kg) and ρ_b= the bulk density (kg/m^3) of the material.

The increase in the production rate P at higher water saturation degrees is due to the presence of water between the pore spaces (Ishimori et al., 2013). The water or film of water on grains hinders radon from transferring a long distance, i.e., to access the adjacent grains. Consequently, when decay of an element occurs, the recoil of the atoms (in the liberation process of an alpha particle) in the atom/particle is more likely to terminate its recoil in the water (pore space). Consequently, more atoms exist in the pores at high degrees of water saturation. Thus, a higher percentage of radon atoms, when the moisture content is high, is likely to be exhaled into the air as excess water in the pore system evaporates (Ishimori et al., 2013). At a moisture content of less than 3 % (weight) or 5-7 % (volume),

there is a rapid decrease of the emanation coefficient (release of radon atoms from adjacent mineral grains or material into the pores of that material).

An increase or decrease in the moisture content of a material can be linked to the diffusion coefficient (m^2s^{-1}) of that material (van der Graaf & Meijer, 2005). The diffusion coefficient describes the movement or rate of movement of the radon atoms within the material/aggregates and pore spaces. The higher degree of water saturation, the slower the atom moves within the pore system and the less radon atoms reach the surface of the material/aggregates per unit time. The diffusion coefficient in soil is largely related to the water saturation factor and varies with a factor of ~4 in magnitude from dry to water saturated soils (Ishimori et al., 2013.). Consequently, the exhalation of radon gas is controlled by the following variables (Ishimori et al., 2013):

1. *R*, the radium activity concentration (Bq/kg)
2. ρ_b, the bulk density of the material (kg/m^3)
3. ϵ, the emanation coefficient (non-dimensional)
4. *D*, the diffusion coefficient of radon (m^2/s)
5. *Z*, the depth of material

Figure 3.4 depicts an overview of the composition of the material and the processes influencing the exhalation rate/ radon production rate from a building material.

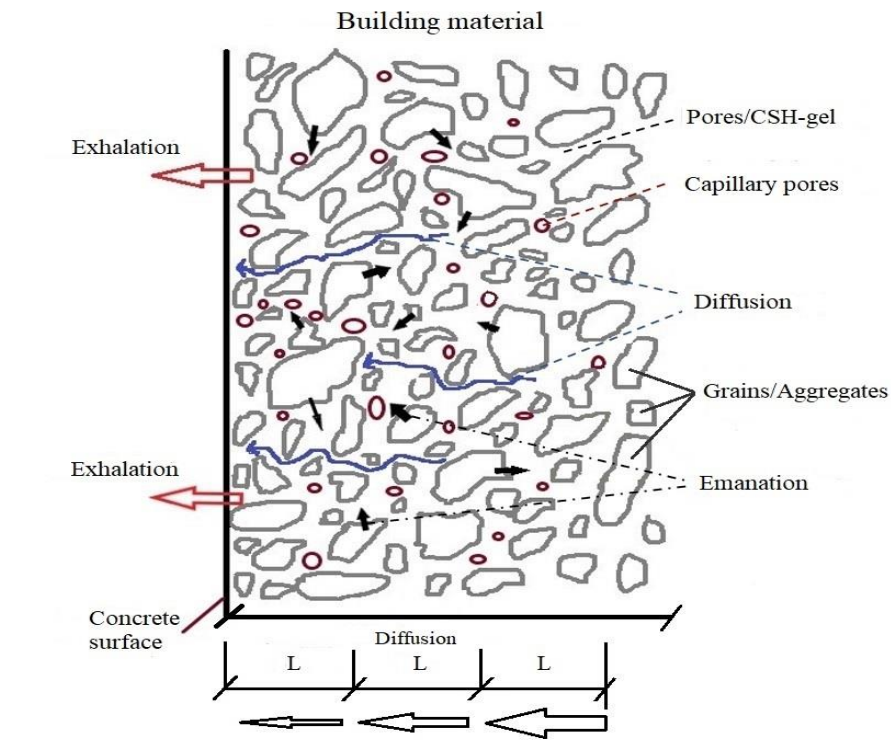

Figure 3.4 Simplified sketch of a building material. Illustrated is a concrete with its constituents. In the lower part of the figure there is a description of the diffusion process, where the diffusion coefficient can be recalculated to the radon diffusion gas length defined as “L”, i.e., the distance the particles diffuse through the material before their number is reduced to 50 % by decay. Figure reworked from Wicke (1979).

In Figure 3.4 also illustrates the emanation process. One cause of emanation is due to the decay process of ^{226}Ra that creates an energy release (recoil energy) as part of the liberation process of the newly formed atoms, namely ^{222}Rn and ^{4}He (alpha particle). The emission, decay and recoil process are illustrated in Figure 3.5. The recoil process (energy release) causes a rebound movement of the newly formed atoms (Isaksson, 2011).

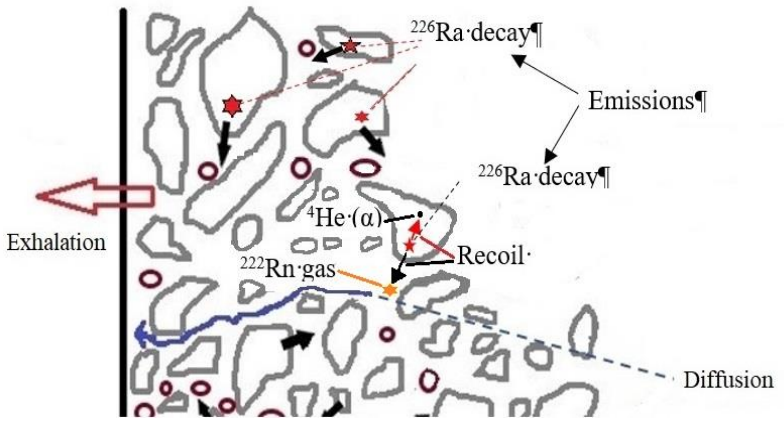

Figure 3.5. Simplified process of the emission of ^{226}Ra atom that decays into ^{222}Rn and ^{4}He (alpha particle). For simplicity, it is only illustrated in the middle of the figure. The energy release during decay causes recoil between the newly formed atoms.

Apart from this ongoing process of decay, factors that influence the final radon gas release rate (exhalation) at a building materials surface is the influence of water content and moisture. These influences have in part been described by Hildingsson et al. (1982), Stranden et al. (1984), de Jong (1985), Rogers and Nielson (1994), Cozmuta et al. (2003), Fournier et al. (2005), Kovler (2012), and Ishimori et al. (2013), among others. There is often a peak in the radon exhalation rate of concrete at 4 to 6 % of moisture content (Petersson, 1992). Stranden et al. (1984) put forward three possible causes as to why an increase in moisture (% weight H_20) often generates a higher radon exhalation rate:

(i) the "direct recoil fraction" of the emanation power (emanation coefficient) is increased when there is a fluid present in the internal pores of the material,
(ii) the fluid may hinder the adsorption of radon gas on the internal surfaces of the material and
(iii) if there is a moisture content gradient in the sample, an active transport of radon on water molecules may take place.

The "direct recoil fraction" is today accepted as a workable theory and presented by several authors (Fournier et al. 2005, Kovler, 2012, Ishimori et al. 2013). The release of ^{222}Rn in the natural decay process from its parent nuclide ^{226}Ra generates as stated a recoil energy (Figure 3.5 and 3.6). The consequence of different mediums is that, as for soils, more radon atoms are likely to stay in partially water saturated pores due to the difference in recoil energy (distance travelled) between water and air. For a radon atom in water the distance travelled by the radon atom is 77 nm, whilst in air, the distance travelled is 53×10^3 nm (Ishimori et al. (2013). Thus, this further strengthens why most radon atoms are likely to be stopped in the water and "higher activity concentrations" in the pores may initially occur in the water/moisture before most water is consumed as part of the hydration process.

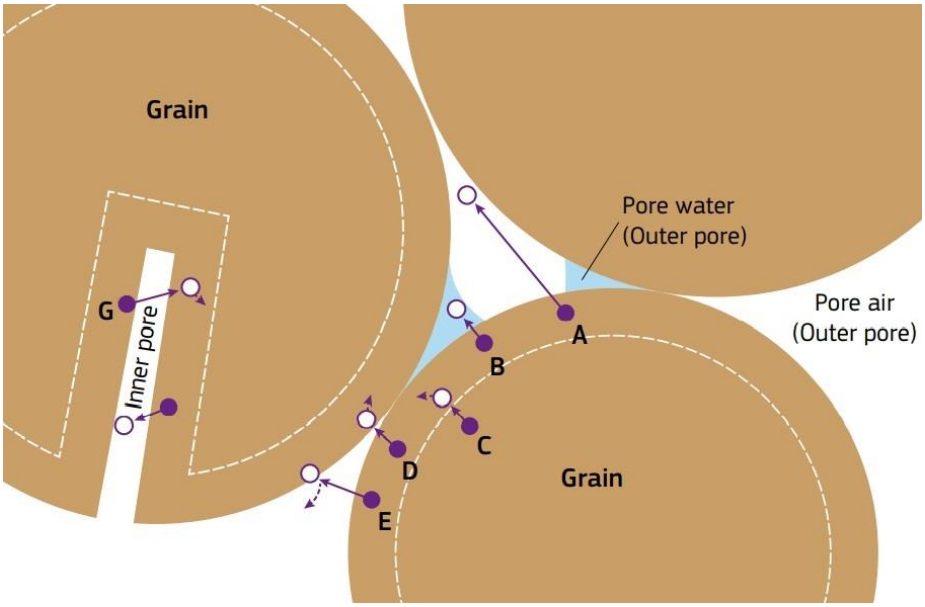

Figure 3.6. Schematic diagram of the radon emanation process (recoil distance in air and water). The purple solid circles indicate start of recoil and the white solid circles with purple ring their travelling distance. The with dashed lines indicates the critical distance of recoil to reach the surface of the grain/pore air. The recoil distance is considerably larger in air (white areas) than in water (blue areas). Copied from Sakoda et al (2011).

3.3 Mechanism of transport

3.3.1 Driving mechanisms of transport

Soil and most building materials have 10^3-10^4 times higher radon gas concentrations than the atmosphere, and thus there is a great radon/thoron concentration gradient between these materials and the open air. The gradient is permanently maintained by the much higher elemental concentrations in the earth of the radioactive decay chains of ^{238}U, ^{232}Th and ^{40}K. The continous and very slow breakdown of, for example, ^{238}U (half-life of 4.5 billion years) contributes to a continous transport of the radon isotopes into the atmosphere (Porstendörfer, 1994).

The ideal gas law applies to changes in the concentrations of radon gas within a confined space (volume) with a set temperature (Eq. 3.14). The flow density is proportional to the concentration gradient (Fick´s first law). According to earlier studies of building materials, the dominant transport mechanism, in building materials, is molecular diffusion, which is driven by a gradient of concentration (Porstendörfer, 1994, Roger and Nielson, 1991, Fournier et al. 2005). Chauhan and Kumar (2015) also demonstrated that the driving mechanisms were basically a diffusion driven transport for dense materials (concrete with a compact density of at least >2000 kg/m^3), due to the low permeability of concrete. Consequently, in the case of the activity concentrations of the ^{222}Rn gas of the concrete specimens, a transport gradient, a flow, will be established between the concrete and its surrounding atmosphere, initially containing much less ^{222}Rn gas (close to zero). Another transport mechanism, except the difference in activity concentration, is the gradient in concrete in the form of moisture content as potential (Nevander & Elmarsson, 2006). This also contributes to the transport mechanism of radon gas, due to a likely difference in the moisture content in the centre of the concrete specimens compared to at the surface of the concretes.

The quantity that describes the process of radon exhalation and radon transport from building materials is, as previously mentioned, the radon production (Ishimori et al, 2013; Fournier et al., 2005). The radon production depends, as noted in Eq. 3.15, on the radium concentration, the emanation coefficient, and the bulk density (volume and mass) as well as the decay constant of radon. Two main parameters of importance for transport in building materials like concrete are porosity and water content (moisture content). The emanation coefficient (Section 3.4.2) is strongly influenced by water or moisture (van der Graaf and de Meijer, 2005, Fatema et al., 2019). According to Fournier et al. (2005), the water content or moisture is the parameter that is the most difficult to predict regarding transport in building materials.

Rogers and Nielson (1991) used a model of the moisture transport in a material according to Fick´s first law.

$$F_{\mathrm{d}} = -D_{\mathrm{o}} \nabla C \qquad (3.16)$$

where F_{d} = the diffusive Rn flux (Bq/m^2/s), C = the Rn concentration (Bq/m^3) and D_{o} = the diffusion coefficient (m^2/s).

The diffusion coefficient D_{o} was calculated regarding different moisture conditions in porous unconsolidated materials such as sand and gravel (Rogers and Nielson, 1991). A multiphase approach was here made to account for the solubility of radon in water (partition coefficient). Also, different moisture conditions in the materials, such as porosity, adsorption and absorption were considered. In short, the results indicated that the adsorption effect is most pronounced for dry materials. At a moisture content in the materials above 30-40 %, the effect of adsorption is very limited and could in many cases be neglected. Nevertheless, the absorption of radon on surfaces influences the diffusion coefficient D and should thus be accounted for.

Using the model (Eq. 3.16) by Rogers and Nielson (1991), Fournier et al. (2005) presented a study of radon transport, including the moisture effect, in dense concrete. Dense concrete in this sense is a typical concrete with a density of ~2.300 kg/m^3. The effect of the moisture content on the emanation coefficient was modelled. The model included a concrete cube, with a radium source of higher concentration placed in the middle of the cube. The concrete cube was enclosed into a large container, to be able to account for the increase of the radon exhalation rate in the surrounding air of the enclosed container. The study also included an approach to combine the molecular diffusion coefficient and the partition corrected porosity with the emanation coefficient under different moisture conditions. This was done to evaluate the radon production at the surface of concrete under different moisture conditions and consequently the release of radon gas (exhalation) into the atmosphere.

According to Fournier et al. (2005), a general equation of continuity involves three important processes:

(i) radon generation/production, which involves the emanation coefficient, i.e., the radon atoms´ ability to leave their surroundings and reach the atmosphere/free air porous system.
(ii) molecular diffusion (radon atoms move) through a medium to reach the atmosphere and
(iii) radon decay.

The total radon transport in building materials can accordingly be described by a general equation of continuity (Fournier et al, 2005, Rogers and Nielson, 1991):

$$\beta \frac{\partial C}{\partial t} = \nabla \times (D \nabla C) - \beta \lambda C + P \qquad (3.17)$$

where β is the partition-corrected porosity, C the radon concentration within the pores (Bq/m^3), D = the bulk diffusion coefficient (m^2/h), P = the radon production rate per unit volume ((Bq/m^3)/h), and λ = the decay constant of radon (per h).

The partition corrected porosity β depends directly on the quantity of water in the material's pores (Rogers and Nielson, 1991). It can be expressed as:

$$\beta = p(1 - m_{vol} + Lm_{vol}) \quad (3.18)$$

where p = the total porosity of the material, L = the Ostwald coefficient that expresses the solubility of radon (0.35 at 298K), and m_{vol} = the degree of saturation.

Van der Graaf & Meijer (2005) developed a one-dimensional radon release model based on the results by Rogers and Nielson (1991). The model was stepwise improved and introduced progress in different literature (Cozmuta & van der Graaf, 2001, Cozmuta et al. 2003, van der Graaf & Meijer, 2005).

Assuming no pressure difference, the release model can be described as,

$$\nabla \times (D\nabla C_a) - \beta\lambda C_a + P = 0 \quad (3.19)$$

where:

- D is the bulk radon diffusion coefficient (m^2/s)
- C_a is the radon concentration in the air-filled pore volume (Bq/m^3)
- β = the partition corrected porosity, $\beta = p(1\text{-}m + Lm) + p_b k_a$
- p = porosity; m is the fraction of water saturation of the pores
- L is the Ostwald coefficient (L = 0.26,value at 293K)
- p_b is the bulk dry density in concrete (kg/m^3)
- k_a is the radon surface-adsorption coefficient (kg/m^3)
- λ = the decay constant of radon ($2.1 \times 10^{-6}/s$)
- P is the radon production rate per unit bulk volume ($Bq/m^3/s$); $P = \epsilon p_b \lambda C_{Ra}$;
- ϵ is the radon emanation factor (coefficient)
- C_{Ra} is the radium content, dry mass (Bq/kg)

The model, like the one described by Fournier et al. (2005), was verified by numerous experiments (Figure 3.7). A concrete cube of 15 x 15 x 15 cm was assessed according to principles developed by Cozmuta & van der Graaf (2001), where it was enclosed into an aluminium airtight box. The radon release rate R was calculated as a function of the moisture content (degree of saturation). The radon release rate was defined as:

$$R = -AD\nabla C \quad (3.20)$$

where A = the area of the concrete (m^2), D = the bulk diffusion coefficient (m^2/s) and C = the radon gas activity concentration (Bq). The total radon release rate R was measured using a closed system with coal absorbers during a preset time. The radon content was thereafter defined by spectroscopy.

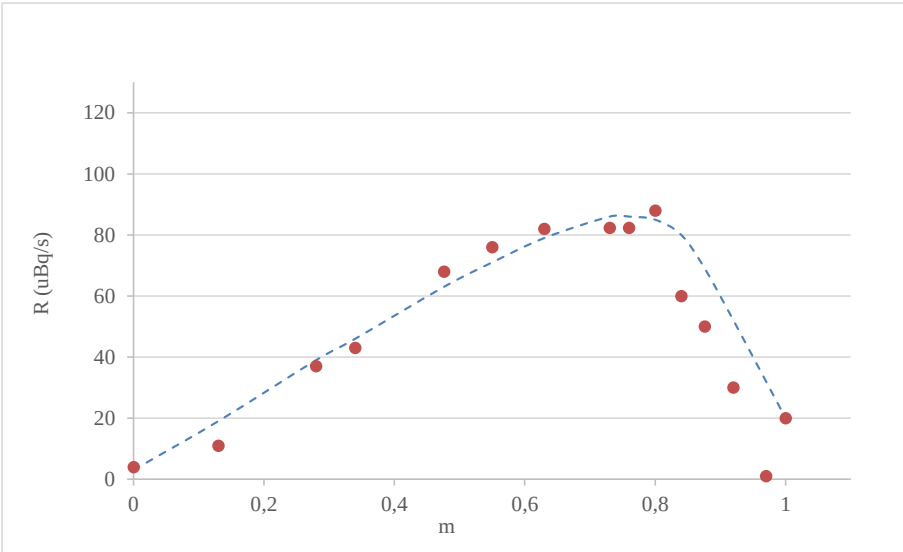

Figure 3.7 The radon gas release rate *R* as a function of moisture content. The modelled approach according to Eq. 3.19 is the dashed blue line. The conducted experiments at different moisture levels are shown with brown circles. Redrawn from Cozmuta et al. (2003).

The independent moisture parameters in the assessments by Cozmuta et al. (2003) and van der Graaf and Meijer (2005) were as follows:

1. C_{Ra} (radium content, dry mass),
2. p (porosity)
3. P_b (bulk dry density of concrete)
4. k_a (adsorption coefficient)

The moisture dependent parameters in the studies were the following:

1. D (diffusion)
2. ϵ (emanation)
3. β (partition coefficient)

Studies by Fournier et al. (2005). Cozmuta et al. (2003) and van der Graaf & Meijer (2005) all indicate a strong dependence of the moisture content on the emanation coefficient and consequently the final ^{222}Rn exhalation rate (Figure 3.6). This has also been documented by Fatema et al. (2019) testing different cements. In the experiments by Cozmuta & van der Graaf (2001), Cozmuta et al. (2003) and van der Graaf & Meijer (2005) the moisture content was assessed by the weight difference of the concrete cube, assuming that a fully water-saturated concrete sample had all voids filled with water. Consequently, a moisture content, i.e., the degree of saturation of 1 represented a fully water-saturated pore system (100 %). Successive drying of the concrete cube with weight documentation and a simultaneous measurement of the radon exhalation rate gave the necessary means to calculate the behaviour of the emanation coefficient as a function of a concrete's moisture content. In the experiments by Cozmuta et al. (2003), the emanation coefficient for concrete as a function of the moisture content indicated an almost linear increase (Figure 3.8).

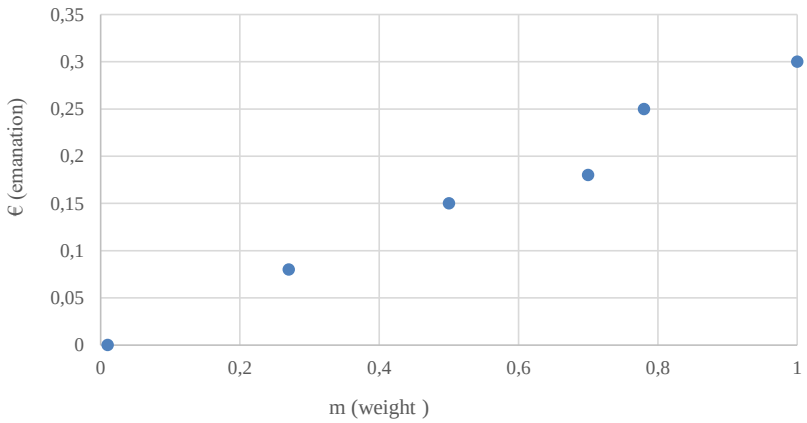

Figure 3.8. Data from Cozmuta et al. (2003). The emanation coefficient € as a function of the moisture content *m* (weight) of a concrete specimen.

As illustrated in Figure 3.8, the total radon production *P* in a building material, such as concrete, may strongly be governed by the emanation coefficient (Cozmuta et al. 2003, van der Graaf & de Meijer, 2005). Fournier et al. 2005 also noted a sharp increase of the emanation coefficient for concrete but specifically at porosity levels < 15 %. Apparently, a sharp increase in the emanation coefficient contributes strongly to a higher ^{222}Rn release rate for building materials.

The influence of the diffusion coefficient *D* of a material as a function of the moisture content was demonstrated by van der Graaf & Meijer, 2005 (Figure 3.9). Several authors reported similar results (Cozmuta et al. 2003, Fournier et al. 2005, Muños et al, 2017, Fatema et al., 2019). This is most reasonably due to the difference in diffusion between air and water, where less water or moisture will increase the amount of air in the pores that increases the rate of diffusion.

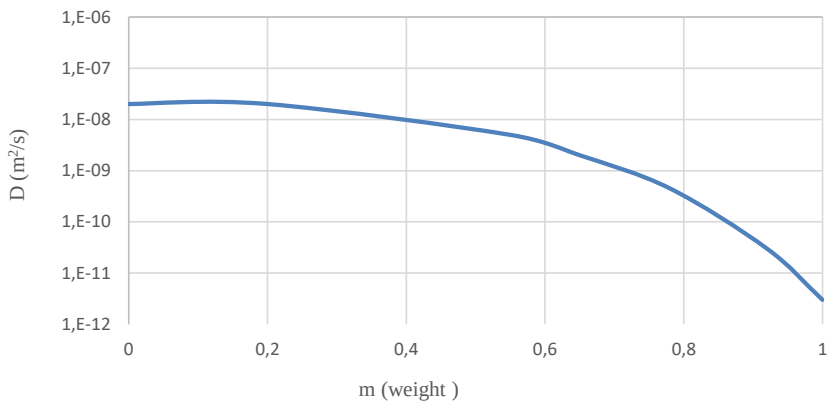

Figure 3.9. The modelled diffusion coefficient *D* as a function of the moisture content *m* (weight) in concrete. Data from Cozmuta et al. (2003).

Fournier et al. (2005) demonstrated a strong influence of the emanation coefficient regarding the relative humidity in dense materials (normal concrete), where a relatively low porosity (< 10-15 %) plays a significant role. The porosity influence was also modelled by van der Graaf and Meijer (2005) where a link between the moisture content m and relative humidity RH of concrete was pursued. The model included a calculation of the final radon gas surface exhalation rate as a function of the relative humidity for a standard concrete (Figure 3.10).

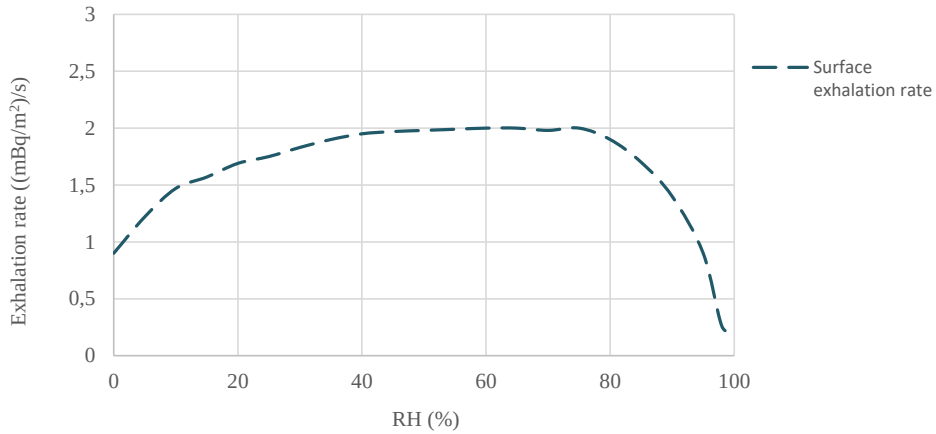

Figure 3.10. A modelled approach of the surface exhalation rate as a function of the relative humidity from a standard concrete. Redrawn from van der Graaf & Meijer (2005).

The modelling data, as verified in experiments by van der Graaf & Meijer (2005) suggest a strong influence on the ^{222}Rn radon gas exhalation rate due to differences in the relative humidity of the concrete (Figure 3.10). The radon gas release rate is most pronounced in the interval 80-100 % RH where a sharp increase is noted. However, at lower relative humidity levels RH <80 % a shift is noted. Thus, even though the diffusion coefficient *D* increases (Figure 3.8) as the moisture content in the gel- and capillary pores decreases, the radon exhalation rate (Figure 3.10) is unchanged or reduces at RH <80 %. This is, according to the model by van der Graaf and Meijer (2005), a result of a change in the partition coefficient β that is a function of the ratio air/water in the pores.

The reason for presenting part of the modelled data by mainly Cozmuta et al. (2003) and van der Graaf & Miejer (2005) is whether they correlate to the experiments in this dissertation. The results in the dissertation have not, however, been compared in detail with van der Graaf & Meijer's the model (2005).

It should be noted, with respect to previous authors, that many experiments often include a drying procedure of the concrete at 100°C or higher before some measurements are commenced. The drying process could severely change the microstructure of the concrete, and thus the porosity and diffusion characteristic of the concrete may change. Consequently, the concrete microstructure may no longer be representative of the concrete examined and may yield incorrect results and conclusions. Consequently, the lack of knowledge of the sensitivity of the hydration process of concrete and the hydration products can influence some research results and final conclusions. The above-mentioned, should in this context only be regarded as a careful notation, noted during the author´s literature studies.

3.4 The diffusivity, coefficients, and pore structure of a concrete material

3.4.1 Diffusion coefficients *D*, radon diffusion length *L* and porosity *p*

Calculation of the radon flux and concentration gradient *J* of a concrete material can be determined by assuming a set of conditions. Assuming two equal radon tight chambers with a concrete sample of thickness *d* clamped between the chambers, the flow/radon flux and gradient can be measured using a radium source in one of the chambers, defined as the source chamber (Kovler, 2012). Letting the radon reach a steady state condition in the source chamber, the measurement of the radon flux can be initiated by setting the ^{222}Rn activity concentration (Bq/m^3) receiver chamber to "zero". This is done by adding a flow of air in short sequences before measurement or pure nitrogen (99,99 %) to assure a very low initial radon concentration in the chambers. Assuming that the initial conditions are met (radon tight chambers), the radon growth in the chamber can be assumed to be linear, during the first hours, and can be written as (Chauhan & Kumar, 2013)

$$J = \frac{C \cdot V}{t \cdot A} \tag{3.21}$$

where J = the radon flux, in Bq/m^{2}s^{-1}; C = the radon concentration, Bq/m^3; V = the volume of chamber (receiver); A = the area of concrete sample in m^2 perpendicular to the flow direction; and t = the time in seconds or hours. Please note that Eq. 3.20 is equivalent to Eq. 3.13 but partly written with different symbols.

The radon flux J ((Bq per m^2/s) across the surface of the material and measured in the receiver chamber can be defined by Fick's first law stating that the flux J *(flow density)* is proportional to the diffusivity D and the negative gradient of concentration dC/dx (Audenaert, 2007)

$$J = -D \left|\frac{\mathrm{d}C}{\mathrm{d}x}\right|_{x=d} \tag{3.22}$$

where x = the point of measurement in the material (in this case the concrete slab with thickness d (m) between source and receiver chamber) and D = the diffusion coefficient in m^2/s.

Thus, the relation between the concentration gradient, its diffusion coefficient, and the material´s radon flux can be assessed. The diffusion coefficient D (bulk diffusion) can be solved numerically (Chauhan & Kumar, 2013) using the radon diffusion length L as

$$L = J \cdot \sinh(d/L)/(Co\lambda) \tag{3.23}$$

where Co = the steady state concentration (Bq/m^3 in source chamber), L = the radon diffusion length (m) and λ = the radon decay constant 0076 h^{-1}.

The radon diffusion length ***L*** (m) can be defined in several ways, but one explanation is "the characteristic distance travelled by the radon atoms during one half-life" (Kovler, 2012).

It can be shown that the square root of the ratio of the bulk diffusion coefficient D and the decay constant λ of ^{222}Rn is equal to the ^{222}Rn diffusion length L under a steady state condition (Chauhan & Kumar, 2013). Consequently, the relation of L to the diffusion coefficient D is described as:

$$L = \sqrt{\frac{D}{\lambda}} \tag{3.24}$$

This was illustrated in Figure 3.4, where L constitutes a specific distance named radon gas diffusion length (m). It could also be addressed that the porosity has a direct dependence on the ratio of the bulk diffusion coefficient D and the effective diffusion coefficient D_e. D_e represents the effective diffusion

coefficient of the pore area of the material and *D* of the bulk area (Unscear, 2000). The relation can be expressed as:

$$p = \frac{D}{D_e} \quad (3.25)$$

Thus, the porosity dependence of a material can be directly related to the radon diffusion length and its effective diffusion coefficient as,

$$p = (L^2 \, x \, \lambda)/D_e \quad (3.26)$$

As a result, a way to describe the "tightness" or "permeability" of a building material can be linked to the diffusion coefficient *D* or vice versa, the radon diffusion length *L*. Further reading in this area can be recommended, and the reader is advised to examine work by Keller (1999), Porstendörfer (1994), Kovler (2012), Chauhan and Kumar (2013) and Ishimori et al. (2013).

3.4.2 Emanation coefficient €

The emanation coefficient is the portion (percentage) of radon atoms produced by radium decay that escapes to the pores in relation to the total amount of radon atoms within that material (Kovler, 2012). It is not to be confused with the exhalation rate (*E*) that describes the release of radon gas from a given surface (per unit time). The emanation coefficient is directly linked to the activity concentration of the sample and the mass exhalation rate of the sample ((Bq x kg)/ h).

The emanation coefficient *€* can be derived by first calculating the radon gas mass exhalation rate Jm (Hildingsson, 1983, Kovler, 2006, 2012, Ishimori et al, 2013) according to the radon gas build-up in a closed system as:

$$\text{Jm} = (V\Delta C)/(\Delta TM) \quad (3.27)$$

where Jm = the mass exhalation rate ((Bq/kg)/h), *V* = the total volume of the closed system entailing the sample (m^3), ΔC = the concentration of radon in Bq/m^3 at equilibrium, *M* = the total dry mass of the sample (kg) and ΔT is the time difference (h).

The mass exhalation rate (Jm) can subsequently be used to calculate the emanation coefficient *€* of the sample according to

$$€ = \text{Jm}/(\lambda R) \quad (3.28)$$

where *€* = the dry sample radon emanation coefficient (non-dimensional) and *R* = the dry weight radium activity concentration (Bq/kg) of the sample.

The emanation coefficient can also be evaluated knowing the equilibrium ^{222}Rn concentration in a specified volume of air (Bq/m^3), as well as the mass of the sample and the material's specific activity (Bq/kg) under dry conditions according to,

$$€ = V \, x \, C \, / \, (\text{M} \, x \, R) \quad (3.29)$$

where C = the ^{222}Rn equilibrium concentration (Bq/m^3), M = the mass of sample (kg), V= the total volume of the closed system entailing the sample (m^3), and R = the ^{226}radium concentration (Bq/kg) of the sample.

Some typical average values of emanation coefficients in different materials can be obtained from Fournier et al. (2005) or Ishimori et al. (2013). For minerals, the value is often < 0.05. For solid rocks the values often vary in the interval 0.01-0.2. For soils, due to their various porosities, it is not

surprising that the values range between 0.1 and 0.4. A pozzolanic binder, such as fly ash, often has a reported value < 0.02 (Kovler, 2012). For building materials, such as concrete, reported values of 0.05-0.35 are often documented (Porstendörfer, 1994, Kovler 2012). A short summary of building materials, such as heavy weight (dense) concrete is presented by Porstendörfer (1994). The data originate from Wicke et al. (1978) and Folkerts (1983), and part of the data are presented in Table 3.1. Note the large difference between the diffusion coefficient D, diffusion length of radon L and porosity p when a heavy weight (dense) concrete (as the concrete mixes/recipes are in this study) is compared to an aerated concrete (blue concrete).

Table 3.1. Data from Porstendörfer (1994) for some typical German building materials and their properties.

Property	**Units**	**Heavy weight concrete**	**Areated concrete**
Density, p_b	kg/m^3	2.3	0.5
Effective porosity, p	%	10	50
Diffusion coefficient, D	m^2/s	$7 \cdot 10^{-9}$	$1.3 \cdot 10^{-6}$
Diffusion length, L	m	0.06	0.79
Concentration, ^{226}Ra	Bq/kg	40-60	12-25
Emanation coefficient, ϵ	%	2-4	10-25
Exhalation rate, E	$(Bq/m^2)/s$	$2\text{-}6 \cdot 10^{-4}$	$1.3\text{-}6.6 \cdot 10^{-4}$

3.4.3 Carbonation

The effect of concrete carbonation on the radon exhalation rate has rarely been reported in the literature (Cozmuta et al., 2003), but diffusion measurements of concrete prior to and after carbonation indicate microstructural changes of the pores system and pore sizes within concrete materials (Utgennant, 2004, Ning et al., 2017, Wu and Ye, 2017, Boumazza et al., 2020, Justnes et al., 2020). This further implies that a change in the radon gas release rate due to carbonation and may take place.

The carbonation of concrete is a process that is initiated by the reaction between CO_2 in contact with the concrete's pore water (Justnes et al., 2020). CO_2 is dissolved and reacts with Ca^{2+} in the pore solution to form calcium carbonate ($CaCO_3$) or similar polymorphs such as vaterite, calcite, and aragonite (Lagerblad, 2017, Justnes et al., 2020). The reaction product $CaCO_3$ normally precipitates in the pore system. The permeability of concrete also changes due to the process of carbonation (Ning et al., 2017, Lagerblad, 2017, Justnes et al., 2020).

Carbonation is a moderately slow process, and the rate is dependent on the CO_2 content in the air. Increasing the CO_2 content accelerates the carbonation process. The carbonation process also requires a humid environment because CO_2 cannot be dissolved without the presence of H_2O (Kurda et al, 2019). The carbonation process, Eq. 3.29-32, can in a simplified approach be described according to, e.g., Lagerblad (2017) as

$$CO_2 + H_2O = HCO_3^- + H^+ \quad (3.30)$$

$$HCO_3^- = CO_3^{2-} + H^+ \quad (3.31)$$

$$Ca^{2+} + CO_3^{2-} = CaCO_3 \quad (3.32)$$

$$Ca(OH)_2 + 2H+ + CO_3^{-2} = CaCO_3 + H_2O \quad (3.33)$$

As shown, an input of carbon dioxide (Eq. 3.30) generates bicarbonate ions, and carbonate ions (Eq. 3.31) are produced in the pore solution. These carbonate ions will react with the calcium ions (Eq. 3.32) to form calcium carbonate (Lagerblad, 2017, Justnes et al, 2020, Qin et al., 2019, Saillio et al., 2021). In the process of carbonation calciumhydroxide ($Ca(OH)_2$), as part of the initial pore solution, is consumed or dissolved causing calcite precipitation/carbonation (Eq. 3.33), preferably in the capillary pores (Ning et al., 2017, Lagerblad, 2017).

The use of pozzolanic additions such as fly ash and slag (hydraulic binder) also generates different volumes of secondary carbonation products and polymorphs, such as calcite, vaterite and aragonite (Justnes et al., 2020).

The carbonation process also includes the consumption of the CSH-gel (Boumazza et al., 2020, Justnes et al., 2020), Lagerblad, 2017, Utgenannt, 2004). Binders containing less CaO (calcium oxid) such as pozzolanic SCMs are prone to start the carbonation of the CSH-gel faster than binders containing only ordinary cement clinkers with a large amount of CaO (Justnes et al., 2020, Lagerblad, 2017). As most of the calcium hydroxide ($Ca(OH)_2$) is eventually used up, the calcium silicate hydrate (C-S-H) will also be dissolved (Justnes et al., 2020, Lagerblad, 2017). Lagerblad (2017) also states that a CSH-pore structure in the concrete matrix, when SCMs (such as fly ash) are used as part of the binder in concrete recipes, can show a more porous capillary pore system.

A fundamental principle of carbonation is the result of the reaction. Papadikis et al. (1989) showed a theoretical model giving a good agreement with experimental results. The considerations of the model take into account that there is a porosity decrease (more solid concrete) due to the fact that calcium carbonate, which formed as a result of the process, has a higher molar volume than calcium hydroxide and calcium silicate hydrates. This is also in agreement with studies by Utgennant (2004) investigating the effect of carbonation with regard to the salt-frost resistance of concrete. He tested different concrete mixes containing SCMs (microsilica and slag) at different w/b ratios. He also compared carbonated and non-carbonated mortars at a w/b ratio of 0.55 with SCMs of slag and silica. In all cases, the carbonation process induced a “coarser” pore structure, even though the total porosity was lowered (as Papadakis concluded) compared to the uncarbonated specimens. It was clearly demonstrated that granulated blast furnace slag at higher amounts in the cement physically generated a coarser pore structure. Normal concrete contains much more calciumhydroxide ($Ca(OH)_2$) than cement pastes with SCMs such as fly ash and silica. Calciumhydroxide also dissolves much more easily than the C-S-H matrix (Lagerblad, 2017). Thus, for a normal concrete, with a binder of mainly ordinary Portland cement (CEM I), it can be assumed that most Ca ions in the carbonation process will meet carbonate ions in the pore solution to precipitate in the capillary pore system, since most of the C-S-H-gel is still intact (Lagerblad, 2017). Consequently, the precipitation of carbonates in the capillary pore system will generate a slow decrease of the porosity and ultimately a densification of the concrete paste, and a lower gas diffusion rate will be the result.

Similar findings have recently been documented by Justnes et al., 2020, Boumazza et al., 2020 and Qin et al., 2019. Justnes et al. (2020) compared the carbonation ingress into cement pastes after 14 and 56 days of carbonation using CEM I and CEM IIB-V (~30 % fly ash) as binders. After carbonation for 56 days the researchers identified two trends:

(i) a decreased diffusion coefficient for a carbonated reference cement paste containing primarily CEM I and
(ii) an increased diffusion coefficient for the binder with CEM II/B-V compared to the non-carbonated reference specimen.

These differences in the diffusion coefficients of the binder mixes containing only OPC as references and cements containing SCMs could, according to Justnes et al. (2020), be explained by changes in the mean pore diameter of the carbonated samples.

Concretes containing SCMs contain much less CH (Saillio et al., 2021, Justnes et al., 2020), as previously stated, and are also continuously consumed in the hydration process by pozzolans. Thus,

carbonation for these types of concrete, containing large amounts of SCMs, may be initiated primarily in the C-S-H-gel. In the carbonation process, the C-S-H-gel is slowly dissolved, and carbonate ions enriched in the capillary pore system may well precipitate as $CaCO_3$, not only in the C-S-H matrix by replacement in the capillary pore system but also in gel-pores (Lagerblad, 2017). This effect will render a coarsening (dissolved carbonate ions) of the capillary pores system as noted by Utgenannt (2004), but also a densification of the gel pore matrix. Lagerblad (2017) also suggested the volumetric aspect, where SCMs often generate much more vaterite instead of calcite. Lagerblad (2017) further emphasised that the role of the polymerisation of the Mg ions may play an important part in increasing the porosity of especially slag (GBFS). In the leaching process of C-S-H with Mg ions, polymerisation occurs, forming clay like sheets. This polymerisation would contract the gel and an increased porosity would result.

These physical and chemical replacement processes as part of the carbonation process of the cement matrix has been of interest in this thesis, particularly when a coarser pore structure can be inferred (Justnes, et al., 2020). The change in pore structure, i.e., changes in pore size, may, of course, influence the radon diffusion coefficient and the radon exhalation rate of different concretes. Consequently, part of the thesis also embraced the possible influence of carbonation upon the radon mass exhalation rate and radon mass transfer (diffusion) at a fixed relative humidity. The results and set up of the carbonation studies are further presented in Chapters 4, Section 4.10, and Chapter 5, Sections 5.13 and 5.14. The findings are also presented in Paper V.

4 Methodology

The study has focused largely on the effects of relative humidity and its influence upon the radon exhalation rate as well as different concrete recipe´s diffusivity as a function of the relative humidity. This has been the core of the dissertation and have been addressed in Paper II and III. The onset of the major experiments (Paper III) presented within this dissertation was due to some preliminary results presented in Paper II, where a distinct difference in the radon gas exhalation rate was observed at an early phase of the experiments. The assessment approach, described in Paper II, was to compare three different concrete recipes at different relative humidity levels; (i) one concrete recipe contained a cement binder of only Ordinary Portland Cement (OPC), (ii) one had an addition of a liquid hydrophobe (Hycrete X1002) as an additive and (iii) one had a combination of binders containing OPC and a Supplementary Cementitious Materials (SCM) of fly ash of 10 % (w.t %). Accordingly, it was noted a large difference between the concrete recipes on the radon gas exhalation rate, that likely was caused by the mixing of cementitious binders and possibly also an influence on the radon gas exhalation rate by adding a liquid additive to one of the concrete mixes. These results initiated the onset of some long-term tests presented within this dissertation of approximately two years, Part of these long-term tests is also presented in Paper III.

The major study, comprising a two-year period, contained twelve different concrete recipes, and focused on the different concretes effects on the radon gas exhalation rates and diffusivity as a function of their relative humidity. Complementary tests were also performed to further assess other external influences on the radon exhalation rate. Such influences included the (i) effects of cracks upon the radon gas exhalation rate (Paper IV) as well as (ii) the influence of carbonation (Paper V) at a fixed relative humidity (figure 4.1). Paper I was focused on gamma radiation and different concretes final effective dose to humans and was presented in Döse´s technical Licentiate, "Ionizing Radiation in Concrete and Concrete Buildings – Empirical Assessment" (2016). Even though interesting, the influence of gamma radiation from a human health perspective is not further elaborated upon within this dissertation.

It can be noted that the concept in Paper I contained testing of ten different aggregates, with different levels of natural radioactivity, but using the same cement binder and similar w/b ratio as in most of the experiments undertaken in the dissertation. In papers II, III, IV and V the approach was different; an identical aggregate was used, but instead a variation in the binder content, with different amounts of mineral additions and additions of different liquid additives was evaluated.

The description of the working procedure under this section relates mostly to the major study, as mentioned presented in part in Paper III. The overall time elapsed of performing all experiments as part of the dissertation was approximately 3 years. This also embraced (i) a minor study to investigate the influence of hydration upon four different concrete recipes in the time interval between three and six months. It also comprised (ii) casting of seven "cement paste recipes" identical to the ones used in the major study apart from that no aggregates were used. These "cement paste recipes" was investigated by Mercury Intrusion Porosimetry (MIP). The influence of cracks as a function of the radon exhalation rate (Paper IV) as well as the influence of carbonation upon the radon exhalation rate of different concrete recipes (Paper V) are presented as separate sections within this Chapter to clarify the working procedure in each case.

Figure 4.1 presents a layout of the experimental plan and respective link to Papers presented.

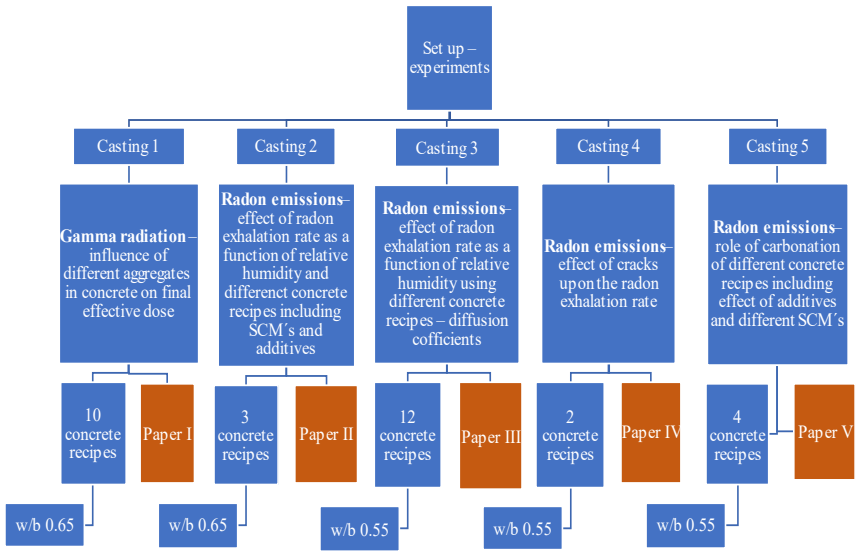

Figure 4.1. The layout of the experiments undertaken as part of the dissertation. In brown colour is the link to each Paper presenting the study.

Those experiments presented within the dissertation that is strongly linked as part of what is defined as "the major study" is shown in Figure 4.2. As illustrated, it can be noted that MIP measurements of the cement pastes of some recipes in part can be viewed separately but compared to the results of the concrete experiments.

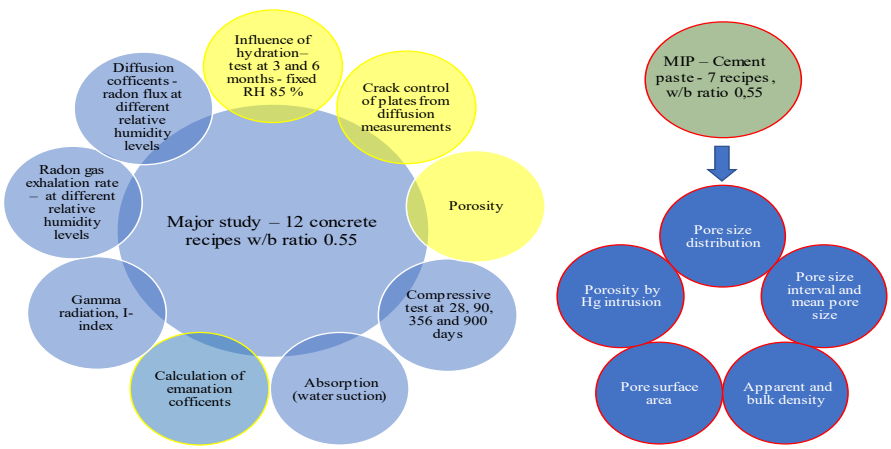

Figure 4.2 Illustration of the different experiments as part of the major study containing twelve different concrete recipes (left part of figure). The right part of the figure shows the set up from the MIP-study by comparing seven different binders of cement pastes with the same w/b ratio as the concrete mixtures. In yellow circles, complementary tests as part of the major study are shown.

4.1 Concrete properties, binders, admixtures and aggregates

4.1.1 General

Prior to initiating the experiments used in the major study, minor research of the commonly used concrete recipes by the precast concrete industry for housing were undertaken. The w/b ratio values used by the industry for housing purposes varied in the interval of 0.4 - 0.65. Even though many industries use casting in place, the precast industry was predominantly asked due to the strong relation to housing and buildings.

The study presented within Paper I and II used a w/b ratio of 0.65 and a binder from Cementa AB/HeidelbergCement Group, Sweden defined as CEM II/ A-LL 42.5 R. For the major study (Paper III) and the forthcoming studies (Paper IV and V) identical aggregates as in Paper II was used in each case. The binder used was an Ordinary Portland Cement - CEM I 52.5 R from Cementa AB/HeidelbergCement Group, Sweden. The w/b ratio was chosen to be 0.55.

The concrete recipes and different binder combinations, including abbreviations for each concrete recipe are presented in Table 4.1. The experimental plans for each separate study (Paper II, III, IV and V) is presented in the following sections.

The experimental plan of the Paper I can be found in Döse (2016) and is not within this dissertation presented further.

Experimental plan

Set up – Paper II

The experiments' purpose was to investigate the effects of fly ash and a hydrophobic agent as parts of different concrete mixes and their effect on the final radon exhalation rate. The radon gas exhalation rates of three concrete mixtures were assessed as a function of the relative humidity (RH). The concrete mixes contained (i) CEM II, (ii) CEM II and fly ash (class N, where 10 % of the Portland cement weight was substituted by fly ash) and (iii) CEM II with an addition (~2 % of the binder weight) of a liquid admixture/ hydrophobic agent (Hycrete 1002).

The principle of the set up for casting and necessary preparations is shown in Figure 4.3

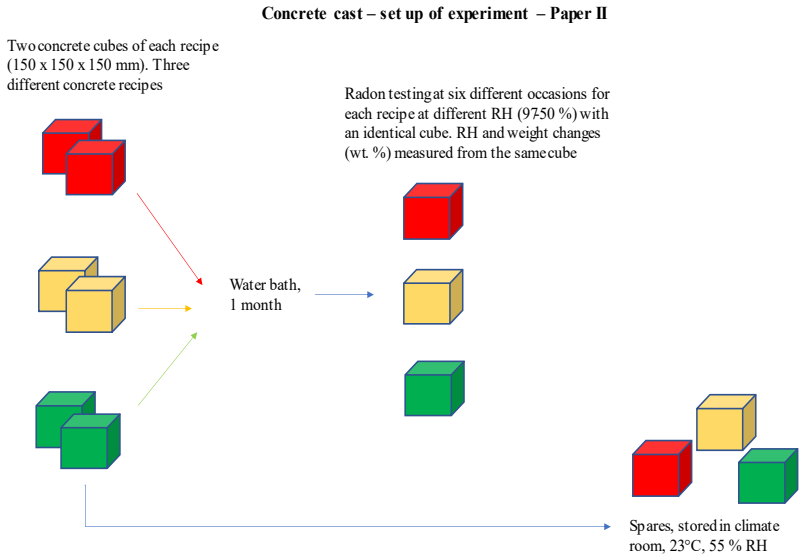

Figure 4-3. Set up for experiment conducted and presented in Paper II.

Set up – Paper III (major study)

The main purpose of the study was to assess the influence of supplementary cementitious materials such as slag, micro-silica and fly ash as part of different binder systems and what effect this would have on the radon exhalation rate at different relative humidity levels. Secondly, the study also embraced the effect of each concrete mixture's diffusion characteristic (diffusion coefficients) at different relative humidity levels. Only initial results at a relative humidity of 75 % are presented in Paper III.

The major study also embraced separate assessments, such as MIP studies including porosity assessment, specific surface and pore radius distribution of each binder system.

The major study included twelve different concrete recipes, where each batch consisted of eight concrete cubes (150 x 150 x 150 mm) and five prisms´ measuring 300 x 75 x 75 mm. The prism´s were cut in half where one part of each prism was used for radon measurements and the other part were used as spare or as a measuring device of relative humidity (RH) for the prism´s at 10 and 25 mm´s depth. Figure 4.4 presents the layout of each cast recipe and its intended use.

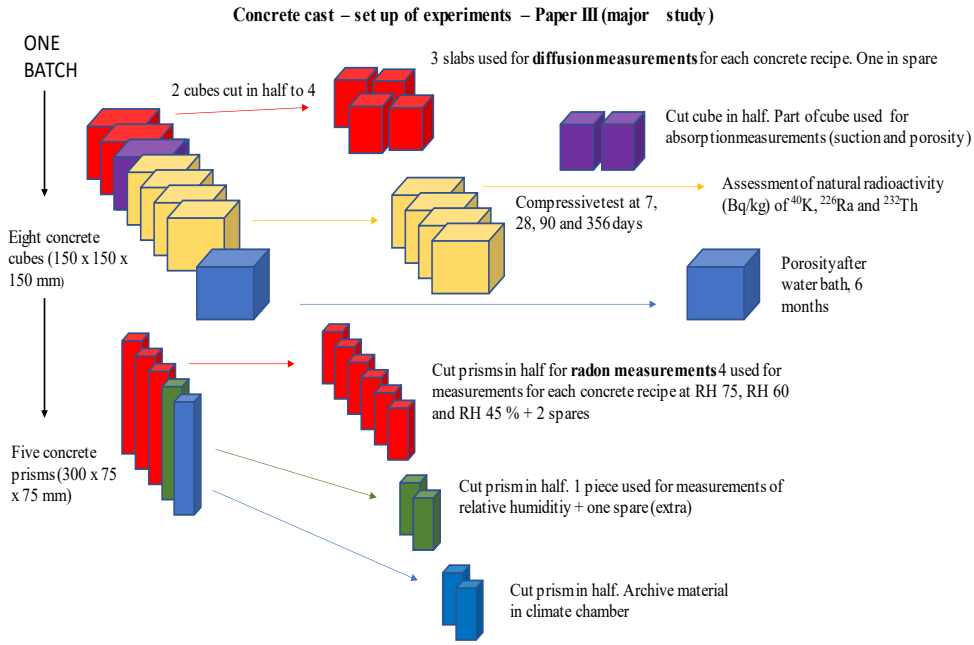

Figure 4.4. Set up for experiment conducted in Paper III (major study).

Set up – Paper IV

The experiments' purpose was to investigate the difference of the radon gas exhalation rate from a concrete slab in a pristine state of a concrete compared to as extensively cracked. Two different concretes recipes were cast. One with Ordinary Portland Cement (C) and one containing and additive (C-H1). Figure 4.5 presents the setup of the experiment.

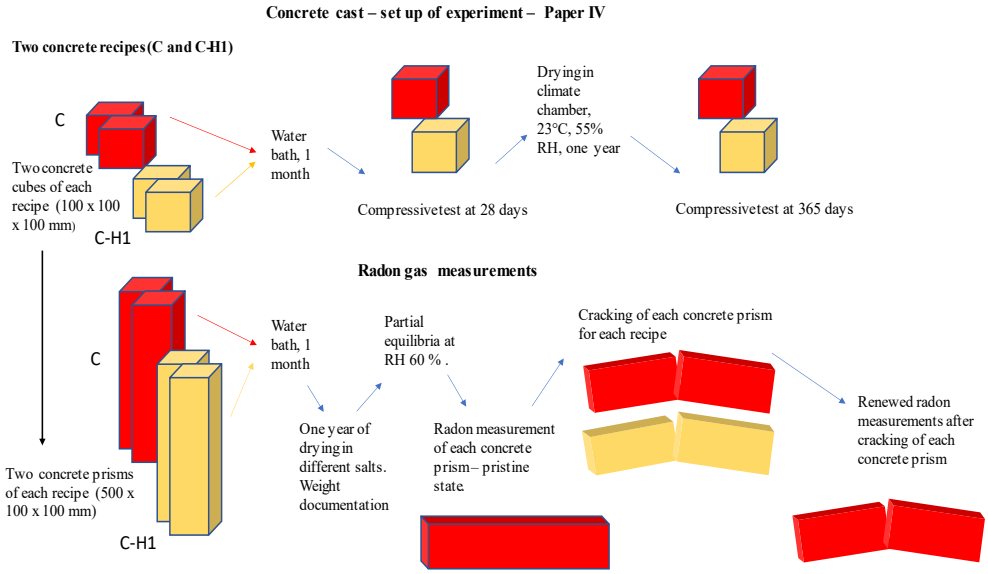

Figure 4.5. Set up for experiment presented in article 4.

Set up – Paper V

The purpose of the study was to investigate the effects of carbonation of four different concrete mixes (recipes) at a fixed relative humidity. The relative humidity was set to 75 %. The recipes included (i) an Ordinary Portland Cement (C), and an almost (ii) identical concrete recipe as "C" with only an added admixture (bulk additive/liquid) as well as (iii) a concrete recipe containing a high share of fly ash (C-F15-MF20) and (iv) one concrete mix containing >60 wt.% of slag (C-S65) as a supplementary cementitious binder (SCM). Figure 4.6 presents the setup of the experiment.

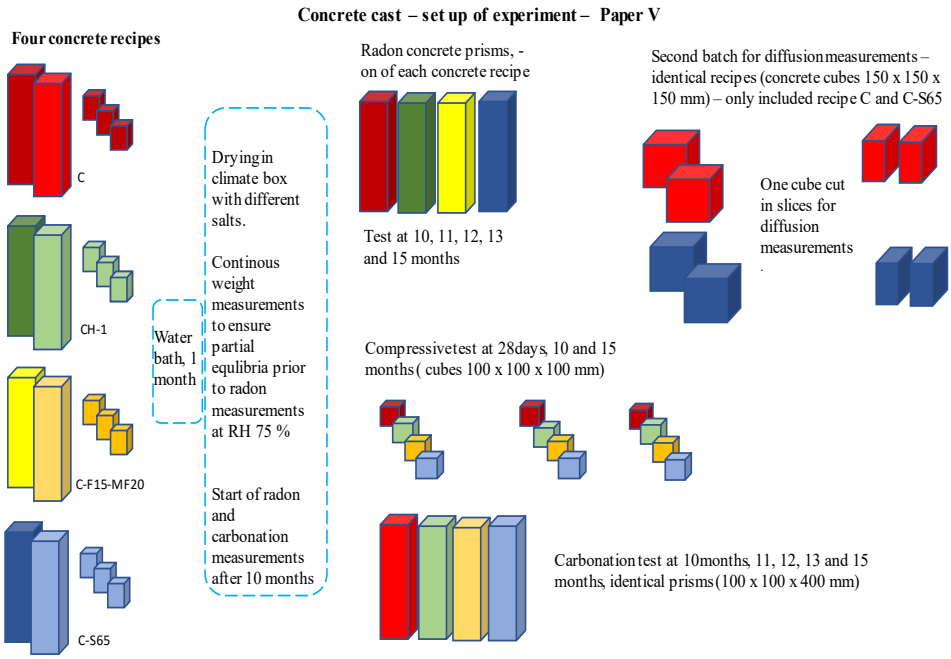

Figure 4.6. Set up for experiment presented in article 5.

4.1.2 Hydration of cement and pore structure – Paper III (major study)

The hydration of cement and combination of binders are essential keys in the measurements conducted in the major study. The concrete cubes, prisms and diffusion plates used in the experiment were dried for at least 5-6 months before a state of partial equilibrium (at 10 and 25 mm into the concrete) at a relative humidity of 75 % could be accepted. After this period of curing, the hydration process of the different concrete recipes was considered "complete". This is of course debatable. Hydration of concrete prevails over several years (Neville and Brooks, 2010), but in the context of comparing the hydration at ca 6 months to 12 months or 24 months it can be argued that a degree of hydration of more than 95 % was achieved (Hewlett & Liska, 2019) nonetheless of binder recipe. The effects using different SCMs (slag, fly ash, silica) and fineness of the SCMs will all affect the rate of hydration (Mehta & Monteiro, 2006).

The hydration of the different binder combinations is as such not examined in detail. Only mechanical strength is within the project used as an indicator. Furthermore, literature data have been reviewed. For the current experiments included as part of the dissertation a water/binder ratio of 0,55 was used. Literature data imply that a setting of the capillary pores where they become segmented varies in the interval of 14 days to six months (Neville & Brooks, 2010, Mehta & Monteiro, 2006). The differences between speed of hydration are due to the type of cement, w/b ratio and as mentioned, particle size (fineness) of the cement used. The higher the blain value (fineness), or the finer a cement is ground, the faster it reacts (Hewlett and Liska, 2019). This implies that the used rapid hardening cement in these experiments (CEM I – 52.5R), that is very fine ground and dominantly composed of calcium silicates should have a complete hydration cycle within this time span. This further suggests that most C-S-H reactions are expected to be complete prior to initiation of measurements.

Similar experiments as in this dissertation were undertaken by Mueller et al. (2017) using different amounts of SCM´s including fly ash, metakaolin and slag (GGBS) as substituting binders. The reference cement used was a CEM I 42.5 SR (low heat hydration cement from Norcem) and a w/b ratio of 0.45 were applied. Two blended binder mixtures with 15 % and 50 % of fly ash were investigated amongst other concrete recipes. Comparative data of the strength increase between 90 days and 365 days indicate that in the former case a strength increase of ~10 % and roughly 15 % in the latter case was documented. But, it should be noted, a low heat hydration cement was used and the comparative data are in this case in the interval 90 days and 1 year. Similar experiments were conducted using slag (GGBS) instead of fly ash in amounts of 16, 30 to 50 % as part of the reference binder. The results, in the interval, 90 days and 1 year, indicated only a minimal difference (~1- 4 %) in mechanical strength between the concrete mixtures containing slag. The research by Mueller at al. (2017) is of specific interest, since the same type of fly ash as well as slag was used as in the actual experiments.

It is often noted that a fly ash content exceeding 20-30 % markedly slows down the mechanical strength and speed of hydration (Hewlett & Liska, 2019), Consequently, a small investigation of the hydration kinetics was undertaken prior to these experiments (Section 6.6). The radon exhalation rate was measured at 90 days and 180 days with a fixed relative humidity (85 %). Four concrete recipes were investigated, where one concrete recipe contained an OPC (Ordinary Portland Cement) in combination with fly ash and one concrete recipe contained OPC and slag as binders. The two other concrete recipes used only OPC and in one case an addition of ca 2 % bulk additive (admixture) were added to this mixture. The assumption regarding hydration implied that a change in pore structure (due to ongoing hydration) would result in a possibly different exhalation rate if a marked change in pore structure would result in this interval (90 to 180 days). The results could however not detect any significant change (uncertainty included), but a small difference (reduced exhalation rate) was observed for the concrete recipe containing fly ash after 180 days compared to 90 days.

To further investigate the microstructural changes occurring in concrete during the first couple of months modelling of the distribution of the gel and capillary pores as a function of time were performed by Cozmuta et al. (2003). The model clearly illustrates the initial conditions of the young concrete and the evolution of the gel and capillary pores within a concrete (Figure 4.7) from initiation of hydration. The material data behind Figure 4.7 do not completely correspond to those investigated in the current thesis but the trends shown in Figure 4.7 are still of value. The hydration kinetics and scheme followed a multicomponent heat of hydration (Maekawa and Kishi 1999) using a w/b ratio of 0.48 where a slag cement was used as binder.

As a result of some of these findings in literature, the approach has been that the cement structure (pore structure) including the continuous hydration and final distribution of gel- and capillary pores as well as the total porosity of the cement matrix can be regarded as “completed” (Figure 4.7). Thus, while maybe questionable, the concrete pore structure of the cement matrix has been regarded as approximately constant from the onset of radon gas measurements (~5-6 months after casting of each concrete recipe).

It should be pointed out, as mentioned, that the use of different binder combinations will show different hydration curves (Hewlett & Liska, 2019), but Figure 4.7 still serves a good illustration of the the transformation of capillary pores, being partially replaced by gel pores as hydration of C-S-H gel commence in the concrete and successively progresses until a more final distribution is set after approximately 4-5 months (~120 days).

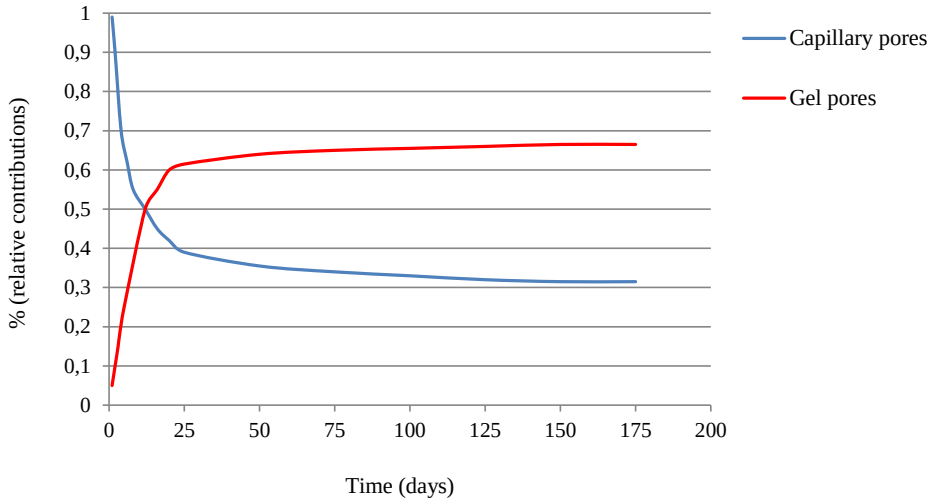

Figure 4.7. Relative contributions of gel and capillary pores within a concrete specimen as a function of time (days). Figure redrawn from work by Cozmuta et al. (2003).

4.1.3 Properties - Consistency, slump and air

For all experiments the slump was measured by a steel cone according to EN 12350-2, *Testing fresh concrete — Part 2: Slump-test.* A slump of 100 mm was regarded as a reference guide to achieve a moderate workability of the concrete. In all cases a slump between 70 and130 mm was reached after final mixing.

The air content was measured by the "pressure gauge method", according to EN 12350-7, *Testing fresh concrete — Part 7: Air content — Pressure methods.* In most cases an air content of 0.9 to 1.3% was recorded.

Regarding the casting, the different concrete recipes was mixed for at least 5 minutes to get a good workability. A plasticizer, "Sikament 56", was in a few cases added in minor amounts if the blend did not mix properly. The pouring of the concrete into the molds followed the recommendations of compaction and filling procedure described in part in EN 12350-6, *Testing fresh concrete — Part 6: Density*. The concrete was vibrated twice (two step filling of the concrete) in short sequences (approximately 15 seconds each time) before the cast was set to rest in the molds.

4.1.4 Supplementary Cementitious Materials (SCMs), hydrophobic admixtures and efficiency factors of the recipes – Paper III

The constituents used in the concrete recipes where: (i) admixtures (hydrophobes) added as liquid solution to the mixture and (ii) and Supplementary Cementitious Materials (SCM´s). The SCMs included different types of fly ash, one type of slag and one type of micro silica. The different recipes included different amounts of SCM's. Table 4.1 presents the recipes used and presented in Paper III with their different constituents of admixtures and SCMs, including their specific amounts. Identical mixtures were later cast for some of the recipes for the experiments presented in Paper IV and V.

To avoid any discussion in relation to different efficiency factors (k-factors, SS-EN 206-1) of different binders, each binder was considered to have an efficiency factor, $k = 1$ implying that an exchange of

an amount of OPC with an equal amount of SCM will give an equivalent compressive strength at 28 days (SS-EN 206-1). The general assumption involves a comparison according to the concept that the "water cement ratio" is replaced by "water/cement + ***k*** x SCM", expressed as w/b ratio. Consequently, the SCMs that substituted the reference cement in some concrete recipes was exchanged in amounts defined by the weight of the reference cement.

Slag, being a hydraulic binder (contains a lot of $Ca(OH)_2$) is under the context of SCM, considered as a supplementary cementitious binder, even though its properties in part differ from the ones of the other SCMs having pozzolanic properties (fly ash and micro silica).

Table 4.1. The concrete recipes and its constituents with defined amounts. "X" indicates its use in the recipe. The admixtures constituted ca 2 % of the total binder weight.

		Aggregates		**Binders**					**Admixtures**		
				Cement	**SCMs (Supplementary Cementitious Materials)**						
Recipes	**Abbreviations in text**	**Aggregate 1**	**Aggregate 2**	**Cement**	**Fly ash, class F**	**Fly ash, microsite**	**Slag**	**Micro-silica**	**Hydrophobic agents**		
				Weight							
				(%)	(%)	(%)	(%)	(%)			
		Granite	Diabase	CEM I - 52.5R					H1	H2	H3
1	C	X		100							
2	C-H1	X		100					X		
3	C-H2	X		100						X	
4	C-H3	X		100							X
5	C-F15-MF20	X		65	15	20					
6	C-MF35	X		65		35					
7	C-S65	X		35			65				
8	C-SF10	X		90				10			
9	C-SF30	X		65				35			
10	C-FM15-SF10-H1	X		75		15		10	X		
11	CGB		X	100							
12	CGB-H1		X	100					X		

The contribution of different SCMs in the recipes also effect the color of the final concrete (Figure 4.8).

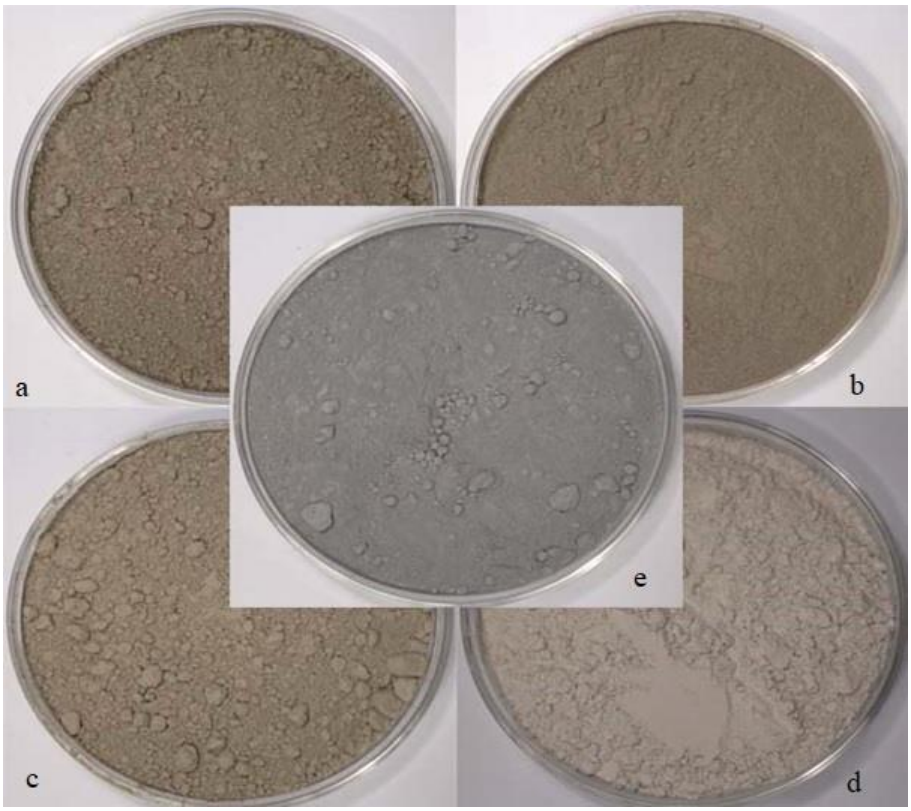

Figure 4.8. Five different SCMs/binders used in the recipe´s. (a) Fly ash, (b) Micro fly ash, (c) Cement (Skövde CEM I-SH 52.5 R). (d) Slag from Bremen and in the middle (e) Micro silica – 940.

4.1.5 Aggregates and concrete recipe – Paper III

The study focused on using one rock type with an activity concentration in Bq/kg of ^{40}K, ^{226}Ra and ^{232}Th, that was slightly above an average value of a Swedish crystalline rock. This approach was used as to ensure high measurable concentrations of ^{222}Rn and subsequently minimize the uncertainty during measurements. As a reference rock type, a diabase/gabbro was chosen, that, in contrast, contains a very low concentration of the radioactive radionuclides (^{40}K, ^{226}Ra, ^{232}Th), Figure 4.9.

Ten different recipes using the same rock type (crushed rock aggregate) were designed. In two cases, a "reference rock type" with a very low activity concentration (Bq/kg) was utilized instead, but with the same prerequisites in its concrete composition as for recipe one and two (Table 4.1). In summation, the concrete recipes "CGB" and "CGB-H1" were identical to recipe "C" and "CH-1", but with another rock type. Thus, overall, twelve different recipes were designed.

Two particle size fractions were used for each recipe. The predominate red granite used had a particle size of 0-5 and 8-16 mm. The diabase used the particle size fractions of 0-8 and 8-16 mm. The lack of the medium size particle fraction 4-8 mm for the red granite was simply due to the that the producer mostly delivers aggregates for asphalt and roads, where the particle size fractions 0-5, 8-11 and 8-16 mm are more commonly used. In preliminary tests of the concrete specimens, the used particles size

fractions of 0-5 and 8-16 seemed to satisfactorily produce a descent concrete quality, and as such, it was concluded as sufficient.

Figure 4.9. Aggregates used in the recipes. (a) Red granite, particle size fraction 8-16 mm. (b) Grey-black diabase/gabbro, particle size fraction 8-16 mm. (c) Red granite, particle size fraction 0-5 mm. (d) Grey-black diabase/gabbro, particle size fraction 0-8 mm.

4.1.6 Different SCMs in the concrete mixes and their mean diameter (d_{50}) and density

A compilation of the used materials regarding their grain size is summarized in Table 4.2. The mean diameter of a particle size distribution is normally expressed as $d_{50.}$ It relates to the fineness of the cement or SCM. The efficiency factor, *k* as described in Chapter 4, Section 4.1.4, was for each recipe set to 1. Table 4.2 presents the different binders, their mean diameter grains size (d_{50}). compact density (Bq/m^3) and k-factor.

Table 4.2. An overview of the different grain sizes (d_{50}) and compact densities as well as used k-factor in the different concrete recipes.

Product	Grain size (µm)	Compact density (kg/m^3)	k-factor in recipes
	d_{50}		
Fly ash	15	2270	1
Fly ash (microsite)	<5	2510	1
Slag (Bremen)	30	2900	1
Micro silica (grade 940)	0.15	2250	1
Cement, RH (Skövde	20	3125	1

4.1.7 Concrete recipe – Paper III

A standard CEM I – Skövde CEM I SH 52.5 R (rapid hardening) from the Skövde cement factory/Cementa AB/HeidelbergCement Group was used as the primary binder. A cement-content of 350 kg/m^3 was applied. For concrete used for dwellings a minimum strength class of at least C40/50 was set as the primary target (Table F.1, SS-EN 206). Using the current w/b ratio, a strength development of approximately 55-65 MPa (28 days) could be anticipated for the concrete specimens (mixes). The component of air was measured to be approximately equal to 1.0 vol %.

A difference in strength development was anticipated due to the different proportions of supplementary cementitious materials, such as fly ash, micro silica and slag (Leung et al. 2016, Neville & Brooks, 2010, Mueller et al. 2017). Table 4.3 presents the general recipe of the concrete specimens using a w/b ratio of 0.55. A summary of the designed concrete mixes as part of the major study are found in appendix A1.

Table 4.3. Quantities (in kg/m^3 and weight %) of the different constituents in the concrete specimens for the reference concrete recipe "C" containing only CEM I – SH R -binder.

Constituents	**kg/m^3**	**Weight (%)**
Cement, CEM I - Skövde	350	14.8
Crushed, aggregate, 0/5 (55 wt%)	821	34.7
Crushed, aggregate 8/16 (45 wt%)	1004	42.4
Water	192	8.1
Superplasticizer (Sikament 56)	~1	-
Total	~2369	100
w/c ratio	**0.55**	

4.1.8 Hydrophobic admixtures – liquid additives – Paper III

In the study in Paper III three different admixtures were used. They are, as previously mentioned, all liquid fluids, that are mixed into the amount of the water of the recipe before being added to the blend of the rapid hardening cement (in one case also fly ash and micro silica) and aggregates in the final concrete mix

The three different admixtures with properties including manufacturer are presented in Table 4.4. In Figure 4.10 their ocular appearance is shown. Their respective amounts were in accordance with the manufacturers' recommendations of approximately 2 % of the total binder weight.

Table 4.4. Admixtures used in three of the concrete recipes.

Additive	**Industrial name**	**Hydrophobic/hydrophilic**	**Company**
C-H1	Silres 1801	Hydrophobic	Wacker
C-H2	Silres 1802	Hydrophobic	Wacker
C-H3	Hydrofob 1	Hydrophobic	SIKA

Figure 4.10. The different additives used in three of the concrete recipes. From left to right; C-H1, C-H2 and C-H3.

4.1.9 Density of materials/constituents (kg/m^3) used in different experiments

The density of the constituents was checked by a gas pycnometer at RISE. The instrument is calibrated on a yearly basis. The densities were also controlled with the information given by the producers (declared values). A strong agreement between measurements and declared values was validated.

4.1.10 Monitoring of concrete samples during the experiments

Concrete casting usually produces some cracks (Neville & Brooks, 2010). The cement paste may shrink up to 8 % during the hydration process (Neville and Brooks, 2010). Normal procedures to minimize cracking to numerous minor tiny cracks is to use reinforcements or an addition of fibres (Mehta & Monteiro, 2006).

The main aim during these experiments was to prevent a major effect from open cracks, that may largely contribute to changes in the release of the radon gas exhalation rate (Paper IV). If major cracks would not be prevented, the evaluation of the binder effect upon the radon gas exhalation rate would be difficult or even impossible to assess. Thus, due to the awareness of this risk, that a "normal concrete" may develop micro-cracks during its initial hydration, a procedure was adapted to minimize this possibility, but also to discover and if so register changes before initiation of measurements.

Crack development was foremost attempted to be hindered by cooling of the concrete recipes in water (first month) with a continued period of high relative humidity (85 % RH) surrounding the samples the following 2 months. An ocular inspection was made after 3 months and prior to initiation of each measurement at RH 75 %. A more thorough review (Section 4.11) was also made after closure of measurements on some of the concrete slabs and prisms (~2 years after initiation of measurements). This approach intended to clarify if cracking may have developed during the time of conducting experiments (Chapter 4, Section 4.11, and Chapter 5, Section 5.8).

At the startup of measurements, a brittle failure occurred for sample C-H1, D3 (150 x 150 x 50 mm), being a plate used for measurements of the radon gas transport (diffusivity). The failure/crack was however likely due to uneven load applied by the equipment onto the sample/plate when "locked in place" by nuts and bolts. Due to this early failure, the plate could be replaced by one of the "spares", C-H1, D2 for measurements at RH 75 % and on forth.

4.2 Analysis of gamma energies of the constituents and the concrete mixes

To properly analyze the activity concentrations of the natural radionuclides most of the different constituents used in the study as well as all the concrete mixes (recipes) produced in the main study were sent for gamma spectrometric analyses to an accredited laboratory. The accredited laboratory, Radiation and Nuclear Safety Authority (STUK) is situated in Helsinki, Finland. Their methodology follows a nationally accredited method, VALO GUIDE 4.5 that applies a measurement technique (semi-conductor measurement) identical to the one suggested by the European technical standard CEN/TS 17216:2018. The technique, as mentioned, using gamma-spectrometry is described in more detail in Döse (2016) and Paper I.

The different constiuents and concrete mixes were prior to analyse prepared at RISE. Investigating the different binders required to sample at least 4 kg of each material. Sampling was taken in small portions from each material at different heights and horisontal locations of their respective volumes (sample not taken from one location). The small test portions taken from each material were thereafter blended to one sample. This was done in order to maintain a good representation of each materials' variations within their volumes.

Each constiuents material was thereafter split once, where 2 kg was sent for analysis and 2 kg kept as archive material.

To properly assess the gamma radiation of each specific concrete recipe, the following procedure was adopted:

(i) one cast cube of each concrete mix was assigned for evaluation of gamma spectrometric analysis,
(ii) each cube from a concrete mix were cut in two halves where one half was archieved,
(iii) the other half was chrushed with a laboratory jaw crusher to achieve a particle size fraction of ~0-16 mm, that was finally sent for analysis.

The reported uncertainity as part of the gamma spectrometic analysis is given, for each investigated radionuclide, with a 95 % confidence level (2σ). In most cases the uncertainity of the radionuclides is in the span of 8-10 % as also reported by Döse (2016).

4.3 Sampling and casting

4.3.1 Aggregates

To have similar conditions and to achieve good workability of the concrete, a reference aggregate sieve curve prescribed in SS-EN 1766 was used as a template before mixing the concrete. The initial sampling of delivered aggregates was made according to the standard SS-EN 932-1 where the material within the bags were collected from different depths and units of the delivered woven bags (approximately 500 kg in each bag). Approximately 60 kg of each particle size fraction were collected for each recipe before mixture of the aggregates commenced prior to mixing the concrete.

4.3.2 Finalizing the concrete recipes of the major study (Paper III)

Figure 4.11 a-d presents different steps during the casting procedure.

(a)

(b)

(c)

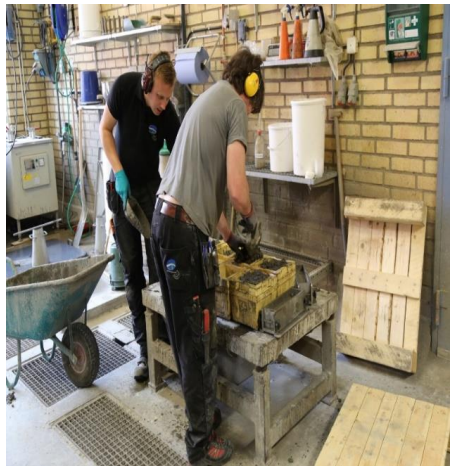

(d)

Figure 4.11. (a) Green buckets containing different binders before mixing with the Rojo concrete mixer/blender. (b) Measurement of slump after casting. (c) Measurement of the air content in the concrete using the pressure gauge method. (d) One concrete recipe being placed in molds prior to vibration.

After casting, the fresh concrete was protected with a plastic sheet to preserve moisture and avoid cracking. Twenty-four hours (24 h) after casting, the cast specimens were demolded and placed in water baths.

After one month in the water bath, the prisms (300 x 75 x 75 mm) intended to be used for radon measurement, were cut in two parts. Each half of the prism was later used as “one prism out of five” in the radon measurements. The final radon prisms had a dimension of approximately 150 x 75 x 75 mm (Figure 4.12).

Figure 4.12 illustrates the different steps of preparation of the concrete cast specimens in its initial phase after casting.

(a) (b)

(c) (d)

Figure 4.12 (a) Concrete cubes and prisms on a pallet after vibrating. (b) Demolding of the concrete cubes after 24h of hydration using air pressure to release the molds. (c) Demolding of concrete prisms resting on a carriage. (d) Prisms, after being cut in two halves resting on a carriage.

From each concrete recipe, two out of the eight demolded cubes, were sawn into plates (50 x 150 x 150 mm) for radon gas diffusion measurements. From each cube, two plates were sawn. All the used measurement plates had freshly cut surfaces. After sawing of one cube, approximately 40 mm's in thickness was left as a "spare slab". The "spare slabs", approximately 40 x 150 x 150 mm, were later used for water absorption measurements and analysis of porosity for ach concrete recipe. So, for the diffusion measurement study, four plates were used for each recipe during the study. Out of the four plates one plate of each concrete recipe constituted the "measurement plate" (Figure 4.13), that were used to calculate the diffusion coefficient (D) and the radon diffusion length (L). Another one (plate) was used to monitor the humidity in the concrete at 25 mm and 10 mm. The others (two extra plates)

were used as “reference plates” of the weight loss during the hydration process but also to check the variation of the diffusion coefficient (repeatability) between the plates of each concrete recipe/mixture.

Figure 4.13. Cut samples from the cast concrete cubes resting on a carriage. The “measurement plates” constitutes one plate from each of the recipes (all in all, 12 different concrete recipes). From lower right corner to upper right corner the recipes numbered from 1-12 are shown clockwise.

4.4 Timeline for evaluation of different materials of the major study

To ease the understanding of the measurements in the major study, a scheme of time is shown, that addresses what and when specific tests were performed. The scheme describes in brief how the specimens were stored, cut, and handled in between all the testing. Table 4.5 describes only an overview but gives an understanding of the general procedure that has been in focus during this study. The blue arrows in Table 4.5 indicate when measurements started for each level of relative humidity (RH 75 %, 60 % and 45 %) and give a measure of the slightly squeezed time frame to finalize the measurements at each relative humidity. The columns with colors, also depicts the stage, when samples after measurement were put in the containers with a new salt (for continued dry out/desorption).

Table 4.5. An overview of the measurement process, starting at a relative humidity of 75 %. Blue arrows indicate approximately start and stop of each measurement interval at different relative humidity levels.

Date	Relativ humidity (%) in the atmosphere surrounding the cubes/prisms			Notes
2017-05-01				After 24 hours - casting and demolding. Water curing during first month
2017-06-01	100			Drilling and mounting directly after finalisation of water bath.
2017-07-01	85			Climate room
2017-08-01	85			Climate room
2017-09-01	75			Climate room
2017-10-01	75			Climate room
2017-11-01	75	60		Climate room
2017-12-01	75	60		Climate room
2018-01-01	75	60		Climate room
2018-02-01	75	60		Climate room
2018-03-01	75	60		Climate room
2018-04-01		60		Climate room
2018-05-01		60	45	Climate room
2018-06-01		60	45	Climate room
2018-07-01		60	45	Climate room
2018-08-01		60	45	Climate room
2018-09-01		60	45	Climate room
2018-10-01		60	45	Climate room
2018-11-01		60	45	Climate room
2018-12-01			45	Climate room
2019-01-01			45	Climate room
2019-02-01			45	Climate room
2019-03-01			45	Climate room
2019-04-01			45	Climate room
2019-05-01			45	Climate room
2019-06-01			45	Climate room
2019-07-01			45	Climate room

4.5 Thickness of materials used for measurements

4.5.1 Thickness of prisms for radon gas exhalation measurements

The chosen thickness of the materials used for radon measurements was due to investigations by Döse (2016). Döse (2016) investigated concrete thicknesses of 150 and 200 mm. The exhalation rates of radon gas using different thicknesses, but the same aggregates and concrete recipe indicated no difference in exhalation rate as a function of thickness. This relates to the thickness as described by Ishimori et al. (2013) as being one parameter to consider relating to the radon production rate (Chapter 3). Consequently, assuming a dense, in part "impermeable" concrete a thickness of ca 150 mm will take into account the longest distances travelled by the radon atoms prior to its final decay of the ^{222}Rn atom. Literature data (Porstendörfer, 1994) also support this conclusion for dense concrete (2.350 kg/m^3). Due to these findings, the cast prism with a length of 300 mm (Figure 4.14) was cut in two halves, were each half was used as separate prism of ~150 mm in length during the radon gas measurements. In all cases, at least four cut prisms were used (where each one was thoroughly sealed with aluminum tape each time on every side except the top). The separate prism surfaces were added together as "one sample" during measurement. Prior to cutting, the cast samples were checked for any noticeable cracks or defects.

Figure 4.14. Concrete cubes and prisms (300 mm in length) resting on top of cubes prior to being cut in two halves for radon gas measurements.

4.5.2 Thickness of plates for radon gas diffusion measurement

The concrete cubes of each recipe were after one month of curing in the water bath taken out and sawn into plates of 50 mm thick concrete. The determined thickness of the plates was due to earlier investigations by several authors in the interval of 30-100 mm (Folkerts, 1983, Chauhan and Kumar, 2016). Except the fact that the thickness of course affects the diffusion coefficient (Kovler, 2012), the cement paste structure (including pore distribution) is the essential key parameter, that can alter the diffusion rate of radon gas in the concrete. With this in mind it was deemed essential to encapsulate most aggregates thoroughly, with an appropriate cover of the cement paste. A "a rule of thumb" guidance for proper measurement practice of concrete (Book of Concrete, materials II, 2021), it is stated that "the thickness of concrete should be at least three times the largest aggregates size for

proper assessments". Consequently, since the largest aggregate size amounted to 16 mm a final thickness of 50 mm was chosen for the experiments of the radon diffusion measurements.

The storage of each concrete mix during the drying procedure is presented in Figure 4.15. The cut plates used for the measurements as well as the concrete prisms from different concrete cubes used for the radon gas exhalation measurements was placed on a plastic floor cover inside prior to closure of the plastic container with a plastic lid. After each measurement at different relative humidity level, the plates and prisms were stripped of their aluminum tape and put back into the plastic box.

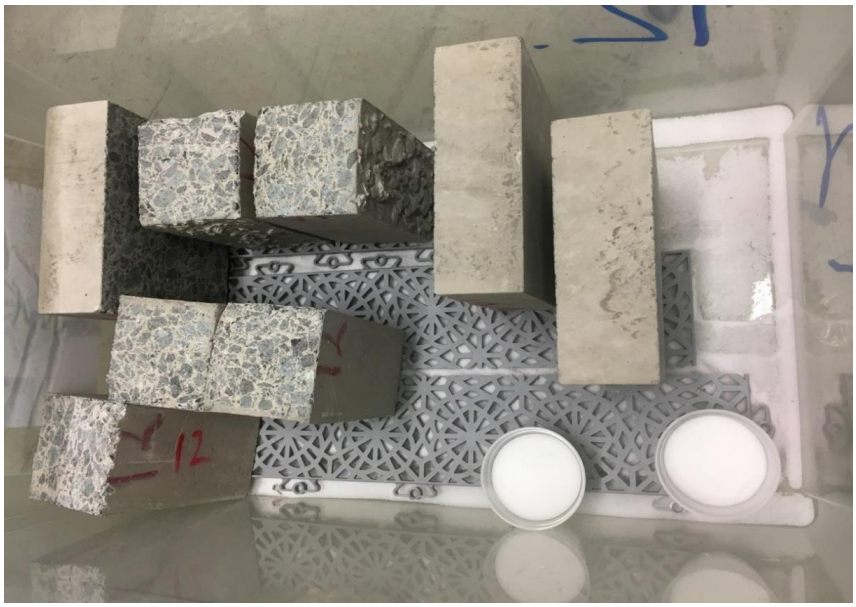

Figure 4.15. Concrete prisms and cut concrete plates (recipe CGB) in their first drying phase to reach approximate equilibrium of RH 75 %. Extra salt is also noted in two small plastic containers.

4.6 Porosity

The porosity of each concrete mix was calculated using its weight difference from initially wet to when the concrete is dry (desorption). The used method resembles the procedure described in SS-EN 130755 (natural stone) at atmospheric pressure. The weight differences of the concrete samples (assuming full water saturation of every pore) are documented and the final weight difference is presumed to account for the pore volume of the concrete specimen, including gel, capillary pores and air voids. Taking the ratio of the pore volume and volume of the specimen gives the porosity p according to:

$$p = V\mathrm{p}/V\mathrm{sp} \qquad (4.1)$$

where Vp is the pore volume and Vsp is the volume of the concrete specimen. Vp assumes water at ~1 liter/kg.

Porosity by use of Mercury Intrusion Porosimetry (MIP) has also been assessed as part of the major study for the cement pastes containing different SCMs as well as the reference cement paste (OPC). However, MIP as a methodology to assess porosity is in part questionable, due to pressure enforced on the materials, that may cause microcracks (Mueller et al. 2017). Therefore, the results, due to some constraints as part of the procedure of the method should be regarded as indicative.

The first set of concrete samples from the main study were documented 6 months after casting. From the main study, one of each concrete specimen/cubes (150 x 150 x 150 mm) from each concrete mix were weighed after 6 months after being water cured since casting. Thereafter the concrete cubes were dried in an oven at 45ºC for 4 weeks. After 4 weeks, the temperature was increased to 55ºC for two weeks and thereafter it was raised to 100ºC. Before each measurement the concrete cubes were placed in a climate chamber at 23°C and 55 % in relative humidity for 24 hours prior to measurements.

A second approach involved using some "concrete spares" available after sawing of the diffusion measurement plates. The size was roughly 60 x 40 x 25 (length x height x width) mm (Figure 4.16). The methodology applied derived from the standard SS-EN 1936 (natural stone method) using vacuum to ensure fully saturated specimens (water filled pores). The drying process included drying of the samples in a small oven at 45ºC until no difference in weight could be registered (assuming dry concrete). The initial step involves that the dry specimens are placed in a vacuum tight container. A pump enables vacuum to be achieved. The samples are then under vacuum for at least 24 hours. Thereafter, water is gently introduced into the container, to assure a good suction of the water into the specimens. After a few hours, the samples are submerged in water and are left for at least 48 hours before measurements are completed.

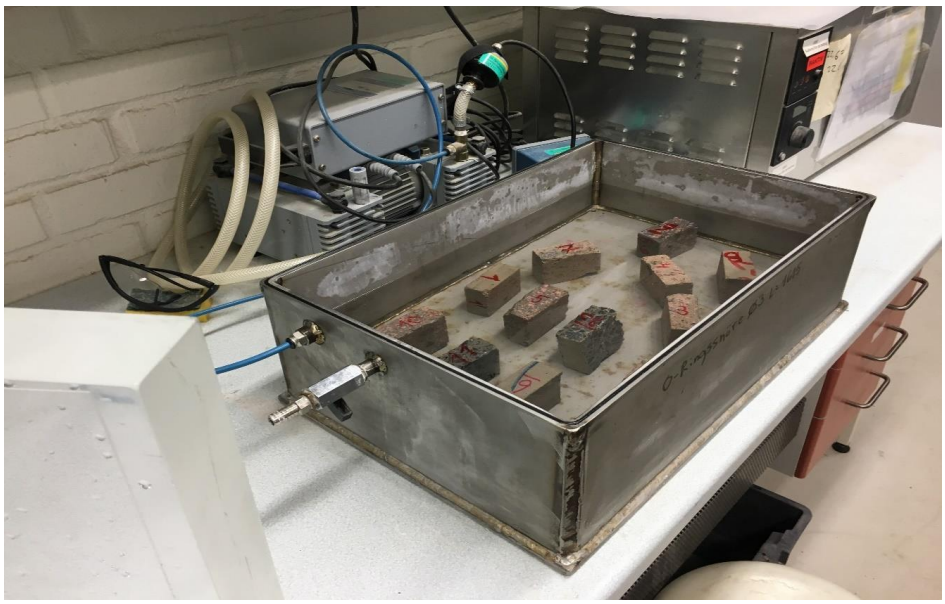

Figure 4.16. Samples immersed in water as part of the assessment of the specimen's porosity.

A third "control study" of four of the recipes were also made. Recipes C, C-H3, C-F15-MF20 and C-S65 (Table 1). The "control study" was done to ensure that the porosities were reasonable in the first study (documented at 6 months), compared to measurements at 28 days of hydration. The control study also served another purpose. Since, this quick drying procedure, previously have been deployed by other authors (de Jong & van Dijk, 1996, Chauhan & Kumar, 2013) it was of interest to check whether any large differences in the concrete mixes porosities would occur due to differences in elapsed time since casting. A small portion was cast of each recipe and at least four cubes (100 x 100 mm) were made. All cubes were after demolding kept in a water bath throughout the hydration phase. Two cast cubes of 100 x 100 x 100 mm for each of the four recipes were assessed and compared with the results of the other studies of porosity.

A slightly more “brutal method” of full water saturation after approximately one month was followed by a quick drying scheme of ~105ºC where the weight difference of each cast prism was documented every 8-12 hours initially. This approach was due to the slightly limited time frame of the project but followed guidance of other authors (de Jong & van Dijk, 1996, Chauhan & Kumar, 2013).

It would likely been advantageous to use the Norwegian PF method (Geiker & Laugesen, 2001), but the author decided to use a simple approach suggested in other articles (de Jong & van Dijk, 1996). Thus, the results may be regarded as indicative. The results are reported in Chapter 5, Section 5.3 and in more detail in Paper V.

4.7 Mercury intrusion porosimetry (MIP) of cement pastes

To better understand the different properties of the concrete mixes containing SCMs, these were also chosen to be evaluated by Mercury Intrusion Porosimetry (MIP). The size and distribution of the gel and capillary pores were of primary interest between the different concrete mixes. Mueller et al. (2017) investigated hydration of concrete binders, including SCMs of fly ash, metakaolin, slag and micro silica. Part of the studies included analysis by use of MIP to understand the different pore size distributions, pore volumes, pore surface areas and total porosities of the different blended cements. Similar investigations have also been conducted by Boumazza et al., 2020, Justnes et al., 2020. Even though apparent, different shares of SCM´s in blended cements will generate different pore sizes and pore distributions in the blended cement paste compared to a reference cement paste (Justnes et al, 2020). Thus, seven recipes were cast including the recipe C, C-F15-MF20, C-MF35, C-S65, C-SF10, C-SF30 and C-FM15-SF10-H1. The recipes included only the reference cement (C) and the different SCMs (only binders, no aggregates) combinations as used in the ordinary concrete recipes. The w/b-ratio was set to 0.55 as for the ordinary recipes. The designed mixes for the study are presented in Appendix A2.

The investigations were performed by BAM (**B**undes**A**nstalt für **M**aterialforschung und -prüfung) in Berlin. The instrument used was a mercury porosimeter PASCAL 140/440 from ThermoFisher Inc. The testing was in accordance with ISO 15901-1 (DIN 66133).

Preparation of the recipes and samples prior to analyze was executed at RISE. The recipes were mixed by a small blender and vibrated thoroughly before being poured into small plastic containers (Figure 4.17a). The containers were thereafter sealed with plastic foil and set for cooling in a water bath for approximately 2 months. Thereafter the samples were stored in a conditioning room (23ºC, 50% RH) for 10 months before preparation of the testing commenced. The samples were sawn and cut into small slices, 4-6 mm thick (Figure 4.17b) and thereafter the slices were cut once again to achieve small specimens, rectangular in shape of 4-6 mm in size (Figure 4.17c). Approximately 6-8 grams of each recipe (minimum, 20 small cubes) were sent to BAM for analysis (Figure 4.17d).

(a)

(b)

(c)

(d)

Figure 4.17. (a) The used plastic container with markers in black for cutting. (b) Cut slices, 4-6 mm thick with a thicker slice to the right. (c) Cut slices in both directions collected in plastic bag with rectangular specimens collected within the plastic bag. (d) Cut slices of each recipe (7 recipes) collected in plastic bags and resting on the laboratory board before delivery.

4.8 Measurements of relative humidity in concrete during experiments

4.8.1 Vaisala equipment

Probes from Vaisala Oy were used to measure the change in relative humidity. The equipment used contains a humidity measurement kit named SHM40 with probes HMP40S. The probes are inserted into plastic hollow pipes that are drilled into the concrete at predefined depths. A yearly calibration has been performed at Vaisala Oy, Helsinki, Finland. The uncertainties are compliant with a confidence level of 95 % and an uncertainty of RH ±1.4 %. To maintain a good certainty and assure limited drifting of the probes, their initial calibration was checked every second month and if necessary corrected at RISE by use of the salt-solutions of K_2SO_4 and LiCl.

The applied technology makes use of a capacitive sensor that consists of two electrodes separated by a dielectric material (Figure 4.18a). The sensor (the probe) is described as a thin film polymer capacitive humidity sensor and has an accuracy of ±1.1% in the range 0-90 % in RH and a temperature accuracy of ±0,2°C in the range 0-40°C (Vaisala, 2019).

The main principle is that; as the water vapor content in the air increase/decreases, the probe sensor's dielectric constant increases or decreases, changing the measured capacitance that corresponds to the

humidity level. As the relative humidity around the sensor changes, the dielectric properties of the covering polymer film change (Figure 4.18a), and so does the capacitance of the sensor. In this case, variations in humidity result in changes in the conductivity (or resistivity) of the sensing layer. The dielectric constant is directly proportional to the capacitance, which is inversely proportional to the relative humidity, RH %, (Inst Tools, 2022).

The instrument's electronics measure the capacitance of the sensor and convert it into a humidity reading. It can be calibrated according to its resistivity as a function of the relative humidity (Figure 4.18b). Figure 4.18c-d illustrates the monitor and the humidity sensor with and without its protective metal cover, respectively.

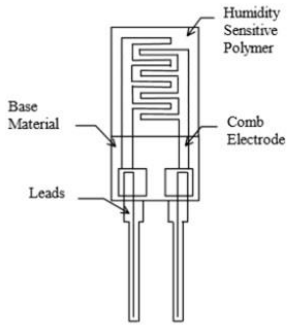

Figure 4.18a. Front view of a bulk polymer resistivity type humidity sensor. Figure copied from Inst Tools (2022).

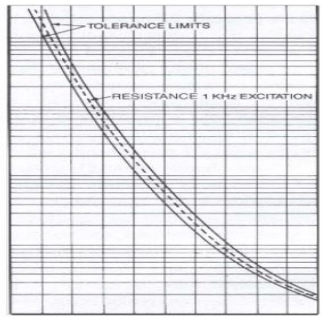

Figur 4.18b. The resistance as a function of the relative humidity. Calibration chart for a polymer resistive sensor. Figure copied and compressed in the y-direction. Figure from Inst Tools (2022).

Figure 4.18c. Monitor from Vaisala Oy connected to the humidity sensor in the lower right corner. In the middle: the black hollow plastic pipe that is mounted into the concrete.

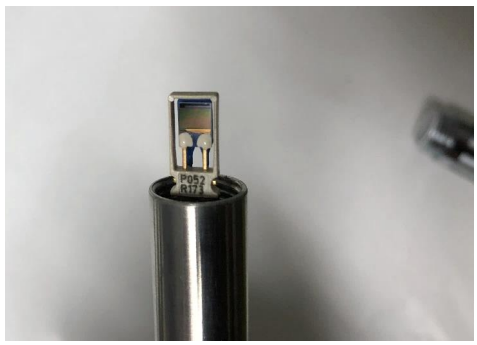

Figure 4.18d. Close up of the humidity sensor as shown in Figure 4.18a with the protective cover taken off.

The SHM40 equipment uses a Pt1000 sensor to display the temperature (figure 4.18c). The Pt 1000 sensor consists of a platinum resistance thermometer. The platinum resistance thermometer is used due to its very low resistance (1000 Ω at 0ºC that produces a high accuracy).

4.8.2 Measurements in concrete and surrounding air during the experiment

In the study the relative humidity was assessed at a depth of 10 mm and 25 mm into the concrete for both the prisms and plates. Each recipe had “one monitoring plate” and “one monitoring prism” to control the relative humidity of the cast recipes’ plates and prisms. The principle relies on that the storage of each concrete mixtures plates and prisms were stored in unification with the monitoring plates and prisms of each concrete recipe. The depth of 10 mm into the concrete was chosen as the determinant for when the cast concrete recipe had reached its specific predetermined relative humidity of 75, 60 and 45 % in RH.

Figure 4.19a-f demonstrate the different steps to monitor the relative humidity of the concrete prisms and plates. In some cases, salt was also placed in small plastic containers within the containers, Figure 4.19d. The relative humidity of the air inside the boxes, after closure (sealed state) was documented using plastic tubes (Figure 4.19e). The tubes were mounted on the plastic lids using epoxy resin. Before measurement of the relative humidity the probes were inserted (Figure 4.19f) inside the hollow plastic tubes and sealed at the top with a rubber gasket.

Each recipe was documented monthly. Measurements of the relative humidity and the concrete recipes’ weights were always documented prior to the measurements of the radon exhalation rate (E) and transport diffusion coefficient (D).

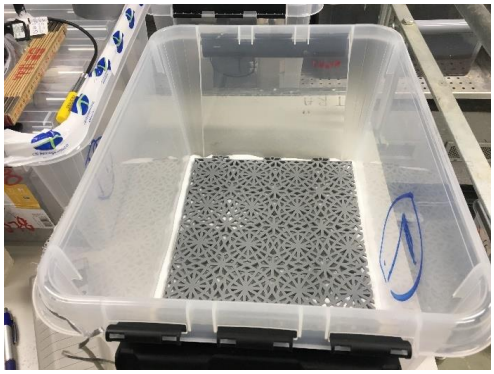

(a)

(b)

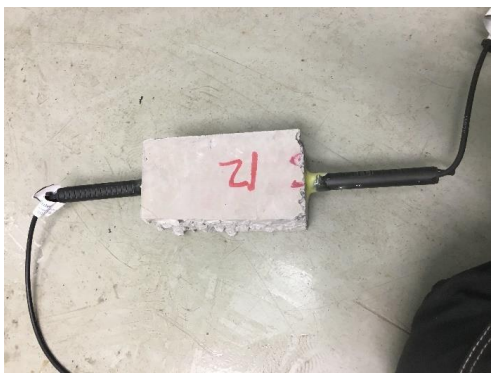

(c)

(d)

(e)

(f)

Figure 4.19. Different steps of the setup to measure and to monitor the drying of the specimens before measurements. (a) The plastic box, with a salt in the bottom and a grey plastic floor to put the samples on. (b) The recording of the RH at two different depths (10 and 25 mm). (c) The setup of recording the RH for the radon prisms. (d) The plates and concrete prisms resting on the grey floor. (e) The plastic box in a sealed state with two hollow plastic pipes used for measurement of the RH inside the box. (f) One measurement probe resting on a cardboard.

The air within the boxes was circulated using a central fan connected to a plastic pipe, drilled with inlets and outlets, to allow for several connections between the central fan and the boxes (Figure

4.20a-c). Each plastic box had an inlet and outlet, and hoses were drawn to connect to the central fan. The circulating air was thus within a “closed” system, with limited access of outside air influencing the relative humidity within the boxes.

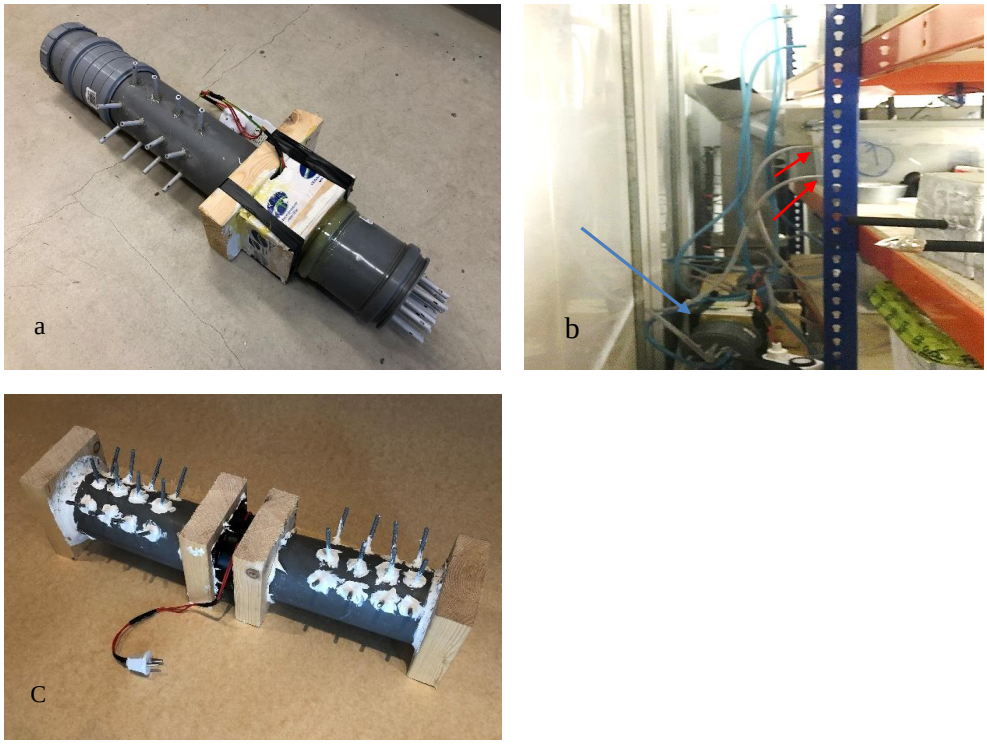

Figure 4.20 (a) Central fan with inlets and outlets for circulation of air within a closed system. (b) Connection of hoses (transparent) from one of the plastic boxes (red arrows) and the central fan in the lower part of the figure (blue arrow), (c) second fan with connectors for hoses on each side and the fan placed in the middle.

The procedure of using a central fan distributing air to each container included at the end two fans identical in performance. Measurements of each concrete mixture started at RH 75 %. After initial completion of measurements including the radon gas exhalation concentration and diffusion characteristics of one concrete mixture, all prisms and plates of that mixture were removed from the container. The NaCl salt where thereafter replaced by NaBr (Table 4.6) to achieve a relative humidity of ca RH 60 %. Thereafter all prisms and plates of that mixture were replaced in the container and the container sealed and connected to the second fan. One by one, after completion of the initial measurements at RH 75 %, the different concrete mixtures were connected to the second fan (RH 60 %) An identical procedure of shifting salts in each container was conducted as the concrete prisms and plates of each mixture were finally exposed to an environment of RH 45 %.

4.8.3 Salts used in the study

Three different salts were used to achieve the predetermined levels of relative humidity. Potassium carbonate (K_2CO_3), sodium bromide (NaBr) and sodium chloride (NaCl). Table 4.6 presents their equilibrium relative humidity at different temperatures.

Table 4.6. Different salts with their respective relative humidity at 20ºC and 25ºC.

Salt	20ºC	25ºC
K_2Co_3	43.2 %	43.2 %
NaBr	59.1 %	57.6 %
NaCl	75.6 %	75.3 %

4.8.4 Weight measurements of samples to ensure partial equilibrium

Weight measurements of the samples (prisms and plates) were decided to complement the initial relative humidity measurements, starting at the relative humidity of 75 %. At the initiation of the "second dry out phase", between RH 75 and 60 % (first dry out phase 100-75 RH), all the used prisms for radon measurements (75 x 75 x 150 mm) and plates (150 x 150 x 50 mm) were measured. Initially with long intervals, 2-3 months, but the closer to the reference value of 60 % in RH, the more often measurements were conducted.

Figure 4.21 presents the monitored data of the drying process to achieve partial equilibrium at different relative humidity levels. The measurements start at 75 % RH. A horizontal line indicates that partial equilibrium between the surrounding air and the concrete sample´s humidity at the predefined depth (10 mm) within the concrete is attained. Some samples quite early showed a weight loss <0,1 gram/week and those measurements were "stopped" under the assumption that partial equilibrium was obtained in the concrete prisms or plates. In most cases, radon measurements and transport diffusion measurements were initiated closely or immediately to when "partial equilibrium" were reached, due to the constrained time frame of the project.

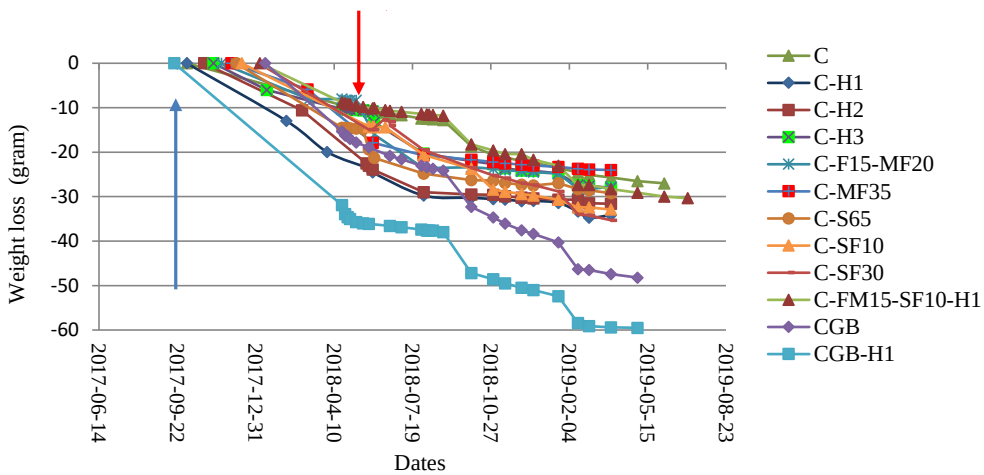

Figure 4.21. Weight loss as a function of time for each recipe investigated. Measurement data of radon "monitoring prisms" at 10 mm depth into the concrete. Blue and red arrows indicate start of measurements at a relative humidity of 75 % and when the second phase of measurements starts at a relative humidity of 60 %, respectively.

A brief overview of when the different measurements commenced at each relative humidity level can also be found in Table 4.5. In appendix A3 all measured relative humidity levels from the concrete´s plates and prisms are summarized.

4.9 Water absorption of the different cast recipes

The water absorption followed the recommended guidelines in ISO-EN 15148. The principle makes use of the initial dry mass of the samples and measures the increase of the masses of the samples when the samples are partially wetted/soaked from the bottom. The increase in mass of the samples as a function of time is documented in close intervals during the first hour and then less frequent during the following 24 hours. The used concrete specimens had its origin from the "spared concrete slabs", that had been dried for 10 months in a climate room (55 % RH and 23°C). Before measurements commenced the samples were dried for 4 weeks in 45ºC until almost no change in mass (0.1 gram/week) could be noticed.

Each cast recipe was represented with at least three concrete specimens (Figure 4.22). In the results an average value of the three specimens from each recipe is calculated. During the assessment, water was added continuously to the boxes to maintain a level just 2-3 mm from the bottom of the slightly immersed specimens.

(a) (b)

Figure 4.22. The different cast concrete recipes, with three specimens of each recipe in different boxes. The samples are resting on wet yellow cloths.

4.10 Control study, fixed RH 85 %, hydration at 3 and 6 months

Although, as previously addressed, the hydration of the cement paste was considered to play a minor part (regarded as negligible) upon the exhalation rate after 4-5 months (Zeng et al, 2012), it was deemed important to launch a minor study. Thus, to validate the hypothesis that the radon exhalation rate after 3 months was quite stable at a fixed relative humidity (RH 85 %) and not affected to a large extent by the continuous hydration of the cement pastes, four recipes were chosen to be further examined and tested at different times during the hydration process. The chosen recipes (Table 4.1 for guidance) included the reference cement C, C-H3, C-F15-MF20 and C-S65 and casting was done in an identical manner as for the first major cast of each recipe with a w/b ratio of 0.55. The radon exhalation rate was determined to be controlled for each recipe after 3 months and 6 months.

The cast cubes consisted of two recipes each with a size of 150 x 150 x 150 mm. The cast cubes were stored in water during the first month and thereafter kept in a climate room with a temperature of 23ºC and a relative humidity of 85 %. The cubes were always stored in the climate room except for during

measurements. One cube was used as the “measurement cube” for each recipe and the second one was used as a spare.

The results are presented in Chapter 5, Section 5.10.

4.11 Evaluation of possible cracks in plates used for diffusion measurements

To ensure some degree of reliability on the diffusion measurements a thorough check by ocular inspection and loupe was made on all “twelve measurement plates” used for the diffusion measurement. In a few cases possible minor cracks could be noticed during the inspection. Consequently, out of the twelve investigated plates, six were further investigated, due to the ocular observations.

The six selected plates (Figure 4.23) were polished and thereafter soaked from the surface with epoxy and fluorescence resin and placed in a vacuum chamber. After hardening of the resin/epoxy the samples were yet again polished (Figure 4.24a-f). This process was performed as to amplify the possibility to discover cracks, since epoxy resin easily is absorbed into cracks and when exposed to ultraviolet light generates a distinct fluorescence.

Figure 4.23. Six of the used plates for diffusion measurements were further examined for any possible cracks. From top left to lower right C, C-H1, C-H2, C-F15-MF20, C-S65and C-SF10 are shown.

The impregnated surfaces revealed that a further checked should be carried out for at least five of the samples. These samples were C, CH-1, C-F15-MF20, C-FM35 and C-S65. Figure 4.24 presents the impregnated samples.

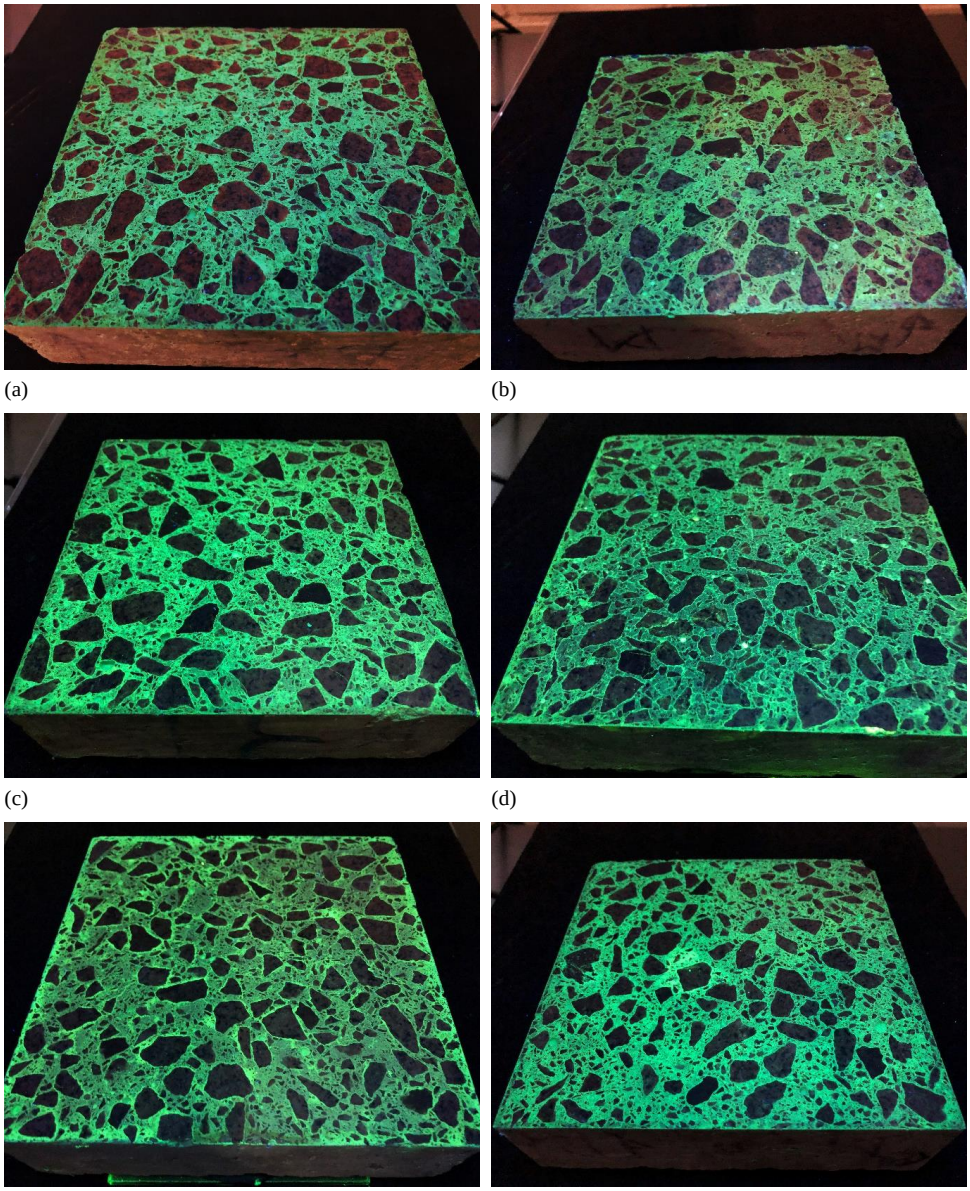

(a) (b)

(c) (d)

(e) (f)

Figure 4.24a-f. Fluorescent-impregnated surface of the diffusion plates exerted to ultraviolet light. From top left to lower right C, C-H1, C-H2, C-F15-MF20, C-S65 and C-SF10 are shown.

The chosen samples were thereafter cut along the middle, transverse to the surface, to further evaluate the quality along the direction of the plate thickness (flow direction of radon gas). The cut surfaces were as such once again impregnated with fluorescent resin and ground. The cut surfaces were further investigated in part by ocular stereoscope but foremost by use of polarizing microscope. Figure 4.25a-c illustrates the chosen part of each plate prior to cutting the plates in half to further assess the crack distribution. A few minor cracks could be observed in Figure 4.25b, c. prior to cutting. Figure 4.25d illustrates the approximate size of the part cut by dotted and red lines.

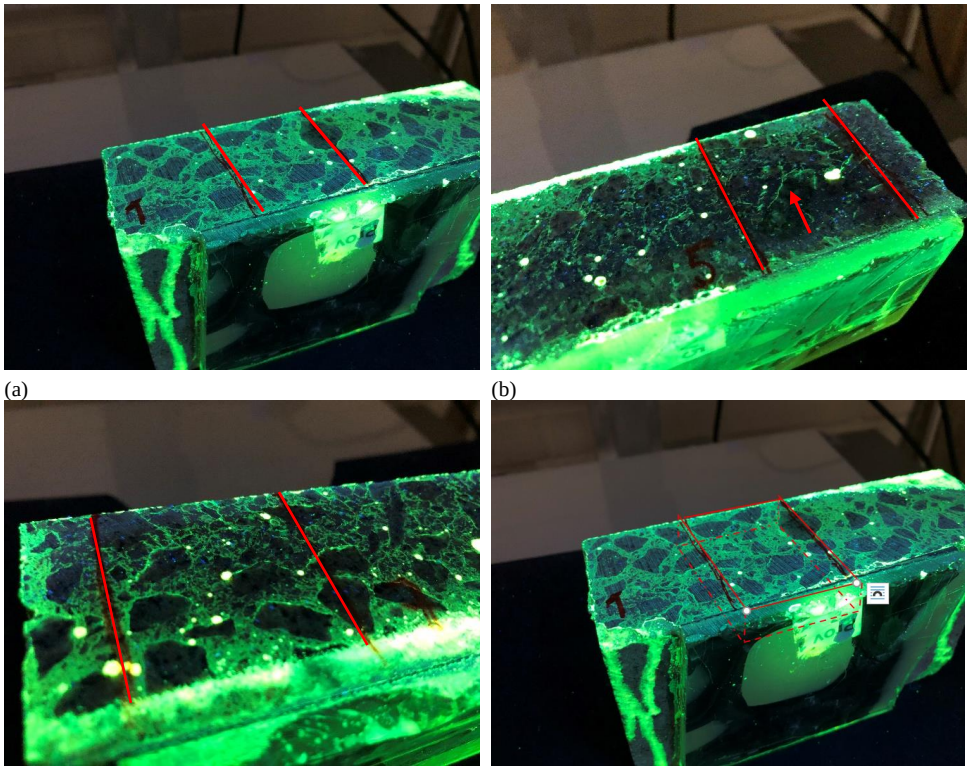

(a) (b)

(c)

Figure 4.25 a-d. Fluorescent-cut surface of the diffusion plates exposed to ultraviolet light. Note red lines marking the area of the investigated thin sections. From top left to bottom, reference sample, C (a), C-F15-FM20 (b) and C-S65 (c) and C (d) with red solid and dotted lines to mark the cut section. The red lines mark an area of 40 mm in width and 50 mm in length. The horizontal scale (= photo width) in each figure is (a) 170 mm, (b) 120 mm and (c) 70 mm. Red arrow highlights a typical cracks seen by green fluorescence.

4.11.1 Thin section examination - preparation and procedure

Thin section analysis was performed at the end for five of the diffusion plates. The procedure is well described in RILEM AAR-1 (2015) and encompasses a selection of an area for further assessment (Figure 4.25d). The thin sections were prepared at RISE. The sections of concrete used for thin sections were cut along the illustrated red lines in Figure 4.25a-c and approximately 20 mm into the concrete slabs. The small concrete cut specimens were thereafter cut in two parts each 10 mm thick. One of these two 10 mm thick concrete specimens were used for thin section examination and mounted onto a glass using epoxy resin (figure 4.26). The other part was archived. Thereafter a new cut of each concrete specimen was made ca 2 mm thick. Thereafter a grinding procedure was initiated to achieve a surface thickness of 25-30 µm i thickness (figure 4.27).

When the thin sections are viewed under the microscope using plan and crossed polars the minerals and hydration products will show different characteristics typical for each mineral phase. Using ultraviolet light will illuminate the fluorescence of the dye. Due to the embedment with fluorescence resins, the micro-cracks will be highlighted with a strong intense light green colour compared to its surroundings.

In brief the procedure after cutting two 10 mm thick concrete plates contained:

(i) the cut sample specimen from each concrete mix were mounted onto a glass (Figure 4.26).
(ii) thereafter the concrete was cut in different steps and ground until only a fraction of 0.1 mm in thickness was left of the concrete.
(iii) Grinding/polishing of the concrete until a thin layer of approximately 25-30 µm thick was left.

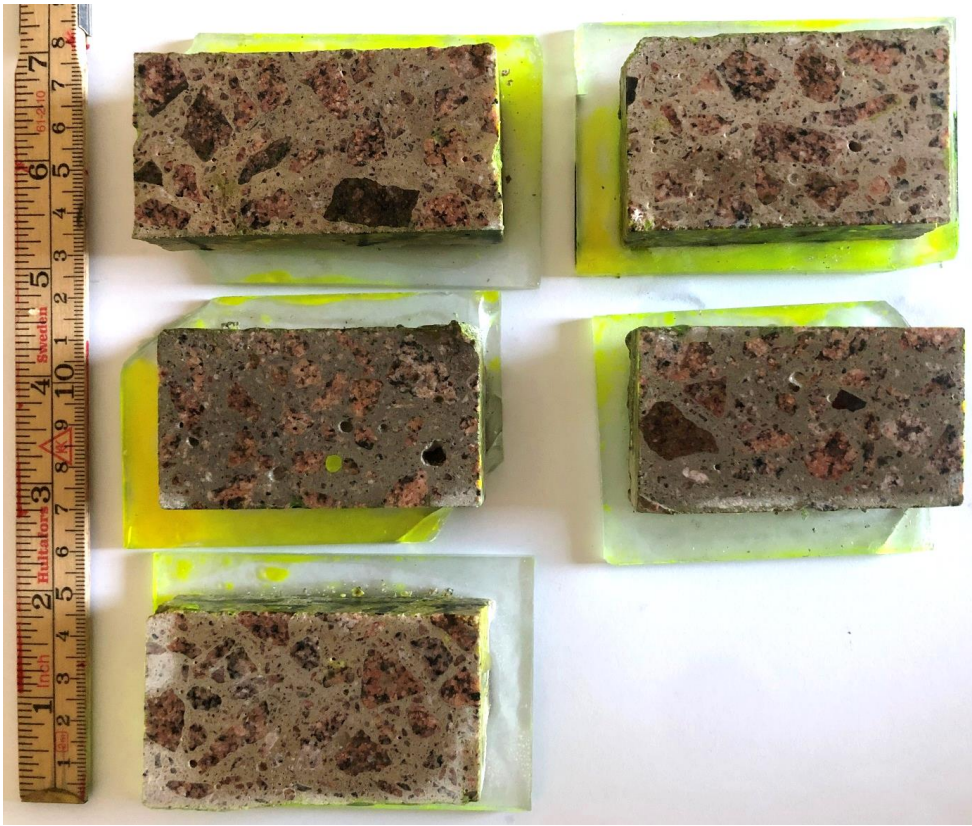

Figure 4.26. The cut concrete specimens prior to preparation of thin section analysis. From top left to bottom right; (a) C, C-H1, C-F15-FM20, C-FM35 and C-S65.

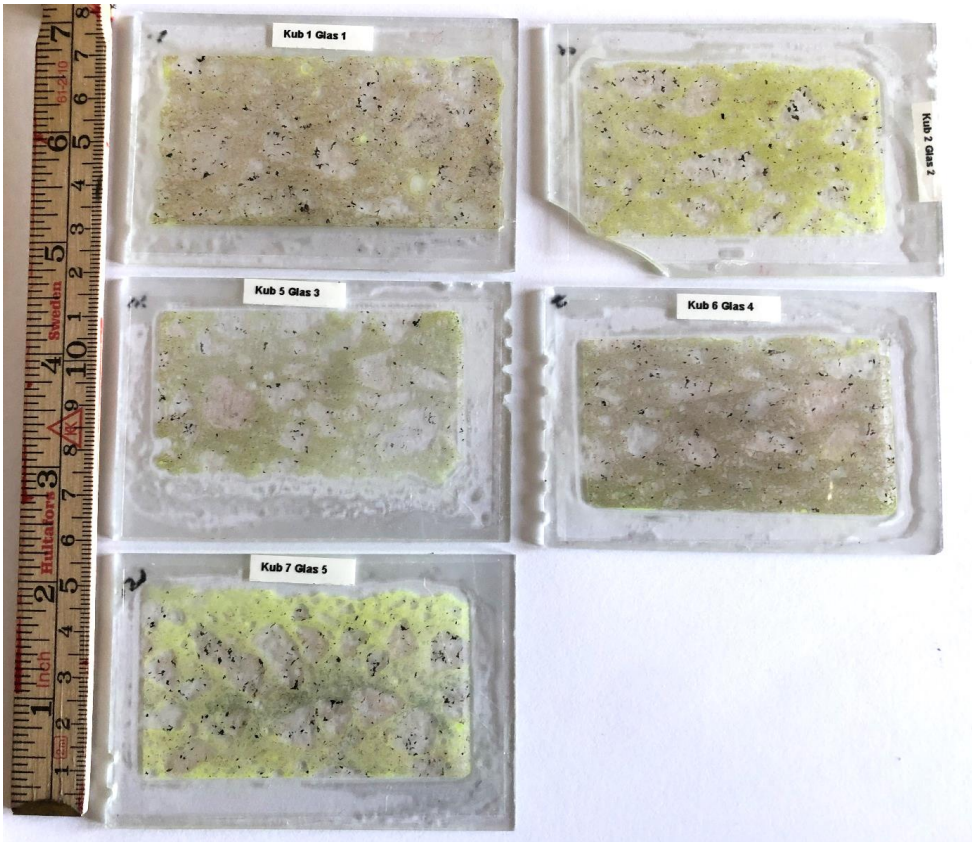

Figure 4.27. Thin section samples prepared for examination with a thickness of 25-30 µm. The thin sections from top left to bottom corner; C, C-H1, C-F15-FM20, C-FM35 and C-S65.

The results are presented in Chapter 5, Section 5.8

4.12 Evaluation of induced cracks in concrete

The influence of cracks on the exhalation rate of concrete was studied using two different recipes with identical w/b ratios, but with a hydrophobic admixture added for one of the recipes. The cement and aggregates in the two recipes were identical. The two recipes investigated were C and C-H1 also used in the major study of the thesis.

The cast prisms consisted of specimens with a size of 400 x 100 x 100 mm. Steel fibers, 40 mm in length were used to prevent cracking. Two of each recipe were cast. Simultaneously two concrete cubes, 100 x 100 mm, were cast of each recipe. The cubes were used for compressive tests at 28 days and after a full year.

The cast prisms and cubes were initially put in a water bath for a month to limit cracking. Thereafter, the prisms were stored in plastic containers, with an initial NaCl-salt (75 % in relative humidity) to achieve a moderate drying rate of the concretes. After approximately 4-5 months the salt was shifted to KCO_3 as to achieve a relative humidity of approximately 60 % in RH, 10 mm into the concrete. The

air was circulated using a closed system with a fan with an external mounted controller device for increased/decreased circulation of the flow.

The process was monitored by measuring the samples/prisms decrease in weight as a function of time. The weight curve of the prisms as a function of time served as partial confirmation of that the concrete prisms at least, close to the surface after one year, was close to a RH of 60 %. As the weight difference of the samples was < 0.1 gram/week, it was decided to initiate the measurements.

After initial radon gas measurements of each prism (pristine state) the same prism was cracked at three different positions along the slab. Thereafter measurements were commenced again on the same prism. An identical procedure was done for each slab (Figure 4.28). The results are presented in Chapter 5, Section 5.14.

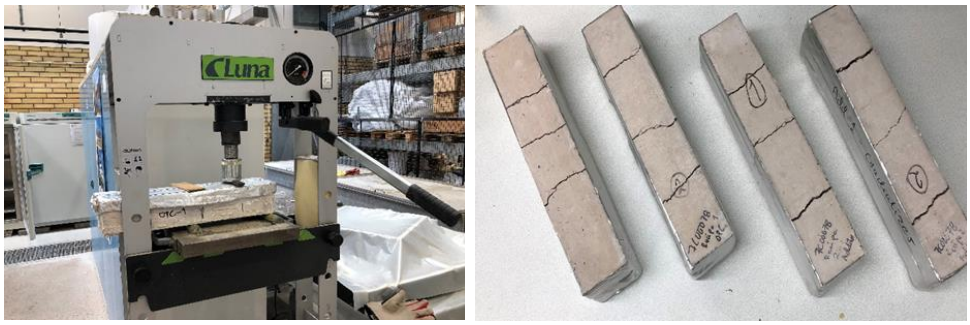

Fig 4.28. (a) Luna pressure press used to induce cracks in concrete prisms. (b) The concrete prism with cracks induced. The first two prisms to the left are from recipe one (C) and the other ones are from recipe two (C-H1).

4.13 Carbonation

During the project's different assignments, it was noticed that the magnitude of carbonation on some of the concrete specimens/samples could be quite substantial during the first two years of drying in climate chambers (23ºC and 50 RH %).

The results revealed that in some cases the carbonation was up to 7-9 mm within the material after 20-22 months. As reported by Boumazza et al. (2020), Justnes et al. (2020) carbonation may in turn effect the rate of diffusion and consequently the radon gas exhalation rate. Consequently, a study was launched (Paper V) to investigate the radon exhalation rate ($(Bq/m^2)/h$) and in part any changes of the diffusion coefficient as a function of carbonation depth for some of the concrete recipes investigated.

For the experiments in Paper V four recipes were cast (Table 4.7). The concrete recipes used identical prerequisites as in the major study (Paper III). A w/b-ratio of 0.55 was maintained. The cast recipes were stored for a month in water before being put in a climate chamber of 75 % RH.

Table 4.7. The cast recipes prepared for experiments presented in Paper V with different amounts of SCMs and admixtures. “X” indicates used in the recipe.

			SCMs – binders -supplementary cementious materials (SCM)				Admixtures		
Recipes	**Abbreviations in text**	**Aggregate**	**Cement**	**Fly ash, class F**	**Fly ash, microsite**	**Slag**	**Hydrophobic agents**		
			(%)	(%)	(%)	(%)			
		Granite	CEM I - 52.5R				H1	H2	H3
1	C	X	100						
2	C-H1	X	100				X		
5	C-F15-MF20	X	65	15	20				
7	C-S65	X	35			65			

To avoid any carbonation of the samples during the hydration period, synthetic air (alphagaz 1 from Air Liquid) was used. It has a purity of 99,99 % (oxygen and nitrogen) and less than 0,5 ppm carbon dioxide. The synthetic air was feed to the air volume within the climate chamber at a rate of 1 l/min (Figure 4.29a-g). Also, sodium hydroxide (NaOH-pellets) was put in small aluminum containers and distributed on the shelves alongside the cast samples as to further promote a carbon dioxide free air within the chamber. The carbon dioxide level was monitored by an equipment from Riken Keiki R1-221 (Figure 4.29e). The level was monitored daily.

Each recipe consisted of two prisms, 100 x 100 x 400 mm in length, accompanied with two cubes (100 x 100 x 100 mm). One of the prisms of each recipe was chosen as the “radon measurement prism” throughout the study. The other prism was defined as each recipe’s “sister” and was exerted to the same climate conditions (23°C, RH 50 %) as the “radon measurement prism”, apart for during ongoing measurement. Simultaneously with each measurement, the “sister” prism was used to measure the actual carbonation depth, where a piece of 100 mm was sawn. The sawn piece, ending up with a cube (100 x100x100 mm) was examined for its compressive strength and thereafter split in two halves (fresh surfaces). The split surfaces were sprayed with thymolphthalein, to get a measure of the carbonation depth at that specific time (Figure 4.30). The cubes of each recipe were used for 28 days compressive strength and prior to commencement of the radon gas measurements (~365 days). Prior to initiation of the radon exhalation measurements the drying of the specimens continued for almost 12 months until the weight difference of each prism was <1 gram per week at the relative humidity of 75 %.

As soon as the first radon gas measurements for each concrete mix was completed, the specimens of the measured mix were moved to another climate chamber, with the same RH (Figure 4.29c). The measurement scheme included in total five measurements of each concrete recipe, where the final phase (3 to 5 months) included an increase of the carbon dioxide level in the chamber (Table 4.8).

Table 4.8. Scheme for radon gas measurements and the actual carbon dioxide level in the atmosphere during drying.

Recipes	Month	CO_2-level (%)
C, C-H1, C-F15-MF20, C-S65	Start value	1
	1	1
	2	1
	3	2 % after ending 3rd month
	5	2

As soon as the first measurements of the concrete mixes were performed (under the condition of being non-carbonated specimens) the carbon dioxide level within the second chamber was raised and monitored as to achieve an air with approximately 1 % CO_2 (volume). This condition prevailed for the first 3 months. After 3 months, the carbon dioxide level was adjusted to 2 % (vol. %) until a final measurement of the radon gas exhalation rate of each prism was conducted at 5 months. The weight of the "radon measurement prism" was also documented during the whole process from casting and prior to each radon exhalation measurement.

The study also included evaluation of the diffusion coefficients for two out of the four investigated concrete recipes (reference concrete, C and C-S65 slag). A separate cast, with identical recipes as in the previous casts was executed. Two concrete cubes (150 x 150 x150 mm) were cast of each recipe. A similar procedure of drying was adopted as for the main study. But these concrete specimens were only exposed for two months in a carbon dioxide atmosphere of 2 %. The cause for only investigating two concrete recipes was due to the limited time frame and that diffusion measurements initially were not intended to be part of the study. The results are presented in more detail in Paper V and briefly in Chapter 5, Section 5.15.

(a)

(b)

(c)

(d)

(e)

(f)

Figure 4.29 (a) Set up using carbon dioxide free air. (b) The initial climate chamber including cast samples. (c) The second climate chamber with carbon dioxide monitor on the right side. (d) Cast samples resting within the climate chamber (e) The monitor used to document the level of CO_2 during the drying phase. (f) Two cast recipes resting on a carriage.

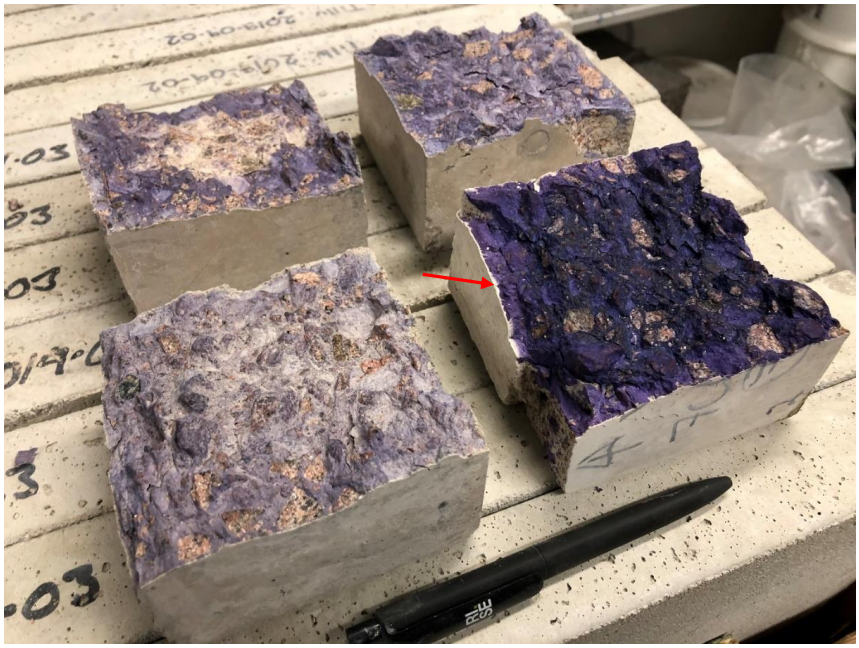

Figur 4.30. Cubes of CH-S65 after being split and checked for carbonation imprints before initation of accelerated carbonation test. Only very vague carbonation is noticable on the surface/side of one of the cubes (red arrow).

4.14 Radon gas exhalation methodology according to ISO 11665-7

The International Standardization Organization (ISO) describes a methodology, ISO-11665-7 (2012), which acknowledges two different ways of calculating the exhalation rate of radon gas. One way is an exponential method (best fit method), where back diffusion (Abo-Elmagd, 2014) is accounted for.

The other approach is according to linear analysis. The latter method is by ISO proposed as the most usable and appreciated, due to its much more constrained time frame of measurement (24 hours instead of at least 144 hours to apply the “best fit method”).

Initially, some experiments between the different proposed methodologies to calculate the exhalation rate were conducted on some of the concrete samples. In most cases very similar results were obtained (± 3 %). However, for a few samples a deviation of approximately 5-7 % could be found. But, due to the project´s amounts of cast specimens for assessment (prisms and plates) and the multiple analyses at different RH, the only reasonable option was to use the suggested linear interpolation method. The linear analysis used in the study applies a regression estimation considering at least 144 analyses (6 analyses per hour x 24 hours = 144 analyses).

4.15 Set up to calculate the radon gas exhalation rate of a surface

Through linear regression analysis an approximation of the radon gas exhalation ((Bq/m^2)/h) can be calculated knowing the initial conditions of the radon gas concentration in a predefined space (volume). Measurements are performed at least for 24h to reduce uncertainties. A measurement is taken every 10 minutes yielding a total of at least (6 × 24 h) = 144 measurements as the basis for the analysis. The linear model assumes no back diffusion of radon and neglects the decay of radon during time. The equation for the linear regression model can be described as:

$$\phi = \frac{\left\{\left[\frac{C-C_0}{t}\right]\times V\right\}}{A} \qquad (4.2)$$

where: ϕ = exhalation of radon gas (Bq/m^{2}h), C = concentration of radon gas measured by the radon gas monitor (Bq/m^3), C_0 = background concentration of radon gas at initiation (Bq/m^3), t = time of duration (h), A = effective surface area of the sample (m^2), V = volume of the container including hoses.

The principle to calculate the exhalation rate is to use a closed system explained in "section B" of ISO-11665-7. Knowing the surface area of the material, and the volume of the air enclosed (includes volume of container and volume in hoses to connect to the radon-monitor) as well as the background of radon gas at initiation of the measurement (C_0), then the necessary variables are known. Figure 4.31 shows the principle of the method.

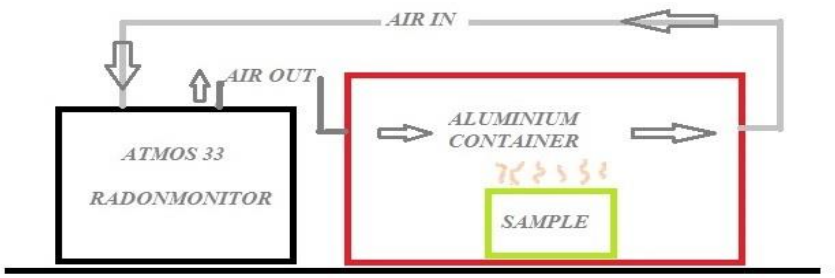

Figure 4.31. Principle to evaluate the radon exhalation rate using a closed system. Figure redrawn and modified from ISO 11665-7.

The sample to be analyzed is sealed on the bottom and each side is covered with a thick non-permeable tape. The tape consists of butylene-rubber (sticky) that is combined with an aluminum folio on top of the tape. This combination ensures a non-permeable tape regarding possibly leakage of ^{222}Rn gas. Figure 4.32 shows the different steps of preparation before final measurement of the radon gas exhalation rate can be conducted.

(a)

(b)

(c)

Figure 4.32. (a) Preparation of samples with tape. (b) Samples inside the chamber before closure. (c) Closed container with tape and clams connected to the measurement equipment.

The principle to evaluate the radon gas content originates in part from a procedure described by Baltzer et al. (1992), where different photo peaks (alpha energies) in MeV of ^{222}Rn, ^{218}Po, ^{214}Bi could be detected, knowing their specific energy. The energy intervals are 5.5, 6.0, 4.8 and 7.7 (MeV) for ^{222}Rn, ^{218}Po and ^{214}Bi and ^{214}Po, respectively. It is thus an indirect method, making use of the proportionality of alpha-decay and its photo peaks of ^{222}Rn, ^{218}Po, ^{214}Bi and ^{214}Po in relation to content of radon gas within the air. ^{222}Rn is in part detected by the summation of the energies of its daughter nuclides before it decays (Isaksson & Rääf, 2017).

The microprocessor within the radon monitor subtracts the ^{214}Po and ^{214}Bi photo peaks before recalculating the photo peak amplitude of ^{222}Rn and ^{218}Po and its relation to content of radon gas (Bq/m^3) in air. The unit displayed in the window of the radon gas monitor is the content of the ^{222}Rn rate in the Bq/m^3.

The instrument is calibrated, on a yearly basis, at the Swedish Radiation Safety Authority (SSM) where a well-defined level of ^{222}Rn gas is maintained in a predefined room volume. Before the final calculations of the measured activity concentrations of each concrete sample, the given correction factor ("*k*") as notified in the calibration letter is applied to the calculation. The *"k-factor*" is the ratio of the measured activity concentration of the ATMOS instrument owned by RISE divided by the

measured activity concentration measured by SSM. SSM uses a calibrated equipment in a specified room with a preset activity concentration of radon gas in that room. This correction is often ~1%.

For the analysis conducted at RISE a steady state temperature at 23ºC has always been maintained during all the analysis.

4.16 Test method used to calculate the radon diffusion coefficient (D) and radon diffusion length (L) of the radon gas

4.16.1 General

The calculation of the radon diffusion coefficients of the different concrete recipes and radon gas diffusion length *L* follows guidelines by Ishimori et al. (2013), Kovler (2012) and Chauhan & Kumar (2013), as described in Chapter 3, Section 3.4.1.

Table 4.9 presents some of the quantities, units, abbreviations and provides a short description of the quantities applied.

Table 4.9 Quantity and units for evaluation of radon and diffusion coefficients.

Quantity	Abbreviation	Unit	Description/short explanation
Radon concentration	*C*	Bq/m^3	Concentration of radon in a volume
Radon flux	*J*	Bq per m^2/s	Concentration of radon that traverses in one direction per unit time.
Diffusion coefficient	*D*	m^2/s	Relates the gradient of concentration of ^{222}Rn gas to the flow density across an area per second
Radon diffusion length	*L*	m	Characteristic distance travelled by the radon atoms during one half-life (3.8 days for ^{222}radon)

The radon diffusion coefficients of each concrete mixture can be calculated assuming a primary source of radon at a steady state condition. The methodology involves a concrete slab/plate, that is placed between the primary source and a secondary source defined as accumulation or receiver chamber (Figure 4.33). By placing the concrete plate (Figure 4.33a) between to hollow steel cylinders (Figure 4.33b, c) assuming a sealed unit one may place a minor uranium source in the primary chamber that will generate radon (primary source). A tight sealing between the primary source, the concrete plate and the secondary source (receiver chamber) assures that only radon can be transported through the concrete plate and the radon growth (radon flux) per unit time can be measured in the secondary or receiver chamber.

Assuring that the primary source reaches secondary equilibrium (steady state condition), that is usually in proximity after ca twelve days (Isaksson & Rääf, 2017), the secondary chamber can prior to radon

flux measurement (after at least 12 days) be flushed by low radon gas air (nitrogen) or outside air for one or two minutes.

This will set the necessary conditions prior to measurement:

(i) that steady state is maintained in the primary chamber
(ii) the secondary/receiver chamber is set to a state of almost “null radon” in the chamber.

As soon as the flushing is finalized the measurements starts. The growth of radon (increase in activity concentration), from almost zero, is monitored for at least 4-5 hours and then ended. An average value of the radon growth is recorded every 10 minutes. This “10-minute measurement”, is a mean value that consists of 60 separate values being registered every 10 seconds by the Atmos 33 (Baltzer et al. 1992).

Monitoring of the activity concentrations prior to measurements is performed by another instrument (solid state detector) To monitor a steady state condition in the primary chamber, whilst measuring with the Atmos 12 DPX monitor from the secondary chamber a radon equipment, named RAD 7 from Durridge Company Inc. was used (Chapter 2, Section 2.3.4). The possible influence of the steady state condition during flushing in the secondary chamber was registered during the ongoing measurements. No effect could be seen of any large fluctuations of the activity concentration in the primary chamber during flushing nor during the ongoing measurements (4-5 hours) and consequently these reflections of maintaining a steady-state condition during measurements were considered fulfilled. Figure 4.33 presents the setup of the diffusion measurements.

(a)

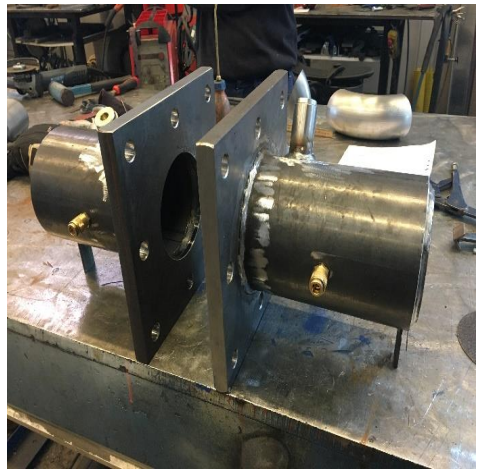

(b)

(c)

(d)

Figure 4.33. (a) Initial wrapping with aluminum tape. (b) The chambers (primary and secondary also named "source" and "receiver". (c) Set up with the concrete specimen between primary and secondary chamber. (d) Test is running with an aluminum taped concrete plate (red arrow) between primary and secondary chambers. Black hoses can be seen being connected to the receiver (secondary) chamber and the ATMOS 33.

After retrieving the final data of each measurement from the Atmos 12 DPX the linear regression analysis of the radon concentration (radon flux) could be evaluated. To smear out possible fluctuations in the linear regression analyses, the study used an "overlapping" technique", defined as "sliding average". Three "10-minute values" were lumped together defining "one value over a 30-minute period" used in the regression analysis. The minor change/ or influence was, that the last value in each "series", became the "first value" in the next "one value over a 30-minute period". Thus, in part, abrupt variations in the radon growth were limited.

Figure 4.34 depicts the growth of radon in the secondary chamber directly after the chamber is flushed. An "R"-value (square root of "R^2") >0.9 was always achieved during regression analysis of the measured data from each concrete specimen/plate. This implies that the "R"-value is trustworthy due to the strong correlation of the "y" value as a function of its "x" value. An R-value in the range of 0.8-0.9 is considered very solid (Garcia, 2010).

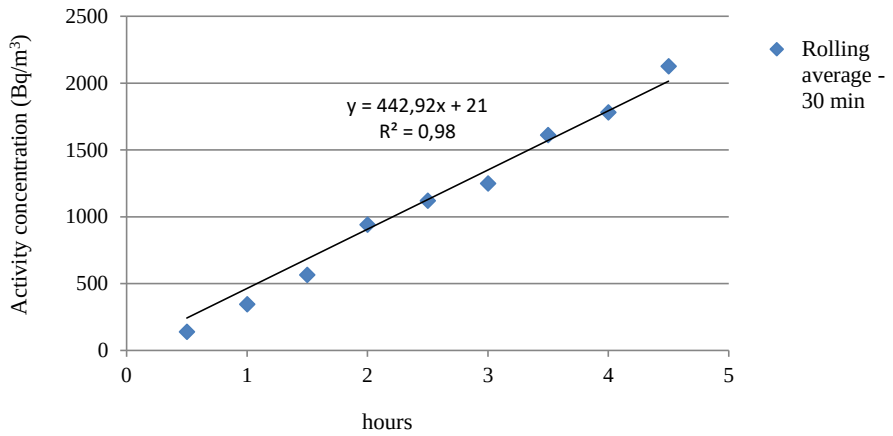

Figure 4.34. Growth of radon (activity concentration per unit volume) in the secondary chamber as a function of time.

5 Results

5.1 Radium activity concentration (Bq/kg) of the constituents

The radium activity concentration (^{226}Ra in Bq/kg) is of interest since it is directly related to the decay process of the uranium chain and the activity concentration of ^{222}Radon being produced in a building material, such as concrete. Thus, the activity concentration (Bq/kg) is essential for calculation of the emanation coefficient €. The interest in building materials` radioactive nuclide content has also increased among contractors, building companies and purchasers due to newly introduced regulations (SSM, 2018) concerning permitted activity concentration threshold levels in building materials.

The activity concentration of ^{226}Ra is normally calculated as part of the total gamma radiation activity where the natural radionuclides of ^{40}K, ^{232}Th and ^{226}Ra are measured simultaneously. In the present study, the binders, aggregates (red granite) and the completed concrete recipes (one cube of each recipe) were analysed according to their concentrations of ^{40}K, ^{226}Ra and ^{232}Th. Most of the materials used, including the reference cement, SCMs and the reference aggregate, were assessed. Also, the gamma index, or the activity concentration index*, defined as I-index, was calculated for each constituent. The uncertainty is normally <10 % and is with a 95 % confidence level (2σ) within the given reference values (VALO Guide 4.5). Table 5.1 presents the results for the constituents used in this study.

Table 5.1. Measurement and calculation of I-index of the natural radionuclides (^{40}K, ^{232}Th and ^{226}Ra) for most constituents used in the concrete recipes.

Constituents	**Radionuclides (Bq/kg)**			**I-index**	**Uncertainty (+-)**		
	^{40}K	**^{226}Ra**	**^{232}Th**		**^{40}K**	**^{226}Ra**	**^{232}Th**
Aggregate 1, 0/5 (red granite)	1180	228	162	**1.96**	140	19	19
Aggegate 1, 8/16 (red granite)	1230	195	191	**2.02**	130	21	21
Cement Skövde (CEM II A/LL)	280	28	17	**0.27**	17	2.1	1.8
Cement - SH (CEM I) 52,5 R	790	32	38	**0.56**	100	6	5
Fly ash, class F	480	118	102	**1.06**	60	10	12
Fly ash - Microsite	710	150	103	**1.25**	100	16	15
Slag (Germany)	151	115	114	**1.00**	22	12	17
Micro-silica (G 940)	99	5	2	**0.06**	14	1.5	0.3
Hydrophobic admixture, H1	<1.6	<.1.1	<0.3	**0.01**	-	-	-
Hydrophobic admixture, H2	<2.1	<2.4	<0.5	**0.01**	-	-	-

*I-index is calculated as ^{40}K, C/3000 + ^{226}Ra, C/300 + ^{232}Th, C/200, where C denotes concentration in Bq/kg (EC, 2014). Unit is dimensionless.

The cast concrete specimens were also measured. Before being analysed, the specimens were stored and slowly dried in a climate room for six months before they were crushed to fraction 0-16 mm and sent for analysis. Table 5.2 presents the results for the 12 concrete recipes analysed. The abbreviations and different amounts of the constituents in the various recipes can be found in Chapter 4, Table 4.1 and Appendix 1.

Table 5.2. Measurement and calculation of I-index of the natural radionuclides (^{40}K, ^{232}Th and ^{226}Ra) for each investigated concrete recipe.

Recipe	**Measured value**			**Calculated**	**Uncertainty (+-)**		
	^{40}K	**^{226}Ra**	**^{232}Th**	**I-index**	**^{40}K**	**^{226}Ra**	**^{232}Th**
C	1070	179	152	**1.71**	*110*	*20*	*16*
C-H1	1070	189	149	**1.73**	*180*	*24*	*22*
C-H2	1150	218	175	**1.99**	*170*	*50*	*26*
C-H3	1050	174	146	**1.66**	*170*	*21*	*22*
C-F15-MF20	1070	199	148	**1.76**	*110*	*22*	*16*
C-MF35	1090	201	154	**1.80**	*110*	*23*	*17*
C-S65	1040	198	154	**1.78**	*170*	*24*	*23*
C-SF10	1030	179	151	**1.70**	*150*	*42*	*22*
C-SF30	1060	184	146	**1.70**	*110*	*21*	*16*
C-FM15-SF10-H1	1050	180	143	**1.67**	*170*	*22*	*21*
CGB	253	6,5	6,1	**0.14**	*42*	*0,8*	*0.9*
CGB-H1	257	6,8	6,4	**0.14**	*37*	*1.1*	*0.7*

It can be noted (Table 5.1) that some constituents are slightly higher in their activity concentration (I-index), such as those containing fly ash (C-F15-MF20, C-MF35) and slag (C-S65). This is also partly the case for the concrete specimens, where a slight increase in the overall I-index of the concrete specimens containing those constituents can be noted (Table 5.2, I-index column). However, this is by and large within uncertainty of the individual measurements, although the slight increase is a good match in relation to measured concentrations of the separate constituents (Table 5.1) analysed in the concrete. Further, the binders containing micro-silica are in line with the reference cement and show a slightly lower I-index value in the final concrete, as expected due to the low activity concentration of micro-silica compared to the other constituents.

With a special focus on the binders, it is apparent that the Swedish cement, except for micro-silica, in general has moderate concentrations of natural activity compared to some of the supplementary cementitious materials such as fly ash and slag, specifically noted for their activity concentrations of ^{226}Ra and ^{232}Th. These are the radioactive elements that contribute to radon gas as ^{222}Rn and ^{220}Rn gas respectively.

It is also worth acknowledging the higher I-index for the recipe C-H3. This hydrophobic admixture (liquid additive) as a single constituent was not measured in the study, but the constituents H1 and H2 were, indicating very small contributions of the natural radionuclides (Table 5.1). Although it cannot be excluded that this admixture contains a higher content of the measured radionuclides of ^{226}Ra and ^{232}Th, it is highly unlikely that any effect would still be noted due to its small share in the final concrete mix. It is more likely that the ratio of aggregates/cement paste was slightly elevated in this sample compared to the other specimens. A higher share of aggregates will evidently (Table 5.1) result in an increased I-index (higher activity concentration).

Finally, the concrete mixes with very low activity concentrations (Bq/kg) shall be addressed. These concrete mixes were the ones using an aggregate (CBG and CBG-H1) with low concentrations of the natural radioactive elements ^{40}K, ^{226}Ra and ^{232}Th. This is a good typical representative of crystalline

rock types defined as gabbro or diabase (in Sweden), which in general contain very low levels of natural radionuclides compared to most granites within Sweden or the Nordic countries.

5.3 Porosity, pore volume and pore radius

5.3.1 Porosity estimate due to weight loss of water

Evaluation of porosity was assessed in three different ways:

(i) The main study used submerged concrete samples (150 x 150 x 150 mm) in water and dried at initially 45°C.
(ii) The second approach used submerged samples in water including initial vacuum (60 x 40 x 25 mm).
(iii) The third approach included only a few concrete mixes (cubes 100 x 100 x 100 mm) that were submerged in water and dried at a high temperature (105°C).

After completion of each assessment, the results of the different methods were compared. The second approach, according to SS-EN 1936 (Chapter 4, Section 4.6) using vacuum, showed in a few cases some doubtful results. This was considered as due to the small volume assessed (uneven mix of aggregates and cement paste) and the results were discarded, although many results were in line with the main study.

From the main study it can be concluded that:

- The results regarding porosity vary in the interval between ~11 and 16 % (Figure 5.1).
- The reference concrete mix shows a porosity value of ~14 %, which is in line or slightly lower than all the concrete recipes using an SCM.
- The highest value recorded was registered for recipe C-SF30, where the amount of micro-silica is rather high (30% weight of binder content).
- Increasing the micro-silica content indicates an increase in the porosity.
- The recipes containing a hydrophobic admixture all show a reduced porosity compared to the corresponding reference concrete (C).
- The values of the porosity for the reference concrete are seemingly in good correspondence with an expected value at the set w/b ratio according to *Concrete Handbook (1997, 2017), material section* (in Swedish Betonghandboken, material).

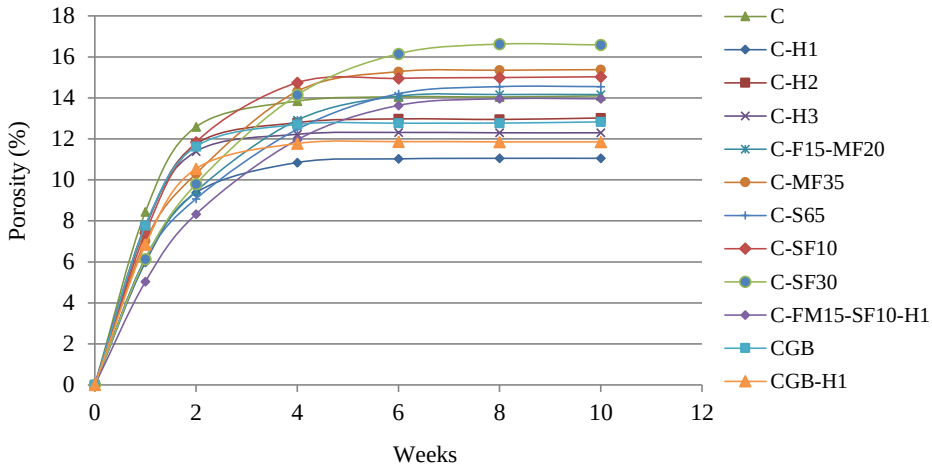

Figure 5.1. The porosity, defined as the total air volume, was estimated as the final value from measurements of loss of water as a function of time during drying of the test cubes (the density of water was set to 1000 kg/m^3).

The control study included four of the recipes (C, C-H3, C-F15-FM20 and C-S65). However, as mentioned in Chapter 4, Section 4.6, a quick drying procedure at 105ºC was here selected. Also, the porosity assessment was started one month after casting of the recipes.

Figure 5.2 presents the results for two out of the four recipes (C and C-F15-FM20). Each recipe used two cast cubes for internal comparison (Figure 5.2). At the final reading (408 hours), the results are compared with the porosities of the identical recipe in the main study. The decision to present only two out of the four assessed recipes is merely in the interest of clarity in Figure 5.2.

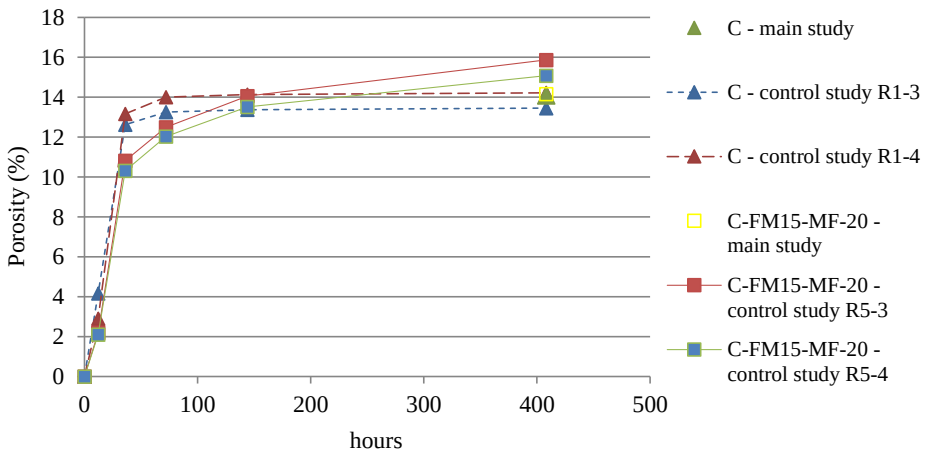

Figure 5.2. The porosity, defined as the total air volume, was estimated as the final value from measurements of loss of water as a function of time during drying of the test cubes (the density of water was set to 1000 kg/m^3). The increase in "porosity" during drying at 105ºC.

Following comparison with the main study, some conclusions can be drawn:

- By and large, the results are in good agreement with the main study.
- The results indicate a slight variation (ca 0,5-1,5 vol. %).
- The "control study" indicates a slightly higher porosity for three out of four concrete mixes compared with the main study.

In the "control study" alone, we can also observe a minor variation in porosity between the cast concrete cubes of each recipe/mixture. It was assumed that the control study may indicate higher porosity values than the main study, due to the short time of hydration and a non-finalised microstructure of the concrete (Hewlett & Liska, 2019). This was also indicated for three out of four concrete mixtures (Table 5.3).

The porosity results from the concrete mixtures were also compared with the porosity of the assessed cement pastes using MIP. Table 5.3 shows a summary which also includes the porosity of the assessed cement pastes one year after casting.

Table 5.3. Summary of the porosity results from concrete assessments also including the calculated porosity of the cement paste using Mercury Intrusion Porosimetry (MIP).

Porosity (weight. %)			
Concrete recipe	**Main study**	**Control study - 28 days (mean value)**	**(MIP) - Hg intrusion (one year after casting)**
C	14,10	13,46	14,10
C-H1	11,05		
C-H2	13,02		
C-H3	12,30	14,60	
C-F15-MF20	14,16	15,87	11,33
C-MF35	15,38		12,1
C-S65	14,55	15,99	11,42
C-SF10	15,03		13,16
C-SF30	16,58		12,47
C-FM15-SF10-H1	13,96		13,48
CGB	12,83		
CGB-H1	11,85		

Comparing some of the results from the MIP study with the porosities of the concrete mixtures in the main study, it was apparent that the assessed porosities of the cement pastes showed lower values. This was clear in all cases where SCMs were used as part of the binder. In many cases, the decrease in porosity was 2-3 %.

5.3.2 Mercury Intrusion Porosimetry (MIP) – Cement pastes

MIP was also used to assess the differences in the average pore and medium pore radius (µm) as well as the "total porosity" of the cement pastes containing different SCMs. Part of the results are summarised in Table 5.4. The measurement range was between 0.0005 and 100 µm.

Table 5.4. A summary of the MIP results from the examined cement pastes.

Cement paste	Total intruded volume	Average pore radius	Median pore radius	Bulk density	Apparent density	Porosity by Hg Intrusion	Total pore surface area
	[mm³/g]	[μm]	[μm]	[g/cm³]	[g/cm³]	[%]	[m²/g]
C	75.10	0.0106	0.0121	1.8780	2.1863	14.10	14.154
C-F15-MF20	60.95	0.0077	0.0099	1.8603	2.0981	11.33	15.885
C-MF35	67.33	0.0100	0.0137	1.8437	2.1050	12.41	13.468
C-S65	60.82	0.0096	0.0130	1.8782	2.1204	11.42	12.660
C-SF10	70.37	0.0052	0.0050	1.8704	2.1539	13.16	27.156
C-SF30	68.44	0.0048	0.0045	1.8219	2.0814	12.47	28.284
C-FM15-SF10-H1	73.87	0.0072	0.0072	1.8244	2.1086	13.48	20.549

Figure 5.3 presents a cumulative curve of the total porosity (by Hg intrusion) as a function of the pore radius size distribution of each investigated cement paste.

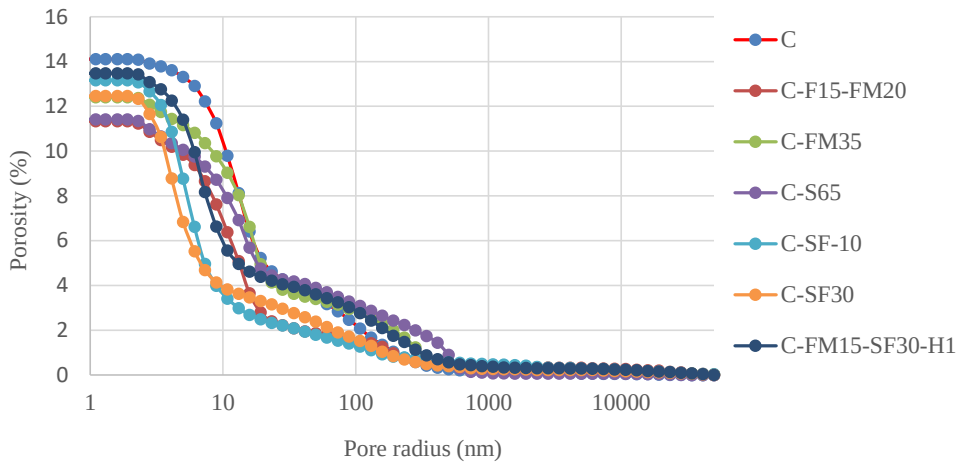

Figure 5.3. Cumulative curve of the total porosity of the cement pastes of each recipe as a function of the pore radius size distribution.

The relative volume distribution of the pores can also be presented as a function of the pore radius of each recipe (Figure 5.4). The relative pore volume is a measure of the “real porosity” measured with a

gas pycnometer.

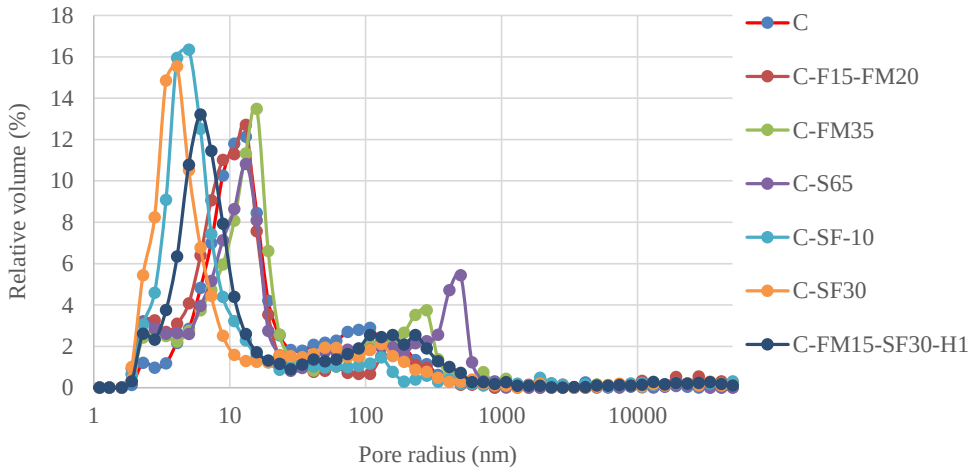

Figure 5.4. Relative volume as a function of the pore radius of each cement paste recipe.

Regarding the porosity as a function of the pore radius, the result implies that the reference cement shows the highest total porosity (Table 5.4). The lowest porosities are shown by C-S65 (slag) and C-F15-FM20 (fly ash).

Regarding the porosity as a function of the pore radius size distribution, the concrete recipes containing silica fume as part of the binder system all show a very high percentage of small pores at a very small pore radius (<10 nm). This is as expected (Hewlett & Liska, 2019). In contrast, the cement paste containing slag as binder indicates a fairly high distribution of pores within a larger span (bimodal size distribution) than the other cement pastes assessed. This becomes more evident when the relative pore volume is plotted as a function of the pore radius (Figure 5.4). The cement paste containing slag (C-S65) displays typical “double neck” behaviour. This is also evident in part for the cement binder systems containing the constituent “fly ash microsite” (C-FM35) but also to a lesser extent for the reference cement (C).

In Appendix A4, data are compiled from the MIP measurements for each recipe investigated.

5.4 Compressive tests at 7, 28, 356 and 900 days

Compressive tests were performed according to SS-EN 12390-3. The analysed cubes of 150 x 150 x 150 mm were all from the first cast batch (major study) of each recipe (Figure 5.5). One concrete cube of each concrete recipe was analysed on each occasion. The uncertainty including operational variations is <5 %.

The results after one year are in the interval of 50-80 MPa for most recipes. A set value of at least 40/50 MPa was set as a target (EN 206) for the reference concrete. Accordingly, the results are in part as expected due to the share of cement and different shares of SCMs in the recipes regarding the set w/b ratio. The highest compressive strength is achieved using silica fume and fly ash. The lowest compressive strength is recorded when an admixture is added to the recipe (C-H3). Slightly lower values are recorded for cement binders containing a high share of fly ash (C-FM35) at 28 days.

However, this is not surprising due to the initial hydration phase requiring a high portion of $CaOH_2$ prior to the onset of the pozzolanic reactivity and formation of C-S-H gel.

There are indications of a minor decrease in the compressive strength for most of the concrete recipes at 900 days compared to 356 days. This is slightly surprising due to the fact that most concrete mixtures increase slightly in strength during their first year after casting (Mehta & Monteiro, 2006; Hewlett & Liska, 2019). Plausible explanations may relate to an increased sensitivity range setting of the compression cell during compressive testing or recalibration of the compression cell. External processes to the concrete specimens may also affect the concrete compressive strength differently, such as initiated carbonation.

The compressive tests clearly indicate the fact that using mineral SCMs/fillers such as micro-silica or fly ash leads to a higher strength of the concrete compared to only using an ordinary Portland cement (C).

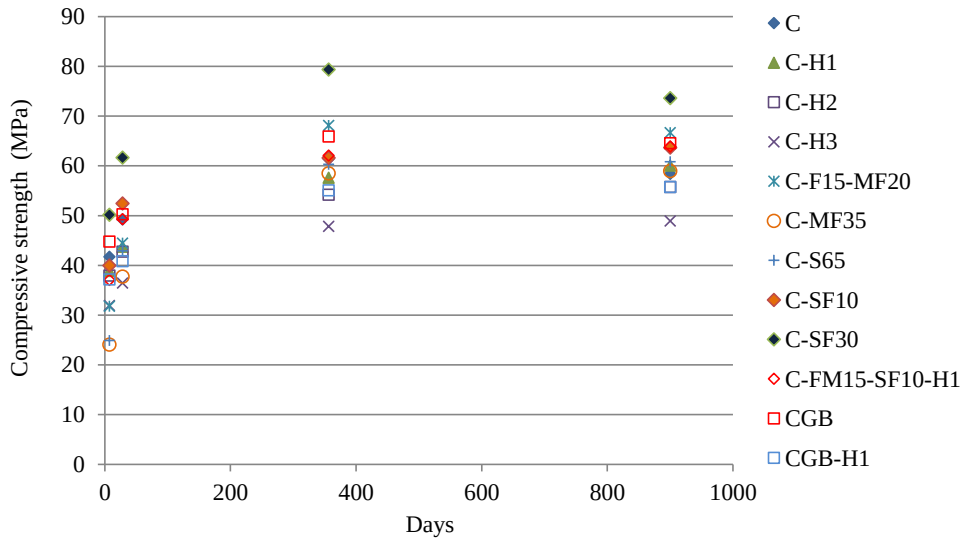

Figure 5.5. Compressive tests as of function of time for each recipe at four different occasions.

5.5 Monitoring to achieve partial equilibrium at 75 %, 60 % and 45 %

The differences in weight among the measured plates and prisms were monitored during the drying process for each recipe. These prisms and plates were weighed prior to commencing measurements of the radon flux and the radon gas exhalation. The initial weights of each specimen were firstly documented at the time when RH 75 % was reached for each concrete mixture. In four cases, the monitoring prisms of C, C-F15-FM20, C-S65 and C-SF30 were also dried in an oven at 105°C to achieve an RH of "0" %.

Figure 5.6 presents the total percentage loss (wt. %) of each prism at RH 60 % and 45 % as a function of the specimen's weight at RH of 75 %. Figure 5.7 presents the same procedure as Figure 5.6 but this time for the plates used for diffusion measurements. In many cases, very similar weight losses were obtained and consequently data are overlapping. As a result, it may seem like the data are not present in the figures.

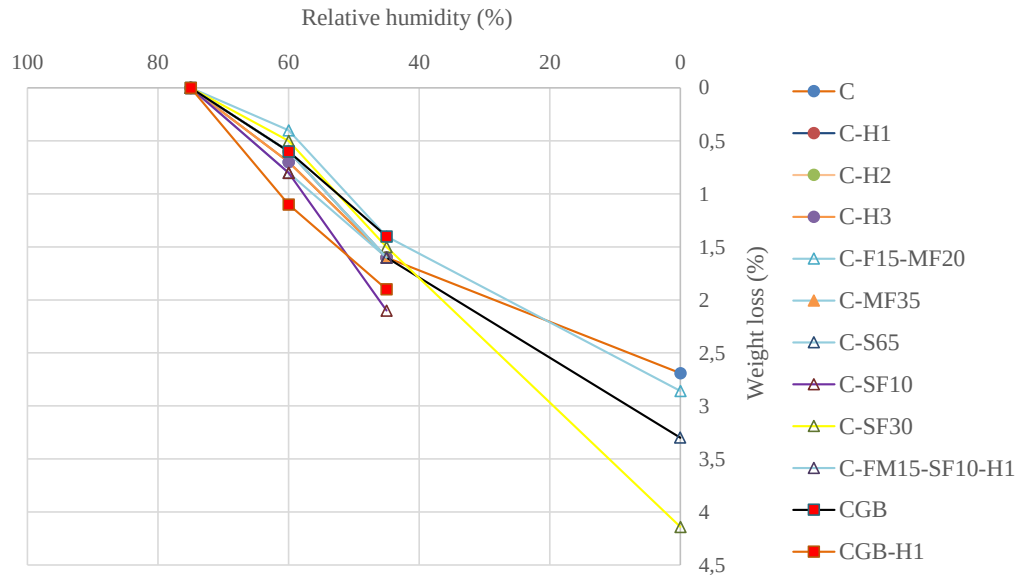

Figure 5.6. The weight loss in percent (%) as a function of the relative humidity of each monitoring prism.

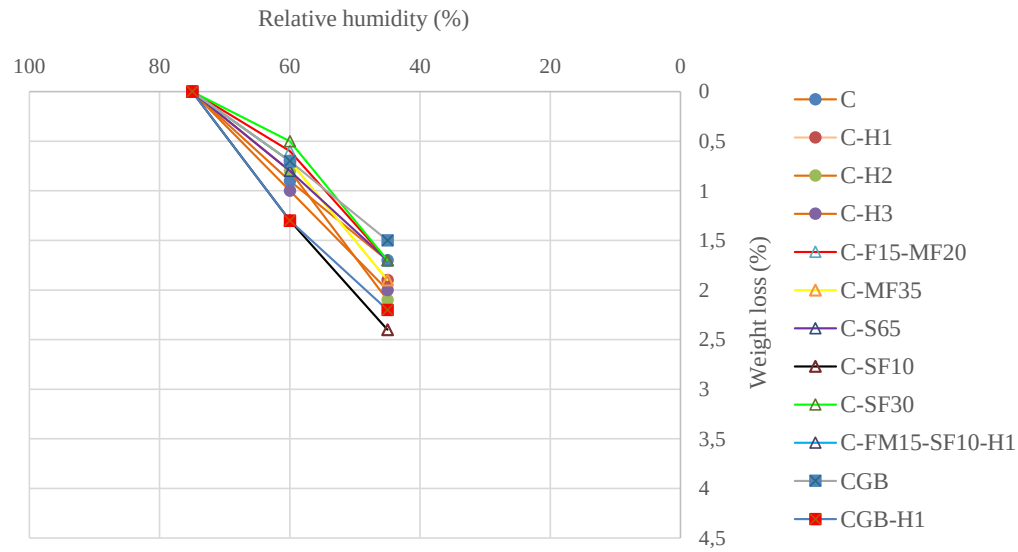

Figure 5.7. Weight loss in percent (%) as a function of the relative humidity (%) of the monitoring plates.

The results imply in general terms that there is a comparable weight loss for most samples during the drying process. This indicates that the setup using salts to achieve a state of at least partial equilibrium in RH between the air and the concrete specimens has been a workable concept, but apparently not ideal. In two cases, the weight loss of the specimens is clearly higher. The data for both the "monitoring prisms" and "monitoring plates" show a similar trend in these cases. This is evident for C-SF10 and CGB—H1. It seems like concretes with a smaller share of micro-silica or a CEM I binder

(OPC) that contains hydrophobic admixtures release a higher fraction of water in the interval, RH 75-RH 60.

The monitoring plates show, in general, a slightly higher percentage loss compared to the prisms. This is in part as expected due to the larger surface/volume ratio of the plates compared to the prisms which would imply a sharper drying gradient for the plates.

5.6 Water absorption (suction) of different concrete recipes

A large spread in the water absorption coefficient between the concrete recipes was measured. The results reveal that the concrete recipes where a hydrophobic admixture had been added, specifically C-H1 and CH-3, have a very low absorption coefficient. This was also noted when the additive C-H1 was combined with the reference aggregate (gabbro). In all cases, where the additive H1 was added to the recipe (C-FM15-SF10-H1) a strongly reduced water absorption coefficient was the result.

The largest water absorption was the combination of the reference cement and different shares of micro-silica (C-SF30, C-SF10) and a high amounts of fly ash (C-MF35). Similar results have been reported by Mueller et al. (2017). The results obtained from the water absorption test were in line with the porosity results, where the highest porosity values were recorded for the same binder combinations as previously mentioned.

Excluding the concrete mixes containing an addition of liquid additive, the lowest water absorption was achieved for the combination of different fly ashes with the reference cement (C-F15-MF20) and slag (C-S65). The difference compared with the reference cement C was more clearly noticeable during the first 10 hours of the measurements. These results agree with MIP measurements of the cement pastes, where the total pore surface area figures for micro-silica, slag and fly ash also have the highest water absorption capability and vice versa.

Figure 5.8 presents the results for each concrete recipe (mean of three individual pieces). The measurements were ongoing during a time interval of 24 hours (86.400 sec.).

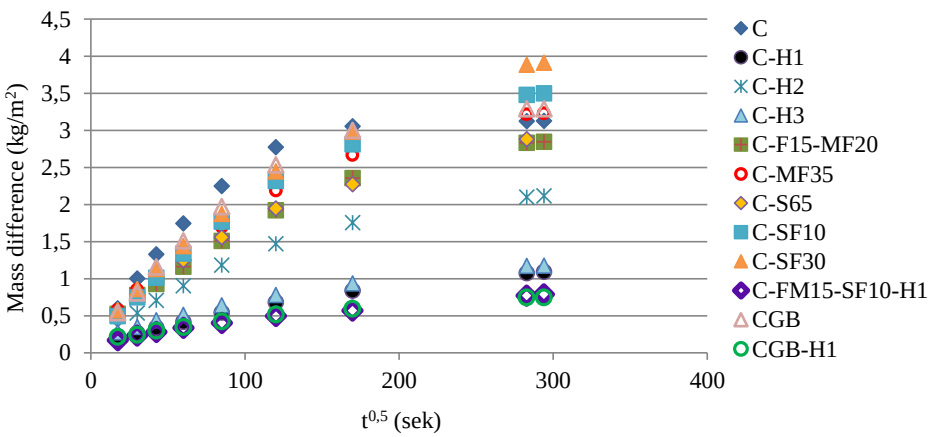

Figure 5.8. Mass difference (kg/m^2) as a function of time (square root) to evaluate the absorption of the different concrete recipes.

5.7 Radon emanation coefficients for the studied recipes

The radon emanation coefficient was investigated using two approaches. The first (Section 5.7.1) included a few concrete recipes (three in total), where the radon gas equilibrium concentration was measured and compared. The second approach (Section 5.7.2) included all concrete recipes (mixtures), where the calculated exhalation rate of each recipe (measured values) was used to theoretically calculate the equilibrium radon concentration (Chapter 4, Section 3.5) of each recipe. Consequently, knowing the activity concentration of each concrete recipe (Table 5.1 and 5.2) and the mass of each prism at the different relative humidity levels, it follows that the emanation coefficient could be deduced.

5.7.1 Emanation coefficients measuring the radon equilibrium concentration

In the first approach, the radon emanation coefficient was calculated according to Eq. 3.26 and 3.27 (Chapter 3) at a relative humidity of ~50 % for three concrete cubes (150 x 150 x 150 mm) from the main study. To allow for a correct estimate, the ^{222}Rn activity concentration (Bq/m^3) was prone to reach secular equilibrium in air. Figure 5.9 presents the build-up of the ^{222}Rn concentration in the enclosed atmosphere during the study of the reference cement C. An average value of the last readings between 29,912 and 32,200 minutes (from 20.8 to 22.4 days) was chosen as the "equilibrium concentration" (red arrow, Figure 5.9).

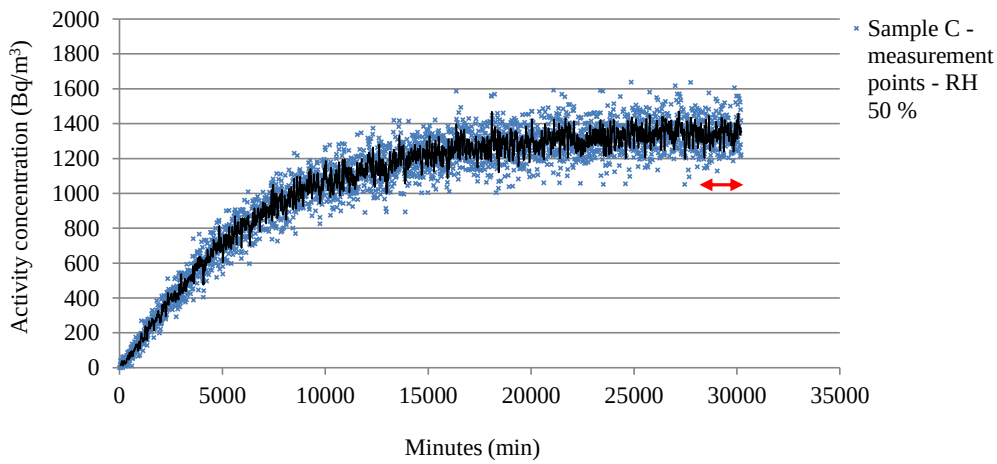

Figure 5.9. The ^{222}Rn concentration in air (activity concentration) building up as a function of time (minutes) for the reference sample C. The red section marks the equilibrium area used for calculation of a mean value.

The reference concrete recipe (*C*) was thereafter compared to the recipe containing two types of fly ash (C-F15-FM20) and the reference concrete, with an aggregate (gabbro) with almost no detected radiation of ^{226}Ra (Bq/kg).

Table 5.5 presents the calculated emanation coefficients (ϵ) of each recipe and the parameters used.

Table 5.5. Calculated emanation coefficient of each recipe and measured parameters.

Recipe	Volume in chamber (m^3)	Mass of sample/cube (kg)	Activity concentration of ^{226}Ra (Bq/kg)	Equilibrium ^{222}Rn concentration (Bq/m^3)	Emanation coefficient (€)
C	0,1424	7,797	177	1370	**0.14**
C-F15-FM20	0,1424	7,783	171	1087	**0.11**
CGB	0,1424	8,534	6,8	35	**0.09**

Note the very large difference in activity concentration of ^{226}Ra (Bq/kg) (Table 5.1) between the concrete recipes C and C-F15-FM20 compared to the recipe CGB. As previously mentioned (Section 4), the difference is due to different aggregates used, which for the recipe CGB contained very small amounts of ^{238}U and consequently, the daughter nuclides and their corresponding activity concentration of ^{226}Ra and its progenies will also be very low. Thus, due to the low activity concentration of ^{226}Ra in this recipe, there are also significant uncertainties (Figure 5.10), where the build-up of ^{222}Rn concentration in the closed chamber is seemingly non-existent. Thus, the calculated emanation coefficient should be taken with some caution. However, it should be noted that, even though the activity concentration (Bq/kg) of the recipe CGB is very low compared to the other recipes, it may very well have a similar or even higher emanation coefficient. The coefficient is only a measure of the portion (percentage) of radon atoms produced by radium decay that escapes through the pores in relation to the total amount of radon atoms within that material.

The calculated emanation coefficients are in line with results reported for concrete (€ = 0.05-0.35) by Fournier et al. (2005) and Kovler (2012). It is also in good agreement with the calculated emanation coefficient values of the concrete recipes taking the mass radon exhalation rate into account (Figure 5.12, Section 5.7.2).

The recipe containing fly ash, C-F15-FM20, has a lower radon gas exhalation rate than most of the recipes investigated (regardless of relative humidity level). This is reflected in the calculated lower emanation coefficient compared to the reference cement C. In general, it can be concluded that only a minor portion (9-14 % from the measured samples) of the radon atoms leaves the concrete´s interior and transfers into the free air at a relative humidity of 45-50 %. This indicates that the dense concrete matrix (constituents and C-S-H matrix) mitigates the ^{222}Rn gas transport and ensures that a large degree of decay of ^{222}Rn occurs within the samples itself, not being released into the free air.

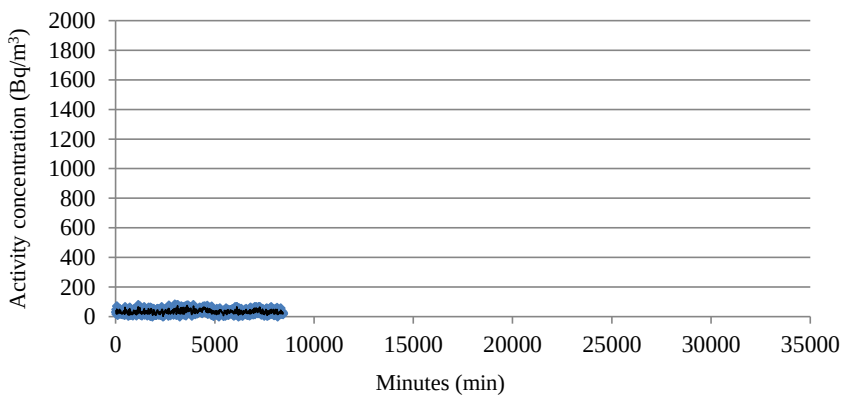

Figure 5.10. The “non-existent” build-up of ^{222}Rn activity concentration as a function of time for recipe CGB.

5.7.2 Calculation of the emanation coefficient and exhalation rate for all recipes

The second approach to measuring the emanation coefficient involved the use of the radon gas mass exhalation rate ((Bq/kg)/h), knowing the mass of the sample and its activity concentration (Bq/kg). In four cases, the concrete prisms were, after finalised measurements, put in an oven at 105ºC for two weeks to achieve a relative humidity as close to 0 % as possible. Figure 5.11 presents the calculated radon gas exhalation rates as a function of the humidity for each concrete recipe. Figure 5.12 presents the calculated emanation coefficients in each case.

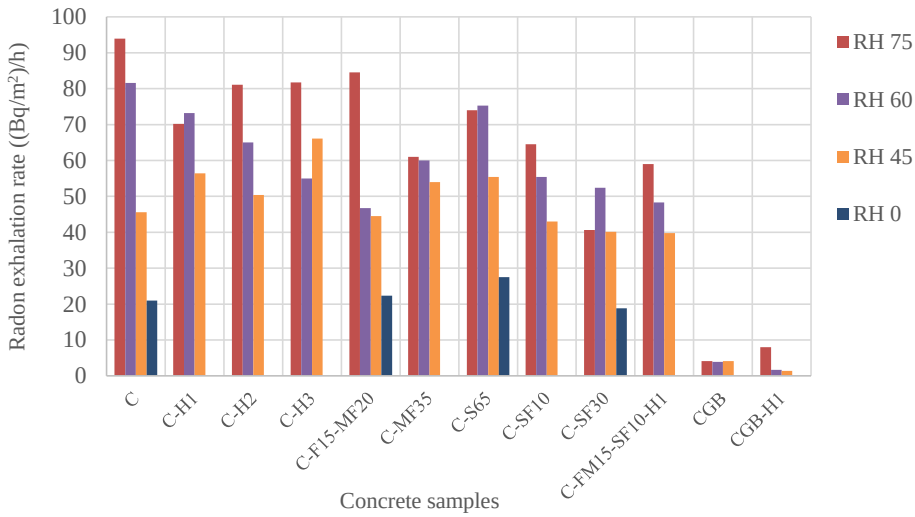

Figure 5.11. The calculated exhalation rates as a function of the studied recipes at different relative humidity levels.

A decrease in the exhalation rate also implies a lower emanation coefficient, being related to the amount of radon atoms reaching the free air and escaping the concrete surface. Figure 5.12 presents the calculated emanation coefficients of each concrete recipe.

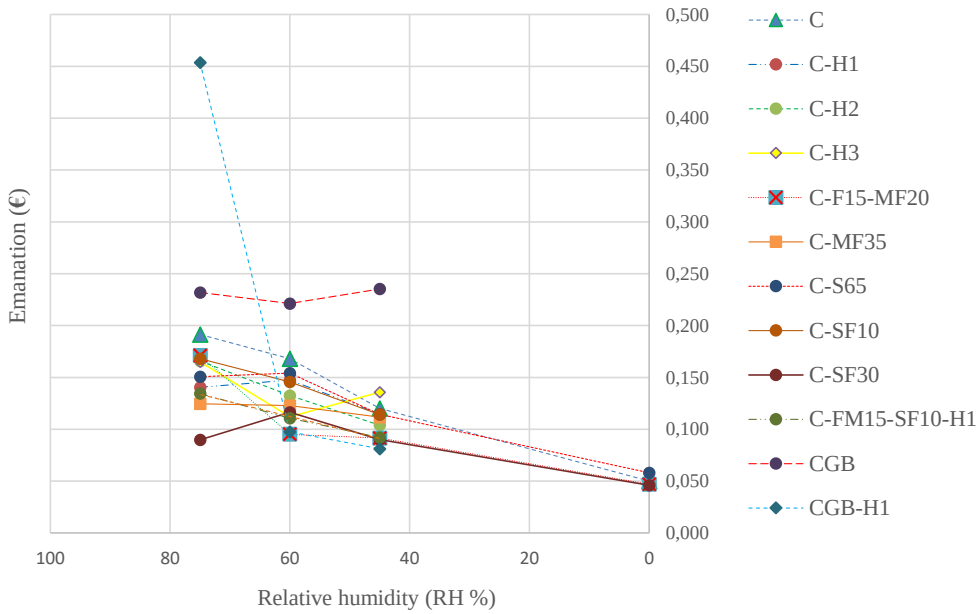

Figure 5.12. The emanation coefficients as a function of the relative humidity of each concrete recipe.

The results imply that the emanation coefficient in most cases successively decreases as a lower relative humidity of the concrete samples is documented. The lowest values almost converge at around 5 % (0.05) at a relative humidity being close to 0 %. The lowest value is calculated for the recipe containing fly ash (CF-F15-FM20). The behaviour of the concrete mixture containing slag is noteworthy, since the emanation coefficient is similar, even though the relative humidity decreases in the span RH 75-RH45.

The calculated results or numerical values of the emanation coefficients for those concrete mixtures used in both approaches were compared. However, since the first approach involved conducting the experiments at an RH of 50 %, a comparison is not fully attainable. What can be noted, though, is that the calculated emanation coefficient values retrieved in the first setup also match the results of the second approach in the interval RH 60-RH45.

It is also evident (Figure 5.12) that there is likely a large degree of uncertainty, causing a wide variation for the reference samples containing gabbro/diabase (CGB and CGB-H1). Specifically, it is worth noting the value of CGB-H1 at RH 75 %. This is due to the previously mentioned very low ^{222}Rn activity concentration (Bq/m^3) being measured for this concrete mix.

5.8 Crack investigation of concrete plates used for diffusion measurements

5.8.1 Stereoscope

Using ocular aid and stereoscope only revealed minor indicative cracks for the reference sample, C, but more apparent minor cracks along some aggregates were noticeable in samples C-F15-FM20 and C-S65. The cracks did mainly occur along the transition zone between the cement paste and the aggregates. Only very few cracks could be noted for each concrete mix in the cement paste under the stereoscope.

5.8.2 Polarising microscope

Possible micro-cracks were further analysed using polarising microscope. Only some minor micro-cracks could be observed for samples C, C-F15-FM-20 and C-S65. The samples C-H1 and C-FM35 had an intact and homogenous C-S-H gel well distributed over the entire sample. Figure 5.13 presents the thin sections of C, C-15-MF20 and C-S65 in plane polarised light and with fluorescent light. The photographs depict the same area for each concrete mix.

The cement paste or C-S-H gel in each case appeared with a homogenous matrix with only a minimum of noticeable fractures/micro-cracks in the cement paste. The fractures were less than 0.5 mm in length and with an aperture of <0.01 mm. In contact with some aggregate edges (transition zone), minor areas with open space were noted (Figure 5.13f). Most parts of the transition zones were filled and substituted with secondary formed calcite, ettringite and portlandite.

The analyses of the concrete specimens using thin sections do not provide any support for larger micro-cracks measuring >0.02 mm (Figure 5.13b, d) or any interconnecting system of micro-cracks within the cement paste in the direction of flow of the radon gas. The limitation is, of course, that only a very small area compared to the total area was examined. It could be added that micro-cracks are noted in the cement paste, but as stated, only to a very small extent and with very limited lengths (<0.5 mm).

Secondly, it should be addressed that carbonation was noted for samples C and C-S65 which varied within the interval of 2-3 mm. However, for C-F15-MF20 the carbonation depth was around 4 mm (Figure 5.13c). The carbonation depth is indicated by a brownish tint, where the fresh cement paste has a darkish colour in plane polarised light.

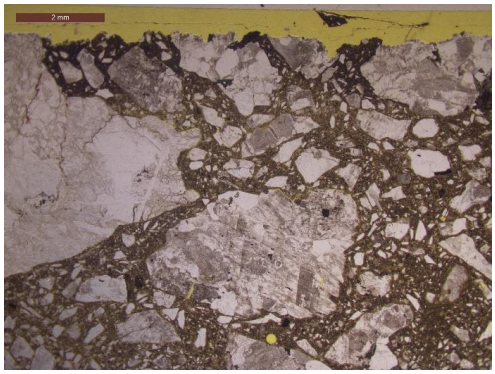

(a)

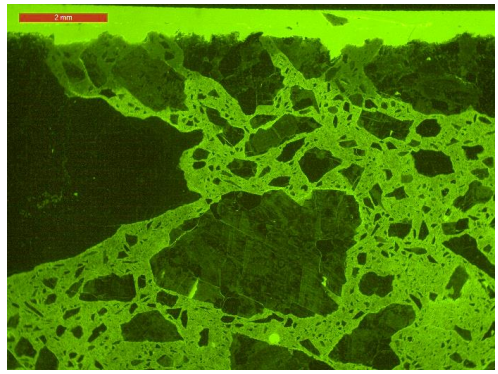

(b)

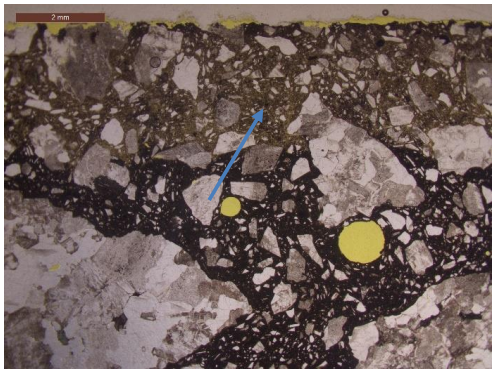

(c)

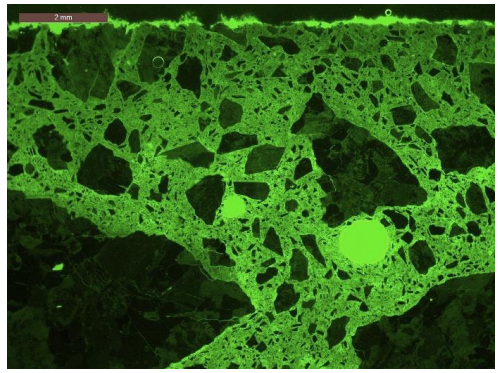

(d)

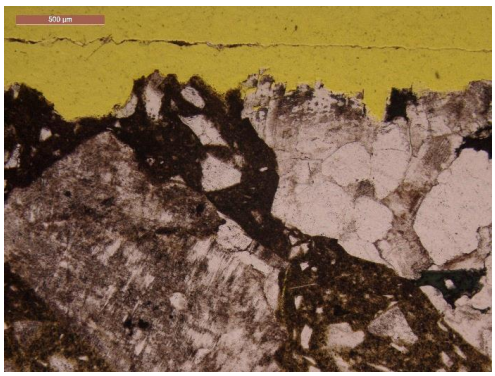

(e)

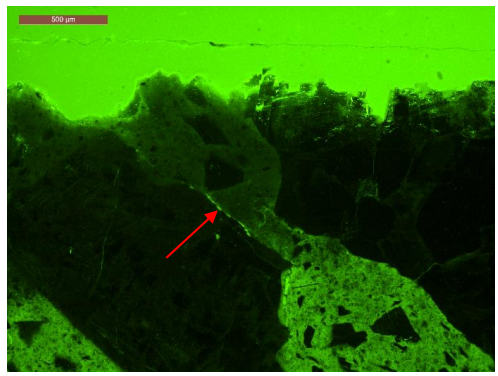

(f)

Figure 5.13a-f. Thin section analysis of the concrete samples C, C-F15-MF20 and C-S65 in plane and fluorescent light. Figures a-b illustrate the reference cement. Figures c-d illustrate C-F15-MF20 and Figures e-f illustrate C-S65. Note minor area of open space along the transition zone of an aggregate (red arrow, Figure f). In Figure c, the carbonation zone is shown by a blue arrow. The horizontal scale (= photo width) in each figure is (a) 10 mm, (b) 10 mm, (c) 10 mm, (d) 10 mm, (e) 2.74 mm and (f) 2.74 mm.

5.9 Diffusion coefficient measurements (D) and radon diffusion length (L)

The diffusion coefficient measurements and radon diffusion lengths of each concrete recipe (cast) have been calculated according to the equations presented in Chapter 3, Section 3.4.1. The different diffusion coefficients of each recipe at different relative humidity levels are presented in Table 5.6 as well as the calculated radon diffusion lengths. The background influence in percent (%) at a relative humidity of 75 % is also included.

Table 5.6. Results of the radon diffusion length and diffusion coefficients, with respect to relative humidities (RH) of each concrete mix.

Recipe	**Radon diffusion length *L* (mm)**			**Background influence (%)**	**Radon diffusion coefficients *D* (m^2/s)**		
RH (%)	**75**	**60**	**45**	**75**	**75**	**60**	**45**
C	9.2	16.6	22.5	32	1.78E-10	5.80E-10	1.06E-09
C-H1	9.0	10.1	25.2	17	1.70E-10	2.12E-10	1.33E-09
C-H2	9.7	14.3	27.2	3	1.98E-10	4.29E-10	1.55E-09
C-H3	7.4	20.1	26.0	32	1.15E-10	8.48E-10	1.42E-09
C-F15-MF20	3.7	3.5	7.6	49	2.87E-11	2.56E-11	1.20E-10
C-MF35	6.7	9.0	15.7	28	9.43E-11	1.70E-10	5.15E-10
C-S65	4.9	10.1	12.9	37	5.04E-11	2.12E-10	3.48E-10
C-SF10	6.4	10.9	16.0	27	8.60E-11	2.49E-10	5.36E-10
C-SF30	8.4	18.2	20.0	12	1.48E-10	6.95E-10	8.43E-10
C-FM15-SF10-H1	8.9	10.5	15.0	18	1.66E-10	2.32E-10	4.74E-10
CGB	7.4	16.0	21.2	36	1.15E-10	5.40E-10	9.43E-10
CGB-H1	3.6	13.6	19.1	44	2.72E-11	3.88E-10	7.65E-10

Figure 5.14 also presents graphically the radon diffusion lengths *L* of the different recipes at the different relative humidity levels.

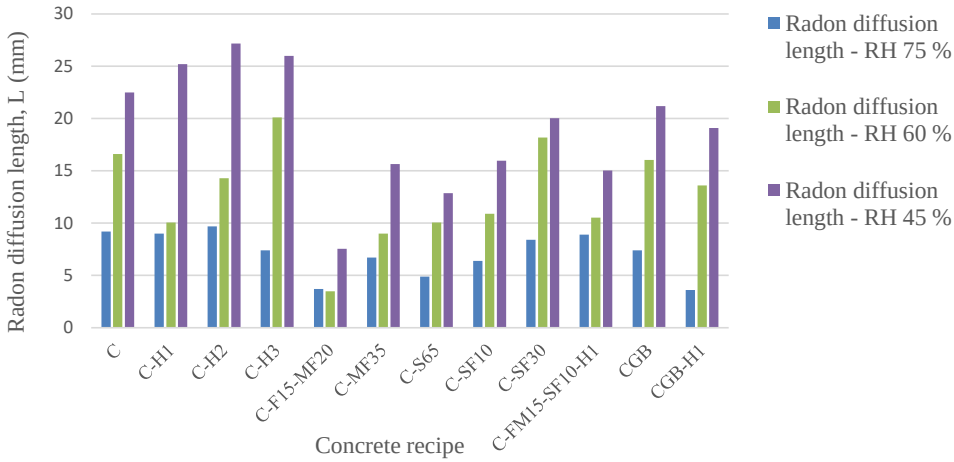

Figure 5.14. The calculated radon diffusion lengths (mm) at different relative humidity levels for each recipe.

The calculated diffusion coefficient of each recipe is normally in the interval of 1 x 10^{-11} to 1 x 10^{-9} m^2/s. In general, the calculated diffusion coefficients of the studied recipes increase as the relative humidity decreases. At a relative humidity of 45 %, the largest diffusion coefficient is for the reference concrete and the smallest coefficients are for those recipes having an addition of fly ash, slag or microsilica. As expected, the radon diffusion length increases as the diffusion coefficient increases, as can be observed in Table 5.6. A low diffusion coefficient generates a shorter radon diffusion length and vice versa.

The influence of humidity upon the diffusion coefficient is also quite apparent. As can be noted in Figure 5.14 and Table 5.6, a high relative humidity in the concrete mixes (RH 75 %) produces a very low diffusion coefficient (and short radon diffusion length), and a lower relative humidity in the concrete specimens (RH 45 %) markedly increases the diffusion coefficient and the radon diffusion length. Consequently, the radon gas transport rate (radon flux) through the concrete plates increases as the relative humidity of the concrete plates decreases. This is in sharp contrast to the results of the radon exhalation rate, where the radon exhalation rate (radon leaving the surface of the concrete) decreases as the relative humidity decreases (Sections 5.10, 5.11).

In Table 5.6, there is also marked a column for background influence in percent (%). This approach was only used during the first setup at a relative humidity of 75 %. The background influence is the amount of radon generated solely from the concrete plate (no mass transfer of radon through the plate, e.g., radon flux is “zero”). As previously noted, for some recipes, the amount of radon produced from the concrete plate itself, and its internal decay of ^{222}Rn gas has a major influence on the total radon gas content (activity concentration, Bq/m^3) measured when the diffusion coefficients are very low (RH 75 %). At higher diffusion coefficients, this influence from the concrete plate reduces drastically. Thus, it has been demonstrated in the experiments that the diffusion coefficient registered (bulk diffusion) would be even lower at higher relative humidities without this “background influence” of the radon gas produced from within the plate.

5.10 Radon exhalation at different RH (75 %, 60 % and 45 %)

The results on the radon exhalation rates from the measured concrete prisms of each recipe indicate in general a clear decrease in the rates as the relative humidity of the samples decreases. By way of illustration, Figure 5.15 presents the results from two of the concrete recipes, namely C 1 and C-H1. The concrete prisms have been measured at three different relative humidity levels: RH 75 %, RH 60 % and RH 45 %.

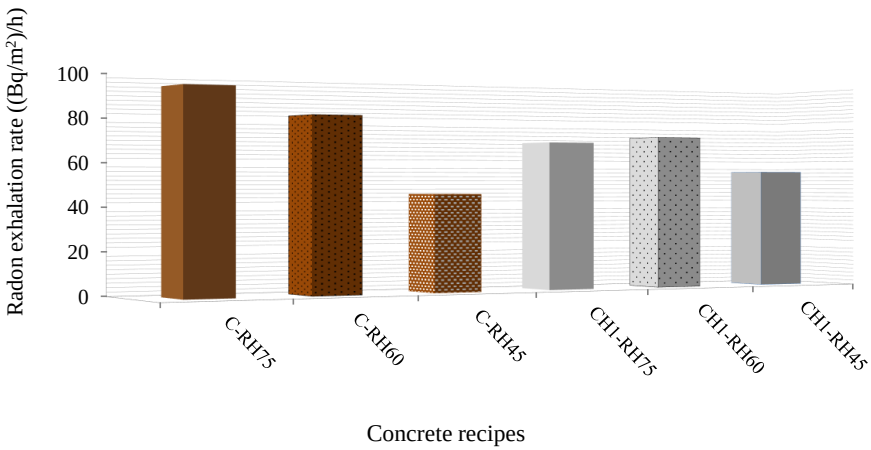

Figure 5.15. Calculation of the radon exhalation rate ((Bq/m^2)/h) of two recipes at different relative humidity levels (RH75 %, RH60 %, RH45 %).

The columns represent the radon exhalation rate ((Bq/m^2)/h) for each measurement, using always the same "prism" in each series (recipe) during the measurement. Accordingly, a conclusive presentation of each concrete recipe is represented in Figures 5.16a-c, which show the radon exhalation rates as a function of each concrete recipe at relative humidity levels of 75 %, 60 % and 45 %.

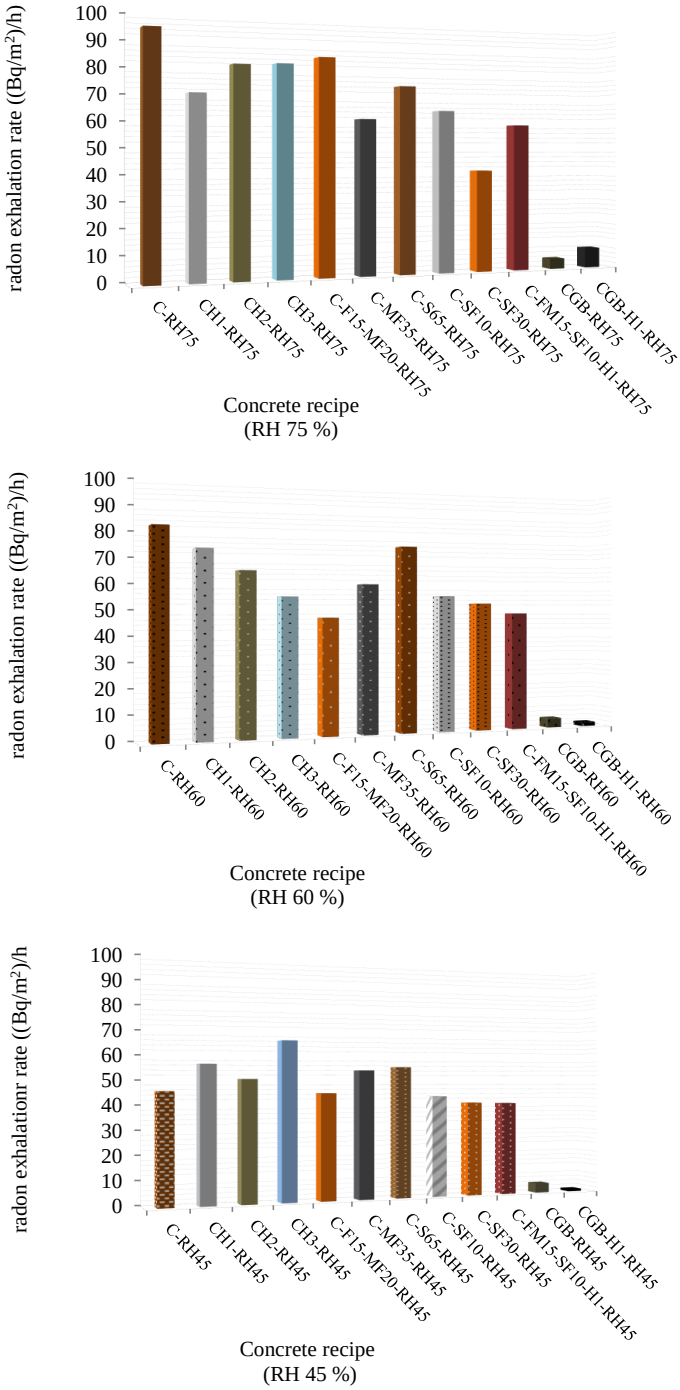

Figure 5.16a-c. The radon exhalation rate ((Bq/m^2)/h) as a function of the relative humidity at 75, 60 and 45 % for the investigated concrete recipes.

At a relative humidity of 75 %, all recipes containing different SCMs or hydrophobic admixtures, or a combination thereof, show a decrease of 10 % or more of the radon exhalation rate ((Bq/m^2)/h) compared to the reference concrete. For SCMs with a high amount of fly ash (C-MF35) or a minor share of silica fume as binder (C-SF10), the decrease is roughly 30-35 %. When the addition of silica fume is further increased as part of the binder system (C-SF30), the decrease is around 57 %.

For the recipes containing hydrophobic admixtures, the largest effect can be seen for the additive C-H1, where the reduction in exhalation rate is around 25 % compared to the reference concrete at a relative humidity of 75 %.

A similar trend can be seen for most recipes where the radon exhalation rates at a relative humidity of 60 % had been calculated. Most recipes show a lower radon exhalation rate compared to the reference concrete. For some recipes, no change in radon exhalation rate compared to the calculated value at a relative humidity of 75 % could be documented. In a few cases (S-C65 and C-SF30), the calculated value was higher compared to the value at a relative humidity of 75 %.

A sharp drop of the radon gas exhalation rate ((Bq/m^2)/h) for the reference concrete (C) is noted between a relative humidity of 60 and 45 %. In many cases, the reference concrete has a calculated radon gas exhalation value that is lower at a relative humidity of 45 %, compared to some of the other concrete recipes.

However, the general trend for each recipe regarding the relative humidity is quite distinct. At higher relative humidity levels of the concrete mixes, the exhalation rate is high and drops as the relative humidity decreases. Only the recipes containing a high share of silica fume (C-SF30) show a more obscure trend, and in part also slag (C-S65).

5.11 Control study of radon exhalation as a function of hydration during the first six months with a fixed relative humidity (85 %)

Four different concrete mixes were examined. The chosen recipes (see Table 4.1 for guidance) included the reference cement C, C-H3, C-F15-MF20 and C-S65. As previously mentioned (Section 4), the cast recipes were stored in a climate chamber with a fixed relative humidity of 85 %.

The calculated results from the control study indicate that the effect of hydration, at least between three and six months, did not have any effect on the rate of radon exhalation. In all cases, only minor differences could be noted between the measurements, regardless of the investigated recipe. Figure 5.17 presents the calculated radon exhalation rates as a function of time at three and six months. Only for the recipe C-F15-FM20 was a slightly lower radon exhalation rate determined. However, this was still within the range of uncertainty (5 % with a 95 % confidence interval). Consequently, the change could not be considered as evidence for any documented change in the radon exhalation rate in this interval, but does imply a possible minor change due to hydration.

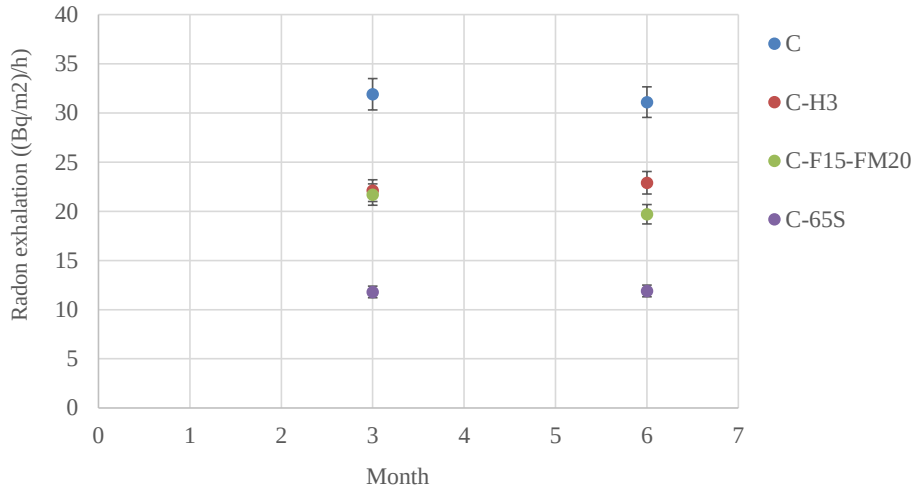

Figure 5.17. The radon exhalation rate as a function of time for four of the concrete recipes with a fixed relative humidity at RH 85 %.

5.12 Hydrophobic admixtures and their implications

Part of the two assessments, where separate studies are presented (Papers II and III), included admixtures with different hydrophobic characteristics. In the main study (Paper III), recipes C-H1, C-H2 and C-H3 constituted a blend of an OPC and an addition of the mentioned hydrophobic admixtures. They are all "liquid hydrophobic admixtures", in the sense that they are fluids and are blended with the water before being mixed into the final concrete.

For Paper II, a different liquid hydrophobic mixture named Hycrete X1002 was used. The results using Hycrete showed a marked reduction of 30-35 % in the radon gas exhalation rate compared to using a CEM I binder at relative humidity in the span of 85-55 %. However, it should be noted that a slightly higher w/b ratio (0.65) and a different binder were used in this experiment compared to the experiments in Papers III, IV and IV.

In the major study (Paper III), a significant reduction in the radon exhalation rate at a relative humidity of 75% could be noted, especially for the recipe C-H1: a reduction of up to 25 % was documented in comparison to the reference concrete C.

The additives' effect upon the radon exhalation rate is more specifically addressed in Papers II and III. The results of this study are otherwise presented in Sections 5.10 and 5.11 regarding the effect upon the radon exhalation rate of using an input of hydrophobic admixtures. A similar trend can be seen for all assessed additives. A reduction of the exhalation rate was evident due to these constituents, at least at higher relative humidity levels (75 % and 60 %).

Alongside some of the experiments, a concrete mix containing another binder, CEM II A/LL 42.5 (Cementa AB/HeidelbergCement Group) was assessed, but the same aggregates and w/b ratio and recipes as in the main study were used. The results were also very similar to the effects achieved using the recipe C-H1, but the effect of using a liquid hydrophobic mixture was in this case even larger at a relative humidity of 75 % compared to the reference cement. The results were presented at the XXIII Nordic Research Concrete symposium in Ålborg, Denmark in 2017 (Döse & Silfwerbrand, 2017).

5.13 Carbonation on cast mixtures stored in a climate room

All concrete recipes had an excess of concrete prisms that were stored in a climate room after initial water cooling of all the cast specimens. The room had a constant temperature of 23°C (±2) and an RH value of 50 % (±2).

After approximately two years (22 months), one concrete prism of each concrete recipe was tested for the effect of carbonation. The samples were sprayed with phenolphthalein according to the procedure described in SS-EN 13295 (2004).

Figure 5.18 presents the different prisms after testing with phenolphthalein, where the pink-purple color represents the non-carbonated area, and the light grey rim is the zone of carbonation.

Figure 5.18. Different concrete castings of the 12 recipes with different carbonation depths. The samples are shown numbered 1-12, in columns, from the upper right corner to the lower left corner.

Table 5.7 presents the results of the measured carbonation depth of each cast recipe after almost two years of drying in the climate room.

Table 5.7. Carbonation depth after two years of drying.

		Measurement ~ two years after casting				
No	**Concrete recipe**	**Side A (mm)**	**Side B (mm)**	**Side C (mm)**	**Max (mm)**	**Mean (mm)**
1	C	4.9	4	3.5	4.9	4.1
2	C-H1	4.8	4.6	3.7	4.8	4.4
3	C-H2	4.9	4.8	5.5	5.5	5.1
4	C-H3	5.7	8.1	6.8	8.1	6.9
5	C-F15-MF20	6.6	6.3	7.1	7.1	6.7
6	C-MF35	8.9	7.6	7.2	8.9	7.9
7	C-S65	7.6	10.3	9.3	10.3	9.1
8	C-SF10	4	4.9	4.4	4.9	4.4
9	C-SF30	7.7	5.3	7.9	7.9	7.0
10	C-FM15-SF10-H1	5.4	7.2	6.9	7.2	6.5
11	CGB	2.9	3.3	3.4	3.4	3.2
12	CGB-H1	4.6	5.3	5.6	5.6	5.2

In Figure 5.19, the values in Table 5.7 are presented graphically.

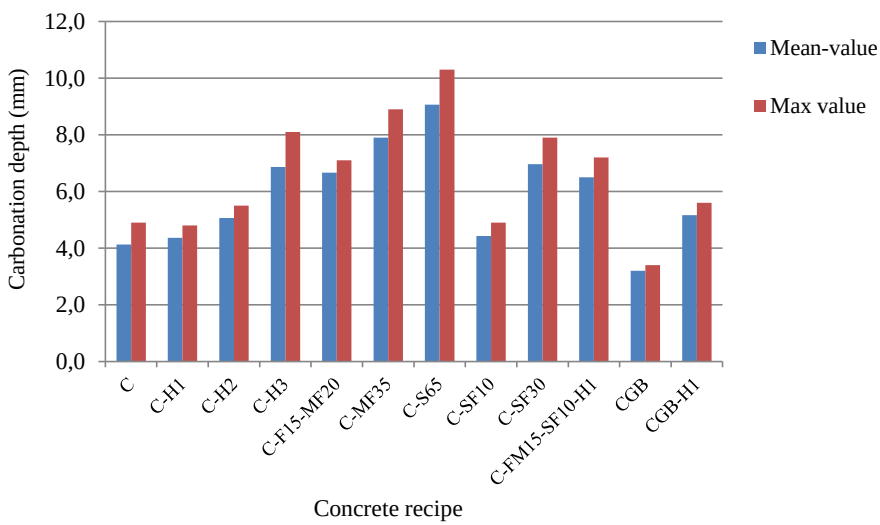

Figure 5.19. The carbonation depth of all measured prisms presented as “max” and “mean average”.

For the recipes containing SCMs of fly ash, slag or a large amount of micro-silica (C-SF30), there was a noticeable increase in carbonation rate compared to the reference cement. This was in part also true when hydrophobic admixtures were added to the recipe. The recipe containing a limited amount of

micro-silica (C-SF10) did not show any noticeable difference compared to the reference concrete prism. The reference concrete mixes (C and CGB) showed the smallest carbonation ingress.

Due to these results, it was decided to further investigate the possible influence of carbonation upon the exhalation rate of radon gas at a fixed w/b ratio and fixed relative humidity of RH 75%.

5.14 Cracks induced into concrete prisms

Two different concrete recipes were investigated, with the same w/b ratio. The two recipes included two analysed concrete prisms each. One recipe contained only ordinary, rapid-hardening cement (reference cement C) and the other contained an addition of a liquid/hydrophobic additive (C-H3).

The results of the study imply a substantial increase in the exhalation rate when cracks are induced. Table 5.8 presents a summary of the radon exhalation rate of each recipe and its percentual increase compared to the concrete's pristine state (no cracks induced).

Table 5.8 – Results of the radon gas exhalation measurements of each prism in a pristine state ("prist.") and after cracks ("cracks") were induced.

Prisms	**OPC 1-1**		**OPC 1-2**		**CH - 1-1**		**CH - 1-2**	
	Prist.	**Cracks**	**Prist.**	**Cracks**	**Prist.**	**Cracks**	**Prist.**	**Cracks**
Exhalation rate ((Bq/m^2)/h)	38.2	67.3	36.1	78.6	31.9	114.6	26.3	79.5
Difference (%)		76		118		259		202

For the concrete mix OPC, an increase in the radon gas exhalation rate was in proportion to the increased area due to the cracks induced. However, for the concrete mix CH, a much more marked increase due to induced cracks was evident. A more comprehensive outline of the results, analysis and discussion is found in Paper IV.

5.15 Accelerated carbonation test regarding the rate of radon exhalation

The test included four different recipes. The prerequisites were according to the same recipes as used in all the other studies. The investigated recipes were C, C-H1, C-FM15-FM20 and C-S65. The setup is described in detail in Chapter 4, Section 4.13. The carbon dioxide level in the climate chamber was set to 1% CO_2 for the first three months. Thereafter, the level was increased to 2 %. Figure 5.20 presents the mean results of the carbonation depth as a function of time for each recipe.

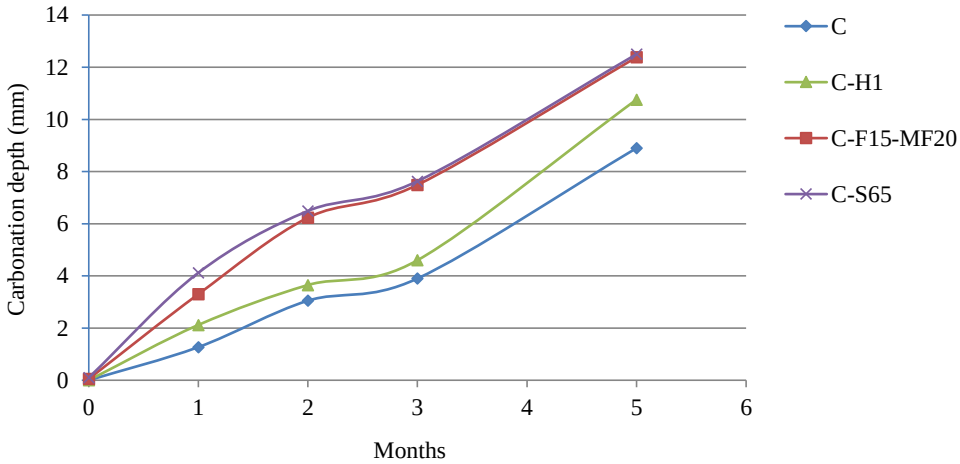

Figure 5.20. The different recipes with their measured mean carbonation depth as a function of time.

It was noted that the binders containing fly ash and slag had a faster carbonation ingress. This phenomenon was also addressed by Helsing (2017) when assessing input of SCMs in binders and their effect upon the salt frost resistance of concrete mixes. Figure 5.21 presents the results of the radon exhalation rate of the concrete recipes as a function of time.

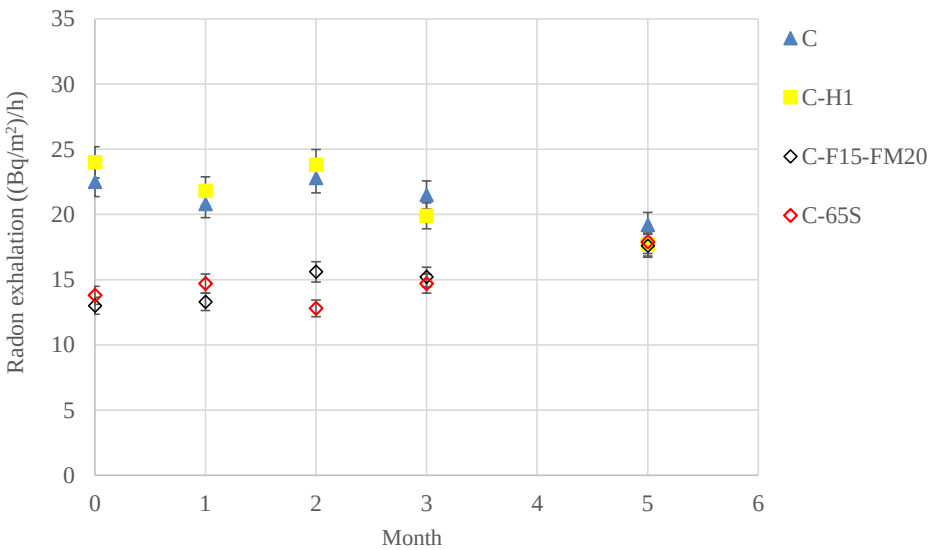

Figure 5.21. Radon exhalation rate ((Bq/m^2/h)/h as a function of time during carbonation.

The results indicate different trends in the radon gas exhalation rate as a function of time depending on the type of concrete mix being assessed. For concrete with binders with a high share of SCMs (C-F15-MF20 or C-S65), the radon exhalation rate apparently increases with increasing carbonation depth. For the reference concrete (C) and the reference concrete including a hydrophobic admixture (C-H1), the radon exhalation decreases.

The carbonation ingress is in good agreement with the difference in results between the concrete mixes measured for the cast recipes after almost two years in the climate room (Figure 5.19). Both measurements, shown in Figures 5.19 and 5.20, indicate a faster ingress rate for concrete recipes containing a high share of SCMs (fly ash and slag) compared to a reference concrete. This has also been documented by several other authors (Boumazza et al., 2020; Justness et al., 2020). The used reference concrete with a hydrophobic admixture also points to a slower ingress rate compared to concretes with SCMs in the first study (Figure 5.19). This is also in line with the results of the second study (Figure 5.20).

A more comprehensive outline is presented in Paper V.

6 Discussion

The thesis deals with ionising radiation in concrete intended for buildings and has primarily focused on:

I. Investigation of the relation between relative humidity and radon gas exhalation (RH 75 %, RH 60 % and RH 45 %) using an approximate fixed porosity value and a constant w/b ratio for several concrete recipes with different binders (SCMs) and hydrophobic admixtures (liquid additives).
II. Determination of the diffusion coefficient or diffusion length of radon of the different concrete recipes measured at different relative humidity levels (RH 75 %, RH 60 % and RH 45 %).
III. Cracks in concrete and their effect on the exhalation rate at a fixed relative humidity (60 %).
IV. Carbonation of different concrete mixes and its effect on the exhalation rate at a fixed relative humidity (75 %).

As a result of the emphasis on the radon exhalation rate and the diffusion coefficients at different relative humidity levels, several parameters influencing this behaviour directly or indirectly have been investigated more closely, such as (i) the role of hydration using different SCMs, (ii) the role of the emanation coefficient regarding the final exhalation rate of concrete mixes, (iii) the influence of porosity, (iv) the effect of the pore radius and pore distribution within the cement mixes, and (v) the water absorption ability of the investigated concrete mixes.

Secondly, some necessary assessments have been conducted to determine and analyse the concrete materials included in the main studies, such as:

- Compression tests of the concrete mixes in the main study at 7, 28, 356 and 900 days.
- Analysis of the gamma energies of the used binders, with or without hydrophobic admixtures, as well as the final concrete mixes to calculate the I-index (activity-index) as part of the main study.
- A complementary study of micro-cracks of the different concrete mixtures was performed. This was regarding the relation to radon gas diffusion measurements. The analysis was conducted by using some of the "diffusion plates" in the study. The analysis included ocular inspection and thin section analysis to check for any presence of cracks.
- Investigation into the effect of hydration in the interval between three and six months for concrete mixes including sole OPC, OPC and a hydrophobic admixture as well as binder combinations of OPC and fly ash and OPC and slag.

6.1 General

A discussion of different properties influencing the radon exhalation rate and the gas diffusion rate (radon flux) is presented in separate sections in the following text. Since there are many factors influencing the radon gas exhalation rate and there are still some relatively unknown factors, it is deemed appropriate to discuss these factors successively.

6.2 Constituents and compressive strength

Regarding different constituents, it can be expected that concrete containing SCMs such as fly ash or slag will initially have a slower strength development (Neville and Brooks, 2010). For micro-silica, it is also expected that it will act as a filler besides being a pozzolanic addition. Being a pozzolanic SCM, it firstly needs calcium hydroxide ($Ca(OH)_2$) to promote the initiation of C-S-H hydration (Mehta & Monteiro, 2006). The filler will make the concrete matrix more closely packed and give the concrete a higher compressive strength after prolonged curing (Hewlett & Liska, 2019).

Binders with hydrophobic admixtures will show a latent hydraulic action, since the use of these admixtures will reduce the early strength (Plank et al., 2015). This has been demonstrated by Spaeth et al. (2008) where the addition of a bulk additive (hydrophobic admixture) results in delayed hydration of the C-S-H linkage. This finding is also validated in this study and has previously been demonstrated by other authors (Plank et al., 2015; Helsing et al., 2017).

It should be recognised that some recipes, especially those including fly ash, may have a prolonged hydration due to high content of SCMs. This has been well documented by Mueller et al. (2017), where recipes containing larger shares of fly ash showed a steady strength increase even after 90 days, and some experiments imply a vague but continued hydration even after a year or two, due to a slow consumption of excess lime. However, this was observed in combination with a coarsely ground cement. Jalal et al. (2015) experimented with different amounts of silica fume and fly ash for concrete with cement amounts of 400 to 500 kg/m^3 (ASTM Portland cement type II) and a w/b ratio of 0.38.

In general, the recipes in this study have been considered as being fully hydrated when the radiation measurements were initiated after approximately five to six months. This is in part supported by the experiments (radon exhalation of four concrete mixes at three and six months) as part of this dissertation. The compressive tests after 28 days imply that most recipes had already gained a strength of at least 70-80 % of their final strength. As expected, the concrete containing micro-silica also shows the highest strength after a full year. Also as expected, those concrete recipes containing a hydrophobic additive (C-H1, C-H2 and C-H3) all show a lower compressive strength compared to the identical concrete recipes without a hydrophobic admixture (C) at every measurement. This is in line with previous studies (Selander, 2010, Helsing et al. 2017).

The successive strength development of the concrete recipes containing slag and fly ash was in part as anticipated, specifically for those recipes containing a large fraction of SCMs (C-FM35, C-S65). The results indicate an initially quite low compressive strength at seven days compared to the other concrete recipes. In the time span of seven to 28 days, the compressive strength of the recipes containing larger shares of SCMs has largely increased. This indicates an initially very slow hydration rate shifting to a more rapid strength development after seven days. The concrete recipes containing micro-silica after only seven days show a higher strength than all other recipes. This is likely due to the effect of micro-silica acting as a filler.

The final measurement at 900 days was however not according to expectations. Most of the results indicated a somewhat lower compressive strength at 900 days compared to measurements executed after 300 days. There is no clear explanation for this behaviour, except possibly a more finely tuned sensitive load cell adjustment, or possibly external factors such as micro-cracking due to uneven drying and/or carbonation, which may have affected part of the concrete specimens negatively.

6.3 Porosity, pore distribution, diffusion coefficients and radon gas exhalation rate/radon flux

The measured porosities in the first tests (main study) were based on concrete cubes (150 x 150 x 150 mm) that were initially submerged and subsequently investigated after six months. That experiment indicated that some mixes containing SCM such as micro-silica (C-SF-30) had a higher porosity than the reference cement concrete. Furthermore, in the “control study”, it was also implied that reference concrete had a slightly lower porosity than the one of the binder mixes containing fly ash (C-F15-MF20). On the contrary, the cumulative measurement results of the porosity of the cement paste using MIP implied that the reference cement paste had the highest porosity, whilst the lowest porosity was measured for the cement paste recipe C-F15-MF20. In other words, the porosities for some recipes show noticeably different results depending on the methodology used. According to Boumazza et al. (2020), this is not surprising, since MIP is a pressure-induced methodology, indicating that not all gel pores are included in the measurement. It should thus also be noted that the MIP measurements only measured the pore radii r in the interval 0,0005 um $\leq r \leq$ 100 μm. Consequently, larger pores or air

voids are not included in the results. Another cause for a generally lower porosity for the cement pastes assessed by MIP compared to the concrete mixes is the mixing of cement, water, and aggregates. The mixing causes cavities along the interstitial transition zone (contact aggregate/cement paste) of the concrete mixes.

Assessing the results of the cement paste (MIP tests), it can be seen that there is a clear connection between the "total porosity" (Table 5.4) and a lower diffusion coefficient (Table 5.6, Figure 5.15). A low diffusion coefficient, as for C-F15-MF20 and C-S65, is in correspondence to a lower total porosity. This is also true regarding the compared reference cement paste (C) which has the largest measured and calculated total porosity in the MIP tests (Figure 5.15) and correspondingly among the highest diffusion coefficient of the measured concrete plates (Table 5.6).

From the main study, it is also evident that those concrete mixes with the lowest porosities are those containing a hydrophobic admixture. In a comparison between the porosities of the concrete mixes of the main study and the ones in the control study (measured after 28 days), it was evident that three out of four recipes in the control study indicated a higher porosity (ca 0.5-1.5 vol. %). The higher porosity values are likely caused by an early and only partially set pore structure of the capillary and gel pores of the concrete mixes (Hewlett & Liska, 2019).

With consideration to the MIP study, the highest porosity was calculated for the reference cement paste, whilst the lowest porosity was calculated for the mixes containing fly ash and slag. It can thus be argued that porosity has a vital impact on the radon gas exhalation rate due to its influence on the bulk/effective diffusion (Eq. 3.24). The porosities calculated from the cement pastes (MIP) suggest this, and it is well reflected by the differences in the calculated radon gas exhalation rates of the mentioned concrete recipes (C, C-F15-FM20 and C-S65) at RH 75 %. High radon gas exhalation rates are as such a function of the porosity in the cement paste and vice versa. This implies that the results of MIP evaluating only the cement paste are consistent and that a lower porosity in the cement paste is largely reflected in a lower radon gas exhalation rate. This indicates that the diffusion coefficient is the important variable at a moderate to high humidity (RH 60-75 %), largely controlling the radon release rate. At lower relative humidity levels (RH 45 %), this trend is much more obscure.

Nonetheless, in the experiments it was also shown that adding micro-silica as part of the binder resulted in a high porosity (Table 5.3, Figure 5.1) compared to the other concrete mixes. The results of the cement pastes (MIP) also indicated that micro-silica (C-SF10 and C-SF30) had a moderate to high porosity compared to the other cement paste mixes.

Therefore, the question arises as to why there is such a large difference in the radon exhalation rates (at RH 75 %) between the concrete mixes of C and C-SF-30, despite the fact that the porosities in both concrete mixes are high. The cause is probably at least partly related to the large differences in the mean pore radius and the pore size distribution of the different cement paste mixes. The mixes containing micro-silica have a mean pore radius that is more than half the size of the mean pore radius of the reference cement paste (ref. cement 0.0121 µm compared to 0.0050 µm and 0.0045 µm for the two micro-silica mixes). In Boumazza et al.'s (2020) comparison of carbonated and non-carbonated cement pastes, it was found that the pore-size distribution and the degree of water saturation could be seen as material properties as a function of the diffusivity of the samples. This is also inferred in the Knudsen diffusion model (Cozmuta et al., 2003; Xi et al., 1994), where the effective diffusion coefficient is proportional to the mean pore diameter.

The experiments by Boumazza et al. (2020) included a reference OPC (CEM I 52.5N) paste that was compared with paste mixes where additions of 30 % fly ash and 60 % slag at a w/b ratio of 0.6 were used, much the same in composition as in this study. Boumazza et al. (2020) demonstrated that, regardless of cement paste mix, a smaller mean pore diameter and pore size distribution also induced a lower gas diffusivity. This is also addressed by some authors as the connectivity of pores (Zeng et al, 2012; Boumazza et al, 2020). Their results suggest that concrete with mainly very small pores, relative

to other concrete mixes, will mitigate the radon gas transfer more strongly. Consequently, a large part of the newly formed radon atoms will decay in the material instead. Thus, adding very finely dispersed mineral additions such as micro-silica as part of the cementitious binder composition will serve two main purposes:

(i) The addition will act as a filler in the cement matrix and as such make the cement matrix denser (Taylor Lange et al., 2012; Chauen & Kumar, 2013; Mueller et al., 2017; Lagerblad, 2017).
(ii) Reduces the average mean pore size diameter within the cement paste.

This results in a less permeable concrete mix with a lower diffusion coefficient that reduces the gas transfer within the concrete mix. This could most evidently be seen for the concrete mix containing silica (C-SF-30) where the radon gas exhalation rate already at a relative humidity of 75 % was reduced by 57 % compared to the reference concrete, although the porosity was quite high compared to many other concrete mixes.

6.4 Water absorption and radiation

The water absorption test was performed to investigate whether any obvious link to the radon exhalation and radon diffusion properties could be documented. It is suggested that a concrete that is less prone to absorb water would show a lower diffusion coefficient or likely a lower radon exhalation rate due to a non-permeable concrete with pore interconnectivity between the capillary pores to enable suction (absorb water). It was thought that the reference cement concrete would show a fairly high water absorption coefficient, whilst likely SCMs (specifically silica and fly ash) may act in part as fillers and give a denser concrete resulting in less absorption of water in these concrete mixes. The hydrophobic concrete mixes were suspected to have a fairly low water absorption coefficient due to their hydrophobic nature (Plank et al., 2015; Selander, 2010;,Helsing et al., 2017).

Using the hydrophobic admixtures had a strong effect on the absorption capability of water on these concrete mixes. The lowest results were from OPC-H1. During the initial stages of the experiment (first eight hours), the highest absorption was from the reference cement concrete (C). Regarding the link to the radon exhalation rate, this could also be demonstrated. This was most evident at RH 75 % and RH 60 %. The results therefore imply that at a high relative humidity, the hydrophobic agent acts as a partly impermeable film to mitigate a high exhalation rate of radon gas. As the relative humidity in the concrete specimens is lowered, this effect apparently disappears or is of secondary importance, probably due to increased access of air through other parts of the pore system at a lower relative humidity.

Regarding the SCMs as part of the concrete, the concrete mix containing micro-silica generated the highest water absorption coefficient after 24 hours. The higher the share of micro-silica as part of the binder, the higher the absorption capacity. The different contributions of fly ash did not show a remarkable difference compared to the reference concrete, but the concrete mix containing two different fly ashes (C-F15-MF20) did show a higher degree of absorption. The contribution of slag (C-S65) did not show any large difference in its absorption capability compared to the reference concrete. Thus, it could be noted that the recipes containing silica fume apparently have a high absorption capacity, likely due to silica fume's very large surface area (Zeng et al., 2012). This is also in agreement with the porosity measurements obtained for the concrete cubes, where concretes containing silica fume also show a higher porosity than the other concrete specimens. From the MIP results (Table 5.4), it is also indicated how much larger the pore surface area is for the cement pastes containing silica fume compared to the ones with other SCMs and the reference cement paste. Consequently, it seems reasonable that the concrete mixes with a large pore surface area also show a high absorption capability. Despite high porosity, the radon exhalation rates (Figure 5.4) of the silica concrete mixes show the lowest radon gas (regardless of the relative humidity level), implying that the micro-silica acts as a filler to make the concrete less permeable and very dense. Thus, it can be

assumed that the water absorption capability test is a poor reflection of the concrete mixes´ ability to exhale radon gas into the ambient air. It may only in part be used as guidance of expected ^{222}Rn gas exhalation rates.

6.5 Hydration and radiation

Hydration results for the concrete specimens were compared as part of the main study. It was expected that some concrete recipes may hydrate slowly due to larger amounts of SCMs, where the SCMs start to hydrate only in presence of portlandite ($Ca(OH)_2$) in the cement matrix. Depending on the cement used (CEM I – 52.2 R), the larger part of the hydration cycle and strength development was accounted for within a few months (Neville and Brooks, 2010; Mueller et al., 2017). Depending on different SCMs and additives added to a mix, this period "before one may consider the concrete strength as more or less final" depends of course upon the binder combinations used, their fineness and composition (Mehta & Monteiro, 2006).

In the experiments, the reference cement CEM I 52.5 R was used, where most (but not all) of the cement clinkers were assumed to be hydrated after three months (Mehta & Monteiro, 2006). It was anticipated that further hydration would not change the pore system substantially. Nonetheless, a minor test was performed to investigate the effects of the hydration of concrete specimens regarding its possible influence on the radon gas exhalation rate (Chapter 5, Section 5.11) at different times of hydration.

The experiments concerning the effects of hydration within this study showed that no clear effect could be documented upon the radon gas exhalation rate regarding hydration influence. It should be noted that these experiments were conducted at a fixed relative humidity of 85 %. A small decrease was noted for the concrete recipe containing fly ash but the difference in the exhalation rate was within levels of uncertainty. Even so, the results, regarding a continued hydration after six months of the concrete specimens, may indicate a small contribution of a more set concrete paste with more C-S-H-gel occupying vacant spaces. This would imply a less permeable concrete and as such a lowered radon exhalation rate may result. This should be considered, since concrete with SCMs normally hydrates slower than OPC (Taylor-Lange, 2012; Setina et al., 2013). As stated earlier and documented by Jalal et al. (2015), it also implies that most recipes containing small to minor amounts of fly ash continue to show more strength increase compared to OPC, well beyond three months. However, the results of this study indicate that hydration after a few months contributes only very little to changes in the radon exhalation rate, in any case compared to influences of other external processes, such as carbonation ingress (Section 6.7 and Paper V).

6.6 Cracks in concrete

Most concrete produces micro-cracks or cracks in due time (Mehta & Monteiro, 2006). As such, it was reasonable to assess the influence of cracks upon the radon gas exhalation rate. It was thought in general that an increase in the radon exhalation rate should be proportional to an increase in surface area as suggested in models and calculations of the radon exhalation rate (ISO-11665-7). Not much is found in the literature regarding cracks in concrete, except where there is a relation between the cracks and the underlying soil (Landman, 1982; Handbook of Radon, 2004).

The results from the study where cracks were induced into the concrete were slightly surprising. An increased radon exhalation rate, as mentioned, should be proportional to an increase of the surface area if the concrete is moderately homogenous. In two cases, however, the increase in the exhalation rates was 200-250 %. Theoretically, a 100 % increase would be more likely regarding a doubled surface area due to the induced fractures. However, the very large increase in the exhalation rates for some of the concrete prisms implies that the applied load cell also induced numerous minor cracks in the concretes, not visible to the naked eye, giving radon gas additional routes to escape into the free air.

The study did show that the radon exhalation rate was strongly affected by cracks in concrete. This serves as a reminder to avoid striving to produce floors and walls with only the economic aspect in mind, where too weak or slender concrete structures may easily break, generating cracks in the concrete and subsequently causing secondary effects such as a strong increase in radon gas emissions.

6.7 Carbonation and radiation

Carbonation of concrete was one of the areas where documentation and literature regarding the radon gas exhalation rate was quite limited, since most research relates to the carbonation process regarding the risk of de-passivation of the surface reinforcements. Due to the limited research available, the expectations of the study (Paper V) within this project were ambiguous and the outcome could not be anticipated

In a doctoral thesis by Utgenannt (2004) the author demonstrated microstructural changes in concrete mixes containing large amounts of slag, indicating a coarser pore structure due to carbonation, but at the same time a decrease in porosity as a result of carbonation. Similar findings have recently been documented by Justnes et al. (2020), Boumazza et al. (2020) and Qin et al. (2019). Justnes et al. (2020) compared the carbonation ingress into cement pastes after 14 and 56 days of carbonation using CEM I and CEM IIB-V (~30 % fly ash) as binders. After carbonation for 56 days, the researchers identified two trends: (i) a decreased diffusion coefficient for a carbonated reference cement paste containing primarily CEM I and (ii) an increased diffusion coefficient for the binder with CEM II/B-V compared to the non-carbonated reference specimen. Similar findings were documented by Leeman (2019) comparing a slag cement and an OPC cement. These differences in the diffusion coefficients of the binder mixes containing only OPC as references and of cements containing SCMs could, according to Justnes et al., be explained by changes in the mean pore diameter of the carbonated samples. According to Justnes et al. (2020), the coarsening of the pore structure is related in part to the aluminate phases, where the cement binder compositions with a high content of Aft/Afm in concrete with high proportions of SCMs lead to an internal volume decrease of these solids when carbonated, due to the release mechanism of large amounts of crystal water in the Aft/Afm phase transformation during carbonation. This in turns leads to a higher porosity and coarser pore structure within the cement pastes. Wu et al. (2017) have also highlighted the coarsening of the mean pore diameter as a cause of better interconnectivity of the gel- and capillary pores, explaining the increase in the diffusion coefficient of carbonated specimens. Using only an OPC binder, most literature indicates a densification or a finer microstructure due to carbonation (Papadakis, 1992; Lagerblad, 2017). This is also in agreement with the findings of Wu et al. (2017) and Justnes et al. (2020).

From the initial assessment (Chapter 5, Section 5.13), it was obvious that the use of SCMs also generated a faster carbonation ingress under favourable conditions (air). This is also in line with studies by Kurda et al. (2019), Boumazza et al. (2020) and Justnes et al. (2020) as well as reported values by Helsing (2017). In two cases, a marked increase in the radon exhalation rate was demonstrated after carbonation. This occurred for the concrete recipes where large contributions of SCMs (C-F15-FM20 and C-S65) were added. In contrast, the ordinary recipe (C) and the recipe containing a hydrophobic admixture (C-H1) showed a slight decrease in the radon exhalation rate.

The author believes that the results are reasonable and in line with the literature addressing carbonation of concrete specimens as a function of diffusion characteristics. Investigations of changes in the micro-texture that occur for SCMs documented by Utgenannt (2004), Wu et al. (2017) and Justnes et al. (2020) among others indicate that a coarser pore structure as carbonation progresses in the concrete will render a higher radon exhalation rate. This is also demonstrated in the study and is considered highly credible (Paper V). A concrete mix containing only CEM I as the reference concrete, however, may precipitate carbonates primarily in the capillary pores, reducing the mean capillary pore size (Justnes et al. 2020). As a result, the radon gas is in part hindered on its transport route to the free air, resulting in a lower radon gas exhalation rate.

6.8 Moisture (relative humidity) and water regarding radon exhalation rate and radon diffusion

Research on the influence of moisture (Petterson et al., 1984; Rogers and Nielson, 1991; Stranden et al., 1984; Cozmuta et al., 2003; van der Graaf & Meijer, 2005; Munoz et al., 2017) indicates a decrease in the radon gas exhalation rate as moisture decreases in building materials, such as concrete. This is also in accordance with the model demonstrated by van der Graaf & Meijer (2005) and in part also in experiments by Döse (2016). Thus, it was predicted prior to the experiments conducted for this dissertation that the gas radon exhalation rates of the concrete mixes would release less radon gas as the relative humidity (moisture content) of the samples decreased. This hypothesis was based in part on the recoil principle (Stranden et al., 1984). Stranden (1984) also stressed that *if there is a moisture content gradient in the sample, active transport of radon on water molecules may take place*. This also seemingly has a bearing on the results presented in this dissertation, where the highest radon gas exhalation rates clearly were measured regarding a higher moisture content.

Regarding the radon gas exhalation measurements, the following discussion is interesting. Radon gas will be generated because of ^{226}Ra decay from the constituents of the concrete material. These constituents are mainly cement binders and aggregates that release radon gas into the pore system of the concrete. Under these circumstances, the recoil principle applies. The recoil theorem can be discussed in the case of a water-filled concrete sample (moisture content and relative humidity of 100 %). According to the recoil theorem, a larger fraction of radon atoms and alpha particles will upon decay end up in the water-filled spaces due to the very short distance travelled in water compared to air. The water in the pores or the film of water on grains slows down or hinders radon or α-particles from travelling long distances. This process is defined by Porstendörfer (1991) as "recoil stopping power". A high recoil stopping power has the consequence that decay of ^{226}Ra to ^{222}Rn in the vicinity of the surface of a material's grain is significantly hindered from reaching the adjacent grains. Consequently, the atoms and α-particles released in these regions of a material are more likely to terminate its recoil, caused by decay, in the water (pore space). This gives rise to an increase of ^{222}Rn concentrations and α-particles in the water pore system that may be expelled into the air. However, due to the very low diffusion rate in water, almost all radon gas will decay in water. Eventually, as the moisture content (relative humidity) in the concrete sample is reduced, the recoil stopping effect will diminish (Porstendörfer, 1994) and a lower share of radon atoms will end up in the pore system of the concrete. This will have two different effects:

(i) as less water or moisture occupies the pore space, more radon gas will be able to escape via the air in the pores, but also
(ii) due to a lower moisture content in the pores, less radon gas (atoms) will end up in the pores themselves (higher probability of recoil to adjacent grain). This will lower the emanation coefficient and consequently the exhalation rate.

Thus, radon exhalation rates are shown to be (for most concrete experiments) at their highest level at ~80-90% of their relative humidity (Döse, 2016; Petterson et al., 1982; Cozmuta et al., 2003). This is in part also indicated in the main study and supports earlier research (Cozmuta et al., 2003; Munoz et al., 2017). Regarding the influence of moisture upon the radon exhalate rate, it can be noted that it is a complex process as described by van der Graaf & Meijer (2005), where the partition coefficient corrected porosity β is a function of the total porosity as well as the fraction of water saturation of the pores. The influence of the moisture content upon the radon exhalation rate of the concrete specimens is also related to the total porosity, where the largest effect is noted on concrete samples with a porosity less than 15 % (Fournier et al., 2005; van der Graaf & Meijer, 2005).

Regarding the diffusion measurements from the experiments, with a clamped concrete slab between two chambers, similar experiments have been conducted by different authors (Kovler, 2012; Maier et al., 2018). The diffusion measurements measure the ability of radon atoms to move from one side of a closed chamber to the other, with a concrete specimen in between. Thus, the permeability (in this case ^{222}Rn gas) of the concrete specimen is measured. Moisture in the concrete specimen, under these

circumstances, merely contributes with an increased resistance to the flow capacity, since diffusion in water is much slower (Table 2.3) than in air (Porstendörfer, 1994). This is also evident in Figure 3.7 regarding the diffusion coefficient in dense concrete as a function of humidity. Thus, for the diffusion measurements, it is reasonable to expect that the diffusion coefficients increase (as does the radon diffusion length), when less water or lower relative humidity (lower moisture content) of the concrete specimens is documented. This is also the case for each concrete mix investigated. This is further highlighted in this study and reported in Paper III, and is in line with the results of previous literature studies (van der Graaf and Meijer, 2005; Fournier et al., 2005; Munoz, 2017; Fatema, 2019).

6.9 Radon exhalation rates of the concrete mixes

From earlier experiments (Chauen and Kumar, 2013b; Taylor-Lange et al., 2012), it was assumed that a contribution of SCMs with a finer particle distribution may act as a filler to generate a denser concrete and possibly hinder the radon gas exhalation release (Section 6.3). Regarding hydrophobic admixtures, it was suspected that this may slow down the diffusion process due to a change in the absorption and diffusion properties of the concrete's surfaces (Plank et al., 2015; Selander, 2010), consequently mitigating radon transport and resulting in a decrease in the radon gas exhalation rate.

In general, a compilation of the different concrete samples´ exhalation rates at different relative humidity levels shows a clear decrease in the radon exhalation rates as the relative humidity decreases. However, for some concrete mixes (and binder combinations), such as the slag concrete (C-S65), a more inconclusive behaviour can be seen. Firstly, the radon exhalation rate is higher at RH 45 % than at RH 60 %, which contrasts with most measurements. Secondly, the calculated emanation coefficient (Section 6.12) for slag (C-S65) was basically unchanged, independent of relative humidity investigated. This may be a consequence of the fact that slag concrete, due to external processes such as carbonation, undergoes a volumetric change and is more porous after partial carbonation (Boumazza et al., 2020; Justnes et al., 2020). Thus, a simultaneous development of a larger pore surface area due to carbonation, implying a higher release rate of radon gas, may counteract the reduced release of radon gas atoms into the free air as the relative humidity decreases. This may explain the behaviour of some concretes containing SCMs, such as slag concrete, where the radon gas exhalation rate is largely unchanged regardless of relative humidity.

Secondly, Kumar & Chauhan (2015) presented results from experiments conducted with different amounts of fly ash in concrete measuring the radon surface exhalation rate. These experiments were also related to moisture. The results indicated that optimum performance (the radon gas release rate was at its lowest) occurred when approximately 20-25 % fly ash was mixed into the binder. An increased amount (up to 50 %) or a smaller share of fly ash in the concrete mix generated a larger surface radon exhalation rate. Thus, some SCMs such as fly ash behave differently than micro-silica (Chauhan & Kumar, 2013; Kumar and Chauhan, 2015), where for example an increased amount of silica fume as part of the binder also signals a lower radon exhalation rate in the concrete. This odd behaviour of fly ash as a constituent in concrete may in part explain the variations in the radon exhalation rates under different relative humidity levels between the concrete mixes C-FM35 and C-F15-MF20 in this study. The chosen proportions or shares of fly ash binders may as such not necessarily reflect their optimum behaviours regarding the radon exhalation rate.

The hydrophobic admixtures act as anticipated and help to promote a lower radon gas exhalation rate at higher relative humidity levels, but with quite different impacts. The result of adding a hydrophobic admixture has the consequence that a "hydrophobic film" acts in part as an impermeable layer (Roos et al., 2008) in parts of the pore system of the concrete. The differences in the radon exhalation rate between the recipes are likely due to the different combinations of silanes or polysiloxanes that make up part of the constituent (hydrophobe) added to the water. The general cause of the reduced radon exhalation rate is the large difference in surface tension between water and silicones, meaning that water cannot easily penetrate the hydrophobic film. However, the pore structure is still open, but with a lower diffusion coefficient (Roos et al., 2008). Selander et al. (2008) demonstrated in a study with

shotcrete the effect of adding a hydrophobic admixture. The capillary absorption of the tested hydrophobic specimen with a w/b ratio of 0.55 was reduced by 85 % in relation to the reference concrete. Thus, the mechanism for capillary suction was clearly mitigated by adding a hydrophobic admixture. This demonstrates an obvious hindrance for capillary transport as described by Roos et al. (2008) within the concrete, and in part a reduced diffusion coefficient should be expected, thus a lowered radon exhalation rate is reasonable. The experiments also indicated to some extent a lower diffusion coefficient for those concrete mixes containing a hydrophobic admixture compared to the reference concrete (C, C-H1, C-H2, C-H3) at higher relative humidity levels. Also, for the reference concrete and reference concrete containing an admixture and gabbro (CGB and CGB-H1), this difference in diffusion is evident at higher relative humidity levels.

6.10 Emanation

During assessments and calculations, emanation, considering the moisture influence, is expressed as the emanation coefficient (ϵ), and is directly related to the final radon production.

As demonstrated within this study, the emanation coefficient varies significantly for most concrete recipes investigated in this study as the relative humidity changes. Studies by Yu et al. (1997) with a fixed humidity at 60 % RH using different amounts of pulverised fuel ash (PFA) indicated a sharp drop during the first two to three months for the emanation coefficient in all concrete recipes tested. Yu et al. (1997) attributed this drop in the emanation coefficient during the first 100 days to the drying of the superficial pores. This is also in line with the process of the evolution of gel and capillary pores during initial hydration up to 120-150 days (Cozmuta et al., 2003). In research by Yu et al. (1997), it was found that the emanation coefficient was almost unchanged after three months regardless of mixing proportions of PFA. Consequently, a fixed moisture level seems to maintain the emanation coefficient at a fixed rate after the initial drop due to the most intense hydration phases of the concretes.

In this study, in almost all cases of the concrete mixes investigated, there is a sharp drop in the emanation coefficient as the relative humidity decreases, except for, as mentioned, the concrete containing slag and the silica fume concrete. The finding of a larger emanation coefficient at higher relative humidity levels is in agreement with other authors (Cozmuta et al., 2003; Fournier et al., 2005; van der Graaf & Meijer, 2005), which emphasise that the emanation coefficient has a strong bearing for dense concrete upon the radon exhalation rate. The cause, as first presented by Stranden (1984), is considered to be the limited recoil transfer of ^{222}Rn atoms in water or a high degree of moisture in contrast to air, which results in an increased activity concentration of ^{222}Rn atoms in the pores of a material. Such a scenario, where the relative humidity is high, involves an increase in the number of ^{222}Rn atoms in the pores that will be exhaled to the surface. Where a fully water-saturated pore system occurs, this will instead block the exhalation of radon gas through the material. This is why, as demonstrated by Cozmuta et al. (2003), the radon gas exhalation is significantly increased in the interval between 100 and 90 %, where the activity concentration of ^{222}Rn as a function of the relative humidity often reaches a plateau in the interval of 90-80 %. Thereafter, the ^{222}Rn activity concentration (Bq/m^3) slowly decreases as humidity decreases. Similar results have since been demonstrated by several other authors (Fournier et al., 2005; de Jong et al., 2011; Munoz, 2017). This decrease is related to the recoil theorem, where less moisture in the pores will not limit the ^{222}Rn gas transfer and most ^{222}Rn atoms will continue their journey to an adjacent grain instead. Consequently, fewer ^{222}Rn atoms will be exhaled through the pores to the ambient air.

The general reasons why the concrete samples´ radon exhalation rate or radon production decreases as a function of their relative humidity is discussed in Section 6.9. However, it can be noted that in this research, the differences between the concrete recipe´s mass and activity concentrations (Bq/kg) of ^{226}Ra were limited. Consequently, the radon emanation will largely be influenced by the moisture content of the concrete mixes influencing the radon exhalation rate. This influence can be clearly observed in Figure 5.12 for each concrete mix.

6.11 Radon diffusion measurements

It was believed that a lower relative humidity would promote an increase in the radon diffusion coefficient. However, different results have been shown in previous studies (Porstendörfer, 1994). The general hypothesis is that fewer water molecules within the concrete capillary pores promote a higher transport rate (radon is transported faster in air than water). This is also, in general, documented in the main study. The radon diffusion measurements indicate a higher diffusion coefficient as the relative humidity of the concrete specimens is lower.

The background influence, defined as "the production of radon atoms from the concrete specimen itself", and its contribution to the "total radon gas concentration", is of interest. At very low diffusion coefficients (most noticeable at RH 75 %), this background influence is rather high in a few cases. In some cases, it constitutes almost 47 % of the total radon production measured. This "contribution", if subtracted from the measured value (Table 5.6), would generate even smaller values of the diffusion coefficients than presented in Table 5.6. In this context, it may be noted that it is the bulk diffusion coefficients that are presented (background of radon from specimen included). Due to time constraints, it was not possible to measure the "background influence" for each concrete mix at each relative humidity, even though the contribution to the current research would have been desirable. This may be illustrated via a comparison between the recipes for reference concretes C and CGB, bearing in mind that the aggregates of CGB contained very low concentrations (Bq/kg) of ^{226}Ra generating radon. If we address the diffusion coefficients of the two concrete samples at a relative humidity of 75 % (Table 5.6), it can be observed that the reference concrete C indeed shows a higher value. The diffusion coefficient of CGB would thus theoretically be closer to a true value, where the influence of the activity concentration of radon gas (Bq/m^3) of the concrete specimen itself can be neglected.

It may also be anticipated that the carbonation of the concrete specimens (concrete slabs) may in part influence some of the assessments made at lower relative humidity levels due to findings in Paper V. It was however noted in the minor internal study using thin section analysis (Chapter 5, Section 5.8), assessing the cement paste, that the carbonation ingress for C, C-F15-MF20 and C-S65 was rather limited. A maximum of 4 mm carbonation depth was documented (after 24 months). This implies that carbonation may have some effect on the results, although this would likely be limited, specifically for the concretes containing different SCMs (due to higher ingress rate).

Furthermore, it cannot be excluded that there may be an effect of a change in the radon gas exhalation rate due to ongoing hydration. This was also partly addressed in Section 6.6. In many cases, hydration will promote a denser C-S-H cement matrix (Hewlett and Liska, 2019). Thus, a smaller diffusion coefficient may arise due to a less permeable concrete (Kovler, 2012). With this in mind, a minor effect during the experiments may relate to the fact that almost 24 months (two years) elapsed between the first and the final measurement. As mentioned in Section 6.6, it may be noted that the concrete specimens were young (six months) during the first study, and the micro-texture of the cement paste may still undergo changes. This could also influence the results slightly and should not be discarded especially for some binder combinations of SCMs.

In the main study, the radon gas diffusion measurements describe the diffusion of a gas through a medium (concrete slab) using an external source of radon for measurements. However, for the measurement of radon gas exhalation, it is an issue of radon gas generated from the concrete specimen itself being exhaled to the ambient air, as described by van der Graaf & Meijer (2005), where several factors (emanation, diffusion, air/water ratio in the pores of the concrete and density) influence the final radon gas exhalation rate.

6.12 Activity concentrations of the investigated concrete mixes and constituents

The activity concentrations investigated were analysed, in part due to the large contributions of the SCMs added to some of the concrete recipes. In general, it was believed that no large differences between the concrete mixtures activity concentrations (I-index) would occur since the main contributor to the activity concentration of the concrete mixes is the aggregates. The control of the activity concentrations for the concrete mixtures and constituents was considered of significance since many calculations within the main study use the ^{226}Ra concentration (Bq/kg) to calculate the radon flux (J) or emanation coefficient (€) of ^{222}Rn.

As expected, no major differences were measured, except possibly for recipe C-H3. It was also demonstrated that some constituents, such as fly ash, may exceed the recommended I-index value, but only to a marginal extent. The addition of some hydrophobic admixtures also indicated that their contribution to the total activity concentration of the concrete mixes was minimal.

The slight increases or decreases of the calculated I-index or ^{226}Ra concentrations between the concrete mixtures were also in line with results from some of the constituents analysed. The slightly higher ^{226}Ra activity concentrations (Bq/kg) of some fly ashes also indicated slightly increased ^{226}Ra concentrations of the concrete mix and vice versa for e.g., additions of micro-silica to the concrete recipe. The results were thus considered consistent and therefore reliable.

7 Uncertainties and sources of errors

7.1 Repeatability of radon gas growth and radon gas exhalation measurements

Sources of errors are related to the measurement and calculation procedures. Some errors are directly linked to the measurement technique used, where an initial "zero" value has to be established due to the nature of proportionality (linear analysis) between the radon gas growth and function of time. The "zero" value is computed in the regression analysis and checked with initial numerical values generated from the ATMOS radon monitor before the test starts. In most cases, there is a very good correlation, but this "zero value" may influence the calculated radon gas exhalation rate and must be reflected upon when analysing the prevailing measurement conditions at each instance.

The instrumental technique using a pulsating ionisation chamber, such as ATMOS 33, was developed from the main measurement techniques described by Baltzer et al. (1992) and has an uncertainty of 10 % (s.d). Calculations according to the ISO standard ISO-11665-7 include a margin of error (uncertainties). As described previously, this uncertainty can be calculated via repeatability measurements on an identical sample. Such an approach was assessed by Döse (2016), where five repetitive measurements from each concrete mixture were assessed. In total three different concrete mixtures were evaluated. The estimated standard deviation of the radon gas concentration measurements demonstrated an interval of variation of 4.2-6.4 % with a 95 % confidence level (2σ).

The standard deviation (s), the uncertainty (u) and the expanded uncertainty (U) were calculated. The expanded uncertainty includes a coverage factor of k=2 (~95 % confidence level). The equations used (7.1-7.3) were calculated according to guidelines by Bell (2001):

$$s = \sqrt{\frac{\sum_{i=1}^{n}(x_i - \bar{x})^2}{(n-1)}} \quad (7.1)$$

$$u = s/\sqrt{n} \quad (7.2)$$

$$U = 1.96 * u \quad (7.3)$$

However, due to the limited number of repetitions, Döse (2016) suggested that a cautious approach was to be adopted. Consequently, Figure 7.1 presents uncertainty bars including a 10 % deviation from the measured values by Döse (2016). The operational uncertainties have been considered negligible.

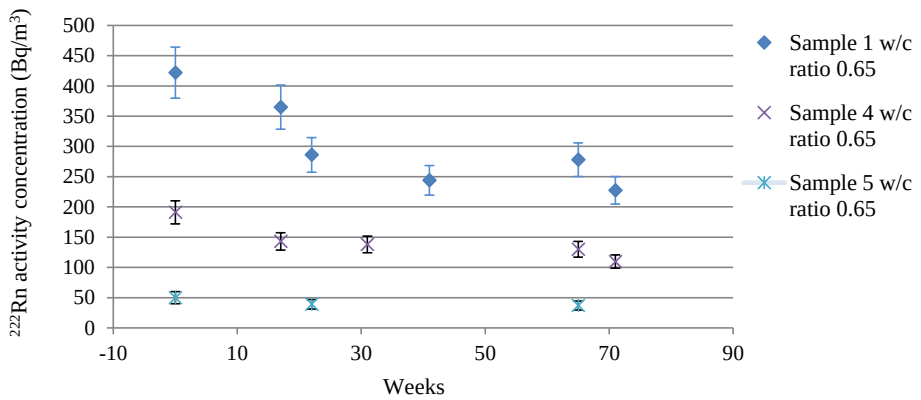

Figure 7.11 Calculated values of the radon gas concentration in the air for a specified room as a function of time (weeks). Included are 10 % uncertainty bars for each measurement.

In the current study only limited assessments were made to investigate the uncertainty. This was mostly due to consistent results (~5 %, 2σ confidence level) in earlier investigations of concrete mixtures (Döse, 2016). Before the main study was launched for each concrete recipe at 75 % in RH, three repetition runs were made for three different concrete mixes: C, CH-3 and C-F15-MF20 (Table 7.1). In this approach, the radon gas exhalation rates were compared for each concrete recipe.

Table 7.1. Summary of repetitions for three concrete recipes in the study.

Repetition	C	C - check	U (95%)	C-H3	CH-3 - check	U (95%)	C-F15-MF20	C-F15-MF20 - check	U (95%)
I	96.5			97.1			99.6		
II		101.1	4.5		103.2	5.9		97.1	2.5

The results were satisfactory and in good correspondence with earlier investigations (Döse, 2016), with a variation (95 % confidence level) of ~3-6 %. Thus, no further action was taken regarding radon gas exhalation measurements and uncertainties.

7.2 Repeatability of radon flux (diffusion) between plates of each concrete mixture

The repeatability of the radon flux (diffusion) was investigated for two concrete recipes at RH 75 % just prior to initiating the first experiments. The available time frame limited the investigations. Recipes CH-1 and C-MF35 were chosen as candidates. In the first case (CH-1), only one measurement was performed for each plate (D1, D2 and D3). A large crack was also discovered in plate three (D3) after finalised measurement. Thus, no further measurement was undertaken for this recipe.

For recipe C-MF35, three plates were tested (D1, D2 and D3). The plate D1, due to almost identical results as D2, was chosen to be "the measurement plate" used for all the experiments at RH 75 %, RH 60 % and RH 45 %. For plate 2 (D2), five consecutive measurements were conducted (Table 7.2).

The analytical error (uncertainty) investigated was chosen to be upon the calculated radon exhalation rate (radon flux) after regression analysis. Thereafter, calculations were made of the standard deviations of each plate, as well as uncertainty (u, 67 % confidence) and total uncertainty (U, 95 % confidence). Table 7.2 presents the numerical values of the radon flux, the number of repetitions and the uncertainties in numerical values and as percentages.

Table 7.2. Repetitive measurements of measured radon flux (concentration gradient, m^2/s).

Sample	Plate	J, flux Bq per (m^2/s)	Rep I	Rep II	Rep III	Rep IV	u (67 %)	%	U (95 %)	%	Note
C-H1											
	D1	0.0011									
	D2	0.0008					0.0001	15	0.0003	29	D1 & D2
	D3	0.0043									visible crack

C-MF35											
	D1	0.0007	0.0007				0.0000	2	0.0000	3	
	D2	0.0008	0.0008	0.0006	0.0005	0.0006	0.0001	10	0.0001	20	
	D3	0.0014	0.0011				0.0001	10	0.0003	20	

The numerical values of uncertainty given for C-H1 only include D1 and D2. It must be considered that low number of repetitions implicate that the results are not fully reliable.

In general, an uncertainty of 20 % (U) for a confidence level of 95 % can be viewed as appropriate. This is regarding the uncertainty of the radon flux measurement of one concrete plate (C-MF35, D2). With a confidence level of 67 % (u), the uncertainty is 10 %.

The results are regarded as acceptable. Perhaps more importantly, however, the variation between the plates of the radon diffusion lengths of one recipe (CH-1 or C-MF35) does also imply some variation within each concrete recipe (e.g., for the series C-MF35, the uncertainty (u) was ~18 %). This should be borne in mind, since only one plate of each recipe was chosen for the study.

8 Conclusions

The investigations of various concrete mixtures in relation to radon gas revealed some important features such as:

- In general, the radon gas exhalation decreases as RH decreases for a concrete mix. This is in line with previous models and experiments where a reduced radon exhalation rate is documented as the moisture content of the concrete decreases.

- In general, the diffusion coefficient of the experiments undertaken for the 12 concrete specimens increases as the moisture content decreases or the relative humidity decreases. This is also in line with previous studies.

- It is shown that the radon gas exhalation rate can to some extent be reduced by the use of SCMs, notable specifically at higher relative humidity levels compared to an ordinary CEM I cement concrete mix.

- In general, hydrophobic admixtures have a positive effect on the radon gas exhalation rate. This result indicates that the admixtures contribute to reduce the exhalation rate compared to the case of using only OPC. This effect is more pronounced at higher relative humidity.

- The calculated diffusion coefficients of the studied recipes containing hydrophobic admixtures are at high and moderate levels of relative humidity (75 % and 60 %) similar to those of an ordinary OPC recipe. This result is mainly attributed to the measured bulk coefficient. Calculating the effective coefficients (background subtracted) of the concrete recipes, the hydrophobic concrete mixtures have slightly lower diffusion coefficient values at a relative humidity of 75 % compared to the reference recipe containing only OPC. The low "background-influence" at RH 75% for C-H1 an CH-2 compared to the OPC-mixture for these to hydrophobic mixtures also indicates a lower emanation coefficient (less radon gas escaping through the pores). This results at the end in a lower exhalation rate from these concrete mixtures, even though the diffusion coefficients are similar to the OPC-concrete mixture.

- The results of the MIP analysis imply that a low mean pore radius and increased pore area surface (m^2/g) of the cement paste increases the possibility of generating a low diffusion coefficient and consequently a low radon exhalation rate in the final concrete.

- The study with induced cracks shows a strongly increased risk of higher radon exhalation rates.

- Carbonation initially has a very low impact on the exhalation rate. As it continues to a more substantial depth (>8-10 mm), a marked influence on the exhalation rate is noted. Depending on the binder composition, different effects will occur. SCMs as part of the binder promote a higher radon exhalation rate due to changes in the pore structure caused by carbonation. The carbonation process induces a coarser pore structure, increasing the interconnectivity between the pores and endorsing an increased rate of radon gas release from the concrete mix. A reference concrete containing only ordinary Portland cement will instead show a reduced diffusion coefficient, due to a denser pore structure as a result of carbonation and precipitation of calcium carbonates in primarily the capillary pores.

- Using different binders or SCMs compared to an ordinary OPC may slightly increase the activity concentration of the concrete mix (I-index) but will, as the experiments have shown, contribute to at least initially (at higher relative humidity levels) substantially reduce the radon gas exhalation rate compared to a concrete mix with only an ordinary reference binder such as

CEM I. The benefit from a health perspective is that a lower effective dose is received by the inhabitants of the concrete building.

9 Recommendations

In light of the study's findings, certain recommendations are deemed appropriate. These are presented as bullet points below.

- A recommendation to assure a low radon gas concentration within the building material is to choose an aggregate with low levels of ^{226}Ra concentration (Bq/kg). This will enhance the possibilities of having low levels of ^{222}Rn (Bq/m^3) in the free air, regardless of crushing procedures of the aggregates or particle size fractions used in production.

- The testing of the radon release rate (activity concentration build-up within the container) from the concrete specimens is recommended to be performed at a relative humidity below 60 %. This is suggested due to the relative humidity levels in houses and buildings measured by Fridh and Lagerbladh (2013) and Bagge (2011). In their studies, the findings indicated relative humidity levels below 60 % in the tested concretes, regardless of where measurements were taken (floor, roof, ceiling). Consequently, the studies within this thesis have demonstrated that the radon exhalation rates can be much higher at a higher relative humidity. Thus, the testing of concrete intended to be used for houses and buildings should be performed with a relative humidity in correspondence to what can be expected in houses and buildings over time (prolonged period). Testing of radon gas production or radon gas exhalation rate under too-dry conditions will likely lead to underestimation of the radon concentration in the air, as shown in this study, and should be avoided.

- Radon gas measurements shall not be performed during the first two to three years of a newly constructed building. This relates to the above findings and will most likely yield non-representative results over a longer time period (>10 years).

- Concretes intended for testing of their radon production rate need to be dried gently (minimum 2-3 weeks) in a laboratory oven at 35-40ºC prior to testing of the radon production/ exhalation rate. The loss of mass of the concrete specimen during drying can be used as an indicator of the relative humidity within the concrete.

- SCMs may well be used to promote a lower radon gas exhalation rate from a concrete mix. Depending on the SCMs used, different results have to be expected. All tested concrete samples containing SCMs within the study however gave beneficial results at a higher and moderate humidity (RH 75 % and RH 60 %) compared to a reference concrete with rapid hardening ordinary Portland cement (CEM I).

- An increased amount of SCMs does not necessarily relate to a lower radon exhalation rate. The specific SCM needs to be tested in different amounts with the Ordinary Portland cement to achieve the specific concrete´s best performance from a radon exhalation point of view.

- Hydrophobic admixtures aid in lowering the radon exhalation rate. This is most pronounced at higher relative humidity levels. In order to achieve optimal results regarding the radon exhalation rate in a short time frame, this may be an option.

- A large part of the radon gas exhalation can be mitigated by using a specific concrete mix with a highly impermeable layer as a topping on floors and walls made up of concrete. Thus, a large fraction of the expelled radon gas exhalation can be hindered. This requires reducing the diffusion rate sufficiently so that a significant part of the radon gas decays within the building material itself. The surface top layer shall consist of a balanced mix of OPC and SCMs in combination with an aggregate with a low concentration of the natural radionuclides. A low porosity would be beneficial.

10 Future research

Döse & Silfwerbrand reported in Paper II results that indicated that the radon gas could be reduced by merely adding hydrophobic admixtures into a pure Portland concrete cement recipe (with no SCMs added). This encourages further research into how to reduce the radon gas exhalation rates by use of new admixtures as radon closures whilst being a part of the concrete.

Furthermore, it is evident that the moisture content of the concrete has a significant influence on the radon gas exhalation rate. A more precise and accurate approach to evaluating or modelling the influence of the relative humidity of different concrete mixes on their final radon gas exhalation rate would be of substantial benefit to researchers, regulators and the concrete industry. Especially interested, not least in the moisture perspective, is to investigate concrete mixes containing SCM's with substantial potential to reduce concrete's environmental impact.

As the model by van der Graaf and Meijer (2005) suggests, there is an intricate system of variables that have an influence on the final radon exhalation rate. The author has not focused in depth on the influence of the different concrete mixes' absorption/desorption behaviours. Absorption/desorption curves for each concrete mix would most likely be very advantageous for a more in-depth analysis. Some moisture-dependent parameters were assessed, such as diffusion and emanation. The author however believes a more thorough analysis of the effect of the partition coefficient would be beneficial, dealing with the effects of partially filled water pores and their influence on the release rate of radon gas. Also, the effect of the adsorption coefficient (k_a) as a function of the concrete pore size would need further elaboration if part of a model for the radon gas release rate. These variables affecting the transport abilities within the concrete would be meaningful to analyse in depth with consideration to the release mechanisms under conditions of different moisture contents and relative humidity levels in building materials. A more general approach has been adopted in this dissertation, with the aim of explaining possible causes of variations in the radon gas exhalation rate as a function of:

(i) the measured relative humidity of the concrete recipes,
(ii) internal differences (pore size, pore distribution and porosity) in the cement paste of the concrete recipes, or
(iii) internal factors such as carbonation or external factors such as cracks.

The results have been evaluated based on these outcomes.

Another approach for further research has in part been presented within this study. Most of the radon gas released for dense concretes, as in this study, derives from the top 60 mm of the concrete. Consequently, it would be most interesting to construct precast concrete elements with an understanding of this in mind. One suggestion, therefore, would be to use the technique of a sandwich element, where the top layer of a concrete mix consists of a low radiating aggregate, to reduce the radon gas levels for inhabitants and to hinder the radon gas from reaching the central parts of the concrete element. The inner part or inner core of an element can, however, consist of a concrete cast with cement and aggregate with higher levels of natural radionuclides.

Other combined effects using a sandwich layer construction may also be investigated, such as an increased heat capacity using e.g., a dark, high-density aggregate such as gabbro with a generally low radon exhalation rate. Indirectly, a two-layered concrete member would also include optional choices for different tints on walls. One might also address a beneficial approach where self-sustaining (self-cleaning) walls could be part of a two-layered construction. As such, future research should seek to employ and combine several of these factors.

Finally, one might address the broad issue of natural radionuclides, their decay and contribution to effective doses to habitants. ^{222}Rn as of today, originating from the ^{238}U decay chain, is considered as

the only potential source of risk in health risk assessments from building materials. However, consideration may also be given to the ^{232}Th (232-Thorium) chain with its progeny ^{220}Rn, often named as thoron. De With et al. (2018) showed that the thoron component of radon isotopes can contribute considerably to the mean effective dose (20-30 %). In conclusion, further research is suggested here, since many Swedish bedrocks are enriched in ^{232}Th, implying a higher risk of increased ^{220}Th in the air, whilst the ^{226}Ra activity concentrations (Bq/kg) generating ^{222}Rn are still moderate. In other words, the ^{220}Rn (thoron) and ^{222}Rn exhalation rates of different building materials should be assessed simultaneously and their total contribution to the effective dose should be considered.

References

Abo-Elmagd M (2014).”Radon exhalation rates corrected for leakage and back diffusion - Evaluation of radon chambers and radon sources with application to ceramic tile”. Journal of Radiation Research and Applied Sciences. Vol. 7. pp. 390-398.

Andersson P, Carlsson M, Falk R, Hubbard L, Leitz W, Mjönes L, Möre H, Nyblom L, Söderman A, Yuen Lasson K, Åkerblom G, Öhlén E (2007). “Radiation environment in Sweden (*Strålmiljön i Sverige*)”. SSI report 2007:02. Stockholm, Sweden, pp. 138. (In Swedish).

Audenaert K (2007). “Durability of Self-Compacting Concrete, RILEM TC 205-DSC, Section 4.1 Carbonation”. State of the Art Report, pp. 63-76.

Bagge H (2011). “Building Performance – Methods for Improved Prediction and Verification of Energy Use and Indoor Climate”. Doctoral Thesis, Report TVBH-1019, Building Physics, Lund University, 202 pp. Lund, Sweden.

Baltzer P, Görsten K G, Bäcklin A (1992). ”A pulse-counting ionization chamber for measuring the radon concentration in air”. Nuclear Instrument and Methods in Physics Research. Vol. 317A. pp. 357-364.

Barros-Dios, J. M., Barreiro, M.A., Ruano-Ravina, A. & Figueiras, A. (2002). “Exposure to residential radon and lung cancer in Spain: a population-based case-control study”. American Journal of Epidemiology, Vol. 156(6), pp. 548–555.

Baskaran M (2016). “Radon: a tracer for geological. geophysical and geochemical studies”. Springer Verlag. Switzerland, 260 pp.

Bell S (2001). “A beginner’s guide to uncertainty of measurement”. Measurement Good Practice Guide No. 11 (Issue 2). National Physical Laboratory. Teddington. Middlesex. United Kingdom. 34 pp.

Boumazza M; Turcy P; Huet B; Aït-Mokhtar A (2020). “Influence of carbonation on the microstructure and the gas diffusivity of hardened cement pastes,” *Construction and Building Materials*, Vol, 253, pp. 1-13.

Catelinois O, Rogel A, Laurier D, Billon S, Hemon D, Verger P and Tirmarche M (2006). “Lung Cancer Attributable to Indoor Radon Exposure in France: Impact of the Risk Models and Uncertainty Analysis”. Environmental Health Perspectives, Vol. 114, No. 9, pp. 1361-1366.

Cember H & Johnson T E (2009). “Introduction to Health Physics. fourth edition”. (Edited by C. A Johnson & C Naglieri). The McGraw-Hill Companies Inc. New York. United States of America. 873 pp.

Chauhan R P & Kumar A (2013). “Radon resistant potential of concrete manufactured using ordinary portland cement blended with rice husk ash”. Atmospheric Environment. Vol. 81. pp. 413–420.

Chauhan R P & Kumar A (2013b). ”Study of radon transport through concrete modified with silica fume”. Radiation Measurements, Vol. 59, pp. 59-65.

Chauhan R P & Kumar A (2015). ”A comparative study of indoor radon contributed by diffusive and advective transport through intact concrete”. Physics Procedia, Vol. 80, pp. 109-112.

Cinelli, G., De Cort, M. & Tollefsen, T. (2019). ”European Atlas of Natural Radiation”. Publication Office of the European Union, Luxembourg, 1st ed., 195 pp.

Concrete handbook (1997). “Concrete guidance, material section (in. Swedish, Betonghandboken, material)”. Svensk Byggtjänst, Stockholm, Sweden, 1127 pp.

Concrete hanbook (2017). Concrete guidance, material section (in Swedish, Betonghandboken, material, del I)”. Svensk Byggtjänst, Stockholm, Sweden, 540 pp.

Cotton FA. Wilkinson G. Bochmann M Grimes RN (1988) Advanced inorganic chemistry: a comprehensive text. 5th edn. Wiley-Interscience, pp. 1488.

Cozmuta I & van der Graaf E R. (2001). ”Methods for measuring diffusion coefficients of radon in building materials”. The science of the total environment. Vol. 272, pp. 323-335.

Cozmuta I, van der Graaf E R, de Meijer R J (2003). ”Moisture dependence of radon transport in concrete: measurements and modeling”. Health Physics. Vol. 85(4). Groningen. The Netherlands. pp. 438-456.

Darby S, Hill D, Auvinen A, Barros-Dios JM, Baysson H, Bochicchio F, Deo H, Falk R, Forastiere F, Hakama M, Heid I, Kreienbrock L, Kreuzer M, Lagrade F, Mäkeläinen I, Muirhead C, Oberaigner W, Pershagen G, Ruano-Ravina A, Ruosteenoja E, Schaffrath Rosario A, Tirmarche M, Tomasek L, Whitley E, Wichmann H-E & Doll R. (2005). “Radon In Homes And Risk Of Lung Cancer: Collaborative Analysis Of Individual Data From 13 European Case-Control Studies”. British Medical Journal, Vol. 330, No. 7485, pp. 223-226.

Darby S, Hill D, Auvinen A, Barros-Dios JM, Baysson H, Bochicchio F, Deo H, Falk R, Forastiere F, Hakama M, Heid I, Kreienbrock L, Kreuzer M, Lagrade F, Mäkeläinen I, Muirhead C, Oberaigner W, Pershagen G, Ruano-Ravina A, Ruosteenoja E, Schaffrath Rosario A, Tirmarche M, Tomasek L, Whitley E, Wichmann H-E & Doll R (2006) “Residential Radon and Lung Cancer: Detailed Results of a Collaborative Analysis of Individual Data on 7148 Persons with Lung Cancer, 14208 Persons without Lung Cancer from 13 Epidemiologic studies in Europe,” Scandinavian Journal of Work, Environment and Health, Vol. 32, pp 1-84.

Daud W Z & Renken K J (1999). ”Laboratory measurements of the radon gas diffusion coefficient for a fractured concrete sample and radon as barrier systems”, Proceedings International Radon Symposium, Las Vegas, USA, pp. 14-19.

De Jong P & van Dijk W (1996). ”The effect of the composition and production process of concrete on the ^{222}Rn exhalation rate”. Environmental International. Vol. 22. pp. 287-293.

Dorn F E (1900. “Die von radioactiven Substanzen ausgesandte Emanation”. Abhandlungen der Naturforschenden Gesellschaft zu Halle 23:1–15 (In german).

Döse M. (2016). “Ionizing Radiation in Concrete and Concrete Buildings – Empirical Assessment”, Licentiate thesis in civil and architectural engineering, School of architecture and the built environment, KTH Royal Institute of Technology, Stockholm, Sweden, 91 pp.

Döse M & Silfwerbrand J (2017). ”Reduction of radon gas in concrete – effects and evaluation of effective dose”. Proceedings of the XXIII Nordic Concrete Research Symposium, Aalborg, Denmark. Nordic Concrete Federation, pp. 185-188.

Döse M & Silferwerbrand J (2018). “Reduction of Radon Gas in Concrete Using Admixtures and Additives”. Nordic Concrete Research, No 58, 2018, pp. 17-34.

EC (1999). Directorate-General Environment. Nuclear Safety and Civil Protection. “Radiological protection principles concerning the natural radioactivity of building material”. Radiation Protection 112”. Luxembourg City. Luxembourg. 24 pp.

EC (2014). “Council Directive 2013/59/Euroatom of 5 December 2013 laying down basic safety standards for protection against the dangers arising from exposure to ionising radiation. and repealing Directives 89/618/Euroatom. 90/641/Euroatom. 96/29/Euroatom. 97/43/Euroatom and 2003/122/Euroatom”. Offical Journal of the European Union. Vol. 13. 73 pp.

EC (2021). “Radon map – Atlas”. Joint Research Group (JRC), Directorate General – Nuclear Safety & Security, REM project, Digital Atlas (europa.eu)

CEN/TR 17113 (2017). “Construction Products - Assessment of Release of Dangerous Substances - Radiation From Construction Products - Dose Assessment of Emitted Gamma Radiation,” European committee for standardization, CEN, pp. 47.

CEN/TS 17216:2018 (2018). ”Construction products - Assessment of release of dangerous substances - Determination of activity concentrations of radium-226, thorium-232 and potassium-40 in construction products using semiconductor gamma-ray spectrometry”. CEN/TC 351/WG 3 - Radiation from construction products, pp. 42.

Fatema S A, Khalid H M, Jawad E (2019). “Humidity effect on diffusion and length coefficient of radon in soil and building materials”. Energy Procedia, Vol. 157, pp. 384-392.

Fridh K & Lagerblad B (2013). “Carbonation of indoor concrete : measurements of depths and degrees of carbonation”. Report TVBM; Vol. 3169. Division of Building Materials, LTH, Lund University, Lund, Sweden, 36 pp.

Fournier F J E, Groetz J E, Jacob F Crolet J M, Lettner H (2005). “Simulation of Radon Transport through Building Materials: Influence of the Water Content on Radon Exhalation Rate”. Transp. Porous Med. 59. pp 197–214.

Garcia E (2010). “A Tutorial on Correlation Coefficients”. http://web.simmons.edu/~benoit/lis642/a-tutorial-on-correlation-coefficients.pdf

Harrison J & Marsh J W (2011). “Effective dose from inhaled radon and its progeny”. ICRP 2011 Proceedings, Annals of the ICRP, pp. 378-388.

Helsing E (2017). “Freeze-thaw testing of concrete with slag and fly ash”, in Swed. Salt-frostprovning av betong med slagg och flygaska, CBI-report 2017:4, Research Institute of Sweden (RISE), Stockholm, Sweden, pp. 133.

Helsing E, Parg L, Mueller U, Ellison T. ”Hydrophobic admixtures in sprayed concrete – influence on properties and the behaviour at spraying”, in swed. Hydrofoberande medel I sprutbetong – Inverkan på egenskaper och beteendet vid sprutning”, (2017), CBI report 2017:5, Swedish Cement and Concrete Research Institute (RISE), Stockholm, Sweden, 53 pp.

Hewlett P C & Liska M (2019). ”LEA´s chemistry of Cement and Concrete, fifth edition”, Cambridge Massachusetts, USA, 858 pp.

Hildingsson O (1983). “Radon from glacofluvial material and crushed rock”, in Swedish, “radon från naturgrus och makadam”), Swedish testing facility, SP, technical report, 1983:28, 45 pp.

M. Hoffmann, Ch. S. Aliyev, A. A. Feyzullayev, R. J. Baghirli, F. F. Veliyeva, L. Pampuri, C. Valsangiacomo, T. Tollefsen, G. Cinelli (2017). ”First map of residential indoor radon measurements in Azerbaijan”. Radiation Protection Dosimetry, Vol. 175 (2), pp. 186–193.

ICRP (2006). “Assessing dose of the representative person for the purpose of radiation protection of the public and the optimization of Radiological Protection: broadening the process” (edited by J. Valentin). Annals of the ICRP. publication 101. publication 101. Elsevier. Vol. 36. London. United Kingdom. 221 pp.

ICRP (2007). ”The 2007 recommendations of the International Commision on Radiological Protection” (Edited by J. Valentin). Annals of the ICRP. Publication 103. Elsevier. Vol. 37. London. United Kingdom. 332 pp.

ICRP (2014). ”Radiological Protection against Radon exposure” (Edited by C. H. Clement). Annals of the ICRP. Publication 126, Vol. 43, No. 3, 73 pp.

Inst Tools (2022). “Humidity Measurement Principles”., Humidity Measurement Principle - Inst Tools (instrumentationtools.com)

Isaksson M (2011). “Basic radiation physics (Grundläggande strålningsfysik). 2nd edition”. Elanders. Studentlitteratur. Lund. Sweden. 330 pp.

Isaksson M (2011b). “Radioisotopes – Applications in physical sciences”. chapter 10. “Environmental Dosimetry – Measurements and Calculations”. (edited by N. Singh). InTech publishing. Croatia. pp. 175-196.

Isaksson M & Rääf C L (2017). ”Environmental radioactivity and emergency preparedness”. CRC Press, Taylor & Francis Group, Boca Raton, Florida, USA, 614 pp.

Ishimori Y, Lange K, Martin P, Mayya Y S, Phaneuf M (2013). “Measurement and calculation of radon releases from NORM Residues”. Technical Reports series no. 474. International Atomic Energy Agency. Vienna. Austria. 85 pp.

ISO 15901-1 (DIN 66133) (2016) “Evaluation of pore size distribution and porosity of solid materials by mercury porosimetry and gas adsorption - Part 1: Mercury porosimetry”. ISO/TC 24/SC 4, pp. 19.

ISO-EN 15148 (2002). “Hygrothermal performance of building materials and products – Determination of water absorption coefficient by partial immersion”. CEN TC 89, European standardization, 12 pp.

ISO 11665-7 (2012). “Measurement of radioactivity in the environment — Air: radon-222 — Part 7”: Accumulation method for estimating surface exhalation rate. International Standard (ISO). first edition. Geneva. Switzerland. 23 pp.

Jalal M, Pouladkhan A, Harandi O F, Jafari D (2015). “Comparative study on effects of Class F fly ash, nano silica and silica fume on properties of high performance self compacting concrete”. Construction and Building Materials, Vol. 94, pp. 90-104.

Jelinek C & Eliasson T (2015). ”Radiation from bedrock (Strålning från Bergmaterial)”. Geological survey of Sweden. SGU-report 2015:34. Uppsala. Sweden (in Swedish). 26 pp.

Justnes H; Skocek J, Östnor T A; Engelsen C J; Sköljsvold O (2020). ”Microstructural changes of hydrated cement blended with fly ash upon carbonation,”*Cement and Concrete Research*, Vol, 137, pp. 1-14.

Keller G, Hoffmann B, Feigenspan T (1999). “Radon permeability and radon exhalation of building materials”. Science of the Total Environment. Vol. 272. iss.1-3. pp. 85-89.

Kovler K (2006). “Radon exhalation of hardening concrete: monitoring cement hydratation and prediction of radon concentration in construction site”. Journal of Environmental Radioactivity, Vol. 86, pp 354-366.

Kovler K (2012). “Radioactive materials, chapter 8”. “Toxicity of Building Materials, Woodhead Publishing, Ed. by F Pacheco-Torgal, S Jalali and A Fucic, pp. 196-240.

Klein C & Hurlbut Jr C S (1993). “Manual of mineralogy”-21st edition. (edited by B Harmon). John Wiley and Sons Inc. New York. USA. 681 pp.

Knoll G F (2010). “Radiation detection and measurement”. 4th edition. (edited by J Welter). John Wiley and Sons Inc. Michigan. USA. 830 pp.

Kropat G, Bochud F, Jaboyedoff M, Laedermann J-P, Murith C, Palacios M, Baechler S (2014). “Major influencing factors of indoor radon concentrations in Switzerland”. Journal of Environmental Radioactivity, Vol. 129, pp. 7-22.

Kumar A & Chauhan R P (2015). ” Effect of moisture and additive on radon exhalation rate from concrete”. Romanian Journal of Physics. Vol. 60, pp. 1589-1597.

Kurda R, de Brito J, Silvestre J (2019). ”Carbonation of concrete made with high amount of fly ash and recycled concrete aggregates for utilization of CO_2”. Journal of CO_2 Utilisation., Vol. 29, pp. 12-19.

Landman K A. “Diffusion of Radon Through Cracks in Concrete Slab”. Health Physics. Vol. 43. Issue 1. 1982. pp. 65-71.

Lagerblad B (2017). “Mechanism and mode of carbonation of cementitious materials”, Swedish Cement and Concrete Research Institute, CBI report 2017:1, Stockholm, Sweden, 32 pp.

Leung H Y, Kim J, Nadeem A, Jaganathan J Anwar M P (2016). ”Sorptivity of self-compacting concrete containing fly ash and silica fume”. Construction and Building Materials, Vol. 113, pp. 369-375.

Maier, A, Weber U, Dickmann J, Breckow J, van Beek P, Schardt D, Kraft G, Fournier C. “Method for measurement of radon diffusion and solubility in solid materials (2018). Nuclear Inst. And Methods in Physics Research B, Vol 416, pp. 119-127.

Maringer F J, Baumgartner A, Siedel C, ”Natural Radioactivity of Building Materials: Radiation Protection Concepts, Measurement Methods and Regulatory Implementation, pp. 15-16, Third European IRPA Congress 2010 June 14−18, Helsinki, Finland.

Markkanen (1995).”Radiation dose Assessments for materials with elevated natural radioactivity”. Department of Radiation Safety. Finnish Centre for Radiation and Nuclear Safety. report STUK B STO-32. Helsinki. Finland. 38 pp.

Mehta P K and Monteiro P J M. (2006). “Concrete: Microstructure, Properties, and Materials. 3rd Edition”. McGraw-Hill, New York, pp. 659.

Mueller U, Lundgren M, Babaahmadi A. (2017). ”Hydration of concrete binders blended with ground granulated blast furnace slag, fly ash and metakaolin”. RISE CBI Betonginstitutet, Samhällsbyggnad. CBI report 2017:6, Borås, Sweden, 78 pp.

Munoz E, Frutos B, Olaya M, Sanchez J. (2017). “A finite element model development for simulation of the impact of slab thickness, joints, and membranes on indoor radon concentration”. Journal of Environmental Radioactivity, Vol. 177, pp. 280-289.

Mustonen, R (1984). “Natural radioactivity in and radon exhalation from finnish building materials”, Health Physics, Vol. 46, No. 6, pp. 1195-2303.

Möre H (1985). “Radioactive substances in building materials (*Radioaktiva ämnen i byggnadsmaterial)”*. SSI-rep 85-08: 56. Stockholm. Sweden (In Swedish).

Mjönes L, Burén A, Swedjemark G A. (1984). “Radon rates in Swedish dwellings (Radonhalter i svenska bostäder. SSI-report-a 84-23”. Stockholm. Sweden (In Swedish). 56 pp.

Nazaroff WW (1992). “Radon transport from soil to air”. Rev Geophys 30 (2), 137–160 pp.

Nevander L E and Elmarsson B (2006). “In Swed. - Fukthandbok” – In Eng. “Book of Moisture”, 3rd rev. edition, Svensk Byggtjänst AB, Sweden, pp. 538.

Neville A M & Brooks J J (2010). “Concrete Technology, 2nd edition”, Pearson Education Ltd, Essex, England, 442 pp.

Ning L; Nima F; Caijun S (2017). “Microstructural changes in alkaliactivated slag mortars induced by accelerated carbonation”. *Cement and Concrete Research*, V. 100, 2017, pp. 214-226.

Nuccetelli C, Leonardi F, Trevise R (2015). “A new accurate and flexible index to assess the contribution of building materials to indoor gamma exposure”. Journal of Environmental Radioactivity. Vol 143. pp. 70-75.

Papadakis V, Vayenas G, Fardis M (1992). ”Effect of composition, environmental factors and cement-lime mortar coating on concrete carbonation”. Materials and Structures, Vol. 25, issue 5, pp. 293-304.

Petterson H, Hildingsson O, Samuelsson C, Hedvall. R (1982). “Radonexhalation of building materials (radonexhalation från byggnadsmaterial)”. Technical report. SP- 1982:32. Borås. Sweden. 52 pp. (In Swedish).

Porstendörfer J (1994). “Properties and behaviour of radon and thoron and their decay products in the air”. Journal of Aerosol Science, Vol. 25, No. 2, pp. 219-263.

Porstendörfer, J (2001). ”Physical Parameters and Dose Factors of the Radon and Thoron Decay Products”. Radiation Protection Dosimetry, Vol. 94, Issue 4, pp. 365–373.

Qin L; Gao X; Chen T (2019). “Influence of mineral admixtures on carbonation curing of cement paste,” C*onstruction and Building Materials*, Vol, 212, pp. 653-662.

Reiniking A & Porstendörfer J (1988). “Activity size distributions of the shortlived radon decay products and their influence on the deposition probability in the human lung”. Journal of Aerosol Science. Vol.19, Issue 4, pp. 1331-1337.

Rogers V C & Nielson K K (1991). “Multiphase Radon generation and transport in porous materials”. Health Physics, Vol. 60, No. 6, pp 807-815.

Roos M, König F, Stadtmüller S, Weyershausen B. (2008). “Evolution of Silicone Based Water Repellents for Modern Building Protection,” Proceedings, 5th International Conference on Water Repellent Treatment of Building Materials”, Brussels, Belgium, 2008, Aedificatio Publishers, pp. 3-16.

Saillio M.; Baroghel-Bouny V.; Pradelle S.; Bertin M.; Vincent J.; d’Espinose de Lacaillerie J-B (2021). “Effect of supplementary cementitious materials on carbonation of cement pastes,” *Cement and Concrete Research*, Vol, 142, pp 1-18.

Sakoda, A., Ishimori, Y. & Yamaoka, K. (2011). A comprehensive review of radon emanation measurements for mineral, rock, soil, mill tailing and fly ash. Appl. Radiat. Isot., 69(10): 1422–1435. doi: 10.1016/j.apradiso.2011.06.009

Scofield P. (1988). “Radon decay product. in-door behaviour – Parameter. measurement method. and model review”. National Institute of Radiation Protection. SSI-report 88-07. Stockholm. Sweden.

SS-EN 206 (2013). “Concrete – Specification. performance. production and conformity”. Swedish Standard Institute. Stockholm. Sweden. 93 pp.

SS-EN 1936 (2006). “Natural stone test methods - Determination of real density and apparent density, and of total and open porosity”. Swedish Standard Institute, Stockholm, Sweden, 12 pp.

SS-EN 12350-6 (2009). ”Testing fresh concrete – Part 6: Density”. Swedish Standard Institute. Stockholm, Sweden. 20 pp.

SS-EN 12350:2 (2009). “Testing fresh concrete – Part 2: Slump test”. Swedish Standard Institute. Stockholm. Sweden. 20 pp.

SS-EN 12350:7 (2009). “Testing fresh concrete – Part 7: Air content – Pressure methods”. Swedish Standard Institute. Stockholm, Sweden, 38 pp.

SS-EN 12390-10 (2019). “Testing hardened concrete – Part 10: Determination of the carbonation resistance of concrete at atmospheric levels of carbon dioxide”. Swedish Standard Institute (SIS), Stockholm, Sweden, 32 pp.

SS-EN 13755 (2008). “Natural stone test methods – Determination of water absorption at atmospheric pressure”. Swedish Standard Institute, Stockholm, Sweden, 20 pp.

SS-EN 1097-6 (2013). “Tests for mechanical and physical properties of aggregates – Part 6: Determination of particle density and water absorption”. Swedish Standard Institute. Stockholm. Sweden. 49 pp.

SS-EN 1766 (2000). “Products and systems for the protection and repair of concrete structures – Test methods – Reference concretes for testing”. Swedish Standard Institute. Stockholm. Sweden. 13 pp.

SS-EN 932-1 (1997). “Tests for general properties of aggregates – Part 1: Methods for sampling”. Swedish Standard Institute. Stockholm. Sweden. 25 pp.

SS-EN 932-2 (1999). “Tests for general properties of aggregates – Part 2: Methods for reducing laboratory samples”. Swedish Standard Institute. Stockholm. Sweden. 15 pp.

SS-EN 12390-3 (2011).” Testing hardened concrete – Part 3: Compressive strength of test specimens”. Swedish Standard Institute. Stockholm. Sweden. 8 pp.

SS-EN 14360 (2006). “Products and systems for the protection and repair of concrete stuctures – Test methods – Determination of carbonation depth in hardened concrete by the phenolphtalein method”. Swedish Standard Institute, Stockholm, Sweden, 8 pp.

Selander A (2010). “Hydrophobic Impregnation of Concrete Structures – Effects on Concrete Properties,” Bulletin 141 (Doctoral Thesis), Dept. of Civil and Architectural Engineering, School of Architecture and Built Environment, KTH Royal Institute of Technology, Stockholm, Sweden, 45 pp.

Selander A, Davant N, Malaga K. (2014): “Hydrophobic Shotcrete – a Method to Waterproof Tunnels,” Proceedings, Hydrophobe VII - 7th International Conference on Water Repellent Treatment and Protective Surface Technology for Building Materials, Lisbon, Portugal, pp. 67-75.

Setina J, Gabrene A, Juhnevica I. “Effect of Pozzolanic Additives on Structure and Chemical Durability of Concrete”. Procedia Engineering 57, pp. 1005-1012 (2013).

Spaeth V, Delplancke-Ogletree M P, Lecomte J P. (2008). “Hydration Process and Microstructure Development of Integral Water Repellent Cement Based Materials,” Proceedings, 5th International Conference on Water Repellent Treatment of Building Materials”, Brussels, Belgium, Aedificatio Publishers, pp. 245-254.

Stein L (1987) Chemical properties of radon. In: Radon and its decay products; Hopke. P.; ACS symposium series; chapter 18. American Chemical Society; Washington DC, USA, pp. 240–251.

Stranden E, Kolstad A K, Lind B. (1984). “The influence of moisture and temperature on radon exhalation. Radiation Protection Dosimetry. Vol 7. No. 1-4. pp 55-58. Nuclear technology publishing.

Swedish National Board of Housing. Building and Planning (2011). “Regelsamling för byggande (*regulations for building*). BBR”. October 2011. Elanders. Karlskrona. Sweden. 356 pp. (In Swedish).

Sweden Green Council Building 3.0 (2017). “Environmental building 3.0 with updates 20170925 (In Swedish - Miljöbyggnad 3.0 Bedömningskriterier för nyproducerade byggnader 170510 170915)”, Stockholm, Sweden, 76 pp., www.sgbc.se

SSMFS 2018:4 (2018). “The Swedish radiation Safety Authority regulations regarding naturally occurring radioactive materials (in Swedish - Strålsäkerhetsmyndighetens föreskrifter om naturligt förekommande radioaktivt material). The Swedish Radiation Safety Authority. Stockholm, Sweden, 6 pp.

Taylor-Lange S C, Stewart J G, Juenger M C G, Siegel J A (2012).” The contribution of fly ash toward indoor radon pollution from concrete”. Building and Environment. Vol. 56. pp. 276-282.

The Swedish Ordinance on Radiation Protection (2018). “Directive for radiation protection, 2018:506”, Environmental and Energy Department, Stockholm, Sweden, 16 pp.

Tolstoy N (1993). “Moisture measurements in Swedish homes. Intermediate moist-level an optimum for the building (in Swedish – Fuktmätningar I Svenska hem. Lagom fuktnivå bäst för bostaden). Building Research (in Swedish -Byggforskning), nr 5, pp, 31-33.

Tomásek L, Rogel A, Timarche M et al. (2008). “Lung cancer I French and Czech uranium miners – risk at low exposure rates and modifying effects of time since exposure and age at exposure”. Radiation Research, Vol. 169, pp. 125-137.

Turner J E (2012). “Atoms. radiation. and radiation protection – third edition”. WILEY-VCH Verlag GmbH & Co. Vernheim. Germany. 585 pp.

Tse L A, Yu I T-S, Qiu H, Siu Kai Au J, Wang X-R (2011). “A Case-Referent Study of Lung Cancer and Incense Smoke, Smoking, and Residential Radon in Chinese Men”. Environmental Health Perspectives, Vol. 119, No. 11, pp. 1641-1646.

UNSCEAR (1988). “Sources. effects and risks of ionizing radiation”. United Nations Scientific Committee on the Effects of Atomic Radiation”. Report to the General Assembly. with Annexes. New York. USA

UNSCEAR (2000). “Exposures from natural radiation sources – Annex B”. United Nations Scientific Committee on the Effects of Atomic Radiation”. New York. USA. pp. 84-156.

UNSCEAR (2008). “Sources and effects of ionizing radiation – Annex B”. United Nations Scientific Committee on the Effects of Atomic Radiation”. Vol 1. New York. USA. pp. 243- 463.

Utgenannt P (2004). “The influence of ageing on the salt-fost resistance of concrete”. PhD thesis. Lunds University of Technology. Div. of Building materials, Report TVB-1021, Lund, Stockholm, 346 pp.

Vaisala (2019). “SHM40 Structural Humidity Measurement Kit”. Technical data sheet, 3 pp., SHM40 Structural Humidity Measurement Kit Datasheet B211187EN-G (vaisala.com)

Valmari T, Arvela H, Reisbacka (2012). ”Radon in Finnish apartment buildings”. Radiation Protection Dosimetry, Vol. 152, No. 1-3, pp. 146-149.

Van der Graaf & de Meijer R J (2005). “Non-destructive evaluation of concrete condition using radon exhalation monitoring:a feasibility study”. Radioactivity in the environment, Vol. 7, pp. 573-579.

Wiedner H & Maringer F J (2018). ” Results of the comparison exercise for gamma-ray spectrometry measurement systems 2017 – Naturally occurring radionuclides”. NEN, CEN/TC 351/WG 3, N 201, 40 pp.

World Health Organization (2009). “WHO Handbook on Indoor Radon: a Public Health Perspective,” World Health Organization, Geneva, Switzerland, 110 pp.

Wu B and Ye G (2017). “Development of porosity of cement pastes blended with supplementary cementitious materials after carbonation on the pore structure,”*Construction of Building Materials*, Vol, 145, pp. 52-61.

Yu K N, Young E C M, Stokes M J, Kwan M K, Balendran R V. (1997). “Radon emanation from concrete surfaces and the effect of the curing period. Pulverized Fuel Ash (PFA) substitution and age”. Applied Radiation and Isotopes. Vol 48. No 7. pp. 1003-1007.

Yu K N, Cheung T, Guan Z J, Young E C M, Mui B W N, Wong Y Y. (1999). “Concentrations of ^{222}Rn, ^{220}Rn and their progeny in residences in Hong Kong”. Journal of Environmental Radioactivity, Vol. 45, pp. 291-308.

Yu K N, Cheung T, Guan Z J, Mui B W N, Ng Y T (2000). “^{222}Rn, ^{220}Rn and their progeny concentrations in offices in Hong Kong”. Journal of Environmental Radioactivity, Vol. 48, pp 211-221.

Zeng Q, Kefei L, Fen-chong T, Dangla P. (2012). “Pore structure characterization of cement pastes blended with high-volume fly-ash”, Cement and Concrete Research, Vol. 42, 194-204 pp.

Åkerblom & Clavensjö (2004). “The book of radon – Preventing measures in new buildings (In Swedish - *Radonboken – åtgärder mot radon i nya byggnader)*”. Formas. Stockholm, Sweden, 106 pp.

Åkerblom & Clavensjö (2007). “The book of radon – Preventing measures in buildings (In Swedish - *Radonboken – åtgärder mot radon i befintliga byggnader)*”. Formas. Stockholm, Sweden, 140 pp.

Appendices

Appendix 1 - Designed concrete recipes for main study

Table 1. Different constituents used in each concrete recipe and weights (kg/m^3).

	Binders					Aggregates								
Recipe	**Cement, CEM I - SH Skövde**	**SCM 1**	**SCM 2**	**SCM 3**	**SCM 4**	**Crushed, aggregate, 0/5 (55 wt%)**	**Crushed, aggregate 8/16 (45 wt%)**	**Water**	**Superplasticizer (Sikament 56)**	**Hydrophobic admixture (1 % of binder weight)**	**Total**	**w/b ratio**	**Air**	**Slump**
Explanation		Fly Ash, Class F	Fly Ash, Microsite	Slag	Slica Fume, Elkem 940									
	kg/m^3											-	**%**	**mm**
C	350					821	1004	192.5	1		**2369**	0.55	1	100
C-H1	350					817	998	192.5	0.7	3.5 (Silres 1801)	**2362**	0.55	1	102
C-H2	350					819	1001	192.5	0.6	3.5 (Hydrofob 1)	**2365**	0.55	1.1	95
C-H3	350					820	1002	192.5	0.7	3.5 (Silres 1802)	**2366**	0.55	1	120
C-F15-MF20	227.5	52.5	70			808	988	192.5	0.35		**2338**	0.55	1.1	120
C-FM35	227.5		122.5			811	991	192.5	-		**2344**	0.55	1.2	105
C-S65	129.5			220.5		816	997	192.5	-		**2355**	0.55	0.9	86
C-SF 10	315				35	817	998	192.5	0.35		**2358**	0.55	1.2	110
C-SF30	245				105	806	985	192.5	0.7		**2334**	0.55	1	105
C-FM15-SF10-H1	262.5		52.5		35	807	986	192.5	0.7	3.5 (Silres 1801)	**2339**	0.55	1.2	125
CGB	350					918	1122	192.5	0.5		**2583**	0.55	1.3	105
CGB-H1	350		0.7			915	1118	192.5	0.5	3.5 (Silres 1801)	**2579**	0.55	1	90

Appendix 2 - Design paste mix for Mercury Intrusion porosimetry

Table 1. Different constituents used in each concrete recipe and weights (kg/m^3) for Mercury Intrusion Porosimetry (MIP).

	Binders									
Recipe	**Cement, CEM I - SH Skövde**	**SCM 1**	**SCM 2**	**SCM 3**	**SCM 4**	**Water**	**Superplasticizer (Sikament 56)**	**Hydrophobic admixture (1 % of binder weight)**	**Total**	**w/b ratio**
Explanation		Fly Ash, Class F	Fly Ash, Microsite	Slag	Slica Fume, Elkem 940					
	kg/m^3									-
C	350					192.5	1		**543.5**	0.55
C-F15-MF20	227.5	52.5	70			192.5	0.37		**542.8**	0.55
C-FM35	227.5		122.5			192.5	-		**542.5**	0.55
C-S65	129.5			220.5		192.5	-		**542.5**	0.55
C-SF 10	315				35	192.5			**542.5**	0.55
C-SF30	245				105	192.5	0.7		**543.2**	0.55
C-FM15-SF10-H1	262.5		52.5		35	192.5	0.7	3.5 (Silres 1801)	**546.7**	0.55

Appendix 3 - Documentation of relative humidity during drying of recipes

A3.1 Monitoring prisms

Table 1. Measured relative humidity (%) at two different depths in each concrete prism.

Sample	Relative humidity (%) - 10 mm into concrete			Relative humidity (%) - 25 mm into concrete		
	75	**60**	**45**	**75**	**60**	**45**
C	74.4	60.8	44.6	74.9	61.0	44.5
C-H1	76.9	61.8	46.4	78.8	63.6	47.1
C-H2	72.5	59.2	46.4	72.3	60.6	47.2
C-H3	77.3	60.2	45.7	78.1	64.2	46.2
C-F15-MF20	74.7	59.4	46.3	75.9	60.4	48.0
C-MF35	76.7	61.4	46.7	77.3	62.3	48.3
C-S65	76.7	58.4	46.5	77.3	60.2	48.3
C-SF10	77.0	62.1	46.7	77.1	63.3	47.9
C-SF30	76.6	61.8	47.1	78.9	64.7	47.9
C-FM15-SF10-H1	74.4	62.0	48.1	75.6	62.9	48.7
CGB	77.1	61.5	47.1	75	63.4	47.9
CGB-H1	76.4	61.1	45.2	77.5	63.2	45.6
Median	**77**	**61**	**47**	**77**	**63**	**48**
Mean	**76**	**61**	**46**	**77**	**62**	**47**

A3.2 Monitoring plates

Table 2. Measured relative humidity (%) at two different depths in each concrete plate.

Sample	Relative humidity (%) - 10 mm into concrete			Relative humidity (%) - 25 mm into concrete		
	75	**60**	**45**	**75**	**60**	**45**
C	78.5	61.3	47.1	78.9	64.1	48.0
C-H1	74.7	61.0	47.3	75.3	62.8	48.3
C-H2	79.4	63.0	46.5	78.7	64.7	47.3
C-H3	76.4	61.6	47.1	76.7	62.7	48.0
C-F15-MF20	75.6	63.9	50.5	75.9	64.9	51.2
C-MF35	75.6	61.2	49.7	75.9	64.8	51.6
C-S65	77.0	64.5	46.8	77.9	66.2	47.8
C-SF10	74.4	62.8	46.9	75.6	65.4	47.6
C-SF30	76.7	61.9	47.5	76.3	62.9	48.2
C-FM15-SF10-H1	73.4	62.0	48.4	75.7	63.7	49.2
CGB	77.8	61.8	45.4	77.5	63.2	45.7
CGB-H1	75.7	62.0	46.7	75.5	61.3	46.5
Median	**76**	**62**	**47**	**76**	**64**	**48**
Mean	**76**	**62**	**47**	**77**	**64**	**48**

Appendix 4 - MIP- measurements

Below is a representation of the different cement paste binder systems. The figures are presented with the relative pore volume (%) on the right axis and the porosity (%) on the left axis. both as a function of the pore size distribution. The “porosity” on the right axis is a measurement of the accumulated porosity from the Hg-measurements. The figures are numbered from a to g, (a) reference cement paste, (b). C-F15-FM20, (c). C-FM35, (d) C-S65, (e) C-SF10, (f) C-SF30 and (g) C-FM15-SF10-H1.

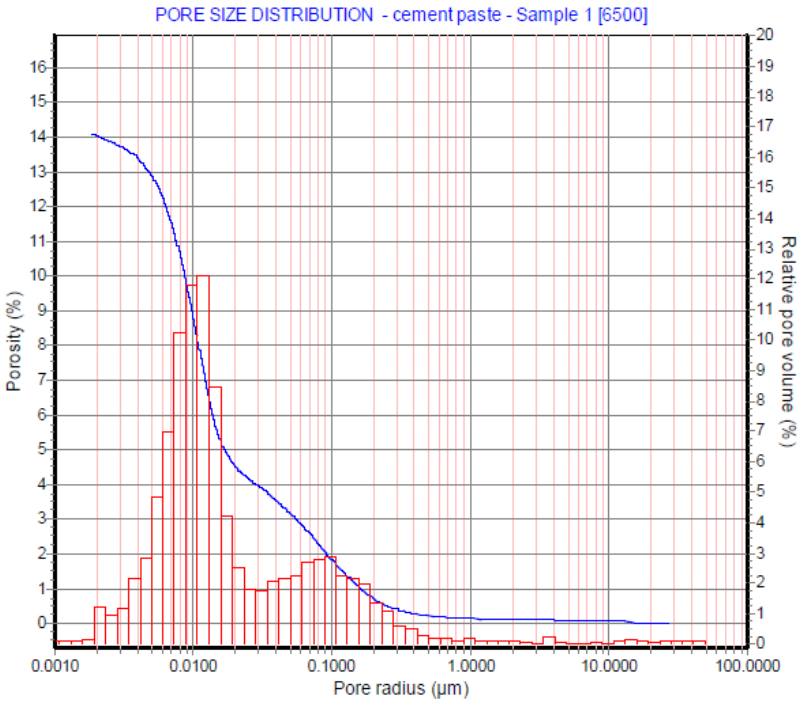

(a)

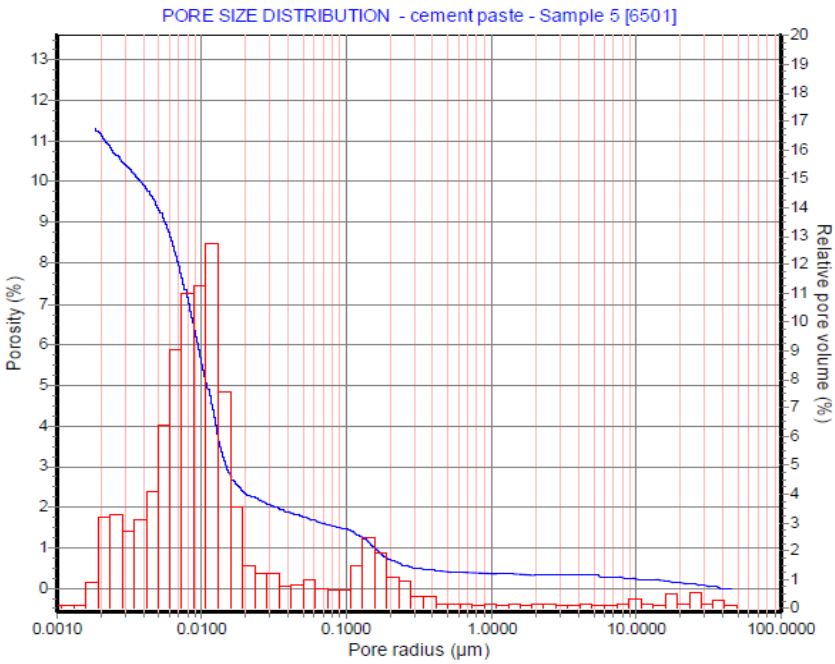
PORE SIZE DISTRIBUTION - cement paste - Sample 5 [6501]
Porosity (%)
Relative pore volume (%)
Pore radius (µm)
0.0010
0.0100
0.1000
1.0000
10.0000
100.0000

(b)

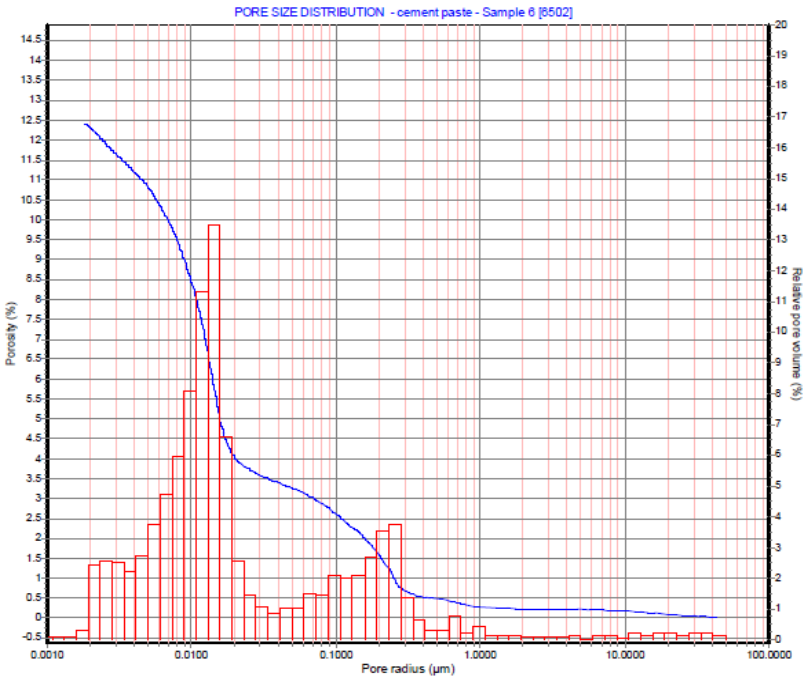
PORE SIZE DISTRIBUTION - cement paste - Sample 6 [6502]
Porosity (%)
Relative pore volume (%)
Pore radius (µm)
0.0010
0.0100
0.1000
1.0000
10.0000
100.0000

(c)

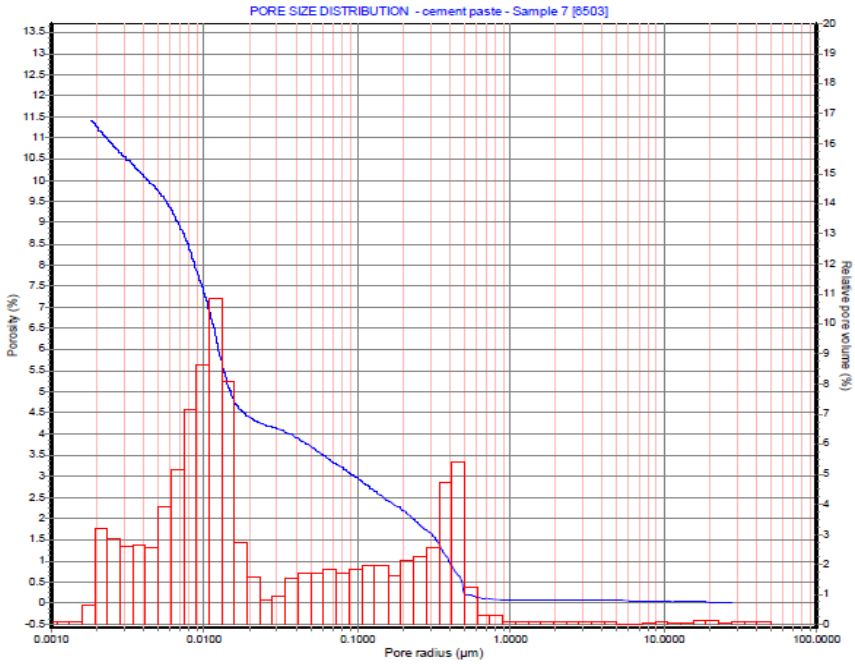
PORE SIZE DISTRIBUTION - cement paste - Sample 7 [6503]
Porosity (%)
Relative pore volume (%)
Pore radius (µm)
0.0010
0.0100
0.1000
1.0000
10.0000
100.0000

(d)

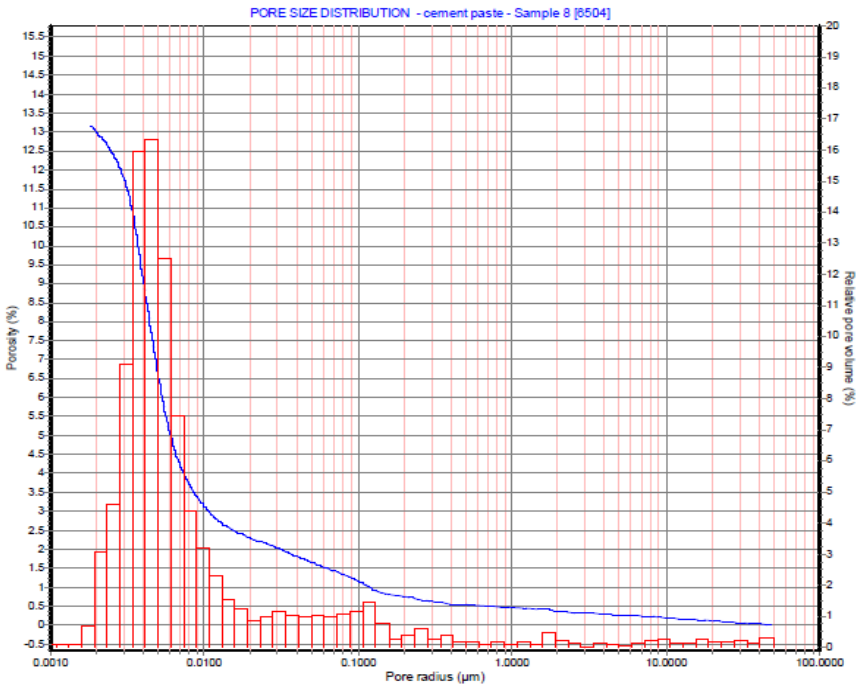
PORE SIZE DISTRIBUTION - cement paste - Sample 8 [6504]
Porosity (%)
Relative pore volume (%)
Pore radius (µm)
0.0010
0.0100
0.1000
1.0000
10.0000
100.0000

(e)

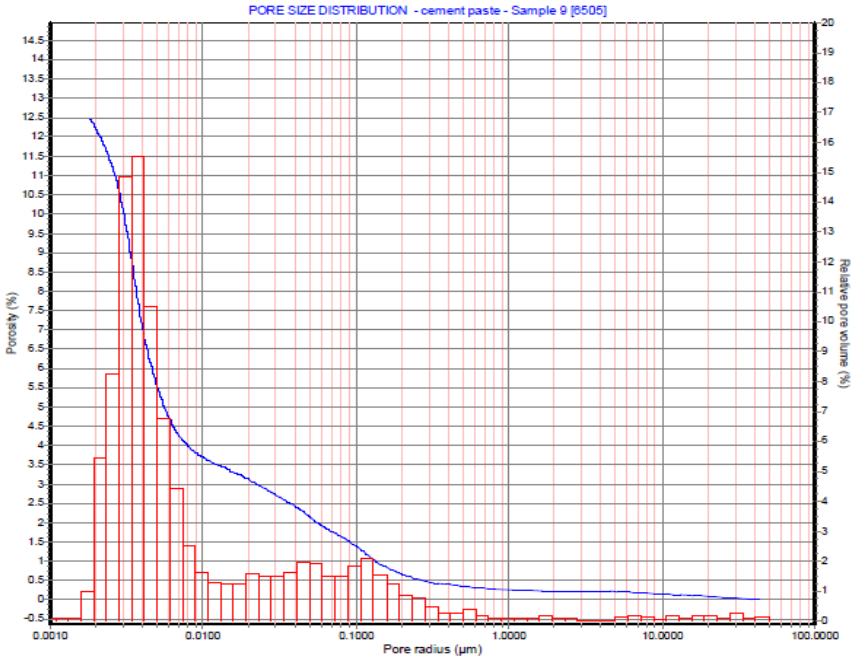

(f)

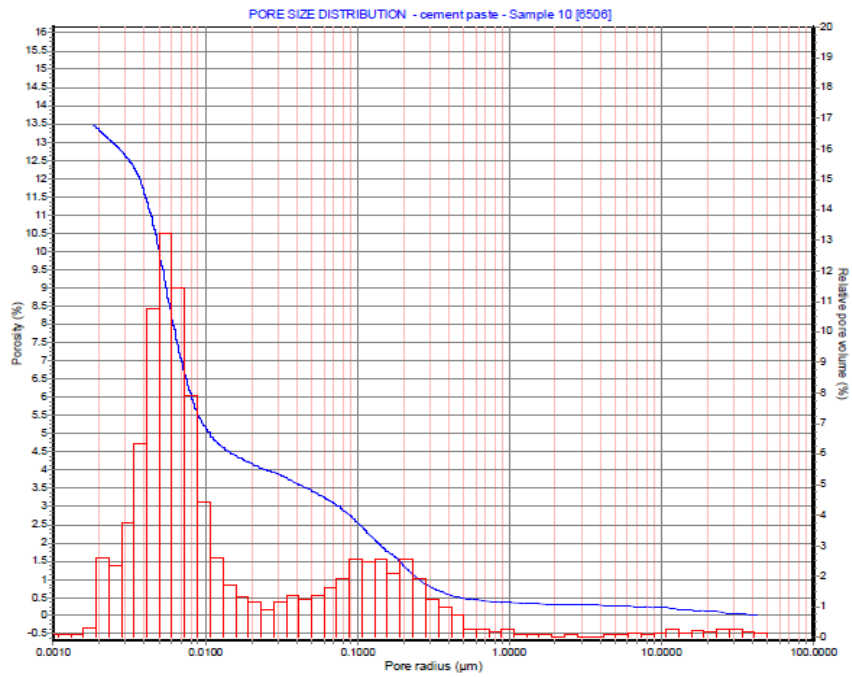

(g)

Figure (a) to (g) present the porosity and relative pore volume (%) as a function of the pore size distribution (µm) of the analyzed cement pastes (binders).

Appended papers